ARCHITECTING AIRCRAFT POWER DISTRIBUTION SYSTEMS VIA REDUNDANCY ALLOCATION

A Dissertation
Presented to
The Academic Faculty

by

Angela Campbell

In Partial Fulfillment
of the Requirements for the Degree
Doctor of Philosophy in the
School of Aerospace Engineering

Georgia Institute of Technology
December 2014

ARCHITECTING AIRCRAFT POWER DISTRIBUTION SYSTEMS VIA REDUNDANCY ALLOCATION

Approved by:

Professor Dimitri N. Mavris,
Committee Chair
School of Aerospace Engineering
Georgia Institute of Technology

Professor Dimitri N. Mavris, Advisor
School of Aerospace Engineering
Georgia Institute of Technology

Professor Daniel Schrage
School of Aerospace Engineering
Georgia Institute of Technology

Dr. Elena Garcia
School of Aerospace Engineering
Georgia Institute of Technology

Dr. Kirsten Duffy
NASA Glenn Research Center

Dr. Gerald Brown
NASA Glenn Research Center

Date Approved: 14 November 2014

DEDICATION

To my family,

your love and support made my dreams possible.

ACKNOWLEDGEMENTS

So many people made this work possible, and I would like to thank everyone. I will begin with my husband. Thank you for being at my side for the past four and half years. Every day you provide me with the love and encouragement that I needed to reach my goals. Next, I would like to thank my parents. Throughout my life you have made me feel loved, and you gave me the confidence that I needed to believe that I could achieve any goal.

I would also like to thank all of my committee members. Dr. Mavris, thank you for your guidance over my last five years at Georgia Tech. Reaching my academic goals would not have been possible without your assistance. Dr. Garcia and Dr. Schrage, thank you for your support of my work during my time at Georgia Tech. Lastly, I would like to thank Dr. Brown and Dr. Duffy of NASA Glenn Research Center for their mentorship for the past four years.

I would also like to thank Dr. Ajay Misra and George Stefko of NASA Glenn Research Center for their support through the NASA Graduate Student Research Program (GSRP). The GSRP made much of the work presented in this thesis possible.

TABLE OF CONTENTS

LIST OF TABLES

LIST OF FIGURES

Nomenclature

α	Tuning parameter
$\bar{\varepsilon}$	Limited error
$\bar{v}$	Limited voltage
β	Tuning parameter
$\dot{m}$	Mass flow rate
$\dot{q_{max}}$	Heat rejection
η_{pump}	Pump efficiency
λ	Component failure rate
μ_0	Magnetic constant
ω	Rotational speed
Φ	State of a system
ρ_{ant}	ant colony tuning variable
$\rho_{coolant}$	Coolant density
ρ_{cu}	Copper density
ρ_{fe}	Ferrite density
$\varphi_{coolant}$	Coolant viscosity
A	Cross-sectional area
$A_{coolant}$	Coolant sleeve cross-sectional area

A_{cp} Cross-sectional area of winding

a_{lower} Lower bound of the acceptable state

a_{upper} Upper bound of the acceptable state

B_c Critical magnetic field

C Capacitance

c_p Specific heat of the coolant

C_w Center leg width

D Diameter

d Diameter

D_h Hydraulic diameter

E_m Magnitude of generator voltage

f Friction factor

F_c Pitch winding factor

I Current

I_c Critical current

i_d Bus current

J_c Critical current density

K_1 Aspect ratio of the center leg

K_2 Aspect ratio of window

k_{ii} Current integral coefficient

k_{ip} Current proportional coefficient

k_{vi} Voltage integral coefficient

k_{vp} Voltage proportional coefficient

L Cable length

l_g Airgap length

n Number of component in a system

n_{turns} Number of turns

p Pressure

p_i Probability of component i functioning

P_{dem} Power demand

P_{load} Power required by load

P_{loss} Power loss

$P_{pumping}$ Pumping power

q_{reject} Cable heat rejection per unit length

R Radius

r Component reliability

R_i Reliability of component i

r_i Inner diameter

r_o Outer radius

R_s System reliability

R_{load} Load resistance

rho Resistivity

T Temperature

t time

T_c Critical temperature

T_e Electromagnetic torque

T_f Shaft static fiction torque

T_m Mechanical torque

$t_{cooling}$ Cooling sleeve thickness

$t_{dielectric}$ Dielectric shielding thickness

$t_{magnetic}$ Magnetic shielding thickness

u_{lower} Lower bound of the unspecified state

u_{upper} Upper bound of the unspecified state

V Velocity

v Bound of he unacceptable state

V_{DC} Bus voltage

v_{max} Maximum allowable coolant velocity

V_{nom} System nominal voltage

V_{wire} Wire voltage

W_a Window area

W_b Bobbin area

W_w Window width

W_{bob} Thickness of bobbin wall

X State of a component

y Selected minimum path

P Particle position

V Particle velocity

APU Axillary power unit

B1 Bus 1

B2 Bus 2

B3 Bus 3

B4 Bus 4

BSCCO Bismuth strontium calcium copper oxide

CPL Constant power load

DOE Design of experiments

DPC Direct power control

ECS Environmental control system

ESS Electric shutdown system

f_o Overall best fitness

F_s Switching frequency

FAA Federal Aviation Administration

G1 Generator 1

G2 Generator 2

G3 Generator 3

G4 Generator 4

GA Genetic Algorithm

GM Gain margin

HTS High temperature superconductor

I1 Inverter Group 1

I2 Inverter Group 2

I3 Inverter Group 3

I4 Inverter Group 4

IDG Integrated drive generators

IPPD Integrated product/process development

J Inertia of rotor and load

M1 Motor Group 1

M2 Motor Group 2

M3 Motor Group 3

M4 Motor Group 4

MEA More electric aircraft

PDS Power distribution system

PEDS Power electronics based distribution system

PM Phase margin

PMF Probability mass function

PMG Permanent magnet generator

PSO Particle swarm optimization

PWM Pulse width modulation

R1 Rectifier 1

R2 Rectifier 2

R3 Rectifier 3

R4 Rectifier 4

RAAPS Redundancy Allocation for Architecting Power Systems

RAT Ram air turbine

Re Reynolds number

RMS Root mean square

SA Simulated annealing

SPWM Sinusoidal pulse width modulation

SR Switched reluctance

TeDP Turboelectric distributed propulsion system

TF Transfer function

TRL Technology readiness level

TRU Tranformer rectifier unit

VOC Voltage oriented control

Y Admittance

YBCO Yttrium barium copper oxide

Z Impedance

SUMMARY

Recently, the environmental impact of aircraft and rising fuel prices have become an increasing concern in the aviation industry. To address these problems, organizations, such as NASA, have set demanding research goals for reducing aircraft emissions, fuel burn, and noise. One outcome of these goals is the shift toward "more electric" aircraft (MEA). In an MEA, heavy, inefficient hydraulic or pneumatic systems, such as actuation, are replaced by a lighter, more efficient electrically driven system. The next evolutionary step is to implement the use of electrical power for propulsion, which has led to the turboelectric propulsion concept.

In a turboelectric aircraft, the mechanical connection between the propulsor and the turbine is replaced with an electrical connection. This allows the propulsor and turbine to be decoupled so that each component can operate at its individual optimum speed. Furthermore, breaking the mechanical connection allows each component to be placed anywhere on the aircraft enabling conceptions such as boundary layer ingestion. Experts have estimated that turboelectric propulsion can reduce aircraft fuel burn by up to 35%.

A significant challenge in realizing a turboelectric system is creating a power distribution system (PDS) that can supply the large electrical loads. For a 300 passenger aircraft, the estimated electrical load for driving the propulsor is 40 MW, which is 40 times larger than the state-of-the-art Boeing 787. Due to the dramatic rise in the number of critical electrical loads on the aircraft, power system reliability is a concern.

Currently, power system reliability is maintained through the use of back-up power

supplies such as batteries and ram air turbines (RATs). However, the increasing power requirements for critical loads will quickly outgrow the capacity of the emergency devices. Therefore, reliability needs to be addressed when designing the primary power distribution system.

Power system reliability is a function of component reliability and redundancy. Component reliability is often not determined until detailed component design has occurred; however, the amount of redundancy in the system is often set during the system architecting phase. In order to meet the capacity and reliability requirements of future power distribution systems, a method for redundancy allocation during the system architecting phase is needed.

This thesis presents an aircraft power system design methodology that is based upon the engineering decision process. The methodology provides a redundancy allocation strategy and quantitative trade-off environment to compare architecture and technology combinations based upon system capacity, weight, and reliability criteria.

The methodology is formulated and demonstrated by architecting the power distribution system of an aircraft using turboelectric propulsion. The first step in the process is determining the design criteria which includes a 40 MW capacity requirement, a 20 MW capacity requirement during an engine-out scenario, and a maximum catastrophic failure rate of one failure per billion flight hours. The next step is determining gaps between the performance of current power distribution systems and the requirements of the turboelectric system. A baseline architecture is analyzed by sizing the system using the turboelectric system power requirements and by calculating reliability using a stochastic flow network. To overcome the deficiencies discovered, new technologies and architectures are considered. Global optimization methods are used to find technology and architecture combinations that meet the system objectives and requirements. Lastly, a dynamic modeling environment is constructed to study the performance and stability of the candidate architectures. The combination

of the optimization process and dynamic modeling facilitates the selection of a power system architecture that meets the system requirements and objectives.

The result of the methodology is an architecture design that meets the reliability requirements with a minimal system weight. While the methodology was formulated for a turboelectric distributed propulsion (TeDP) system, it can be applied to a variety of power distribution architecting studies. The application of the methodology provides the user with insight into the effect of component and path redundancy on system reliability and weight. During the creation of the methodology, a number of contributions to power system architecting were made including: a method to rapidly determine required component capacities in a network, a sizing method for a variety of aircraft power cables, a method for evaluating power system reliability, and an architecture optimization strategy.

CHAPTER I

INTRODUCTION

Some alarming trends have been recently observed in regarding the environmental impact of aircraft [118]. Although aircraft are responsible for only 2% of fossil fuel consumption today, consumption is rising due to the increase in air traffic. [82]. In the United States alone, air traffic is expected to increase by a factor of 2 to 4 by 2025 [79]. The surge of air travel is expected to increase aircraft contribution to global emissions by 5% by 2050 [114].

Another significant aircraft environmental concern is noise. Strict regulations have kept airport noise at a tolerable level; however, as air traffic continues to grow and urban populations expand causing more people to live near airports, aircraft noise will become more of a problem [25]. Because of the nuisance created by aircraft noise, citizens in areas near airports have resisted airport expansion or development. Due to this matter, officials at 29 of the 50 busiest U.S. airports have cited noise as their most serious environmental concern [35].

A third issue is rising fuel prices; this is shown in Figure 1 [72]. For the average airline in 2011, fuel contributed to 35% of operating costs; in contrast, fuel costs were only 10% of operating costs in 2001 [114]. The rising fuel cost has adversely affected airlines' profits. The sharp increase in fuel prices in 2008 caused profits to rapidly drop for airlines, thus putting many on the verge of bankruptcy [48].

The environmental and economic concerns listed have led several organizations to set goals for the aviation industry regarding fuel consumption, emissions, and noise. One example is NASA's technology goals for future subsonic fixed wing vehicles, which are shown in Table 1 [60]. (The improvements are relative to a B737-800 with

Figure 1: Fuel Prices in the United States since 1993

CFM56-7B engines for the N+1 and N+3 goals. The N+2 goals are relative to a B777-200 with GE90 engines). In order to reach these goals, new technologies and aircraft architectures that can significantly improve aircraft efficiency will have to be implemented. One important paradigm shift that is occurring as a result of fuel burn and emission goals is the movement toward "more electric" aircraft (MEA) and electric propulsion [136].

Table 1: NASA Subsonic Fixed Wing Program Goals

Corners of the trade space	N+1 (2015)	N+2 (2020)	N+3 (2025)
Noise	-32 dB	-42 dB	-55 dB
LTO NOx Emissions	-60%	-75%	-80%
Cruise NOx Emissions	-55%	-70%	-80%
Aircrat Fuel/Energy Consumption	-33%	-50%	-60%

In an MEA, heavy, inefficient mechanical systems are replaced by lighter, more efficient, and more reliable electrical systems [74]. The movement toward MEA is dependent on the development of many different technologies such as electromechanical actuation [128]. Traditionally, actuation is performed through a hydraulic system, which requires heavy hydraulic piping throughout the aircraft. The system is prone to leaks that lead to a low system efficiency. In an electromechanical actuation system, the hydraulic system is replaced by electric motors that are used to move the actuators. The hydraulic lines can be replaced by light electric cables, and hydraulic leaks are no longer a problem. This same trend can be observed in other systems as well, such as the environmental control system [53].

After replacing hydraulic and pneumatic systems with their electrical counterparts, the next evolutionary step is to move toward electric propulsion. Two examples of electric propulsion concepts are hybrid propulsion and turboelectric propulsion. In a hybrid propulsion system, the propulsors are driven using a combination of mechanical and electric power. During flight conditions that have low power requirements (e.g. cruise), the engines can be run using stored electric power from storage devices such as batteries, or they can be run using fuel cells. During periods of high power demand, fuel can be used to power the engines. The second option, turboelectric propulsion, provides thrust for the aircraft by using electrically driven motors.

1.1 The Turboelectric Aircraft Concept

Turboelectric propulsion is a revolutionary system that can potentially reduce aircraft fuel burn, emissions, and noise. In a turboelectric system, the mechanical connection between the propulsor (fans) and turbine is replaced with an electrical connection, which allows each component to run at its individual optimum speed and creates a more efficient system. Furthermore, the decoupling of the turbine and fans allows each component to be placed anywhere on the aircraft, so efficiency can be further

optimized. By using this new propulsion system, experts have estimated that fuel burn could be reduced by up to 70% [9]. The reduced fuel burn will also contribute to the reduction of harmful emissions. In addition, this architecture can be modified to allow for the use of alternative fuels such as hydrogen or fuel cells, which can further aid in the reduction of harmful emissions [79].

Another major advantage of the turboelectric propulsion system is that it enables the use of distributed propulsion, a concept which uses many small fans distributed across the aircraft in the place of the traditional two or four propulsors. The expected application for distributed propulsion is a hybrid or blended wing body aircraft. Using this configuration offers several advantages. First of all, fuel consumption can be reduced by ingesting boundary layer flow and filling the wake generated by the airframe with the output stream of the fans. Other advantages of distributed propulsion include the elimination of control surfaces by enabling differential and vectoring thrust for pitch, roll, and yaw moments; reduction of noise by using airframe shielding; and increased lift by using trailing-edge nozzles for vectored thrust, boundary layer control, and supercirculation around the wing [79].

An example of a turboelectric aircraft concept is the NASA N3-X, which is shown in Figure 2. The N3-X is a blended wing body aircraft that can carry approximately 300 passengers and has a range of 7,500 nautical miles. The aircraft will cruise at Mach 0.84 at an altitude of 30,000 feet [21]. The N3-X has a distributed propulsion system consisting of 16 fans driven by electric motors which span the upper body of the aircraft. The gas turbines and generators are located at the wing tips so that they receive undisturbed air and supply a bending moment for the wings [45].

A turboelectric propulsion system consists of six primary components: gas turbine, superconducting generator, power distribution system (PDS), thermal management system, superconducting motors, and fans. An overview of the system architecture is shown in Figure 3. The connections are color coded based on the connection type.

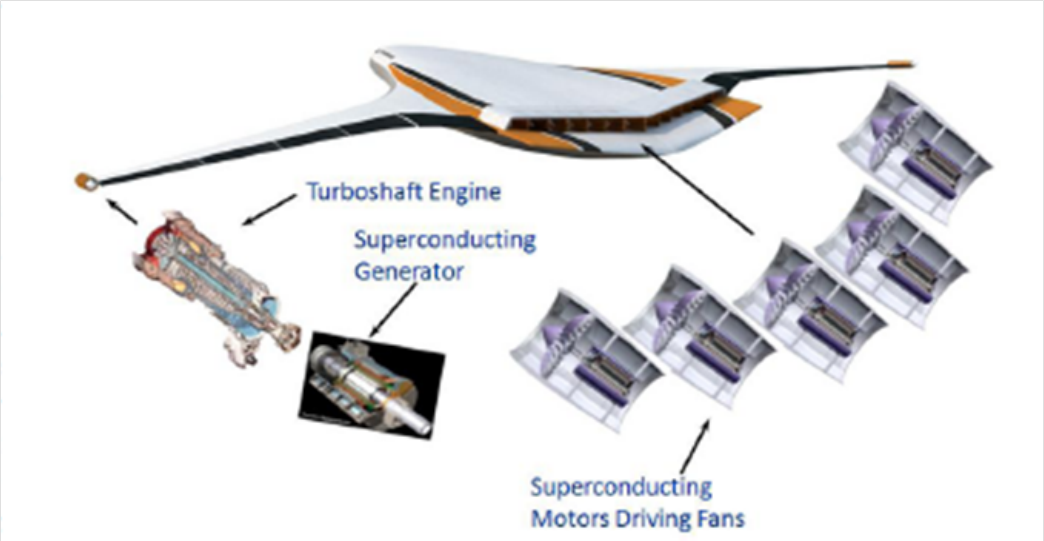

Figure 2: NASA N3-X

The green lines show a mechanical connection. The direction of the arrows shows which component is the source of energy and which component receives it (at the arrow head). The red lines represent an electrical connection. The direction of the arrow shows the direction of power flow from source to load. The blue lines show the flow of coolant. The arrows are in both directions for each line because the coolant will circulate through the system.

Like gas turbines being used today, the primary purpose of the gas turbine in the turboelectric architecture is to convert chemical energy into mechanical energy. One difference between the turboelectric gas turbine and current gas turbines is that jet fuel and hydrogen may be burned in the turboelectric system since liquid hydrogen may already be on-board as a cryogenic coolant for the superconducting elements [89]. The mechanical power generated by the gas turbines will be used to power generators.

The generators convert the mechanical power supplied by the gas turbine to electrical power that can be used to drive the electric fans. In addition to the fans, the generator may also supply all other electrical loads on the aircraft. In a study conducted by NASA, the estimated electrical load demand for the N3-x is 40 MW. Since

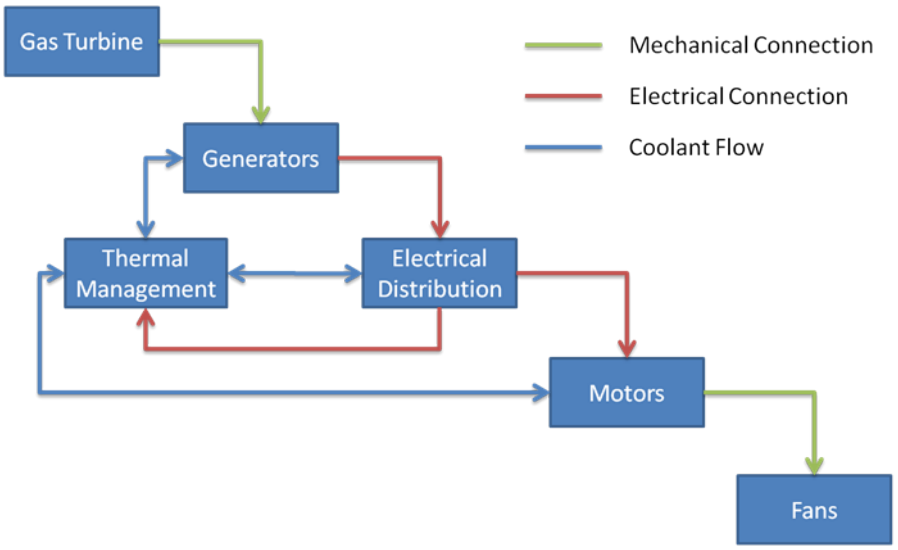

Figure 3: Turboelectric System Architecture

the power demand is so large, the power density of the generator must be high so that the weight does not greatly hinder the performance of the aircraft and negate any benefit of using turboelectric propulsion. The best option to get a high power density is to use a wound rotor synchronous machine. The machine will likely need to be fully superconducting, meaning that the rotors and stators must be made of a low-AC-loss superconducting material and be cooled cryogenically [22]. The expected losses in each generator is estimated to be only 0.01% [79].The superconducting motors used to drive the fans are similar to the superconducting generators; simply, the power flow is in the opposite direction. NASA has estimated that the required power for each of the 14 motors on the the N3-X will be approximately 5.74 MW.

One of the challenges of using superconducting machinery is to keep it cooled to cryogenic temperatures. Depending on the superconducting materials used, the temperature of the components must be maintained between 20K and 65K. Meeting this constraint is the task of the thermal management system. To maintain cryogenic temperatures in superconducting components, a cryogenic coolant will be needed. The most likely choices are either liquid hydrogen or liquid nitrogen. The coolant will be circulated through the system (through transmission lines, generators, and

motors) in order to remove excess heat from components. The heat the coolant gains is removed using a cryocooler. A cryocooler is a Brayton, Stirling, Gifford-McMahon, or Joule-Thomson type refrigerator that can be used to maintain a cryogenic temperature in the coolant [124]. The performance of the cryocoolers is defined by the fraction of Carnot efficiency attained, which is expected to be 30%. The expected weight of the cyrocoolers is 5 lb/input-hp][21].

The final component that links the power source components to the power sink components is the power distribution system. The PDS will consist of power transmission cables, power converters, and fault protection devices. Since the PDS acts as a link between the components in the system, its performance will affect the entire system. The PDS must be able to reliably supply electricity to all components, and must also be robust against disturbances and failures in the system. In order to meet the capacity and efficiency requirements of the system, new technologies such as superconducting cables and cryogenic inverters may be used [24] [156].

1.2 Previous TeDP Studies

As shown in the previous section, the achievement of a turboelectric system will require the use of many new technologies, which has led to the need for new design methods and created a variety of areas of research including: airframe integration; generator, motor, and fan design; thermal management; and power distribution system design. Each of these areas presents a unique set of challenges, which have been the subject of many publications.

One of the most highly researched areas for the turboelectric concept is airframe integration and the effects of distributed propulsion. Studies include the integration of the system with the airframe, the effects of boundary layer control, and vectored thrust. Papers by Gibson et al. illustrate how to integrate the fans with the airframe by investigating inlet, ducting, and nozzle design [57] [56]. Studies by Felder and

Kim [46] [44] [78] have outlined designing for boundary layer control and boundary layer ingestion and have calculated the benefits of using such a system. Another publication by Sato et al. discusses the effect of turboelectric propulsion on aircraft sizing [134].

A second highly researched area is superconducting machinery and fans. Superconducting machinery is being studied in order to develop power dense generators and motors for the turboelectric concept. Many studies have been published on how to size and design superconducting machinery [79] [95] [96] [56]. Furthermore, research on fan design for optimal efficiency can be found in a study by Felder [45].

Thermal management is another research area that has received a respectable amount of attention. Much of the focus has been on the sizing and design of cryocoolers to provide cryogenic cooling for the PDS, generators, and motors [79] [95] [45] [21]. Most of these studies are based on using liquid hydrogen or nitrogen to cool superconducting components of the system.

Currently, the least researched element of the turboelectric system is the power distribution system. The only studies available are basic architecture analyses and preliminary weight estimates using data from other applications [45]. The sizing of the cables is based upon a Japanese superconducting cable study; using this study, NASA estimated a preliminary weight of 9.2 kg/m for a 70 MW transmission cable. Weight and efficiency estimates for the inverters based upon coolant type are available in a paper by Felder [45]. The first PDS architecture study was presented in a paper by Armstrong et al. [10]. This publication discusses the effect of architecture selection on electrical stability, electric grid safety, and aircraft safety. It also addresses the effect of engine failure for the aircraft. If an engine fails, symmetry needs to be maintained among the motors to decrease the load requirement on the vertical tail. Futhermore, the paper highlights the need for redundancy in the system to meet propulsion reliability requirements, but lacks a detailed reliability analysis. While

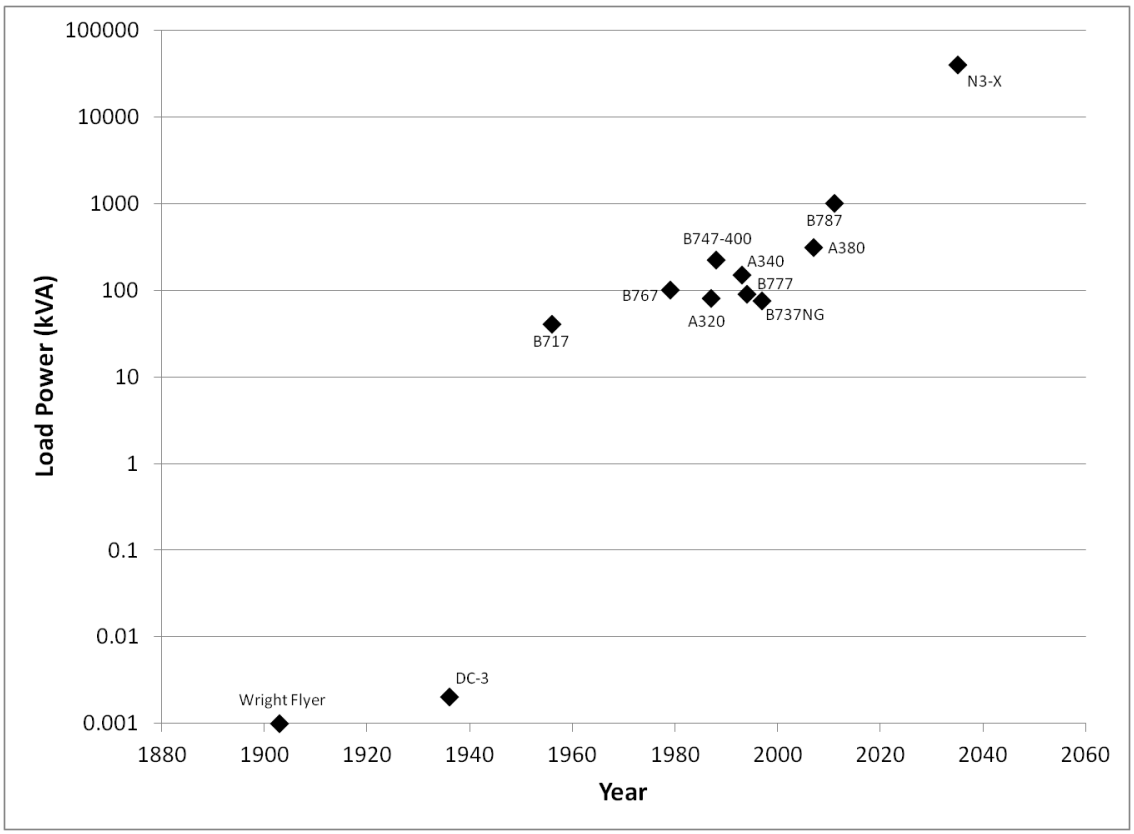

Figure 4: Progression of Commercial Aircraft Power Loads [13]

the PDS information presented in the literature is useful for a first-cut analysis, much more information will be required to architect the power distribution.

1.3 Problem Definition

The reliability and performance of the power distribution system will be critical to the overall propulsion system performance since it serves as a link from the power source to the propulsors. One challenge in creating a design approach is that a PDS of this scale has never been developed for an aircraft. Figure 4 demonstrates that the 40 MW of electrical loads on the N3-X are 40 times higher than the loads found on any commercial aircraft flying today. (The largest electrical load on an aircraft that is currently flying is 1 MW, which is the load for the Boeing 787 Dreamliner.)

Since there is such a large gap between the loads on aircraft today and turboelectric aircraft, new architectures and technologies will have to be used creating uncertainty in the design. (Architecture is defined as "entities and their underlying structure whose combined attributes accomplish a task or sets of tasks" [8] .) When architecting the system, the system functions must be met while delivering the required power capacity from the sources to the sinks. Also, system reliability is of utmost importance since the power distribution system is a critical component of the aircraft propulsion. (If the PDS fails, the aircraft could be put in catastrophic danger.) The reliability of the overall system must be equivalent to or better than the reliability of commercial propulsion systems used today. The first step in determining whether the reliability of the turboelectric system will meet the requirements is to understand what factors drive system reliability. Then, an approach to architecting the system such that the reliability requirements are met can be formulated.

1.4 System Reliability Considerations

Today, the electrical loads on aircraft are relatively small compared to those that would be present in a turboelectric aircraft. Reliability is currently maintained by integrating energy source back-ups into the system such as batteries and auxiliary power units. The auxiliary power sources can provide enough power to operate critical aircraft functions in the case of a primary system failure. The required amount of the reliability for the system can be met by adding these redundant devices. However, with the increase in critical electrical loads, small battery and APU back-ups will not be able to meet the power demand. For this reason, reliability needs to be addressed in the primary system design so that the need for redundant power sources can be reduced.

The first step in determining how to address system reliability during the system design is to have an understanding of the definition of reliability and the system

design features that drive reliability. Reliability is defined as "the probability of a device performing its purpose adequately for the period of time intended under the operating conditions encountered" [14]. First, this definition states that reliability is a probability. It also states that probability is defined over a period of time, which suggests that analyzing reliability is a stochastic problem. Another consideration is that reliability is defined for "the period of time intended", which conveys that the expected lifetime of the system must be specified. Another piece of the definition to consider is the statement that the device "performs its purpose adequately". To carry out a reliability analysis, what is considered to be "adequate performance" must be explicitly defined. Lastly, the definition declares that the device must perform adequately "under the operating conditions encountered"; therefore, the operating conditions of the system must be understood and the reliability calculation will only hold for the assumed conditions.

The next step in determining how to address reliability for the power distribution design problem is determining the driving factors of reliability. Consider the simple series system shown in Figure 5. In this system, "adequate performance" would be that there is an available path from the source to the sink. In a series system, a system failure occurs if any component in the system fails. The formula for determining system reliability is Equation 1; that is, system reliability is the product of the component reliabilities. Therefore, the reliability of this system is dictated by the reliability of each component in the system. If a component design change makes a component in the system more reliable, the overall system reliability will increase. For example, suppose that each component in the system has a reliability of 0.95 at a given time. Then the system reliability would be 0.86. If the reliability of each component was increased to 0.96, then the system reliability would be 0.88. This concept can be extrapolated to more complex systems. In general, a change in the reliability of the components will affect overall system reliability.

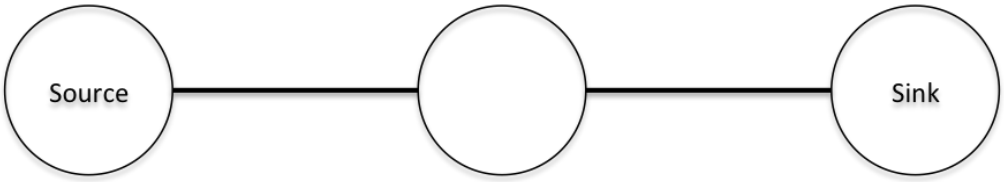

Figure 5: Simple series system

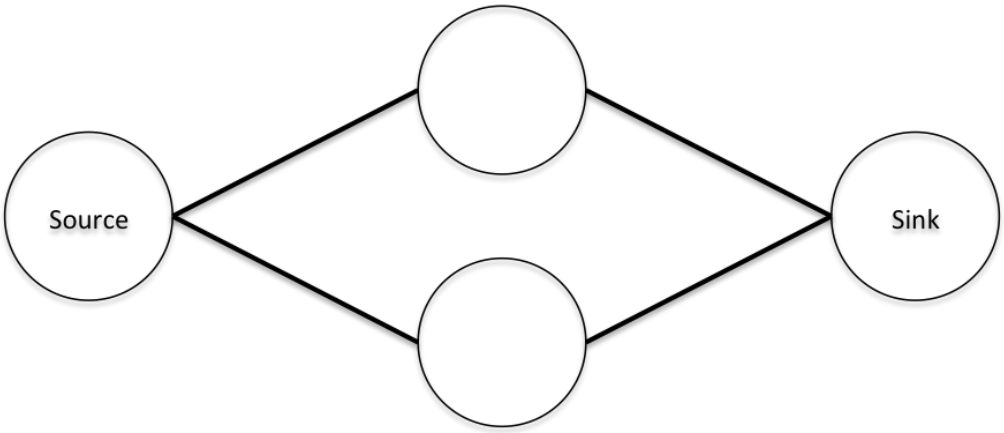

Figure 6: Simple redundant system

$$R_s = \prod_{i=1}^{n} r_i \tag{1}$$

A second consideration in system reliability is redundancy. Consider the system previously shown with a new component in parallel with the middle component of the simple series system. This new system is shown in Figure 6. Now, if one of the center components fails, there is still a path from the source to the sink. The new formula for system reliability, R_s, is shown in Equation 2. If the component reliabilities are 0.95, the reliability of the system would be 0.90. Now suppose that a third component is added in parallel as shown in Figure 7. The formula for calculating the reliability of this system is shown in Equation 3. If the reliability of the components is still 0.95, then the system reliability is now 0.902 rather than 0.900. This example demonstrates that the addition of a redundant component has a major impact on system reliability; however, there are diminishing returns when adding components.

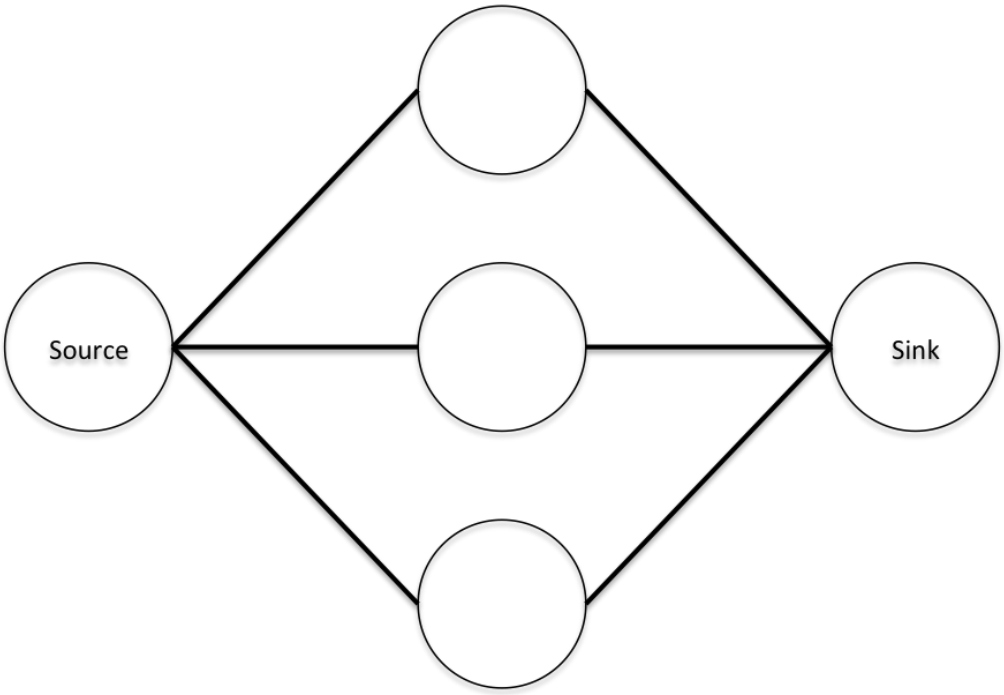

Figure 7: Triple redundant system

$$R_s = r_1 * (1 - (1 - r_2)^2) * r_3 \tag{2}$$

$$R_s = r_1 * (1 - (1 - r_2)^3) * r_3 \tag{3}$$

This suggests a major design question. When should redundancy be addressed in the system design process? One consideration is that not all the information required for an accurate reliability calculation will be available early in the design phase. Specifically, component reliabilities can only be estimated at this point, and there is uncertainty in what their exact reliability profile will be since detailed component analysis will not be completed at this design phase. However, ignoring system reliability early in the design process can lead to the formation of infeasible designs.

System redundancy is often set during the system architecting phase. If the system architecture does not have the appropriate amount of redundancy, the reliability requirement of the system may not be met since there is a practical limit to how

much component reliability can be increased. Also, the example from before showed that increasing component reliability by a percentage point had a small impact on system reliability. Nonetheless, if too much redundancy is included, the system weight will be dramatically increased with little benefit of increasing reliability.

The discussion has shown that reliability must be considered during the system architecting phase. While there is uncertainty in component reliabilities at this point in the design process, redundancy allocation needs to be addressed so that infeasible or overly redundant designs are not considered during the detailed design phase. Therefore, a method for redundancy allocation during the architecting of a power distribution system is needed. Along with finding architectures that can lead to successfully meeting the system reliability requirement, a balance between additional redundancy and system weight must be found. The formulation of this methodology is the objective of this thesis. The overall research objective is stated as:

Research Objective: Develop a power distribution design methodology that provides a redundancy allocation strategy and a quantitative trade-off environment to compare architecture and technology combinations based upon system requirements.

The next chapter will discuss the formulation of the methodology in order to meet the research objective. Then the specific steps used to carry out the methodology will be discussed in following chapters.

CHAPTER II

METHODOLOGY OVERVIEW

The research objective stated in the previous chapter implies that the development of a methodology is the primary goal of this thesis. The methodology will be constructed to address power distribution system redundancy allocation for an aircraft using TeDP. In order to fulfill this task, the methodology must address several issues; the first is the composition of systems, which can be achieved using systems engineering methods. One of the challenges in developing the PDS for a turboelectric aircraft is that identifying specific technologies to use in the design could be difficult early in the design process. Therefore, a top-down approach is the most practical for system composition. The methodology must guide the user to first determine the requirements and high-level functions of the system. After this step, the system can be decomposed and functions can be allocated to specific technologies. After candidate systems have been identified, a computer-integrated environment is needed to evaluate the systems based on a predetermined set of criteria [112]. Attributes of the design approach needed for the TeDP PDS system design problem can be found in the Engineering Decision Process.

2.1 The Engineering Decision Process

The Engineering Decision Process is the cornerstone of the Georgia Tech Integrated Product/Process Development (IPPD) methodology which is shown in Figure 8. The IPPD methodology was developed to bring knowledge forward earlier in the design process by creating a systematic approach to the integration and concurrent application of all the disciplines that affect a product [98]. The methodology uses a top-down approach where a problem is decomposed and enables system trades to be performed.

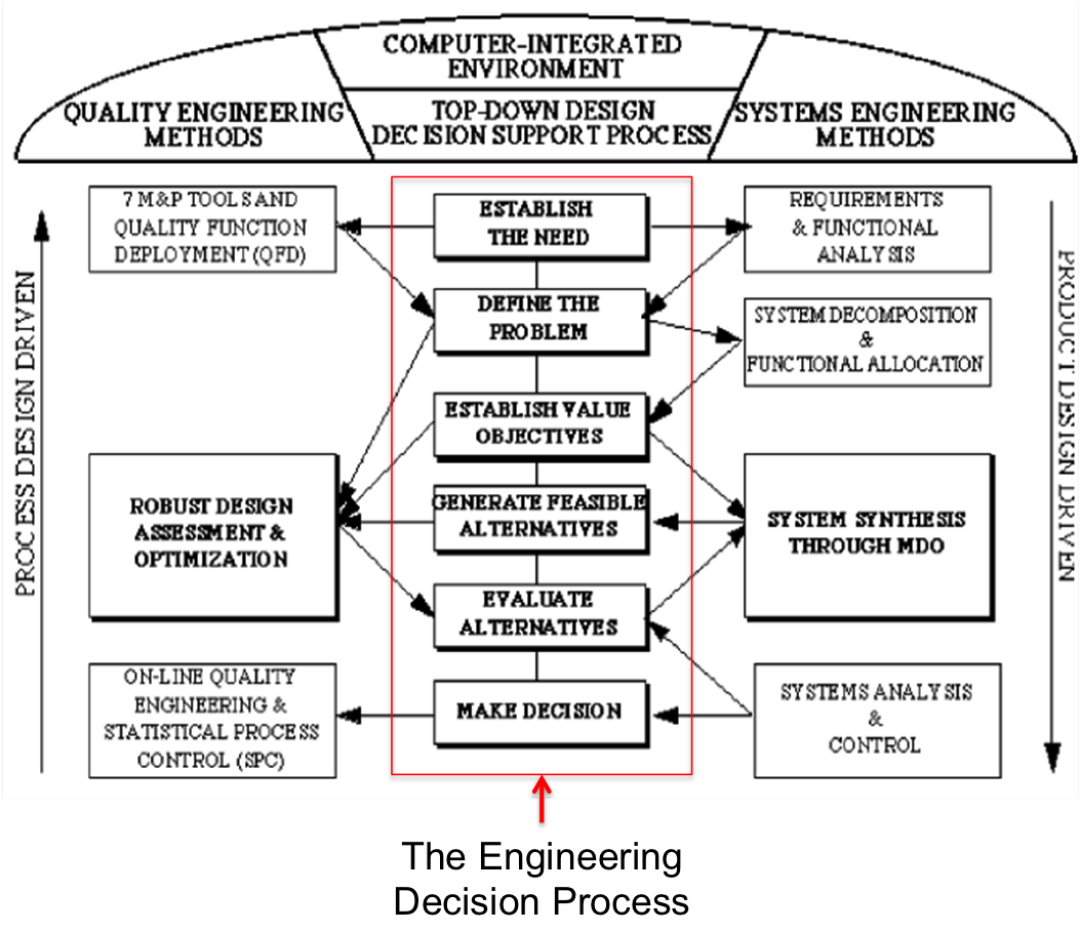

Figure 8: The Georgia Tech IPPD Methodology [98]

The Georgia Tech IPPD methodology is divided into three columns. The columns fall under an umbrella which contain quality engineering methods, a computer-integrated environment, a top-down design decision support process, and systems engineering methods. The columns of interest for formulating the methodology are the center column and the right side column. The center column under the umbrella is the Engineering Decision Process. The first step, as shown in Figure 8, is to establish the need. In this step, the user is asked to identify a problem that requires the development of a new product. The second step in the middle column is "define the problem"; the user must determine what needs to be accomplished and what the scope of the project is. Other requirements in this phase are to determine who the decision makers are and what the external environment is. The third step is to establish value objective. Here factors for determining the project's feasibility and criteria for evaluating the success of the project/product will be determined. The fourth step is to generate feasible alternatives. In this step, many different product designs are generated and then evaluated for feasibility. The feasible designs are then sent to the fifth step in the process, evaluate alternatives. Each design is analyzed based on the criteria set in step 3. The final step in the engineering decision process is the make a decision; the "best" design is chosen based upon the analysis performed in step 5.

In the Georgia Tech IPPD methodology, system and quality engineering methods are used in conjunction with the engineering decision process. The systems engineering methods are shown in the right hand column in Figure 8. The first block in the right hand column is requirements and functional analysis. This step is performed after the establish the need step and is used to define the problem. The requirements define specific objectives that the product must meet. The functional analysis determines all the high level functions that the product must perform. The second system engineering method to be applied is system decomposition and functional allocation, which occurs after the define the problem stage and feeds into the establish value

objectives stage. The system decomposition facilitates the top-down approach. The high level functions of the system are broken down into low level functions; then the requirements are allocated to the lower level functions. The third systems engineering method is system synthesis through multi-disciplinary optimization (MDO) which requires information from the establish value objectives and evaluate alternatives steps. In turn, it provides information for the generate feasible alternatives step. In the system synthesis step, physical components are assigned to the low-level functions from the system decomposition stage. In complex products or systems, many disciplines are needed to complete this process. Also, a large number of alternatives may be possible; therefore, optimization is required to find the best options. The final systems engineering method is systems analysis and control, which includes techniques and tools for analyzing the systems engineering process.

The methodology for the PDS design problem will be formulated based upon the engineering decision process and the right column of the Georgia Tech IPPD methodology. Some of the steps in the Georgia Tech IPPD methodology will be modified for the PDS design problem, also some steps will be added or removed. In the Georgia Tech IPPD methodology there is a focus on process development; for example, the quality engineering methods are concentrated on building robustness into the manufacturing of a product to achieve product reliability. At this stage in turboelectric system design, process design is not a concern. The reliability of the system will be addressed through product design rather than process design causing the PDS design methodology to diverge from the Georgia Tech IPPD methodology.

2.2 Formulation of RAAPS and Research Questions

The PDS design methodology will consist of a series of steps based upon the engineering decision process. Some systems and quality engineering methods will be applied as well. For each step, a set of alternatives will exist for possible actions.

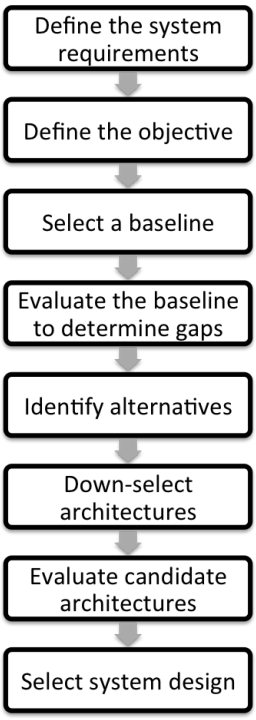

Figure 9: The RAAPS methodology

The decisions that are made will be the defining characteristics of the PDS design methodology proposed. The name given to the PDS design methodology is RAAPS - Redundancy Allocation for Architecting Power Systems. The RAAPS methodology is shown in Figure 9.

2.2.1 Define the Problem

The first step in RAAPS is to determine the system requirements. This is loosely equivalent to the "define the problem" step in the engineering decision process. The goal of this step is for the user to determine system specifications, such as the required capacity and reliability for the system. The requirements will determined by the aircraft's size and purpose. Other requirements are derived from PDS design standards, such as the amount of transient fluctuations allowed. The requirements defined will serve as the constraints on the problem.

As stated in the introduction, the N3-X will be the case study for the thesis which

requires 40 MW of electrical power for takeoff. According to FAA regulations, an aircraft must have enough thrust to complete a takeoff and land if an engine fails. For the N3-X system, if one of the gas turbines fails, the system must still be able to supply 20 MW of power to the motors to meet the engine-out requirement. The other requirement that will be addressed in the design is reliability. According to Boeing, the catastrophic failure rate of commercial aircraft propulsion systems, that is the rate of complete propulsion loss for an aircraft, is about 1 failure in 1 billion flight hours [17]. Since the PDS will be an integral part of the turboelectric propulsion system, the failure rate of this system must be as good as or better than the current failure rate.

Now that the requirements have been defined, the next step is to define an objective. This step is modeled after the "establish value objectives" stage in the IPPD methodology. In this step, the user determines the goals of the design process. For the turboelectric system, the two most desired qualities are light weight and high efficiency. In any aerospace application, weight is always a concern. The weight of the PDS will have an effect on the overall aircraft sizing. If weight is minimized, less thrust will be needed for the aircraft, reducing the overall size of the entire propulsion system. Also, the aircraft will require less lift, so the size of lifting surfaces can be reduced. Furthermore, a reduction in PDS weight means that the aircraft payload weight can increase for a set aircraft size.

A second important issue is efficiency. In an electrical system, any losses will generate heat. In a 40 MW system, even small inefficiencies can lead to massive heat loads. Furthermore, if the system is not efficient as possible, the justification for moving from a turbofan engine to a turboelectric system may be lost; therefore, for the viability of the system, efficiency is paramount.

Having both the weight and efficiency objectives lead to a multi-objective problem. Having two objectives creates a trade-off situation that may make selecting a final

design difficult. The two objectives must be weighted against each other to determine which qualities in the system are more important. Often having multiple objectives in a problem cannot be avoided; however, in this instance, the two objects can be combined. Inefficiencies in the system will lead to heat losses. The heat will have to be dissipated by a thermal management system. The larger the inefficiency, the higher the weight of the thermal management system. So, inefficiency can be treated as a weight penalty on the system. Inefficiency will also lead to the aircraft requiring more fuel, which in turn will increase the takeoff weight of the aircraft. Therefore, the problem can be addressed as a single objective design problem which will simplify the analysis while addressing both objectives.

2.2.2 Select a Baseline

Once the system requirements and objectives have been set, the search for designs that meet the set criteria begins which leads to Research Question 1:

Research Question 1: What improvements are needed to current power distribution systems to meet the electrical load demand of a turboelectric aircraft?

To address this question, step 3 of the methodology, "select a baseline", commences. By creating a baseline, the user can quantify the improvements needed to current PDS designs to fulfill the turboelectric requirements.

The research question asks what improvements are needed compared to today's systems. Selecting a baseline that is truly representative of a current system is difficult since the turboelectric system is not yet a reality. To create the baseline, a literature search was conducted on current power distribution technologies and architectures. The research will begin by examining the power distribution system architectures for a variety of state-of-the-art commercial aircraft; then, a functional decomposition

will be performed on the architectures. Technologies to fulfill each function will then be scrutinized. Observations will be made about current PDS using the information from the literature search, and then a hypothesis will be formed about the deficiencies that will have to be overcome.

2.2.2.1 Architectures

The architecture of a PDS has a direct impact on system capacity, weight, and efficiency. The PDS architectures for several aircraft currently in service will be discussed. The topics covered will include the primary mode of power transmission, the voltage levels used in the aircraft, and the layout of components.

Airbus A319/A320/A321 The electrical system for the Airbus A319, A320, and A321 is shown in Figure 10. The system primarily consists of three-phase 115/200 V 400 Hz constant-frequency AC power, and for DC loads, the power is converted to 28 V DC [75]. The primary electrical power sources for the A319, A320, and A321 are two engine-driven generators, and the aircraft uses an axillary power unit (APU) for secondary power. The power from the generators and APU's is fed to two main AC buses, which distribute power to all AC loads. Fault protection is provided by the AC electronic switching system. In the case of an electrical emergency, the AC electric shutdown system (ESS) will cut-off all loads that are connected to the AC ESS SHED bus. Any load that is connected to the SHED bus is considered non-critical and will not be supplied if the aircraft is lacking electrical power.

Three transformer rectifier units (TRU's), a device that can convert AC power to DC power, can be found on this aircraft. Each TRU can supply up to 200 A of DC current. Two TRU's are connected to the main AC buses (one per bus), and the third TRU is connected to the emergency generator. The power converted using the TRU's is used to supply two main DC buses. The DC buses transmit power to all the DC loads on the aircraft. This class of Airbus aircraft also has two battery

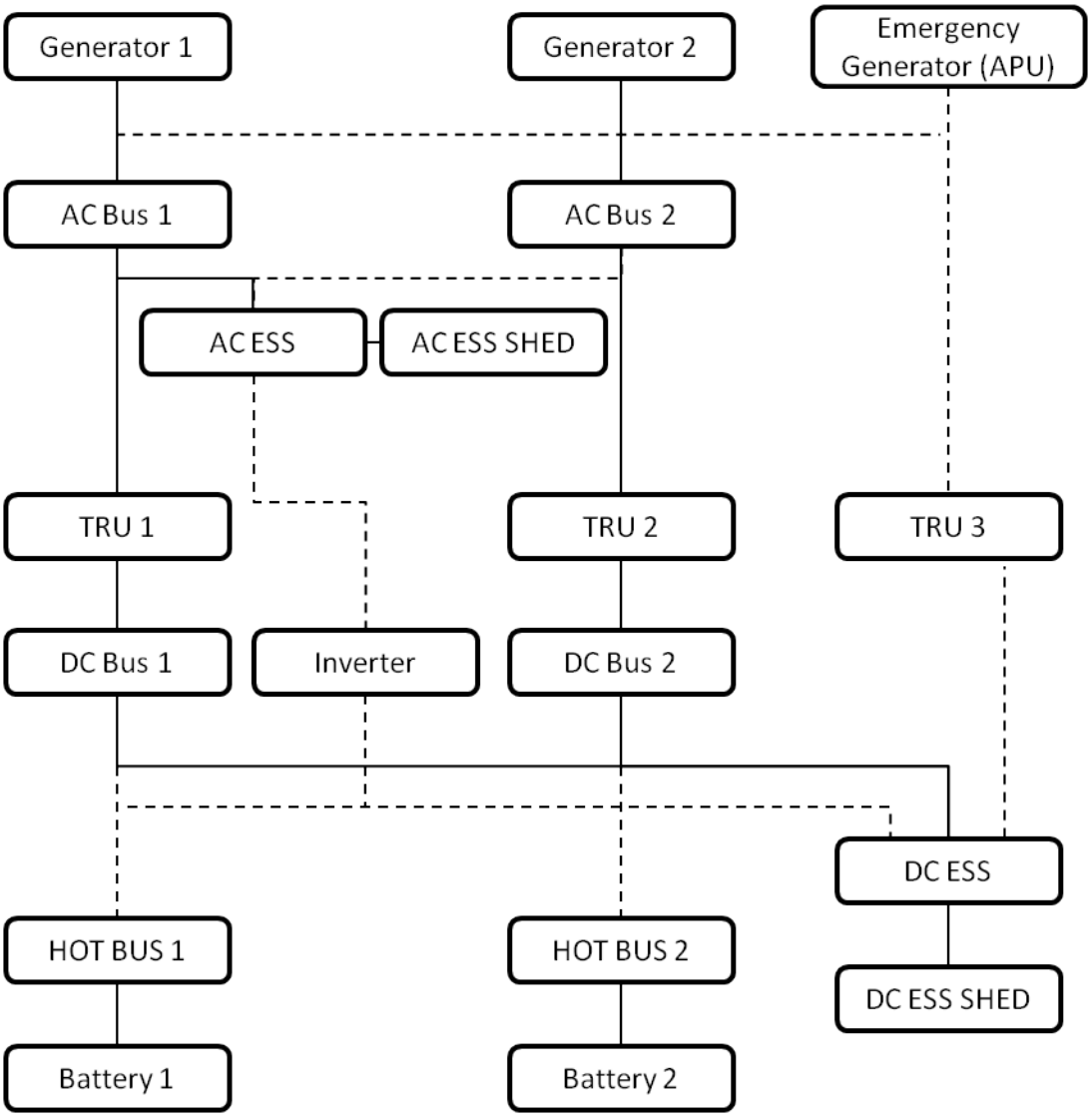

Figure 10: Power distribution system of the A319/A320/A321 [4]

units which are connected to the DC buses through another series of buses called the "hot" buses. The batteries are used primarily to start the APU; in addition, they can supply backup power to the aircraft in the event of an emergency. Lastly, an inverter, a device that can transform DC power to AC power, is used to convert the DC power from the batteries to single-phase 155 V 400 Hz AC power to supply critical AC loads [75].

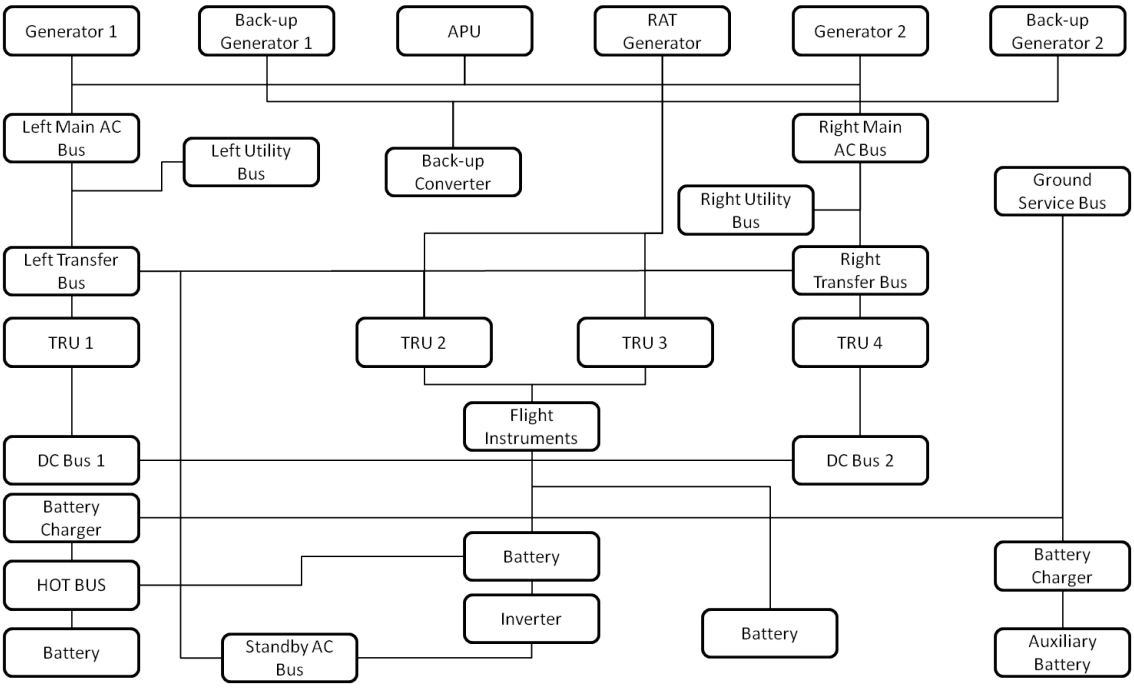

Figure 11: Power distribution system of the B777 [49]

Boeing 777 The Boeing 777 is a commercial aircraft that can transport between 300 and 550 passengers, making it a similar class vehicle to the N3-X. The architecture of the PDS is shown in Figure 11. Like the aircraft previously discussed, the primary power for the aircraft is three-phase AC, 115/200 V, 400 Hz, constant-frequency power which is created by two engine driven generators. The generators are capable of supplying 120 KVA each. Other sources of power are a ram air turbine (RAT) generator and an APU [6]. The aircraft has two main AC buses and two main DC buses. The architecture also contains transfer buses, utility buses, and a standby bus. The primary distribution occurs in AC, and then TRU's are used to convert the power to supply the DC loads. The B777 architecture consists of 4 batteries – two main batteries, an axillary battery, and a battery to power the flight instruments.

Airbus A380 The Airbus A380 is one of the first commercial aircraft to employ a "more electric" architecture. The A380 can carry up to 853 passengers and can supply up to 600 kVA in electrical loads. Its electrical system's architecture is shown

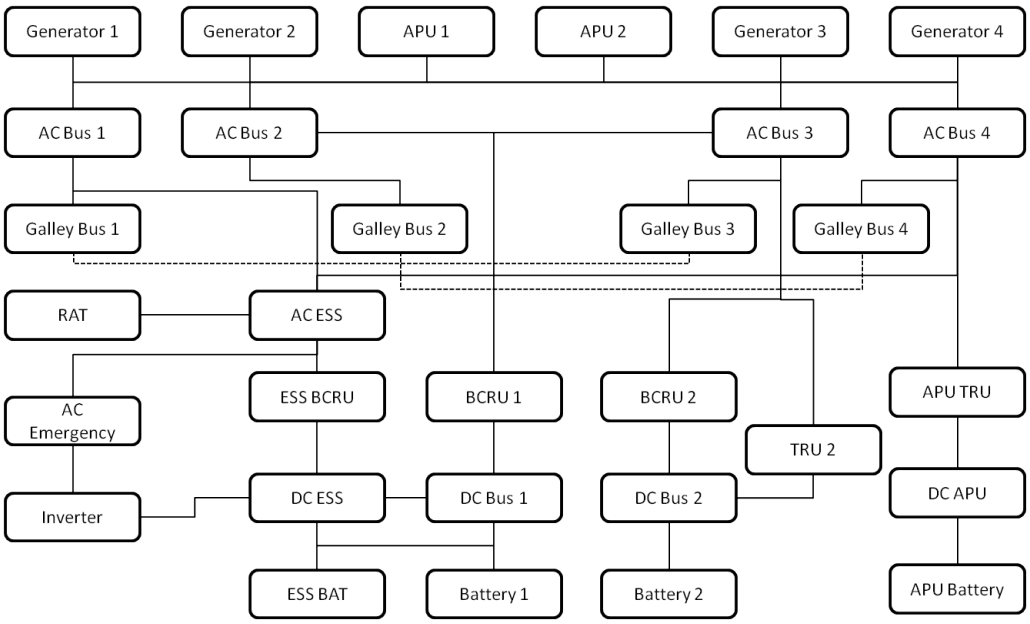

Figure 12: Power distribution system of the A380 [104]

in Figure 12. The aircraft's power is supplied by four 150 kVA variable frequency generators, two 120 kVA APU's, and a 70 KVA ram air turbine (RAT). The A380 is the first modern aircraft to use a variable frequency system. Variable frequency systems have the advantage of being light weight and cost efficient. The power is distributed to the loads via four main AC buses. Four buses are needed because the AC buses cannot be paralleled due to the variable frequency power. The power from the AC buses is transformed to DC using 3 battery charge regulator units (BCRU's) and a TRU. The DC system provides no-break power (uninterrupted power supply) for critical loads and includes three 50 Ah batteries for supplementary power. The system also has a static inverter to convert DC power back to AC for emergency situations [104].

Boeing 787 The PDS of the Boeing 787 Dreamliner is the most advanced to date. The voltages and loads on the B787 are much higher than any other commercial aircraft; the total power loads reach 1 MW [76]. One reason abundant electrical power is needed is that the B787 has an electrical environmental control system (ECS), a

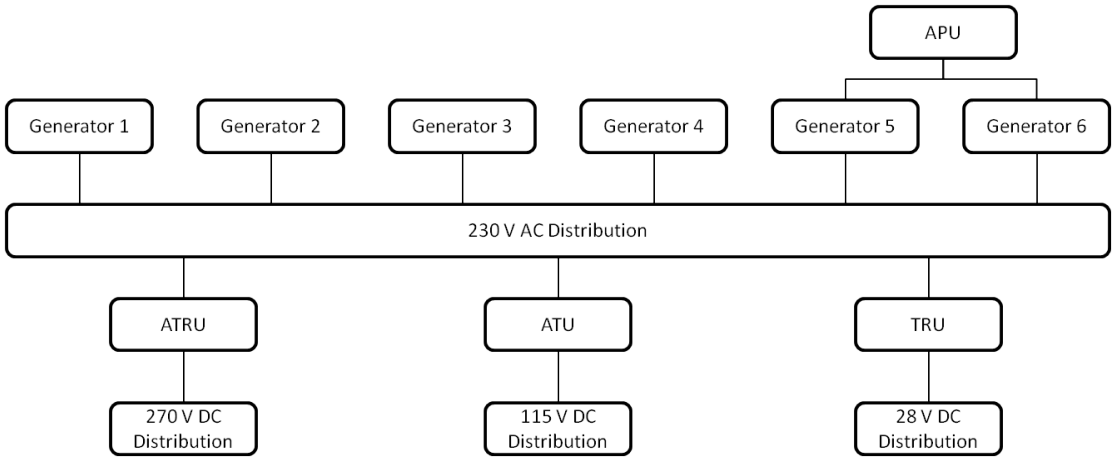

Figure 13: Power distribution system of the B787 [49]

"more electric" technology. Due to the novelty of this PDS, limited information is available on its architecture; however, a basic schematic is shown in Figure 13. The figure shows that the primary AC distribution is at 230 Volts which is double the voltage that has been used on commercial aircraft in the past. Another major difference between this architecture and previous aircraft is that it employs three separate DC buses with different voltages. One DC bus operates at the conventional 28 V DC. A second bus operates at 115 V DC, and a third operates at 270 V DC, almost 10 times the normal aircraft DC voltage. The high voltage DC buses are primarily used to power the ECS. Because of the high loads, the variable frequency generators produce 250 kVA each. The aircraft also has two APU's which can supply 225 kVA each [109]. Another difference between the B787 and other aircraft is that it uses more advanced power converters, namely autotransformer rectifier units (ATRU). An ATRU is a new technology, known as a multi-pulse converter, that is lighter and has less harmonic distortion than a traditional TRU [147]. The Dreamliner also makes use of lithium-ion batteries which provide significant weight savings.

2.2.2.2 Technologies

A functional decomposition of the architectures reveals four primary functions: energy sources, energy storage, energy conversion, and energy transfer. In this section, the components used to carry out each of these functions will be discussed.

Energy Sources On commercial aircraft today, the primary sources of electrical power are the engine-driven three-phase AC generators. Most commercial aircraft use integrated drive generators (IDG's) which contain several stages. The primary "raw" power is created by an exciter of a permanent magnet generator (PMG). The power output by the PMG is sensed by a controller which regulates the the flow of current. The power is then fed to an excitation stage where the voltage is controlled via the excitation stator. A set of diodes is then used to rectify the power. Finally, the power enters a "power" stage where the rotation of a rotor induces an AC voltage in a stator. This stage is protected and supplies the aircraft electrical loads [104].

The amount of power that the generator can provide is aircraft dependent and is not necessarily related to aircraft size. Smaller aircraft that use several "more electric" technologies will require more electrical power output from the generators. Table 2 provides the generator power output for several commercial aircraft. The table shows that the B787 generators have a much larger output than any other aircraft; this is mostly to supply the electrical ECS.

In recent years, new generator technologies have been developed. New aircraft such as the A380 and B787 have been moving toward using a variable frequency generator due to its light weight and low cost. The disadvantage is that components must be more robust to the changing frequencies. Because of these issues, research has begun on using switched reluctance (SR) machines. The SR machine is much easier to manufacture and is more robust than its counterparts. The main drawback of SR machines is that they need extensive use of power electronics; however, recent

Table 2: Commercial aircraft generator capacities

Aircraft(s)	Capacity (kVA)
A319/A320/A321 [4]	90
B777 [16]	120
A380 [104]	150
B787 [109]	250

advances in power electronics design could make SR machines a reality for an aircraft in the future.

Along with the primary engine-driven generators, auxiliary power units (APUs) are typically used [150]. An APU is a small gas turbine that runs independently of the main engines. The primary purpose of the APU is to provide power to start the main engines. The APU can also be used to provide power to electrical loads on the aircraft when the primary generators are not operating. Normally, the APU is capable of providing about the same amount of power as a single engine-driven generator. Along with the APU, aircraft also have a ground connection which can be used to start the engines if the APU is not functioning properly.

The final source of electrical power is the ram air turbine (RAT). The RAT is an air-driven turbine that is usually located at the ventral or nose section of the aircraft. It is powered by the passage of air over a turbine that drives a small generator. The RAT is used only when emergency power is required for critical components such as flight instruments.

Energy Storage The primary type of energy storage used in modern aircraft is a battery. The primary purposes of the batteries are to dampen transient loads in the DC system, provide start-up power when no other options are available, and provide power during emergency conditions. The batteries are charged by a specialized TRU; a reasonable charge is always maintained so that the batteries can properly fulfill their tasks.

Typically, aircraft use a nickel-cadmium (Ni-Cd) type battery; the exception is

Table 3: Commercial aircraft battery capacities

Aircraft(s)	Capacity (Ah)
A319/A320/A321 [4]	23
B777 [146]	47
A380 [104]	50
B787 [52]	65

the B787 which uses lithium-ion batteries. Lithium-ion batteries have a number of advantages: they are lighter, more efficient, and have a higher energy density than the Ni-Cd option. However, lithium-ion batteries have one major disadvantage; they are prone to fires. Because of the high energy potential in the batteries, even a small imperfection or short circuit in the battery can cause a cell to overheat and catch fire. A fire in a single cell can cause a chain reaction that engulfs the entire battery. This phenomena is more likely to occur in batteries with large cells because they store more energy and, consequently, operate at a higher temperature. The B787 was grounded due to several battery fires. The Dreamliner uses eight large cells that seem to be prone to catching fire. Test flights are now being conducted with a new casing around the battery that helps contain and stop fires. Even with the added insulation, if the safety problem is fixed, Boeing will still realize large weight and efficiency savings by using a lithium-ion battery versus a Ni-Cd battery.

Other devices for energy storage are capacitors and fuel cells. An ultracapacitor has the same function as a battery. It has less capacity than a battery, but can charge and discharge much quicker. Possible applications for capacitors are providing a means for regulating DC bus voltage and storage for regenerated energy on the DC bus. Fuel cells have also attracted a lot of attention by researchers in recent years. A fuel cell is a device that converts chemical energy to electricity using a chemical reaction with oxygen. Unlike a battery or capacitor, a fuel cell requires a constant source of fuel and oxygen to operate. In the short term, fuel cells are being researched as a power supply for systems such as actuation. In the future, scientists hope to use

fuel cells as a power source for propulsion.

Energy Conversion Power conversion is needed since both AC and DC power are used on modern aircraft. A transformer rectifier unit (TRU), the most widely used power converter, transforms AC power to DC power. Generally, all power on the aircraft is generated in AC; however, certain loads ,such as batteries, require DC power. The TRU's are needed for the transition. Typically, aircraft TRU's can convert a large amount of power; for example, the B767 TRU's can supply 120 amps continuously and 180 amps during peak conditions. Usually, the output of the TRU's is not regulated; however, if the DC system contains sensitive components, regulated TRU's may be required. One major problem associated with TRU's is heat, so often they have to be forced air cooled. The Dreamliner makes use of more efficient multi-pulse converters known as automatic transformer rectifier units (ATRU's). The ATRU's can also provide higher quality power than TRU's which is an important aspect in some "more electric" applications.

Another type of power converter found on most aircraft is a static inverter. The static inverters are high power, rapid switching devices that transform DC power to AC power [132], typically 28 V DC to 115 VAC. Static inverters are often used to transform DC power to supply critical loads after an AC power failure.

Energy Transmission The electrical buses are the primary devices for energy transmission. All of the commercial aircraft discussed have both AC and DC buses. The primary components in the buses are busbars and cables. Busbars are thick pieces of conductive material that act as a means for connecting supplies and loads. Busbars are also used to interconnect electrical systems in the aircraft to create redundancy in fixed frequency systems. Furthermore, they can be used to split essential and non-essential loads so that only essential loads receive power in emergency situations [116].

The cables are the other primary component in the electrical buses. The cables consist of a conductor and insulating materials. The two primary conductors used in aircraft power cables are copper and aluminum. They have about the same resistance; the primary difference is that aluminum is lighter, but requires a larger volume and is more expensive. The shielding for the cables must prevent electrical interference, protect the conductor from fluids, and thwart arcing. The cable design must ensure flexibility and a tolerance for vibration [148]. The most widely used type of cable is a coaxial cable which consists of a supply and return conductor, an inner shielding layer to protect the cable from electric and magnetic fields, and an outer jacket to protect the cable from containments such as fluid [148].

2.2.2.3 Observations from Literature Search and Hypothesis 1

In the literature search, several commercial aircraft PDS were studied. Although this study included aircraft of different classes and from different manufacturers, many of the technologies and basic architectures were the same. All of them primarily use AC distribution and use TRU's and batteries to supply DC loads. Most power in the architectures is supplied by engine driven generators and APU's. The "more electric" aircraft, the A380 and the B737, have led to the use of variable frequency power generation. The use of variable frequency power has led to light weight and more cost efficient systems. The AC power is mostly supplied at 115 V, except for the B787 which uses 230 V. The increased AC voltage is another upcoming trend in MEA, which also has led to the use of higher voltage DC power. Many "more electric" components such as an electric ECS have led to the need for higher amounts of DC power on the aircraft. The primary advantage of using a higher voltage is that it is more efficient because current losses are higher than voltage losses. A major drawback is that higher voltage can lead to the formation of corona which can lead to an electrical fire. In order to mitigate this risk, more electrical insulation will be

needed in the system.

The literature search has shown that even with movement toward MEA, the electrical loads on current aircraft fall well short of the N3-X. The capacities of the elements will have to be increased 40 times their current values to meet the turboelectric requirements. Creating this large capacity raises many concerns. The first obvious problem is weight. The physical size of the components will have to be much larger to accommodate the increased loads. Benchmarking is needed to determine how much improvement in weight will be needed for the components in the system. A second concern is efficiency. Even if the system is 99% efficient (which is a difficult goal), 400 KW of heat will be generated. This heat will have to be dissipated by a thermal management system which will further increase the weight of the system. The third issue is safety. The voltages and currents used on aircraft today have little risk of causing fires or shocks. In a turboelectric system much higher voltages and currents will be needed. The proper safety precautions for such a system need to be determined. The final issue is that the standards used today will not apply to a turboelectric system. New standards will have to be written and verified for a turboelectric PDS.

Based upon the literature search Hypothesis 1 is formed:

Hypothesis 1: The amount of redundancy required to meet the reliability requirement will result in an unacceptable system weight if current technologies are used.

To test the hypothesis a baseline system must be formed, and then a modeling and simulation environment needs to be created to evaluate the baseline architecture. The modeling and simulation environment must be able to evaluate the system capacity requirement, weight, and reliability. Based upon the results of the modeling and

simulation, hypothesis 1 can be evaluated.

2.2.2.4 The Baseline System

Based upon the observations from current PDS systems, the baseline architecture shown in Figure 14 was created. Although many systems today use AC distribution, new high power systems like that of the B787 use a high voltage DC transmission to increase efficiency. The baseline follows this trend and uses DC distribution. Since the generators and motor rely on AC power, rectifiers and inverters are needed to convert power from AC to DC and vice versa. Four buses were chosen based upon the number of buses used in the A380 architecture, and the amount of redundancy found in B777 architecture was included.

All of the components in the baseline architecture operate at room temperature. The generators and motors are room temperature synchronous machines. The rectifiers are simple diode bridges. The buses will consist of room temperature, copper conductor cables. The motors are grouped in a 4-4-4-4 configuration. Each group of four contains 2 motors on the left side of the aircraft and two motors on the right side of the aircraft. An actual PDS would also require the use of protection devices such as fault current limiters and circuit breakers. The methodology presented can be expanded to include these devices, but for demonstration purposes only the primary distribution components were included in the analysis performed in this thesis.

2.2.3 Evaluate the Baseline to Determine Gaps

Once a baseline architecture has been selected, it must be evaluated to determine gaps between its performance and the objectives and requirements. To accomplish this task, models were built to calculate system capacity, weight, and reliability. The models created are robust enough to evaluate a variety of architectures. The development of the models and the results is the focus of chapter 3.

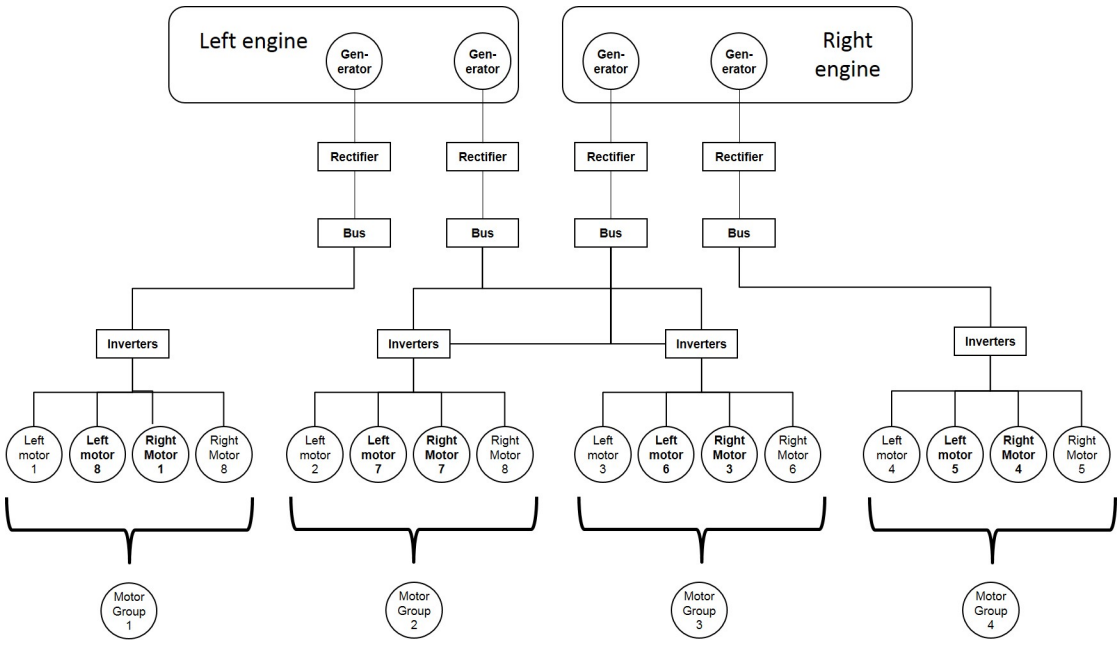

Figure 14: Baseline architecture

2.2.4 Identify Alternatives

If the baseline system does not meet all the system requirements, a designer must proceed to the next step in RAAPS which is to identify alternatives; this is the equivalent of the "generate feasible alternatives" step in the IPPD methodology. The gaps can be closed by either relaxing the system requirements or implementing new architectures and/or technologies. In most cases, including the test case used in this thesis, the first option is not viable. The requirements are set using aircraft size and safety standards which leads to Research Question 2:

Research Question 2: What power distribution architecture and technologies could potentially meet the requirements of a turboelectric system?

In Chapter 4, a literature survey is performed to identify new technologies and

architectures that may be able to bridge the gap between the baseline and the requirements.

2.2.5 Identify Candidate Architectures

When considering new technologies and architectures, a large number of possible system designs will be presented. To pick a final design, in-depth analysis will be needed of the designs. Due to the large number of possible combinations and the amount of time that is needed to evaluate each one, it is not possible to evaluate all possibilities. This leads to research question 3:

Research Question 3: How can new architecture and technology combinations be identified that meet the requirements and objectives of the turboelectric PDS?

A method of down-selecting from the design space is needed. A method will be presented in Chapter 5 to find system architecture candidates that meet the system requirements and objective.

2.2.6 Evaluate Candidate Architectures

After the alternatives are selected, they must be quantitatively evaluated in order to find systems that meet the requirements set in step one. System weight, capacity, and reliability are evaluated during the down-selection process; however, complex electrical systems must be checked for stability as well. Stability is primarily a function of the control used for the system but may require fine tuning of the component design. The candidate architectures will be built in the dynamic simulation environment so that trade-offs between the system requirements, objectifies, and stability can be performed. The dynamic simulation and stability analysis will be presented in Chapter 6.

2.2.7 Select a Design

Once the dynamic simulation and stability analysis for the selected architectures is complete, the final step of the methodology, "select a design", commences. In this step, a designer will have to make a choice based upon the trade-off studies shown the 'Evaluate Candidate Architectures' step. In most cases, a single solution will not exist. The designer must weigh the importance of the different requirements and objectives to select a design. This step of the methodology will be presented in Chapter 7.

CHAPTER III

BASELINE SYSTEM EVALUATION

In the previous chapter, the baseline system shown in Figure 15 was presented. The baseline must be evaluated in order to determine gaps between its performance and the system requirements and objectives. To accomplish this task, a computer modeling environment is built.

The first step in building the modeling environment to evaluate the system is to determine what calculations need to be performed; this is determined by the system requirements and objectives. The first requirement is ensuring that the system can meet the capacity requirements of 40 MW for normal operation and 20 MW during an engine-out scenario. At this point of the analysis, the configuration of the system has been set, but the components have not yet been sized. Therefore, the capacity requirement can be met by sizing all the components in the system based upon the system configuration and the load requirements.

Once the capacities of the components is calculated, the next step is to address the objective of minimizing system weight – meaning a model for calculating system weight is required. The system weight will be dependent on the weight of each component in the system. Component weights will be a function of the capacities calculated in the previous step and the component designs.

Lastly, the failure rate requirement must be addressed. In order to evaluate this requirement, a model for calculating system reliability will be needed. As previously discussed, the reliability of the system will be a function of the system configuration (redundancy) and component failure rates.

The integration of the models needed to evaluate the system requirements and

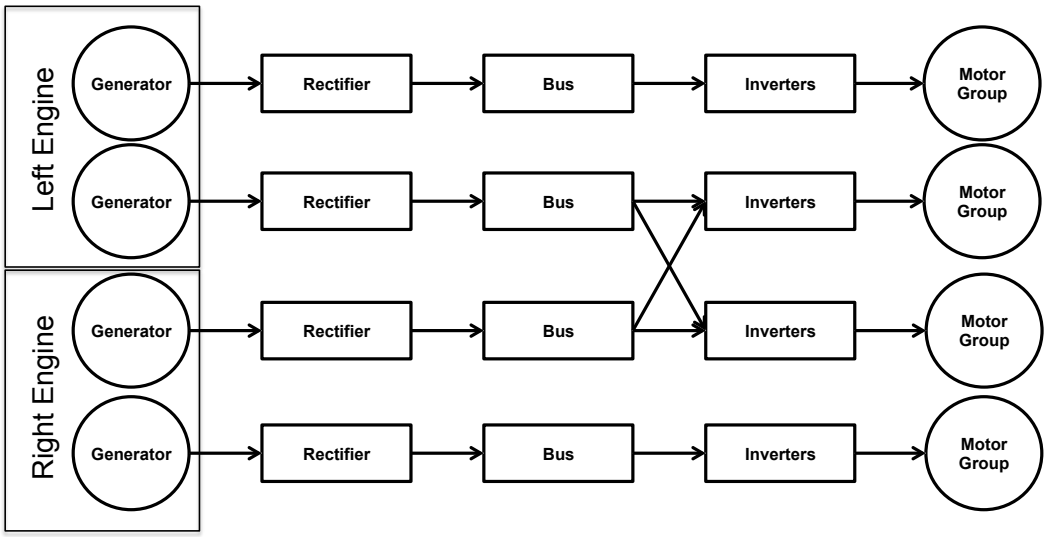

Figure 15: Simplified baseline architecture

objectives is demonstrated in Figure 16. The evaluation begins with the capacity requirement, which will be described in Section 3.1. After the component capacities are calculated, the component capacities flow to the weight calculation. The component weights are calculated using a variety of models, which are described in Section 3.2. Lastly, the failure rate requirement is evaluated using the technique that is described in Section 3.3. Once the modeling environment is complete, the baseline is evaluated and the results are summarized in Section 3.4.

3.1 Capacity Requirement

As shown in Figure 16, the capacity requirement evaluation is the first step of the baseline evaluation. The system capacity requirement can be treated as an equality constraint on the system design problem. In order to generate enough thrust for takeoff, 40 MW of power must be delivered from the generators to the motors. During an engine-out scenario, 20 MW of power needs to be delivered to the motors to meet FAA regulations. The architecture must be sized such that the nominal 40 MW of loads can be met during normal operation and 20 MW of power is delivered to the motors during an engine-out scenario. Solving this problem for a single architecture is

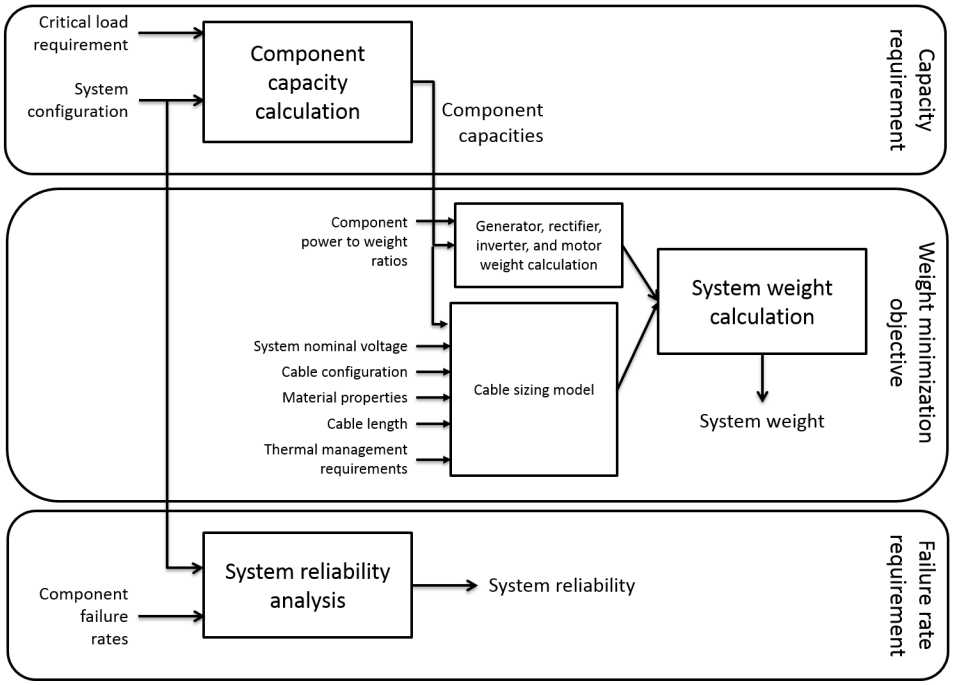

Figure 16: Modeling Environment Overview

trivial; however, in the case that a designer needs to evaluate multiple architectures, a robust method for applying the capacity requirement is needed.

To achieve this goal, a method for finding paths between the generators and the motors in a failure scenario is needed. This will determine the required capacity of the components dictated by the engine-out scenario. Finding paths between a source and sink is commonly addressed in the design and analysis of communication and computer networks. Many of the techniques used in the evaluation of networks have a foundation in graph theory. Once the components are sized for the engine-out scenario, the values are updated to ensure that the 40 MW of power for normal operation can be met.

3.1.1 Graph Theory Application

In order to use graph theory methods, the PDS must be viewed as a graph comprised of nodes and edges. The components in the system will be treated as nodes and the connections betweens the components are treated as edges. Furthermore, the graph

Table 4: Baseline adjacency matrix

	G1	G2	G3	G4	R1	R2	R3	R4	B1	B2	B3	B4	I1	I2	I3	I4	M1	M2	M3	M4
G1	0	0	0	0	1	0	0	0	0	0	0	0	0	0	0	0	0	0	0	0
G2	0	0	0	0	0	1	0	0	0	0	0	0	0	0	0	0	0	0	0	0
G3	0	0	0	0	0	0	1	0	0	0	0	0	0	0	0	0	0	0	0	0
G4	0	0	0	0	0	0	0	1	0	0	0	0	0	0	0	0	0	0	0	0
R1	0	0	0	0	0	0	0	0	1	0	0	0	0	0	0	0	0	0	0	0
R2	0	0	0	0	0	0	0	0	0	1	0	0	0	0	0	0	0	0	0	0
R3	0	0	0	0	0	0	0	0	0	0	1	0	0	0	0	0	0	0	0	0
R4	0	0	0	0	0	0	0	0	0	0	0	1	0	0	0	0	0	0	0	0
B1	0	0	0	0	0	0	0	0	0	0	0	0	1	0	0	0	0	0	0	0
B2	0	0	0	0	0	0	0	0	0	0	0	0	0	1	1	0	0	0	0	0
B3	0	0	0	0	0	0	0	0	0	0	0	0	0	1	1	0	0	0	0	0
B4	0	0	0	0	0	0	0	0	0	0	0	0	0	0	0	1	0	0	0	0
I1	0	0	0	0	0	0	0	0	0	0	0	0	0	0	0	0	1	0	0	0
I2	0	0	0	0	0	0	0	0	0	0	0	0	0	0	0	0	0	1	0	0
I3	0	0	0	0	0	0	0	0	0	0	0	0	0	0	0	0	0	0	1	0
I4	0	0	0	0	0	0	0	0	0	0	0	0	0	0	0	0	0	0	0	1
M1	0	0	0	0	0	0	0	0	0	0	0	0	0	0	0	0	0	0	0	0
M2	0	0	0	0	0	0	0	0	0	0	0	0	0	0	0	0	0	0	0	0
M3	0	0	0	0	0	0	0	0	0	0	0	0	0	0	0	0	0	0	0	0
M4	0	0	0	0	0	0	0	0	0	0	0	0	0	0	0	0	0	0	0	0

will be directed showing the flow of power. The generators are treated as source nodes and the motors are the sink nodes. A path in the graph will denote a set of nodes that connect a source with a sink. In the case of the PDS system, a path will consist of a generator, rectifier, bus, inverter, and motor. To evaluate the system, it must be represented in a mathematical form which can be accomplished by using an adjacency matrix.

3.1.2 Adjacency Matrix

An adjacency matrix represents a graph of n components using a nxn matrix. Each row and each column of the adjacency matrix represents a component in the system. A zero in a given position in the matrix means that there is no connection between the component represented by the row to the component represented by the column. A 1 represents that there is a connection that allows power to flow from the component represented by the row to the component represented by the column. As an example, the adjacency matrix for the baseline system is shown in Table 4.

Using the adjacency matrix, any system configuration can be represented in matrix

form. The next step is to use the adjacency matrix to evaluate the ability of the system to deliver power from the generators to the motors in the event of an engine failure.

3.1.3 Calculating Component Capacities

The first step in calculating the required capacity of the components in the system is determining which motors will have power in the event of either a right or left engine failure. One method to accomplish this task is finding path sets. A path set is a set of nodes and edges that link a source with a sink. A variety of algorithms for finding path sets in a network exist. The most widely used algorithms are Floyd's Algorithm and Dijkstra's Algorithm with path reconstruction; however, traditionally these algorithms find all paths in the system (does not differentiate between source, sink, and other nodes) or can only find paths from a single source. To find the capacities of the components, not every path in the system needs to be known. Also, multiple sources will be in use making the algorithms difficult to use.

Another method that can be used to determine which motors will have power during a gas turbine failure makes use of the adjacency matrix. Adjacency matrices have an interesting property; if an adjacency matrix is multiplied by itself, the result will show connections in the graph that are two steps away. In other words, for the baseline architecture, the multiplication will show the number of generator to bus connections, rectifier to inverter connections, and bus to motor group connections. Also, if there are multiple paths between a generator and a bus, the multiplication will reveal the number paths between those two components.

If the matrix with the two-step connections is multiplied by the adjacency matrix, the three step connections will be revealed; that is, the connections between the generators and inverters and the rectifiers and motor groups. The multiplication process can be repeated a third time to reveal the four step connections. This will show the generator to motor connections. The resulting matrix for the baseline system

Table 5: Baseline four-step connections

	$G1$	$G2$	$G3$	$G4$	$R1$	$R2$	$R3$	$R4$	$B1$	$B2$	$B3$	$B4$	$I1$	$I2$	$I3$	$I4$	$M1$	$M2$	$M3$	$M4$
$G1$	0	0	0	0	0	0	0	0	0	0	0	0	0	0	0	0	1	0	0	0
$G2$	0	0	0	0	0	0	0	0	0	0	0	0	0	0	0	0	0	1	1	0
$G3$	0	0	0	0	0	0	0	0	0	0	0	0	0	0	0	0	0	1	1	0
$G4$	0	0	0	0	0	0	0	0	0	0	0	0	0	0	0	0	0	0	0	1
$R1$	0	0	0	0	0	0	0	0	0	0	0	0	0	0	0	0	0	0	0	0
$R2$	0	0	0	0	0	0	0	0	0	0	0	0	0	0	0	0	0	0	0	0
$R3$	0	0	0	0	0	0	0	0	0	0	0	0	0	0	0	0	0	0	0	0
$R4$	0	0	0	0	0	0	0	0	0	0	0	0	0	0	0	0	0	0	0	0
$B1$	0	0	0	0	0	0	0	0	0	0	0	0	0	0	0	0	0	0	0	0
$B2$	0	0	0	0	0	0	0	0	0	0	0	0	0	0	0	0	0	0	0	0
$B3$	0	0	0	0	0	0	0	0	0	0	0	0	0	0	0	0	0	0	0	0
$B4$	0	0	0	0	0	0	0	0	0	0	0	0	0	0	0	0	0	0	0	0
$I1$	0	0	0	0	0	0	0	0	0	0	0	0	0	0	0	0	0	0	0	0
$I2$	0	0	0	0	0	0	0	0	0	0	0	0	0	0	0	0	0	0	0	0
$I3$	0	0	0	0	0	0	0	0	0	0	0	0	0	0	0	0	0	0	0	0
$I4$	0	0	0	0	0	0	0	0	0	0	0	0	0	0	0	0	0	0	0	0
$M1$	0	0	0	0	0	0	0	0	0	0	0	0	0	0	0	0	0	0	0	0
$M2$	0	0	0	0	0	0	0	0	0	0	0	0	0	0	0	0	0	0	0	0
$M3$	0	0	0	0	0	0	0	0	0	0	0	0	0	0	0	0	0	0	0	0
$M4$	0	0	0	0	0	0	0	0	0	0	0	0	0	0	0	0	0	0	0	0

is shown in Table 5.

Using the four-step matrix, it can be determined which motors will have power during an engine-out scenario. The analysis will begin by assuming that the left gas turbine has failed - meaning that generators 1 and 2 will no longer be able to provide power. By examining the third and fourth rows of the matrix, the motors that will have power under this scenario are shown. In the baseline case, motor group 1 will no longer have power. Enough power for takeoff must be delivered to motor groups 2, 3, and 4; therefore, each group must be sized for at least 33% capacity, which is 33% of required takeoff power.

33% is the minimum requirement. A designer may choose to increase the capacity of the motors so that the aircraft can function with less than the number of motors that have paths from the generator during an engine failure (sizing the motors in this fashion would increase the reliability of the system, but would also increase weight). For this preliminary analysis, it will be assumed that all motors that are available during a gas turbine failure must be functioning and the minimum requirement will be used.

Table 6: Room temperature component efficiencies

Component	Efficiency
Generator	95%
Rectifier	97 %
Bus	98 %
Inverter	97 %

Once the required capacity for the motors is known, the algorithm works backwards through the system to determine the required capacity for the rest of the components. In order to do this, the algorithm makes use of the adjacency matrix again. The capacity of an inverter must be equal to the cumulative capacity of the motor groups that it feeds. The algorithm examines the row of the adjacency matrix of the inverter capacity being calculated. From the matrix, it can be determined which motor groups are being fed by that inverter. If there is a one in the column of a motor, then the capacity of that motor is added to the capacity requirement for the inverter. For example, the adjacency matrix shows that inverter 1 feeds motor group 1. Since the required capacity of motor group 1 in a left gas turbine out scenario is 0, then the capacity of inverter 1 is also 0. If the row for inverter 4 is examined, it is shown that inverter 4 feeds motor group four. Since motor group four needs 33% power, then inverter 4 will also need 33% power plus any additional power needed to account for inefficiencies. (The efficiency of each component is shown in Table 6) Therefore, the required capacity of inverter 4 is 33% power divided by the efficiency of the inverter. which equals 34% power. In this configuration, each inverter only feeds one motor group, so all of the inverters will be sized for 34% of takeoff power.

Once the inverter capacities are known, the buses are sized. The same procedure is used as in the case of the inverters. The row of each bus in the adjacency matrix is examined to determine which inverters are being fed by a given bus. The capacity of the bus will be equal to the capacity(ies) of the inverter(s) that it feeds plus any additional power required due to inefficiencies. For example, the adjacency matrix

Table 7: Component capacities required by the engine-out scenario

$G1$	$G2$	$G3$	$G4$	$R1$	$R2$	$R3$	$R4$	$B1$	$B2$	$B3$	$B4$	$I1$	$I2$	$I3$	$I4$	$M1$	$M2$	$M3$	$M4$
33%	66%	66%	33%	33%	66%	66%	33%	33%	66%	66%	33%	33%	33%	33%	33%	33%	33%	33%	33%

shows that buses 2 and 3 each feed two inverters during an engine-out scenario. Therefore, both buses need to be sized to feed two inverters which means that they will be sized for 66% of takeoff power plus any additional power needed to account for inefficiencies. Buses 1 and 4 only feed one inverter in an engine-out scenario, so they are both sized for 33% power.

The process is repeated for the rectifiers and generators. Once all of the components have been sized for a left gas turbine out scenario, it is repeated for a right engine-out scenario. After the component capacities for both scenarios are found, the required capacity for each component will be the maximum of the two scenarios. Using the algorithm described, the required capacities for the baseline system were calculated and are shown in Table 7.

The values shown in Table 7 show the required component capacities relative to the 20 MW engine-out scenario; however, this analysis does not ensure that the 40 MW of power for normal operation is met. For any architecture, there will be a set of paths that are considered the "primary" paths. These are the paths that are used during normal operation of the system – meaning that a failure has not occurred. For the baseline architecture there are four primary paths: generator 1 to motor group 1, generator 2 to motor group 2, generator 3 to motor group 3, and generator 4 to motor group 4. In order to meet the 40 MW power requirement, each path must have a capacity of 10 MW; that is, the required capacity for each path is 50% of the 20 MW engine-out takeoff requirement. Therefore, each component in the primary paths must be sized for at least approximately 50% capacity. (The capacities are updated to account for losses in the system.)

Based upon the 40 MW requirement, the updated capacity values for each component in the baseline system are shown in Table 8. The results of the capacity analysis

Table 8: Updated component capacities

$G1$	$G2$	$G3$	$G4$	$R1$	$R2$	$R3$	$R4$	$B1$	$B2$	$B3$	$B4$	$I1$	$I2$	$I3$	$I4$	$M1$	$M2$	$M3$	$M4$
56.8%	69.3%	69.3%	56.8%	54.1%	68%	68%	54.1%	52.5%	67.3%	67.3%	52.5%	51.5%	51.5%	51.5%	51.5%	50%	50%	50%	50%

will be used in the next step for the evaluation of the baseline – estimating system weight.

3.2 Weight Calculation

Once the required capacity for each component is known, the weight calculation can begin. The level of fidelity used for the sizing can vary from detailed modeling to estimates solely based on component capacity. When detailed modeling is used, components are broken down into their simplest sub-components, and each sub-component is sized in order to find the size of the component. The detailed sizing algorithms will require more information than just capacity; material properties, operating condition, and other information is needed to calculate an accurate weight. To demonstrate this type of sizing, a detailed cable sizing model was created.

While detailed sizing models are desirable, they can be time consuming and the information required to generate the model may not be available early in the design phase. The simplest form of sizing components is using a power to weight ratio (also referred to as specific power). The ratios can be found by examining data on components and often manufacturers will provide this value for their products. Also, power to weight ratios can be used when low TRL level technologies are being included in the conceptual design of a system since researchers often estimate the expected power to weight ratios of new electric technologies.

Power to weight ratios will be used to size the remaining components in the architecture. The literature search performed to find these values and a list of the expected power densities for each component will be discussed.

3.2.1 Cable Sizing

The sizing of the cables is performed by determining the cable's structure and then using a mixture of physics based models and information from literature. The sizing estimation is completed by calculating the thickness and weight of each layer of the cable. The structure selected for the cable is based upon the most common types of cable used in current aircraft. The purpose of each layer of the cable will be discussed, along with the approach taken for sizing.

3.2.1.1 Cable Sizing Model

Most room temperature cables have a cylindrical core which acts as a conductor. The conductor material is an important design choice. The material must have a sufficient current density to transmit and accommodate the power load while maintaining a reasonable weight and cost. The most popular choices for this type of cable are copper and aluminum. Copper is the most widely used because of its high current density, good conductivity, and relatively low cost.

In addition to the conductor, protective layers must be added to the structure to complete the cable including: a dielectric layer, a magnetic shield, and a cooling sleeve [15]. The purpose of the dielectric layer is to resist the potential between the wire and the magnetic shield. Its thickness is selected based on the system nominal voltage. Many standards for the selection of the dielectric thickness are created by organizations such as the International Electrotechnical Commission (IEC) and the Association of Edison Illuminating Companies (AEIC). The AEIC standards are the most widely used in North America and were used to determine dielectric thickness in this study [7]. XLPE is selected as the dielectric insulation for the cable do to its long term reliability [23]. The purpose of the magnetic shield is to protect the wire from the magnetic field induced by the current flow, so the thickness of this layer is dependent on the maximum current flow through the wire. The magnetic shield is

Table 9: Cable model variable list

Variable name	Variable description
I	Current through wire (A)
ρ	Conductor resistivity (Ohm m)
L	Cable length (m)
V_{wire}	Cable voltage (V)
P_{load}	Power to be delivered to the load (W)
A	Cable cross-sectional area (m^2)
V_{nom}	System nominal voltage (V)
d	Cable diameter (m)

often made out of aluminum. For this cable, a cooling sleeve will be necessary in order to maintain a safe temperature for the wire. The maximum allowable temperature is an important constraint on the design process so that excess heat does not damage the cable or any surrounding electronics, such as the power converters. Also, in situations where the cable may be in close proximity to fuel lines, the designer must ensure that the heat expelled by the cable will not ignite the fuel.

The weight calculation begins with the required capacity for each bus which is defined as P_{dem}. The value is the sum of the power that needs to be delivered to connected converters and the losses along the cable.

$$P_{dem} = P_{load} + P_{loss} \tag{4}$$

The amount of power lost per meter in transmission can be calculated as

$$P_{loss} = I \times V_{wire} = \frac{\rho \times L \times P_{load}^2}{A \times V_{nom}^2} = \frac{4 \times \rho \times I^2 \times L}{\pi \times d^2} \tag{5}$$

The variables used in the equation are listed in Table 9.

In order to solve Equation 5, either the system nominal voltage or the current must be known. System nominal voltage can be set through the use of an actively controlled power converter; so, system nominal voltage will be a design variable in this problem. In a commercial aircraft today, the nominal voltage of the network is usually set between 20 and 270 Volts.

In the new architecture, the power transmitted by the distribution system is almost 40 MW. According to the capacity requirement, a bus may need to supply 66% of the total load for the baseline system - meaning a bus may need to supply 26.4 MW of power. In order to reach that power demand with a 28 VDC bus, the current in the wires would have to reach 942.9 kA. Since the current is so high, other voltage levels will need to be explored.

One method of sizing the wire is to set a maximum allowable power loss or heat rejection ($\dot{q_{max}}$). For an aircraft, this value can be taken as 0.2% of the maximum power load [37]. In this case, the diameter of the wire would be

$$d = 2 \times I_{max} \sqrt{\frac{\rho}{\pi \times \dot{q_{max}}}} \tag{6}$$

Once the cable conductor is sized, the protection layers need to be added. The first layer to be added is the dielectric shield. The thickness of the layer is calculated as the dielectric constant multiplied by the cable voltage. The next step is to size the magnetic shield. The magnetic shield thickness is the product of the magnetic shield constant and current.

The final layer to be sized is the cooling sleeve. Even if only 0.2% of the power is rejected as heat, a significant heat load will be created and will cause a significant temperature rise in the cable. If the temperature rise is too large, the cable and surrounding power electronics could be damaged. Most electronic components start to fail at temperatures of 125 degrees Celsius. The purpose of the cooling sleeve is to guarantee that the cable temperature will not exceed the 125 degree Celsius limit.

The first step in sizing the cooling sleeve is to determine the amount of mass flow of coolant that will be required using equation 7.

$$\dot{m} = \frac{\dot{q}_{max} L}{c_p \Delta T} \tag{7}$$

Where $\dot{q}_{max}$ is the maximum heat output of the cable,

$$\dot{q}_{max} = \frac{8 * \rho * P_{dem}^2}{\pi * d^2 * V_{nom}^2} \tag{8}$$

c_p is the specific heat of the coolant and ΔT is the maximum allowable temperature rise across the cable.

The next step is to derive the cross sectional area of the cooling sleeve using equation 9.

$$A_{coolant} = \frac{\dot{m}}{\rho_{coolant} v_{max}} \tag{9}$$

$\rho_{coolant}$ is the density of the cooling fluid and v_{max} is the maximum allowable velocity of the coolant in the cooling sleeve.

If the maximum allowable velocity is not known, the thickness of the cooling sleeve can be determined using a scaling parameter:

$$t_{cooling} = d * q_{reject} * .000465 \tag{10}$$

Where q_{reject} is the cable heat rejection per unit length. If this approach is used, the cross-sectional area of the cooling sleeve can be calculated as:

$$A_{coolant} = \frac{\pi}{4}[(d+2*t_{dielectric}+2*t_{magnetic}+2*t_{cooling})^2-(d+2*t_{dielectric}+2*t_{magnetic})^2] \tag{11}$$

Once the cross-sectional area and thickness of the cooling sleeve is known, it is important to calculate the amount of pumping power that will be needed to move the fluid through the sleeve. A trade-off between the power and thickness of the sleeve can be examined. Increasing the size of the cooling sleeve will reduce the amount of pumping power needed, but will construe to a higher cable weight. If the cooling sleeve thickness is reduced, more pumping power will be required which will increase the size of the pump and the overall power consumption of the system.

The first step in calculating pumping power is to determine the velocity of the coolant in the sleeve using equation 12.

$$V = \frac{\dot{m}}{\rho_{coolant} A_{coolant}} \tag{12}$$

The next step is to determine the amount of flow resistance that has to be overcome which requires the calculation of a friction factor, f. The first step in calculating friction factor is to calculate Reynolds number.

$$Re = \frac{\rho_{coolant} * V * D_h}{\varphi_{coolant}} \tag{13}$$

D_h is the hydraulic diameter of a concentric pipe and $\varphi_{coolant}$ is the viscosity of the coolant.

$$D_h = 2 * (r_o - r_i) \tag{14}$$

If the flow is laminar (Re<2000), the friction factor is 64/Re. If the flow is turbulent (Re> 4000), the Colebrook equation is used to calculate the friction factor.

$$1/\sqrt{f} = -2log_{10}(\frac{\varepsilon}{3.7D_h} + \frac{2.51}{Re\sqrt{f}}) \tag{15}$$

Where ε is the roughness of the pipe. The Colebrook equation must be solved iteratively.

Once the friction factor is known, the pressure loss in the pipe can be calculated as:

$$\Delta p = f * \frac{(\frac{L}{D})\rho_{coolant}}{2} * V^2 \tag{16}$$

Finally, the pumping power required is calculated as:

$$P_{pumping} = \frac{\Delta p * \frac{\dot{m}}{\rho_{coolant}}}{\eta_{pump}} \tag{17}$$

η_{pump} is the efficiency of the pump.

After all the layers of the cable have been sized, an overall cable weight and diameter can be calculated. The diameter will simply be the addition of the wire diameter, twice the dielectric thickness, twice the magnetic shield thickness, and twice the cooling sleeve thickness. The weight of the cable will be the density of the material of a cable layer multiplied by the layer cross-sectional area and the cable length.

3.2.1.2 Cable Sizing Results

The design variables used to size the cable are power demand and system nominal voltage. Power demand is varied from 1 MW to 40 MW, and system nominal voltage is varied between 4000 volts and 10,000 volts. The parameters used for the model are shown in Table 10. The responses that are examined are cable diameter and cable weight. The results of the sizing tool for the cable are shown in Figures 17 and 18. The coloring of the graph shows how weight and diameter changes with power and voltage. The red areas of the graph should be avoided, and the blue areas are the most desirable.

Figure 17 shows that cable diameter increases with power rating since a larger conductor is needed. The diameter decreases as voltage increases since less current needs to be carried; however, the relationship is not linear since the amount of insulation needed increases with voltage. The same trends are observed with the cable weight (shown in Figure 18).

The weight and diameter of the copper cables are difficult to compare to what is currently being used on aircraft today due to the high power load; however, the cable sizing results match well to power transmission cables that are manufactured for other applications with a similar power load [144].

Table 10: Cable model parameters

Parameter	**Value**
Cable length	9.1 m
Conductor resistivity	1.68 * 10^{-8} Ohm m for copper
Conductor density	8,933 kg/m^3 for copper
Dielectric constant	5*10^{-8} m/V
Dielectric density	940 kg/m^3 for XLPE
Magnetic shield constant	4.65*10^{-7} m/A
Magnetic shield density	2,700 kg/m^3 for aluminum
Specific heat of coolant	4,180 J/kgK for water
Coolant density	1,000 kg/m^3 for water
Coolant viscosity	1.002*10^{-3} Pa.s for water
Pump efficiency	90%
Allowable temperature rise	50 K

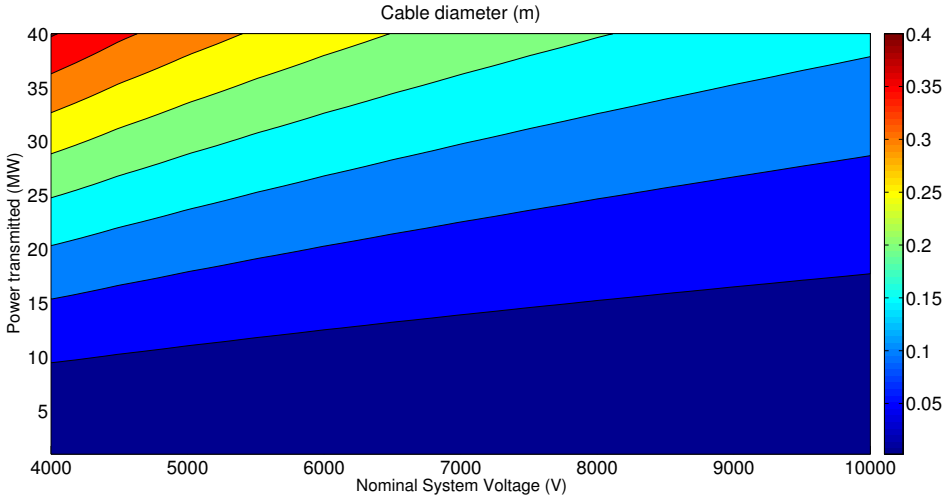

Figure 17: Room temperature cable diameter (m)

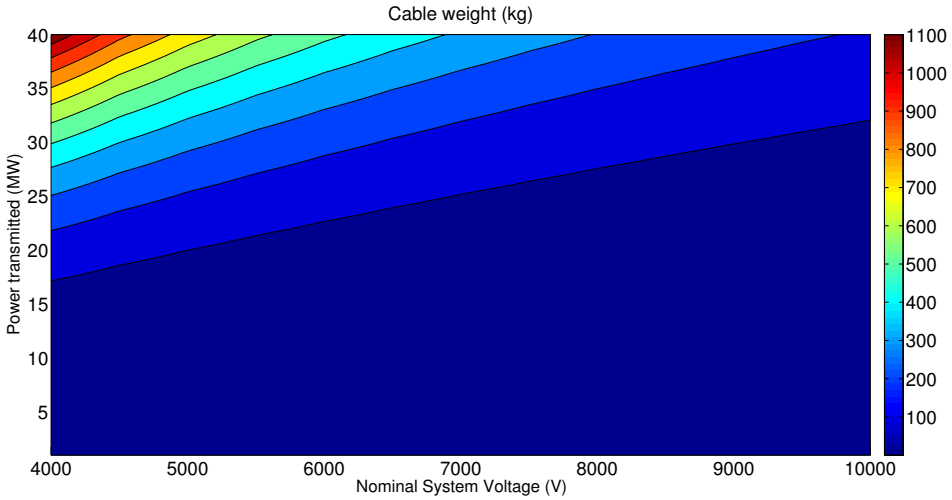

Figure 18: Room temperature cable weight (kg)

Another design consideration is the pumping power that will be required to circulate the coolant which is dependent on the allowable temperature rise, the system voltage, and the length of the cable. In order to not exceed temperatures that could potentially damage the cable or surrounding power electronics, the allowable temperature rise of the cable is set to 50 degrees Celsius. Figure 19 shows the required pumping power versus the length of the cable. The pumping power increases as voltage increases because the cable diameter decreases with voltage. Since the overall cable diameter is decreasing, the cooling sleeve cross-sectional area also decreases; therefore, a higher flow rate of coolant is needed since the flow area is being decreased. The pumping power increases as length increases because of additional friction and the allowable temperature rise per meter of cable decreases.

Table 11: Bus weights (kg)

Component	Weight (kg)	Diameter (mm)	Pumping Power (W)
Bus 1	24.72	2.68	960
Bus 2	49.85	3.04	367
Bus 3	49.85	3.04	367
Bus 4	24.72	2.68	960

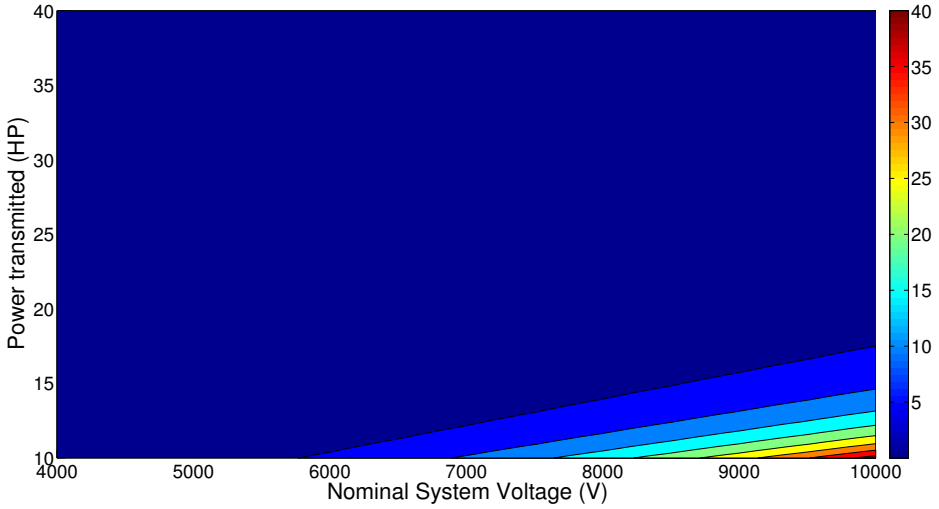

Figure 19: Pumping power required for coolant (kW)

In order to get a cable weight for the baseline architecture, a system nominal voltage must be selected. For this case study, a 4,000 V system voltage is assumed. Based upon this assumption, the bus weights, diameters, and required pumping power for the baseline architecture are shown in Table 11.

3.2.2 Converter and Machine Sizing

Exact weights for the converters and machines are hard to estimate at this point in the design phase since detailed analysis on the design of each component would be required. Detailed component design information is not available at this point in the design process, so power to weight ratios are used to estimate the weight of the components. While they will not provide an exact weight, they will provide weight estimates for the components in the correct order of magnitude.

Table 12: Component power to weight ratios

Component Type	Power to Weight Ratio (kW/kg)
Rectifier	10
Inverter	10
Generators	8
Motors	3

To determine the proper power to weight ratios for each component, the state of the art in high power, low weight technologies was examined. A variety of designs for each component has led to varied estimates for the power to weight ratio. The components needed are not widely used on aircraft today, so research for electric naval propulsion and electric cars was used.

The power to weight ratios of power converters have a wide range. Novel aircraft power converters only have a power to weight ratio of about 1.3 kW/kg [63]; however, manufacturers of inverters for electric cars claim that they have reached a power to weight ratio of 10 kW/kg [126]. This was the value used for this analysis with the expectation that as electric propulsion moves forward, 10 kW/kg could be met for aircraft power converters.

The power to weight ratio of gas turbines was used to estimate the value for the generators. According to the research of Luongo et al. [89], this is a reasonable assumption for an electric aircraft. Gas turbines have a power to weight ratio of around 3-8 kW/kg. [89] [119] [71] The high end of the range is selected for the study assuming that increasing this value is primary focus of generator development in upcoming years.

Like the other components, the power-to-weight ratio of the motors is highly variable based upon motor design and power rating. Values can range from 1-9 kW/kg. [145] [55] [138] [126] However, high power motors have been capped at 3 kW/kg, so this is the value that will be used in the baseline study. A summary of all power to weight ratios for each component is shown in Table 12.

Table 13: Baseline component weights

Component	Weight (lbs)
Generator 1	1490
Generator 2	1733
Generator 3	1733
Generator 4	1490
Rectifier 1	1082
Rectifier 2	1360
Rectifier 3	1360
Rectifier 4	1082
Inverter 1	1030
Inverter 2	1030
Inverter 3	1030
Inverter 4	1030
Motor Group 1	3333
Motor Group 2	3333
Motor Group 3	3333
Motor Group 4	3333

Given these power-to-weight ratios and the required capacity of the baseline system components, the component weights are shown in Table 13.

Given the component weights, the overall system weight would be 28,971 lbs. Based upon the outcome of baseline sizing study, Hypothesis 1 is partially confirmed. Since the weight and efficiency of current PDSs need to be vastly improved, new architectures and technologies must be explored.

3.3 Failure Rate Requirement

After the capacity requirement has been met and the weight of the system is known, the next step is to calculate the reliability of the system. As described in the introduction, reliability is the probability of a device performing its purpose adequately for the period of time intended under the operating conditions encountered. In this thesis, the system is considered to be adequately performing if enough power is being supplied to the motors for takeoff. The operating time should be equivalent to the time of an aircraft which can approach 90,000 flight hours [111].

Determining the reliability of a system is simple if the system can be broken down into a series or parallel system. The first step in calculating the reliability of a simple system is to define a structure function. The structure function determines the state of the system based upon the state of the components. The structure functions for a series and parallel system of n components are:

$$\Phi_{series} = \prod_{i=1}^{n} X_i \tag{18}$$

$$\Phi_{parallel} = 1 - (1 - \prod_{i=1}^{n} X_i) \tag{19}$$

Where X_i is the state of component i and Φ is the state of the system. The reliability of the systems can be calculated by replacing X_i by the reliability of the component.

3.3.1 Reliability of Complex Systems

If the system being evaluated cannot be broken down into a series or parallel system, the reliability analysis becomes immensely more difficult; this type of system is referred to as a complex system and is representative of the power distribution system being studied. There are two basic strategies for determining the reliability of a complex system – a simulation approach or an analytical approach.

3.3.1.1 Simulation Approach

The simulate approach uses a computer simulation to change the states of the components and then determines the state of the system. The most accepted method used for the simulation approach is Monte Carlo simulation. [3]

The first step in Monte Carlo simulation is to define the reliability distribution for each component and an operating time range for the system. Then, a random point in time is selected. Each component is put in a working or failed state with some

probability based upon the time selected and the component distribution. Next, using the structure function, the state of the system is determined [140] [85]. The process is repeated for thousands of trials to create a probability mass function (PMF) for the system. The PMF can be used to determine if the system meets the reliability requirements.

The advantage of Monte Carlo simulation is that it easy to program and allows the use of both continuous and discrete distributions. The major downfall of Monte Carlo simulation is that it can be time consuming; creating the system PMF requires thousands of runs. If the runs take a large amount of time, Monte Carlo simulation may not be feasible. Furthermore, Monte Carlo simulation is not as accurate as exact analytical methods and can only provide the system's PDF. It cannot be used to determine other properties such as the system failure rate or mean-time-to-failure.

3.3.1.2 Analytical

Analytical methods provide mathematical expressions that can be used to determine the system reliability, failure rate, and mean-time-to-failure. There are three analytical approaches that can be used: the decomposition method, the event space method, and the path-tracing method. [2]

Decomposition Method The decomposition method uses the law of total probabilities to determine the system reliability by evaluating the system's response to failing a critical component in the system. The law of total probabilities relates marginal probabilities to conditional probabilities. For example, the probability of event A and event B occurring is the probability of event A occurring given that event B has occurred multiplied by the probability of event B occurring.

$$P(A \cap B) = P(A|B) * P(B) \tag{20}$$

To calculate the reliability of the system, s, a key component, A, is failed. Then

the system reliability is calculated given that A has failed. Next, the calculation is repeated given that A is available.

$$R_s = P(s \cap A) + P(s \cap \bar{A}) = P(s|A) * P(A) + P(s|\bar{A}) * P(\bar{A}) \tag{21}$$

For the equation to remain simple, when the key component fails, the remaining components must be in series or parallel to determine the reliability of the system under this condition. If this is not the case, then the decomposition must continue until the only series or parallel components remain.

Event Space Method The event space method decomposes the sample space into sets of mutually exclusive sets to calculate reliability.

If E_1 and E_2 are mutually exclusive, the probability of both events occurring is the sum of the probabilities of the events.

$$P(E_1 \cap E_2) = P(E_1) + P(E_2) \tag{22}$$

To use this method, all mutually exclusive system events must be determined. Normally, this means evaluating every combination of working and unavailable components. From the combinations, the events that will result in a system failure are determined. Then the probability of system failure is the union of the probability of each event.

Path-tracing Method To use the path-tracing method, all paths from the source of the system to the sink must be considered. Consider the example system shown in Figure 20. The possible paths are:

Path Name	Path
MP1	a1,a5
MP2	a2,a7
MP3	a3, a7

The system reliability would be the probability that at least one of the paths is available. The probability of a path being available is the product of the component reliabilities. Calculating the probability that a path is available is not straight forward since the probabilities of each path being available are not independent because some components are used in multiple paths. This can be demonstrated using the Venn diagram shown in Figure 21. Considering the path set availability independently would overestimate the system reliability. The proper way to calculate the availability of sink 1 is:

$$\begin{aligned} \text{Availability of sink } 1 &= P(MP1 \cup MP2 \cup MP3) \\ &= P(MP1) + P(MP2) + P(MP3) \\ &- P(MP1 \cap MP2) - P(MP1 \cap MP3) - P(MP2 \cap MP3) + P(MP1 \cap MP2 \cap MP3) \end{aligned} \tag{23}$$

The analytical approaches described can become difficult for highly complex systems. Computer algorithms that can construct the mathematical expressions are essential for applying the methods. The best analytical approach varies with the type of problem and the system structure.

A literature search was performed to find whether the techniques had been applied to a system with a similar configuration to the turboelectric power distribution system. The algorithm must be able to handle a system with multiple sources and sinks. Also, the ability for multi-state analysis is desired. Multi-state analysis considers the amount of flow in a system where components can function between a broken and full

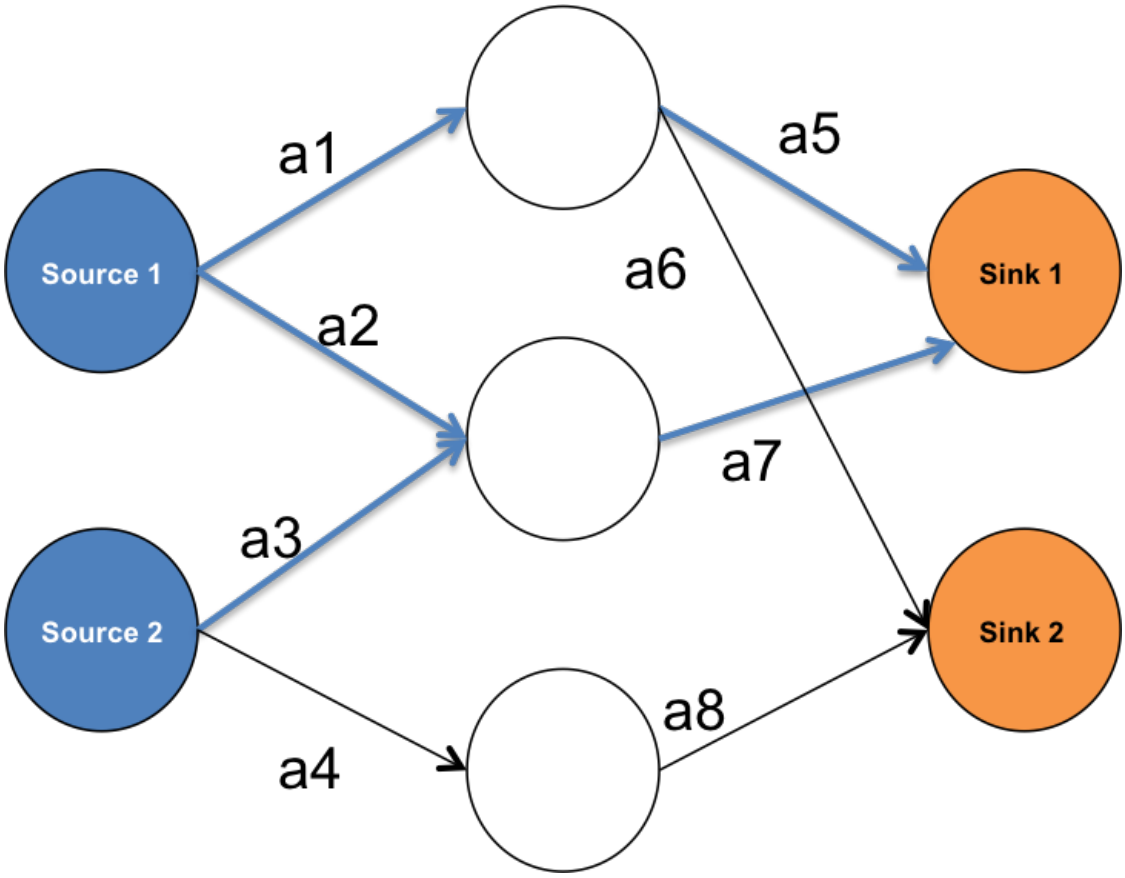

Figure 20: Example system

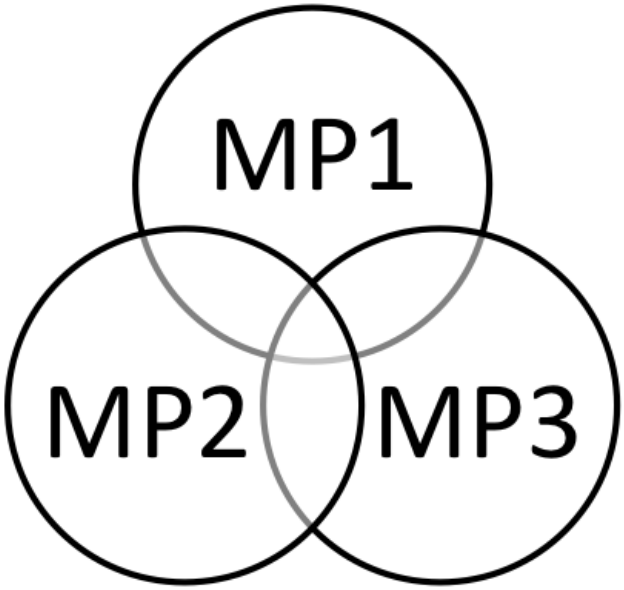

Figure 21: Path set Venn diagram

capacity state. While some studies on power systems were found, they were generally oversimplified and were not well suited for analyzing a multiple source and multiple sink problem. More information was found by studying computer and communication networks. Rather than power, these systems must be able to deliver data packets from multiple sources to multiple destinations [68]. To evaluate the reliability of these systems, an analysis technique emerged referred to as stochastic flow networks.

3.3.2 Stochastic Flow Networks

In stochastic flow networks, the probability that a component will be able to deliver its flow to its loads is considered to be a random variable changing in time. Stochastic flow networks are designed to specifically address the probability that flow can be delivered from source nodes to sink nodes.

The network is composed of nodes and edges. Each node will have a probability mass function that determines the probability of the state of the node over time. The PMF will not only dictate whether the node is functioning or not, it will dictate the amount of flow that a node can carry at a given time. After each node has an assigned PMF, the Doulliez and Jamoulle Decomposition Method is used to determine system reliability.

3.3.3 Component Reliability

Calculating system reliability using the decomposition method relies on specifying the probability that a component could provide the amount of flow corresponding to the acceptable state. In a binary approach (each component has two states - functioning at maximum capacity or unavailable), this is simply the reliability of the component at a given time.

Component reliability is defined using lifetime distributions or by fitting reliability data. Since data is limited, generic parametric lifetime models will be used to estimate the reliability of the components. Common lifetime distributions include the survival

function, probability density function, and the hazard function. The most commonly used lifetime distribution to describe reliability is the survival function. It determines the probability that a component is functioning at a given time. The survival function is often represented using a parametric lifetime model. Some popular distributions that are used for the model are: the exponential distribution, Weibull distribution, and Gamma distribution.

The exponential distribution is widely used to model electronic component reliability. The exponential distribution is unique since it has a constant hazard function (h(t)) [83]. The hazard function is representative of the amount of risk associated with a component at time t. In this case, the constant hazard function is set equal to the failure rate (λ), the expected number of failures per unit time.

Since the hazard function is constant, the exponential distribution has the memoryless property - meaning that in order to use this distribution, a used component that has not failed is statistically as good as a new component; this is a large assumption that rarely applies in real-world situations. In reality, most components actually have a bathtub shaped distribution which is shown in Figure 22 [102]. At the beginning of the component's lifetime (often referred to as the infant mortality period), there is normally a high rate of failure. Then, the failure rate is fairly constant during the intrinsic failure period. At the end of the useful life of the component, the failure rate then dramatically increases due to wear-out. In order to apply the exponential distribution, two assumptions must be made. First, the components must under-go a burn-in period at the factory; that is, the components are operated before they are placed into the aircraft to eliminate parts that fail during the infancy stage. The second assumption is that the components are replaced before they reach the end of their useful life when the failure rate dramatically changes. Therefore, the component will only be in operation on the aircraft during the intrinsic failure period, so the exponential distribution can be used to predict the reliability of the components.

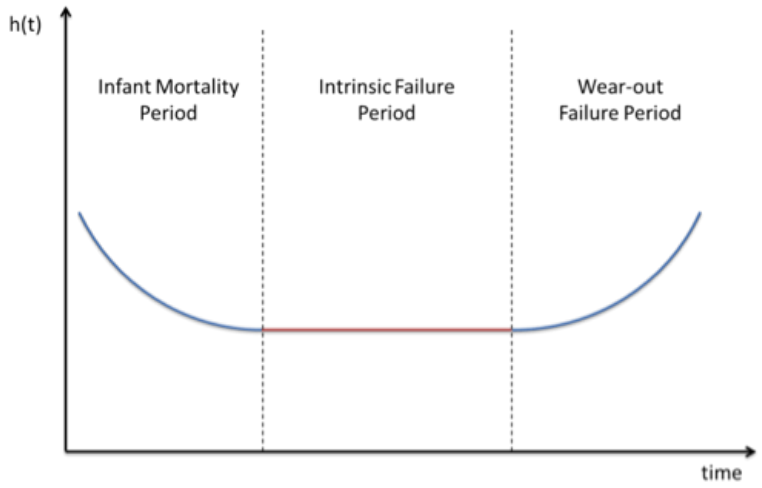

Figure 22: bathtub hazard function

In order to apply the exponential distribution in the modeling environment, the failure rate for each component must be known. Because reliability data is considered to be a competitive advantage by many firms, the amount of information available publicly is limited. The two primary sources of electronic component reliability data available in the public domain are MIL-HDBK-217F [113] and the Handbook of 217plus Reliability Prediction Models [26]. MIL-HDBK-217F is a military document that was published by the Department of Defense in 1991 as a guide for failure rates of electronic components that are used in military technology design. Since this was the first published documents with electronic component reliability data and is fairly comprehensive, it is the most widely used source in electric system reliability analysis. Nevertheless, since the document is over 20 years old, most of the data is outdated. Many analysts still apply this data by using correction factors to estimate the failure rate of updated or new technologies that did not exist when the document was published.

The Handbook of 217plus Reliability Prediction Models is an update to MIL-HDBK-217F. Published in 2006, this document presents the data used to create the 217plus environment. 217plus is a reliability analysis software created by Reliability

Table 14: Room temperature component failure rates

Component	Failure rate (failures per hour)
Generator	0.0007
Rectifier	0.00102
Bus	0.0000114
Inverter	0.000102
Motor	0.0007

Information Analysis Center for the Department of Defense. The information contained within the software was made publicly available through this handbook. Since the data from the 217plus Handbook is more up-to-date than that of MIL-HDBK-217F, it was used to estimate the failure rates of the components.

The 217plus Handbook provides failure rates for a variety of electrical components such as capacitors, resistors, switches, diodes, etc. For each component type, a base failure rate is available for a variety of component designs and materials. The base failure rate can then be altered based upon correction factors provided to account for operating environment, temperature, electrical stress, and duty cycle. All the base failure rates and correction factors are presented in a series of look-up tables. Formulas are also provided to explain proper use of the correction factors to the base failure rates.

The failure rate for some components, such as a converter, will not be readily available in either handbook. Instead, the failure rates of the subcomponents such as resistors, capacitors, switches, etc. must be used [26]. The failure rate of the component can then be calculated by simply adding the failure rates of the subcomponents.

As eluded to by the correction factors provided in the 217Plus Handbook, the failure rate of each component will be dependent on a number of factors such as quality, temperature, stress, and operating environment. Generally, higher quality components will have a lower failure rate, but they are more expensive. The reliability of electronic components is also highly dependent on operating temperature; therefore, an analysis of the temperatures encountered throughout the flight envelope is needed

in order to accurately predict the component failure rates. Furthermore, this analysis may reveal that a thermal management system is required to maintain component temperatures so that a favorable failure rate can be achieved. Additionally, the electrical stress that the component endures will greatly affect its reliability. The stress is often determined using a ratio of applied voltage to rated voltage. Components that have a low ratio tend to be more reliable than components that are used at their full rated voltage. Dynamic system modeling is important to predict the stresses that the components will encounter. Lastly, the operating environment is an important consideration. Components that are placed on an aircraft tend to be less reliable than those used in ground based applications due to the extreme environments encountered and large forces on the components [26].

As described, detailed information about the system environment and operation is needed to accurately predict the reliability of the components; however, this detailed analysis falls outside the scope of the preliminary study. Hence, it is assumed that the operating conditions for the components never exceed nominal levels. With this assumption, basic reliability data available through the Handbook of 217plus can be used to determine the failure rate of the components.

3.3.3.1 Doulliez and Jamoulle Decomposition Method

After the survivor function for each component has been defined, the system reliability calculation begins using the Doulliez and Jamoulle Decomposition Method. The method decomposes the system states into three categories: acceptable states, non-acceptable states, and unspecified states. The algorithm is iterative so that the unspecified states are decomposed into acceptable and unacceptable states until no unspecified states remain. The reliability of the system is the probability that the system is in an acceptable state. This method is based on the event space method that was described in the previous section.

Before the primary algorithm can be applied, the acceptable states of the system must be defined. Of particular interest are the combinations with a minimum number of functioning components that results in a functioning system. This can be found by defining all the minimum path sets in the system and then selecting combinations of path sets that result in a functioning system.

Determining Minimum Path Sets A path set is a set of nodes that link a source with a sink. A minimal path set is a path set that does not contain any loops; that is, no component is used twice. Finding path sets is a common problem and has received a great amount of attention in graph theory research.

Methods for Finding Path Sets There are three primary methods for finding minimal path sets in a system: the Boolean determinant method, the node searching method, and the adjacency matrix method [157]. The Boolean determinant method becomes complex for a network with a large number of nodes. The node searching method finds all connections is a system, not just the minimal paths which unnecessarily increases the evaluation time. For the system being evaluated, the adjacency matrix method will be the fastest and least convoluted.

Adjacency matrix method The adjacency matrix method of finding path sets is derived using the property of adjacency matrices discussed in the capacity calculation section; that is, multiple step connections can be found by multiplying the adjacency matrix by itself. To review, the adjacency matrix and the four-step matrix are shown in Table 16 and Table 17.

The algorithm begins by examining the four-step matrix. A path is initialized for each generator to motor connection possibility. First the G1 row is studied. In the baseline case, one motor group is connected to G1, so a path is initialized including G1 and M1. Next, move to the G2 row which shows that there is a path from G1

Table 15: Path set initialization

G1	G2	G3	G4	R1	R2	R3	R4	B1	B2	B3	B4	I1	I2	I3	I4	M1	M2	M3	M4
1	0	0	0	0	0	0	0	0	0	0	0	0	0	0	0	1	0	0	0
0	1	0	0	0	0	0	0	0	0	0	0	0	0	0	0	0	1	0	0
0	1	0	0	0	0	0	0	0	0	0	0	0	0	0	0	0	0	1	0
0	0	1	0	0	0	0	0	0	0	0	0	0	0	0	0	0	1	0	0
0	0	1	0	0	0	0	0	0	0	0	0	0	0	0	0	0	0	1	0
0	0	0	1	0	0	0	0	0	0	0	0	0	0	0	0	0	0	0	1

to M2 and M3; therefore, two more paths are initialized. The process is repeated for the remaining generators, and the paths shown in Table 15 are initialized.

The next step is to use the three-step matrix (shown in Table 18) to determine the generator to inverter connections, and then cross-correlate those connections to the inverter-motor group connections using the adjacency matrix. Start by taking a vector from the three-step matrix that defines the generator to inverter connections. Use one vector for each generator. Select the row of the generator and the inverter columns. For generator 1 and motor group 1, the vector would be:

$$A = [1000] \tag{24}$$

Next, use the adjacency matrix to select a second vector that defines the inverter and motor group connections. Use the rows of the inverters and the column of the motor group.

$$B = \begin{bmatrix} 1 \\ 0 \\ 0 \\ 0 \end{bmatrix} \tag{25}$$

Next, determine the placement of the inverters using:

$$P = A^T \cdot B = \begin{bmatrix} 1 \\ 0 \\ 0 \\ 0 \end{bmatrix} \tag{26}$$

This will result in a (number of inverters) X 1 vector that determines where to place the inverters in the path sets. The first value in the vector will determine how many times inverter 1 is used connecting generator 1 to motor group 1. Since there is a 1, a 1 is placed in the inverter 1 slot for the path sets that demonstrate a connection for generator 1 to motor group 1. The second value in the vector P shows if inverter 2 is used in connecting generator 1 and motor group 1. Since this value is zero, inverter 2 is not used. This process is repeated for the 3rd and 4th inverter. Once that is complete, the analysis is repeated for all generator and motor group combinations.

After the inverters are placed in the path sets, the next step is to place the buses. The same technique is applied that was used to place the inverters, but now the two-step connection matrix is used. The vector, A, will now be the generator row from the two-step matrix and the bus columns. The B vector will the the bus rows and the motor group column from the two-step connection. The resulting P vector will determine where to place the buses in the path sets for each generator and motor group combination.

Lastly, the rectifiers need to be placed. This is accomplished using the adjacency and 3-step matrix. Again, the correlation technique that was described is used. The A vector is now the generator row and rectifier columns from the adjacency matrix. The B vector will be the rectifier rows and the motor group column from the three-step matrix; then, the P vector is used to place the rectifiers in the path sets. After the algorithm is completed, the path sets will be complete. The path sets for the baseline system are shown in Table 20. The six path sets are denoted as P1, P2, ...,

Table 16: Baseline adjacency matrix

	G1	G2	G3	G4	R1	R2	R3	R4	B1	B2	B3	B4	I1	I2	I3	I4	M1	M2	M3	M4
G1	0	0	0	0	1	0	0	0	0	0	0	0	0	0	0	0	0	0	0	0
G2	0	0	0	0	0	1	0	0	0	0	0	0	0	0	0	0	0	0	0	0
G3	0	0	0	0	0	0	1	0	0	0	0	0	0	0	0	0	0	0	0	0
G4	0	0	0	0	0	0	0	1	0	0	0	0	0	0	0	0	0	0	0	0
R1	0	0	0	0	0	0	0	0	1	0	0	0	0	0	0	0	0	0	0	0
R2	0	0	0	0	0	0	0	0	0	1	0	0	0	0	0	0	0	0	0	0
R3	0	0	0	0	0	0	0	0	0	0	1	0	0	0	0	0	0	0	0	0
R4	0	0	0	0	0	0	0	0	0	0	0	1	0	0	0	0	0	0	0	0
B1	0	0	0	0	0	0	0	0	0	0	0	0	1	0	0	0	0	0	0	0
B2	0	0	0	0	0	0	0	0	0	0	0	0	0	1	1	0	0	0	0	0
B3	0	0	0	0	0	0	0	0	0	0	0	0	0	1	1	0	0	0	0	0
B4	0	0	0	0	0	0	0	0	0	0	0	0	0	0	0	1	0	0	0	0
I1	0	0	0	0	0	0	0	0	0	0	0	0	0	0	0	0	1	0	0	0
I2	0	0	0	0	0	0	0	0	0	0	0	0	0	0	0	0	0	1	0	0
I3	0	0	0	0	0	0	0	0	0	0	0	0	0	0	0	0	0	0	1	0
I4	0	0	0	0	0	0	0	0	0	0	0	0	0	0	0	0	0	0	0	1
M1	0	0	0	0	0	0	0	0	0	0	0	0	0	0	0	0	0	0	0	0
M2	0	0	0	0	0	0	0	0	0	0	0	0	0	0	0	0	0	0	0	0
M3	0	0	0	0	0	0	0	0	0	0	0	0	0	0	0	0	0	0	0	0
M4	0	0	0	0	0	0	0	0	0	0	0	0	0	0	0	0	0	0	0	0

P6.

For a system that only requires a single path to be operational for success of the system, the path sets can be used in their present form. However, for the power distribution system, multiple sources and sinks must be available for the system to be operational. A path would only lead to one operational motor group - meaning that the aircraft would not have enough power for takeoff.

The engine-out scenarios used for the capacity calculation showed that three-motor groups were available during each failure scenario. The motors and system were sized with the minimum requirement that the three groups combined capacity was equal to that of the minimum takeoff power; therefore, groups of path sets that lead to at least three functional motor groups now become the new path sets.

The combinations of motor groups that meet the capacity requirement are:

- M1, M2, M3
- M1, M2, M4
- M1, M3, M4

Table 17: Baseline 4-step connections

	G1	G2	G3	G4	R1	R2	R3	R4	B1	B2	B3	B4	I1	I2	I3	I4	M1	M2	M3	M4
G1	0	0	0	0	0	0	0	0	0	0	0	0	0	0	0	0	1	0	0	0
G2	0	0	0	0	0	0	0	0	0	0	0	0	0	0	0	0	0	1	1	0
G3	0	0	0	0	0	0	0	0	0	0	0	0	0	0	0	0	0	1	1	0
G4	0	0	0	0	0	0	0	0	0	0	0	0	0	0	0	0	0	0	0	1
R1	0	0	0	0	0	0	0	0	0	0	0	0	0	0	0	0	0	0	0	0
R2	0	0	0	0	0	0	0	0	0	0	0	0	0	0	0	0	0	0	0	0
R3	0	0	0	0	0	0	0	0	0	0	0	0	0	0	0	0	0	0	0	0
R4	0	0	0	0	0	0	0	0	0	0	0	0	0	0	0	0	0	0	0	0
B1	0	0	0	0	0	0	0	0	0	0	0	0	0	0	0	0	0	0	0	0
B2	0	0	0	0	0	0	0	0	0	0	0	0	0	0	0	0	0	0	0	0
B3	0	0	0	0	0	0	0	0	0	0	0	0	0	0	0	0	0	0	0	0
B4	0	0	0	0	0	0	0	0	0	0	0	0	0	0	0	0	0	0	0	0
I1	0	0	0	0	0	0	0	0	0	0	0	0	0	0	0	0	0	0	0	0
I2	0	0	0	0	0	0	0	0	0	0	0	0	0	0	0	0	0	0	0	0
I3	0	0	0	0	0	0	0	0	0	0	0	0	0	0	0	0	0	0	0	0
I4	0	0	0	0	0	0	0	0	0	0	0	0	0	0	0	0	0	0	0	0
M1	0	0	0	0	0	0	0	0	0	0	0	0	0	0	0	0	0	0	0	0
M2	0	0	0	0	0	0	0	0	0	0	0	0	0	0	0	0	0	0	0	0
M3	0	0	0	0	0	0	0	0	0	0	0	0	0	0	0	0	0	0	0	0
M4	0	0	0	0	0	0	0	0	0	0	0	0	0	0	0	0	0	0	0	0

Table 18: Baseline 3-step connections

	G1	G2	G3	G4	R1	R2	R3	R4	B1	B2	B3	B4	I1	I2	I3	I4	M1	M2	M3	M4
G1	0	0	0	0	0	0	0	0	0	0	0	0	1	0	0	0	0	0	0	0
G2	0	0	0	0	0	0	0	0	0	0	0	0	0	1	1	0	0	0	0	0
G3	0	0	0	0	0	0	0	0	0	0	0	0	0	1	1	0	0	0	0	0
G4	0	0	0	0	0	0	0	0	0	0	0	0	0	0	0	1	0	0	0	0
R1	0	0	0	0	0	0	0	0	0	0	0	0	0	0	0	0	1	0	0	0
R2	0	0	0	0	0	0	0	0	0	0	0	0	0	0	0	0	0	1	0	0
R3	0	0	0	0	0	0	0	0	0	0	0	0	0	0	0	0	0	0	1	0
R4	0	0	0	0	0	0	0	0	0	0	0	0	0	0	0	0	0	0	0	1
B1	0	0	0	0	0	0	0	0	0	0	0	0	0	0	0	0	0	0	0	0
B2	0	0	0	0	0	0	0	0	0	0	0	0	0	0	0	0	0	0	0	0
B3	0	0	0	0	0	0	0	0	0	0	0	0	0	0	0	0	0	0	0	0
B4	0	0	0	0	0	0	0	0	0	0	0	0	0	0	0	0	0	0	0	0
I1	0	0	0	0	0	0	0	0	0	0	0	0	0	0	0	0	0	0	0	0
I2	0	0	0	0	0	0	0	0	0	0	0	0	0	0	0	0	0	0	0	0
I3	0	0	0	0	0	0	0	0	0	0	0	0	0	0	0	0	0	0	0	0
I4	0	0	0	0	0	0	0	0	0	0	0	0	0	0	0	0	0	0	0	0
M1	0	0	0	0	0	0	0	0	0	0	0	0	0	0	0	0	0	0	0	0
M2	0	0	0	0	0	0	0	0	0	0	0	0	0	0	0	0	0	0	0	0
M3	0	0	0	0	0	0	0	0	0	0	0	0	0	0	0	0	0	0	0	0
M4	0	0	0	0	0	0	0	0	0	0	0	0	0	0	0	0	0	0	0	0

Table 19: Baseline 2-step connections

	G1	G2	G3	G4	R1	R2	R3	R4	B1	B2	B3	B4	I1	I2	I3	I4	M1	M2	M3	M4
G1	0	0	0	0	0	0	0	0	1	0	0	0	0	0	0	0	0	0	0	0
G2	0	0	0	0	0	0	0	0	0	1	0	0	0	0	0	0	0	0	0	0
G3	0	0	0	0	0	0	0	0	0	0	1	0	0	0	0	0	0	0	0	0
G4	0	0	0	0	0	0	0	0	0	0	0	1	0	0	0	0	0	0	0	0
R1	0	0	0	0	0	0	0	0	0	0	0	0	1	0	0	0	0	0	0	0
R2	0	0	0	0	0	0	0	0	0	0	0	0	0	1	1	0	0	0	0	0
R3	0	0	0	0	0	0	0	0	0	0	0	0	0	1	1	0	0	0	0	0
R4	0	0	0	0	0	0	0	0	0	0	0	0	0	0	0	1	0	0	0	0
B1	0	0	0	0	0	0	0	0	0	0	0	0	0	0	0	0	1	0	0	0
B2	0	0	0	0	0	0	0	0	0	0	0	0	0	0	0	0	0	1	1	0
B3	0	0	0	0	0	0	0	0	0	0	0	0	0	0	0	0	0	1	1	0
B4	0	0	0	0	0	0	0	0	0	0	0	0	0	0	0	0	0	0	0	1
I1	0	0	0	0	0	0	0	0	0	0	0	0	0	0	0	0	0	0	0	0
I2	0	0	0	0	0	0	0	0	0	0	0	0	0	0	0	0	0	0	0	0
I3	0	0	0	0	0	0	0	0	0	0	0	0	0	0	0	0	0	0	0	0
I4	0	0	0	0	0	0	0	0	0	0	0	0	0	0	0	0	0	0	0	0
M1	0	0	0	0	0	0	0	0	0	0	0	0	0	0	0	0	0	0	0	0
M2	0	0	0	0	0	0	0	0	0	0	0	0	0	0	0	0	0	0	0	0
M3	0	0	0	0	0	0	0	0	0	0	0	0	0	0	0	0	0	0	0	0
M4	0	0	0	0	0	0	0	0	0	0	0	0	0	0	0	0	0	0	0	0

Table 20: Baseline system path sets

	G1	G2	G3	G4	R1	R2	R3	R4	B1	B2	B3	B4	I1	I2	I3	I4	M1	M2	M3	M4
P1	1	0	0	0	1	0	0	0	1	0	0	0	1	0	0	0	1	0	0	0
P2	0	1	0	0	0	1	0	0	0	1	0	0	0	1	0	0	0	1	0	0
P3	0	1	0	0	0	1	0	0	0	1	0	0	0	0	1	0	0	0	1	0
P4	0	0	1	0	0	0	1	0	0	0	1	0	0	1	0	0	0	1	0	0
P5	0	0	1	0	0	0	1	0	0	0	1	0	0	0	1	0	0	0	1	0
P6	0	0	0	1	0	0	0	1	0	0	0	1	0	0	0	1	0	0	0	1

Table 21: Updated path sets

	G1	G2	G3	G4	R1	R2	R3	R4	B1	B2	B3	B4	I1	I2	I3	I4	M1	M2	M3	M4
PS1	1	1	1	0	1	1	1	0	1	1	1	0	1	1	1	0	1	1	1	0
PS2	1	1	0	0	1	1	0	0	1	1	0	0	1	1	1	0	1	1	1	0
PS3	1	0	1	0	1	0	1	0	1	0	1	0	1	1	1	0	1	1	1	0
PS4	1	1	0	1	1	1	0	1	1	1	0	1	1	1	0	1	1	1	0	1
PS4	1	1	0	1	1	1	0	1	1	1	0	1	1	1	0	1	1	1	0	1
PS5	1	0	1	1	1	0	1	1	1	0	1	1	1	1	0	1	1	1	0	1
PS6	0	1	1	1	0	1	1	1	0	1	1	1	0	1	1	1	0	1	1	1
PS7	0	1	0	1	0	1	0	1	0	1	0	1	0	1	1	1	0	1	1	1
PS8	0	0	1	1	0	0	1	1	0	0	1	1	0	1	1	1	0	1	1	1
PS9	1	0	1	1	1	0	1	1	1	0	1	1	1	0	1	1	1	0	1	1
PS10	1	1	0	1	1	1	0	1	1	1	0	1	1	0	1	1	1	0	1	1

- M2, M3, M4

Each motor group combination is examined to determine which combinations of path sets would lead to a motor group being available that meet the combinations listed. The new path sets that meet the motor group combinations are shown in Table 21. For example, the first acceptable motor group combination is M1, M2, and M3. If Table 20 is examined, it can be found that there are four path set combinations that will lead to that motor group combination: P1, P3, P4; P1, P2, P5; P1, P2, P3; and P1, P4, P5. These combinations are represented by paths PS1, PS2, and PS3 in Table 21. (The P1, P3, P4 and P1, P2, P5 combinations lead to the same component combination and is represented by PS1.)

At this point, one more modification is needed. The sets that are used for the decomposition also need to represent capacity. That is, not only does the existence of a component in a path need to be known, also that capacity of the component must be represented. One way to achieve this is by relating the capacity to the design capacity of the component. In this analysis, it will be assumed that each component has two possible states: either it is operating at its design capacity or it is not functioning. If a component is operating, it is represented by a 1 in the path set; however, a modification needs to be made for the motor groups. Each group contains several motors. Therefore, the path sets need to reflect the number of motors that are operational in a group.

Table 22: Baseline path sets used for decomposition

G1	G2	G3	G4	R1	R2	R3	R4	B1	B2	B3	B4	I1	I2	I3	I4	M1	M2	M3	M4
1	1	1	0	1	1	1	0	1	1	1	0	1	1	1	0	4	4	4	0
1	1	0	0	1	1	0	0	1	1	0	0	1	1	1	0	4	4	4	0
1	0	1	0	1	0	1	0	1	0	1	0	1	1	1	0	4	4	4	0
1	1	0	1	1	1	0	1	1	1	0	1	1	1	0	1	4	4	0	4
1	0	1	1	1	0	1	1	1	0	1	1	1	1	0	1	4	4	0	4
0	1	1	1	0	1	1	1	0	1	1	1	0	1	1	1	0	4	4	4
0	1	0	1	0	1	0	1	0	1	0	1	0	1	1	1	0	4	4	4
0	0	1	1	0	0	1	1	0	0	1	1	0	1	1	1	0	4	4	4
1	0	1	1	1	0	1	1	1	0	1	1	1	0	1	1	4	0	4	4
1	1	0	1	1	1	0	1	1	1	0	1	1	0	1	1	4	0	4	4

For the baseline, the motors were sized such that all motors in a group must be functioning for a path to be available, so the path sets need to be modified to show the requirement. This is accomplished by replacing the one in a motor group column with a 4 to reflect that all 4 motors in the group need to be functioning. The path sets that will be used for the system decomposition are shown in Table 22.

Once all the path sets have been defined, the next step is to apply the decomposition method.

State-space decomposition and reliability calculation The state-space decomposition algorithm can be defined in six steps [12]. The steps will be explained, and then an example problem will be presented to demonstrate the algorithm.

Step 1: Initialization Set the system reliability to zero, and set a counter, k, to 1. Specify the lower bound of the system, u_{lower}. In this case, it will be a 1Xn vector of zeros, where n is the number of components in the system. Next, the upper bound on the system, upper, needs to be defined. This will be a 1xn vector that has the maximum capacity of each component in the system. For all the components other than the motor group, this will be set to 1. The maximum capacity for each motor group will be set to four.

$$u_{lower} = [00000000000000000000] \tag{27}$$

$$u_{upper} = [11111111111111114444] \tag{28}$$

Step 2: Path Selection In this step, one of the minimum paths will be selected. Select a minimum path $\mathbf{y}$ that maximizes:

$$H(\mathbf{y}) = \sum_{i=1}^{n} (u_{upper,i} - max\{y_i, u_{lower,i}\}) \tag{29}$$

Given that $\mathbf{y} \leq \mathbf{u}_{upper}$ - meaning that all of the elements in the minimum path vector is less than the upper limit. The calculation will select a path set that is furthest from the upper limit of the unspecified states. Create an x-by-n matrix, where x is the number of paths that fit the criteria and n is the number of components.

Once a path set has been selected, set:

$$v_i = min\{y_i, \mathbf{y} \leq \mathbf{u}_{upper}\}, i = 1, 2, .., n \tag{30}$$

v is the bound of the unacceptable state. First examine the expression $\mathbf{y} \leq \mathbf{u}_{upper}$. For every path set, specify a vector if all elements in that path set are less than or equal to the upper limit of the unspecified state. For each column of the matrix, take the minimum of the column and the path set which will specify the bound on the unacceptable state.

Step 3: Define bounds of the acceptable state The upper bound is the maximum of the of the path capacity and the lower bound of the previously unspecified state. The lower bound is the maximum of the minimum of the path and the lower bound of the previously unspecified state.

Set $\mathrm{a}_{upper} = \max\{\mathrm{y}_i, \mathrm{u}_{lower}\}$

Set $\mathrm{a}_{lower} = \max\{\mathrm{v}_i, \mathrm{u}_{lower}\}$

Step 4: Compute the probability of the acceptable state Now that the bounds of the acceptable and unacceptable state have been found, the probably that the system state is within those bounds is calculated.

$$R \leftarrow R + \prod_{i=1}^{n} p_i \tag{31}$$

Where,

$$p_i = R_i(a_{upper,i}) - R_i(u_{upper,i} + 1), i = 1, 2, .., n \tag{32}$$

R(x) is the probability that component i has the capacity x at a given time. This calculation will have to be repeated at several different time points so that the system reliability function can be derived.

For components other than the motors, if the state of the component reliability being examined is 1, then the reliability is the value of the reliability of that component. If the state is zero, then the reliability is 1. (A state is the the probability that the components can deliver at least that amount of flow.) Under any condition the component would be able to generate a flow of zero; contrarily, a flow of 1 would require the component to be functioning. If the state of the component goes to 2, then the reliability is zero. There is no possibility that the component can deliver more than its maximum rating of 1.

The motors require a modified analysis since their state can range from 0 to 4 (that is, 0 motors are operational in a group or all 4 motors are operational in a group). A 1X6 vector needs to be defined that contains the probability of each possible state of the motor groups. To construct the vector, a k-out-of-n reliability analysis has to be carried out; that is, finding the probability that k motors out of the number of motors in the group are functioning.

The k-out-of-n reliability formulation begins with the binomial distribution which determines the probability that exactly k units are functioning out of n total units

[36].

$$Pr(X = k) = \binom{n}{k} p^k (1-p)^{n-k} \tag{33}$$

Using this information, the probability that at least k-out-of-n motors are available can be calculated. The vector that defines the probability of the states of the motor groups is defined as:

$$\mathbf{R}_i(x) = \begin{bmatrix} R_i(0) \\ R_i((1) \\ R_i(2) \\ R_i(3) \\ R_i(4) \\ R_i(5) \end{bmatrix}$$

$$= \begin{bmatrix} Pr(X=0) + Pr(X=1) + Pr(X=2) + Pr(X=3) + Pr(X=4) \\ Pr(X=1) + Pr(X=2) + Pr(X=3) + Pr(X=4) \\ Pr(X=2) + Pr(X=3) + Pr(X=4) \\ Pr(X=3) + Pr(X=4) \\ Pr(X=4) \\ Pr(X=5) \end{bmatrix} \tag{34}$$

$$= \begin{bmatrix} 1 \\ p^4 + 4p^3(1-p) + 6p^2(1-p)^2 + 4p(1-p)^3 \\ p^4 + 4p^3(1-p) + 6p^2(1-p)^2 \\ p^4 + 4p^3(1-p) \\ p^4 \\ 0 \end{bmatrix}$$

Where p is the probability that a motor is functioning at a given time.

Step 5: Determine the unspecified states Once the bounds of the acceptable and unacceptable states are known and the probability of an acceptable state has been calculated, the next step is to redefine the bounds of the unspecified states. For i = 1, 2, ..., n, find the i's such that $a_{lower,i} < a_{upper,i}$. Record each i as a_d, d = 1, 2, ..., s. (If no such i exists, set s=0.) If s $\geq$ 1, set for d = 1, 2, ..., s and i = 1, 2, ..., n:

$$b_{upper,i}(d+k-1) = \begin{cases} a_{upper,i} - 1, & \text{for i} = a_d \\ u_{upper,i}, & \text{otherwise} \end{cases}$$

$$b_{lower,i}(d+k-1) = \begin{cases} a_{upper,i}, & \text{for i} < a_d \\ a_{lower,i}, & \text{otherwise} \end{cases}$$

The number of unspecified states is:

Set k $\leftarrow$ k - 1 + s

Step 6: Check for unspecified states If k $\neq$ 0 (an unspecified state exists),

$$u_{upper,i} = b_{upper,i}(k) \tag{35}$$

$$u_{lower,i} = b_{lower,i}(k) \tag{36}$$

For i = 1, 2, ..., n, then return to step 2.

If k = 0, then end and the system reliability has been found.

The amount of time needed to complete the calculations changes significantly based upon the number of possible states in the system. If only two states are taken into account (0 meaning the component is functioning and 1 meaning that the component is functioning at full capacity), the reliability of a given system can be calculated in about a tenth of a second. If the number of possible states is increased to 8 possible states for each component in a system with 16 components, the reliability calculation can take up to an hour.

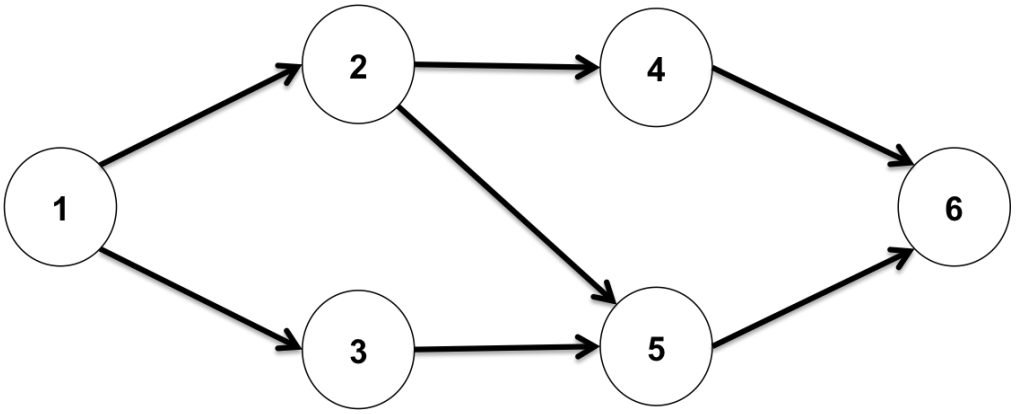

Figure 23: Example system

Table 23: Component Reliabilities

Component 1	Component 2	Component 3	Component 4	Component 5	Component 6
.99	.98	.96	.97	.95	.99

For this study, a binary approach was used to minimize calculation time. The procedure that is described would be the same for a multi-state analysis, but the computational time for optimization would be increased with each state added to the analysis.

Doulliez and Jamoulle Decomposition Example To demonstrate the methodology, consider the simple system shown in Figure 23. The system is considered to be functioning if a path from node 1 to node 6 is available.

First, the path sets must be determined. In this case there are three minimum paths shown in Table 24. The reliability of each component in the system is shown in Table 23. The reliabilities listed correspond to $R_i(1)$. $R_i(0)$ would be 1 in each case, and $R_i(2)$ would be 0.

Table 24: Example system path sets

Component 1	Component 2	Component 3	Component 4	Component 5	Component 6
1	1	0	1	0	1
1	1	0	0	1	1
1	0	1	0	1	1

Step 1 The counter is set to 1. The lower bound on the system is that no components are functioning. The upper bound on the system is that all components are functioning.

$$k = 1 \tag{37}$$

$$u_{lower} = [000000] \tag{38}$$

$$u_{upper} = [111111] \tag{39}$$

Step 2 – Iteration 1 During the first iteration, all the path set vectors are less than the upper bound of the unspecified state. In all cases, the maximum of a path set and the lower bound will simply be the path set. The distance between the upper bound and each path set will be the same during this iteration; therefore, the first path is selected. The bound of the unacceptable state will be the minimum of the vectors (that is, the minimum value for each component across all the path sets), since all vectors are less than or equal to the upper bound.

$$y = [110101]; v = [100001] \tag{40}$$

Step 3 – Iteration 1 The upper bound of the acceptable state is the maximum of y and the lower bound. In this case, this will simply equal y. The lower bound of the system is the maximum of v and the lower bound of of unknown state. In this case, the lower bound will equal v.

$$a_{upper} = [110101]; a_{lower} = [100001] \tag{41}$$

Step 4 – Iteration 1

$$R = (R_1(1) - R_1(2))(R_2(1) - R_2(2))(R_3(0) - R_3(2))* \\ (R_4(1) - R_4(2))(R_5(0) - R_5(2))(R_6(1) - R_6(2)) = \\ (.99 - 0)(.98 - 0)(1 - 0)(.97 - 0)(1 - 0)(.99 - 0) = .93 \tag{42}$$

Step 5 – Iteration 1

$$\mathrm{s} = 2;\ \mathrm{a}_1 = 2;\ \mathrm{a}_2 = 4$$
$$\mathrm{b}_{upper}(1) = [101111]$$
$$\mathrm{b}_{lower}(1) = [100001]$$
$$\mathrm{b}_{upper}(2) = [111011]$$
$$\mathrm{b}_{lower}(2) = [110001]$$
$$\mathrm{k} = 2;$$

Step 6 – Iteration 1

$$u_{upper} = b_{upper}(2) = [111011] \tag{43}$$

$$u_{lower} = b_{lower}(2) = [110001] \tag{44}$$

Since k > 0, return to step 2.

Step 2 – Iteration 2 Now path 1 can no longer be selected since y_4 is greater than $\mathrm{u}_{upper,4}$.

$$maxy_i, u_{lower} = \begin{bmatrix} 1 & 1 & 0 & 0 & 1 & 1 \\ 1 & 1 & 1 & 0 & 1 & 1 \end{bmatrix} \tag{45}$$

The largest distance between arrays computed and the upper bound of the unspecified state is if path 2 is selected. so,

y = [110011].

v is the minimum of path 2 and path 3, since path 1 has an element greater than the unspecified state upper bound.

v = [100011]

Step 3 - Iteration 2

a_{upper} = [110011];

a_{lower} = [110011];

Step 4 - Iteration 2

$$R = R + (R_1(1) - R_1(2))(R_2(1) - R_2(2))(R_3(0) - R_3(2))* \\ (R_4(0) - R_4(1))(R_5(1) - R_5(2))(R_6(1) - R_6(2)) = \\ 0.93 + (.99 - 0)(.98 - 0)(1 - 0)(1 - .97)(.95 - 0)(.99 - 0) = .96 \tag{46}$$

Step 5 - Iteration 2 Since a_{upper} is equal to a_{lower}, a new unknown state is not generated and k is reduced from 2 to 1.

Step 6 - Iteration 2

$$u_{upper} = b_{upper}(1) = [101111] \tag{47}$$

$$u_{lower} = b_{lower}(1) = [100001] \tag{48}$$

Since k is still greater than zero, another iteration is needed.

Step 2 – Iteration 3 Since paths 1 and 2 now have elements that are greater than the upper bound of the unspecified state, the only option is to select path 3.

y = [101011]; v = [101011]

Step 2 – Iteration 3

$a_{upper} = [101011];$

$a_{lower} = [101011];$

Step 4 - Iteration 3

$$R = R + (R_1(1) - R_1(2))(R_2(0) - R_2(1))(R_3(1) - R_3(2))* \\ (R_4(0) - R_4(2))(R_5(1) - R_5(2))(R_6(1) - R_6(2)) = \\ 0.96 + (.99 - 0)(1 - .98)(.96 - 0)(1 - 0)(.95 - 0)(.99 - 0) = .98 \tag{49}$$

Step 5 - Iteration 3 Since a_{upper} is equal to a_{lower}, a new unknown state is not generated and k is reduced from 2 to 0.

Step 6 - Iteration 3 Since k is 0, the algorithm is concluded and the system reliability is 0.98.

3.3.4 Baseline Reliability Results

The decomposition method was applied to the baseline system with the methodology that was explained. The resulting system reliability is shown in Figure 24. The results show that the baseline does not meet the reliability requirement; therefore, two options need to be explored: increase the redundancy of the system or increase the reliability of the system components.

3.3.4.1 Maximum Reliability Case

Since the baseline system did not meet the reliability requirement, another experiment was formed. A system with a maximum amount of redundancy was considered to determine whether the reliability requirement could be met by adding redundancy rather than increasing component reliability.

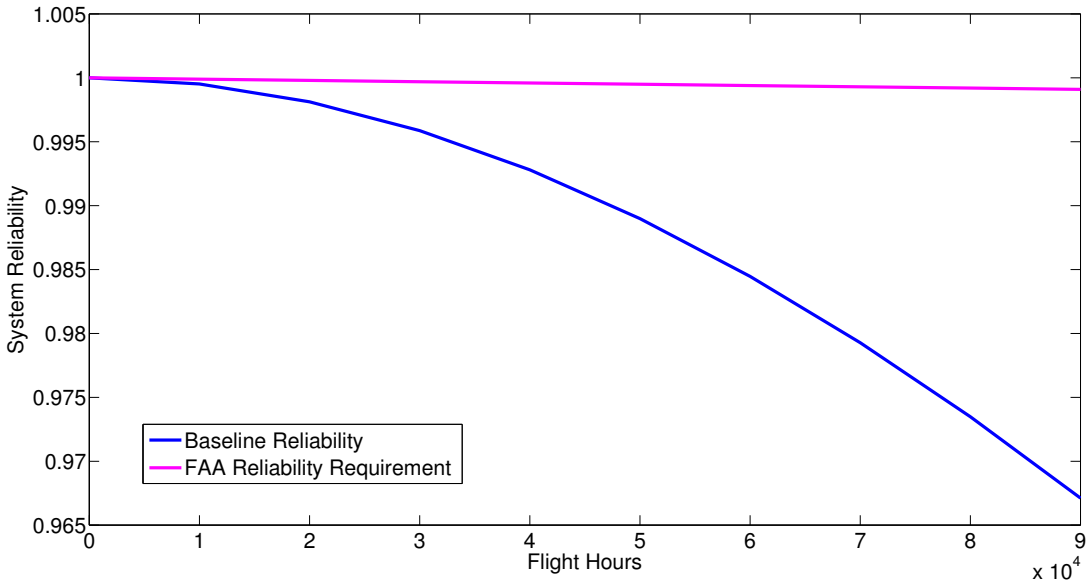

Figure 24: Baseline reliability

The maximum redundancy condition was set at using 4 buses and 16 motors. Also, every possible rectifier to bus connection and every bus to motor groups connection were activated. Furthermore, the sizing of the motors was revisited. The baseline system was sized such that 12 motors had to be operational to meet the minimum critical power requirement. This was selected based upon the engine-out failure scenario. The sizing was altered to study different sizing conditions by adding a design variable to the modeling environment. The new design variable changes the sizing of the motors such that the system can function on fewer motors than required by the engine-out scenario. The updated modeling environment schematic is shown in Figure 25.

The new design variable was perturbed to demonstrate the effect of motor sizing on the system. First, the condition which requires all 16 motors to be operational was studied. Also, the condition that requires only 2 motors out of each group (8 motors in total) to be operational was considered. The reliability for each system along with the constraint is shown in Figure 26, and the updated system weights are shown in

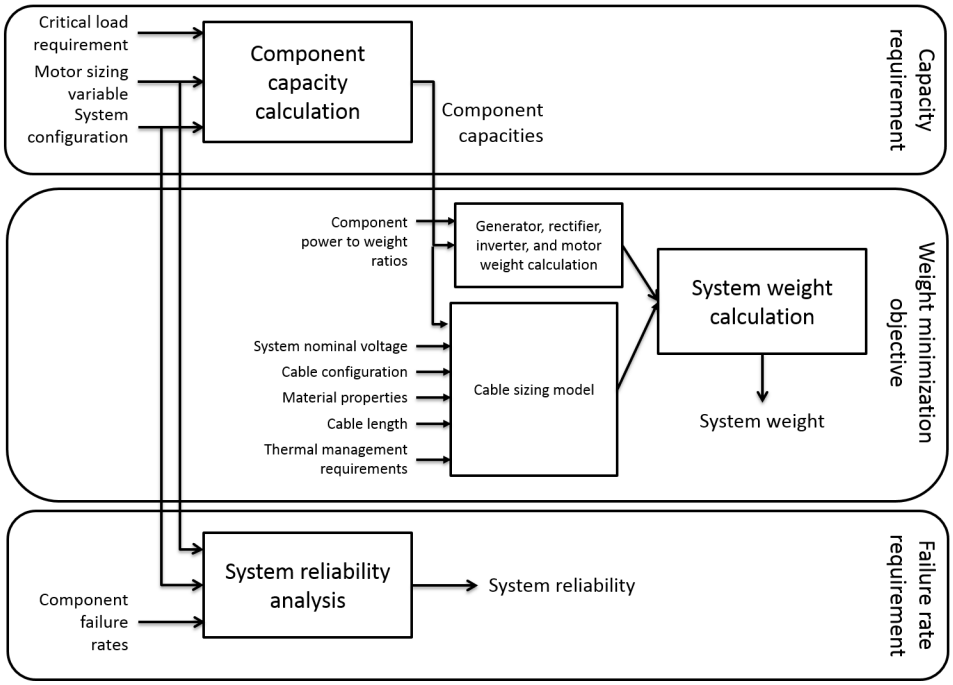

Figure 25: Updated Modeling Environment Overview

Table 25: System weights (lbs) for maximum reliability cases

4 out of 4 motors required	3 out of 4 motors required	2 out of 4 motors required
29,616	29,616	41,611

Table 25.

Figure 26 demonstrates that the reliability of the system is greatly altered based upon the number of motors that must be operational to meet the critical power requirement. The baseline case is that 3 out of 4 motors in a group must be operational. If the requirement is changed so that all motors in the system are required for acceptable operation of the system, the reliability of the system is greatly reduced. If the motors are sized so that only 2 motors out of each group must be operational (that is half of the propulsors must be functioning), then the reliability of the system is about equal to the reliability limit. However, Table 25 shows that the weight of the system would almost double in this case. The increase in the size of the motors has a ripple effect and causes every component in the system to increase in size. Table 25 also shows that the system weight is the same whether 4 out 4 motors are required

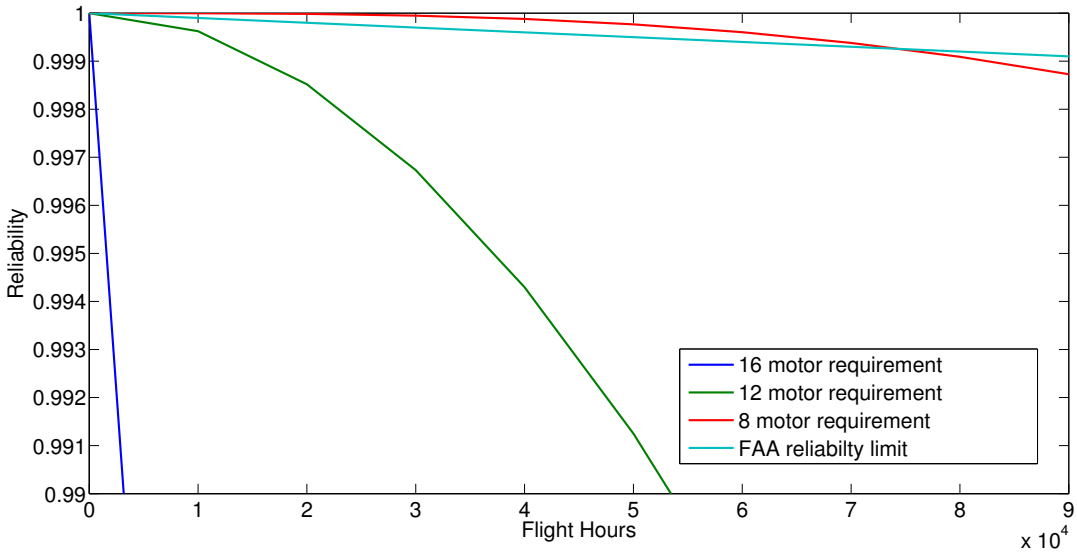

Figure 26: Maximum reliability cases

or 3 out of 4 motors are required, which occurs because of the engine-out scenario constraint. Based upon the system configuration, the motors must be sized so that the system can operate with 12 motors because only 12 motors would be available during an engine-out scenario. Even under the 4 out of 4 condition, this remains true and the motors are sized so that 12 motors can meet the critical power requirement.

3.3.4.2 Reliability Sensitivity Study

The baseline evaluation showed that the reliability requirement could not be met with that architecture and technology combination. The maximum reliability study showed that the reliability constraint could be met by increasing the redundancy in the system and sizing the motors such that the aircraft could operate with only half the motors being operational. However, meeting the requirement meant that system weight would have to be doubled, which is not a feasible solution.

As previously discussed, reliability is not only a function of redundancy but also component reliability. To further understand the gap between the baseline reliability and the reliability requirement, a study was conducted to evaluate the effect of

component reliability on the system reliability.

To carry out the sensitivity study, the mean time to failure of each component was varied by +/- two orders of magnitude. The five component types were studied individually; that is, a given component's mean time to failure was varied while all other component types' mean time to failures were held constant. The results of the study are shown in Figures 27 to 31.

The generator sensitivity study shown in Figure 27 demonstrates that decreasing the reliability of the generator will have a large detrimental impact on the overall system reliability. However, increasing the reliability of the generator will not have an impact on overall system reliability. This reveals some important design considerations; when the system design moves into detailed component design, it is important that any design changes do not increase the failure rate of the generator. However, time and effort should not be spent on improving the generator reliability since it will have little to no impact on the overall system reliability.

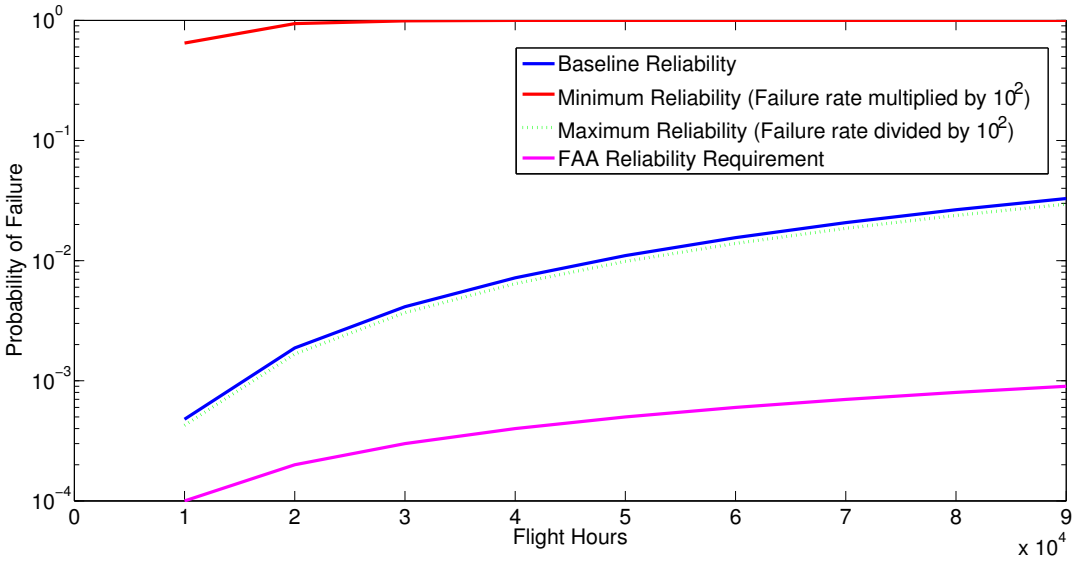

Figure 27: System reliability sensitivity to the generator failure rate

A similar trend was observed with the rectifier as shown in Figure 28. Like the

generator, increasing the reliability of the rectifier will not have a measurable effect on the overall system reliability; conversely, decreasing the reliability of the rectifier will have a large detrimental effect to overall system reliability.

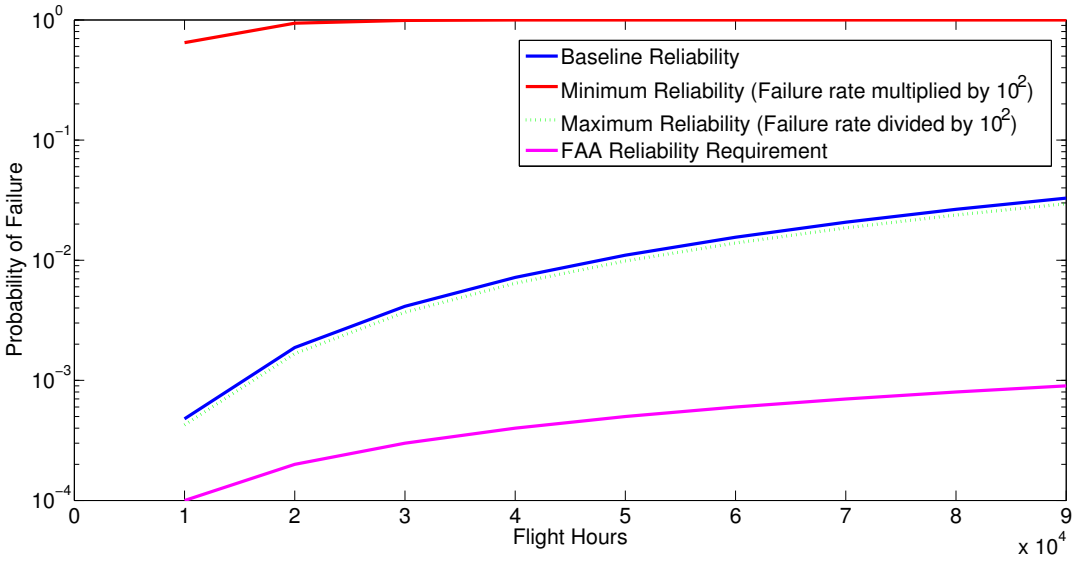

Figure 28: System reliability sensitivity to the rectifier failure rate

Figure 29 demonstrates that the bus reliability has almost no effect on overall system reliability. This is because the reliability of the bus is much higher than the other components. Therefore, it is unlikely to be the failure point of the system and does not drive system reliability. Since the bus has little effect on the system, research effort should not be concentrated on improving the bus reliability. Also, if weight can be saved by reducing the reliability of the bus, there will be little measurable effect on the overall system reliability and could be the proper design choice.

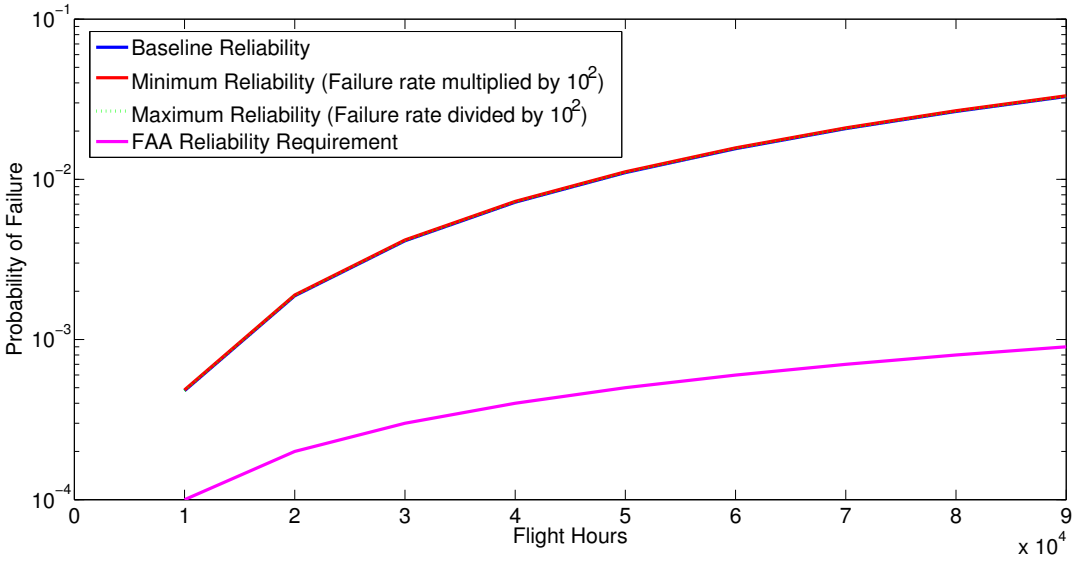

Figure 29: System reliability sensitivity to the bus failure rate

Figures 30 and 31 show that the inverter and motor failure rates have about the same effect on the overall system reliability. Decreasing their failure rate dramatically decreases overall system reliability. This occurs because if the components fail, there is no way to reroute power. For example, if bus 2 fails, power can be rerouted from bus three so that all the loads have power. If a load itself fails, there is no possibility of recovery. Figure 31 shows that increasing the motor reliability causes the system reliability to approach the reliability requirement. However, a two order of magnitude increase in reliability would be difficult, if not impossible, to achieve given current motor designs.

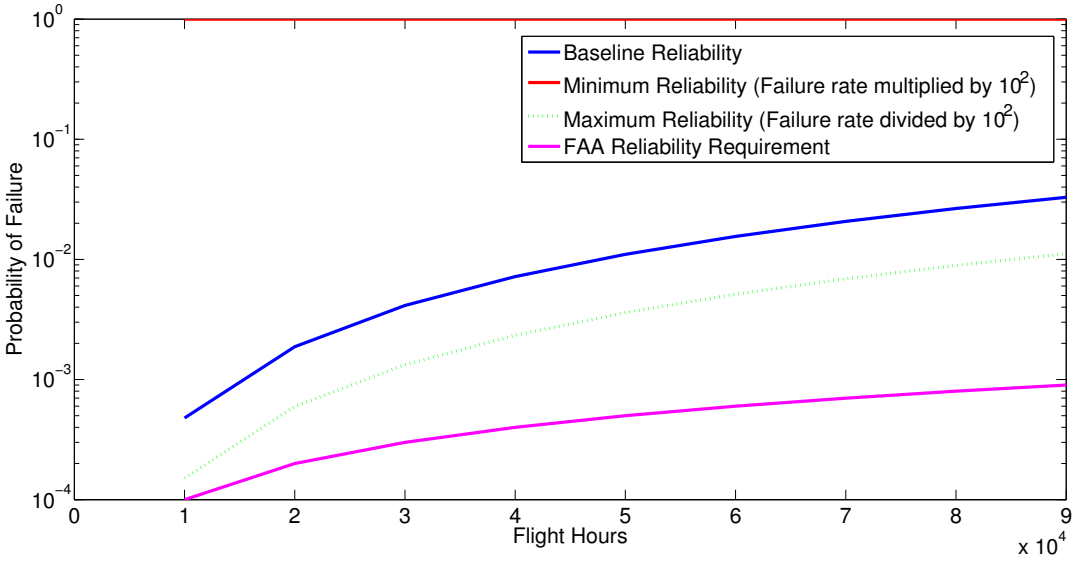

Figure 30: System reliability sensitivity to the inverter failure rate

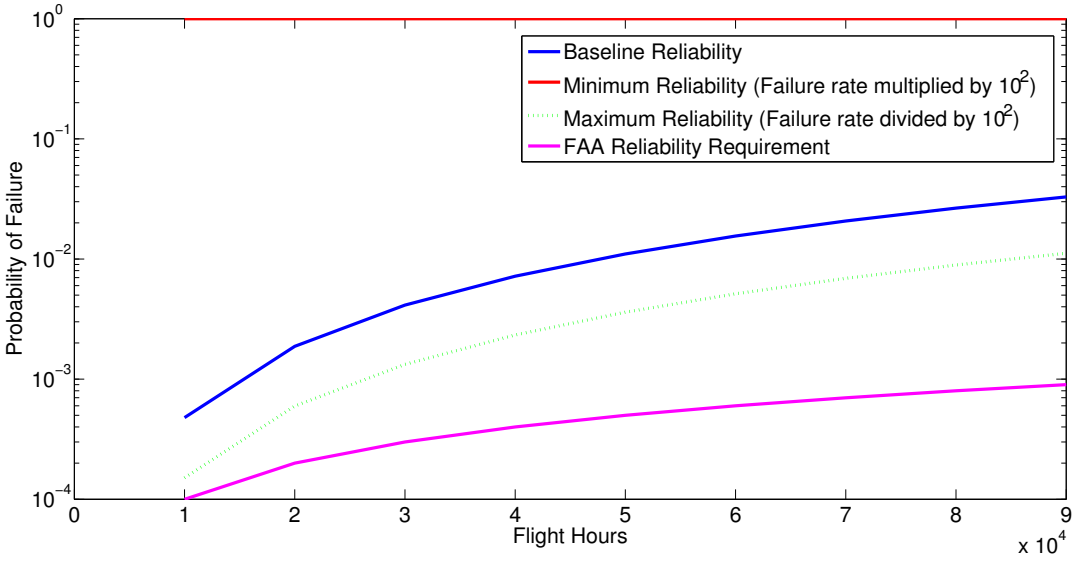

Figure 31: System reliability sensitivity to the motor failure rate

3.4 Baseline Evaluation Summary

The sizing and reliability analysis of the baseline architectures demonstrated a gap between the system performance the the system requirements. The weight of the

system using current technologies was massive and would not be viable for an aircraft. The reliability analysis showed that given the failure rate of components today, the baseline could not meet the reliability requirement. The maximum reliability study demonstrated that the reliability requirement could be met by increasing the size of the motors and increasing redundancy, but this resulted in a system weight that was double of the baseline system. The component failure rate sensitivity study showed that decreasing component reliability had large detrimental effect on system reliability. However, even a two order of magnitude decrease in failure rates for the components would not be sufficient to increase the system reliability to the reliability requirement.

To close the gap, either a new architecture with increased redundancy is needed or lighter, more reliable components will be required. Significantly increasing the component reliabilities would require new component technologies and designs. The next chapter will explore some technology options that could produce lower component weights and increase component reliability. Furthermore, the next chapter will explore the possibilities for changes to the architecture that could lead to a system that can meet the reliability requirement.

CHAPTER IV

IDENTIFY ALTERNATIVES

The analysis presented in the previous chapter has proved that current PDS architectures and technologies cannot meet the requirements of a turboelectric system. The gaps have led to the third stage in the RAAPS methodology – identify alternatives.

To implement this step of the methodology, a literature search is performed to identify PDS architecture and technologies that can offer capacity, size, efficiency, and reliability improvements over current designs, and the potential effects of the design choices are considered. Similar to how the baseline system was formulated, architectures are studied first. Next, a functional decomposition of the architectures is performed, and technologies to fulfill the functions are identified. Using the information from the literature search, a hypothesis will be formed about which architecture and technology combination can meet the system requirements and objectives.

4.1 Architecture Options

The architecture selection has an effect on the system feasibility, safety, availability, size, weight, efficiency, reliability, and cost [18]. The architecture level decisions that must be made include determining the required component types and the amount of redundancy needed.

4.1.1 Required Components

The first step in the architecture design is determining the components needed for the primary functions of the system including power production, conversion, and transmission. Regardless of the architecture designs made, generators will be the primary power source for the system and the motors will be the primary power sink.

The next step is address whether power transmission should be AC or DC. For the baseline study, DC transmission was chosen based upon the movement toward DC distribution in state-of-the-art power systems. This decision needs to be revisited to see if any improvements to the system performance can be made through the use of AC distribution.

As shown in Chapter 3, most commercial aircraft today primarily use AC distribution. AC distribution is used since the power from the generators is three-phase AC and many loads require AC power. Only a small amount of power has to be transformed for DC loads, so the size and number of power converters required is reduced.

The primary advantage of using AC distribution is reducing the amount of power conversion needed. Only AC transformers would be needed to change the frequency of the source power to the frequency needed to drive the loads. The lack of light weight, efficient power conversion has led to the supremacy of AC distribution in aircraft today; however, power conversion is quickly becoming lighter and more efficient allowing the use of DC distribution. DC transmission can offer many advantages over AC; some of these advantages include [88]:

- Reduced losses
- Reduction in insulation requirements
- The frequencies of the source and load do not need to be synchronized
- Storage elements such as batteries can be directly connected to the bus to provide supplemental power
- Regenerated power can be returned to the bus

DC transmission tends to be more efficient than AC transmission due to less line resistance. The increase in efficiency will be extremely important for the turboelectric

system. An issue with AC power is that it acts as a cyclic loading on the cable and will cause fatigue in the insulation. Since the DC power is relatively steady, fatigue is less of an issue, so less insulation can be used and the size of the cables can be decreased. Another consideration is that if AC transmission is used in the turboelectric architecture, the frequency of the generator and the motors would have to be synchronized or an AC/AC converter would have to be used. Synchronizing the frequencies of the generator and motor would work against one of the main advantages of turboelectric propulsion – decoupling the turbine and fan. The use of an AC/AC converter would add complexity and weight to the system. If DC transmission is used, synchronization of frequency is not a concern.

One possibility when using a turboelectric architecture is to use batteries or other storage devices for supplementary power which provide DC power. DC distribution would allow storage devices to be directly connected to the bus with limited use of power converters.

A final consideration is that many "more electric" technologies are capable of supplying regenerated power under certain operating conditions. If AC distribution is used, this can be a major problem. The regenerated power can contaminate the bus causing energy quality and frequency synchronization problems. In a DC system, regeneration is less of an issue. In most situations, any power could be fed directly back to the DC bus with minimal filtering and regulation.

Although DC transmission has its advantages, it creates a new set of challenges including the need for extensive power conversion. As shown by the DC distribution used in the baseline, a rectifier is needed to convert the three-phase AC power from the generators to DC; then, to supply AC loads such as the motors, the DC power must be converted back to AC using inverters. The power converters can significantly impair the system weight, efficiency, and reliability if the system is not properly designed; however, recent advances in power converter design will help mitigate these issues

[40]. On the other hand, the use of power converters may have its advantages. With proper design, they can add protection to devices by isolating zones of the architecture during a fault.

Given the advantages of DC distribution over AC distribution, it will be used for the turboelectric system which dictates the required components for the system. The components will be: generators, rectifiers, buses, inverters, and motors.

4.1.2 Redundancy Considerations

After the types of components needed for the system have been identified, the next step is to consider system redundancy. Redundancy is needed to provide the required capacity and reliability for the system. One part of determining redundancy is setting the number of each type of component.

Some design decisions have already been made for the N3-X power system. First of all, four generators will be used (two driven by each gas turbine). Furthermore, each generator will have its own rectification unit - meaning there will be four rectifiers. The exact number of buses has not yet been determined; three bus and four bus architectures are being considered. The number of motors is also a point of debate, yet two primary configurations have emerged. One uses 14 motors in a 4-3-3-4 grouping, and the other configuration uses 16 motors in a 4-4-4-4 grouping. (The 4-3-3-4 configuration refers to motors being grouped so that all motors in the group are fed by the same buses.) Lastly, each motor will need its own inverter - meaning that the number of inverters in the system will be equal to the number of motors. Depending on the motor and inverter design, the inverter may be used to help control the motor.

The second redundancy consideration is adding connection between components which is referred to as path redundancy. Whenever a connection is added to the system, redundancy will be increased, but switching and transmission components will need to be added which will increase the weight of the system. Another consideration

when adding redundancy to the system is component weight. As the number of connections increase, component weight upstream of the inverters and motors will also increase since components are sized to be able to feed all loads that are connected to it. A trade-off between system reliability and weight will have to be performed.

A final consideration for the system architecture is voltage. The detailed cable model created for the baseline evaluation demonstrated the system nominal voltage will affect component weight. In fact, the voltage selected will affect the size and efficiency of the entire system. Higher voltages lead to less current, so components become smaller and more efficient to a certain extent. However, increasing voltage will lead to significant safety risks due to possibility of shocks and arcing. Arcing is an important issue to consider in designing a PDS for aircraft. The voltage levels on aircraft are often regulated based on Paschen's Law. This law determines the possibility of arcing based upon voltage, distance between conductors, and surrounding air pressure [34]. The law is often presented as Paschen's curve which is shown in Figure 32. At any point below the curve arcing is not an concern; nevertheless, at any point above the curve arcing is possible. Tracking the system's operating point on Paschen's curve is a problem in aerospace applications because pressure is changing throughout the flight envelope and vibration could affect gap distance. Low voltages have always been used in aircraft so that there is no chance of reaching an operating point above the curve. Yet, in a turboelectric system low voltages will not be sufficient; accordingly, the proper safeguards must be built into the system to prevent arcing problems which includes increasing the amount of electrical insulation used. The increase in insulation will have a detrimental effect on component weight and will eventually begin to outweigh the benefits of decreasing current through the system. A detailed voltage analysis is outside the scope of this study, but could be included in future applications of the methodology.

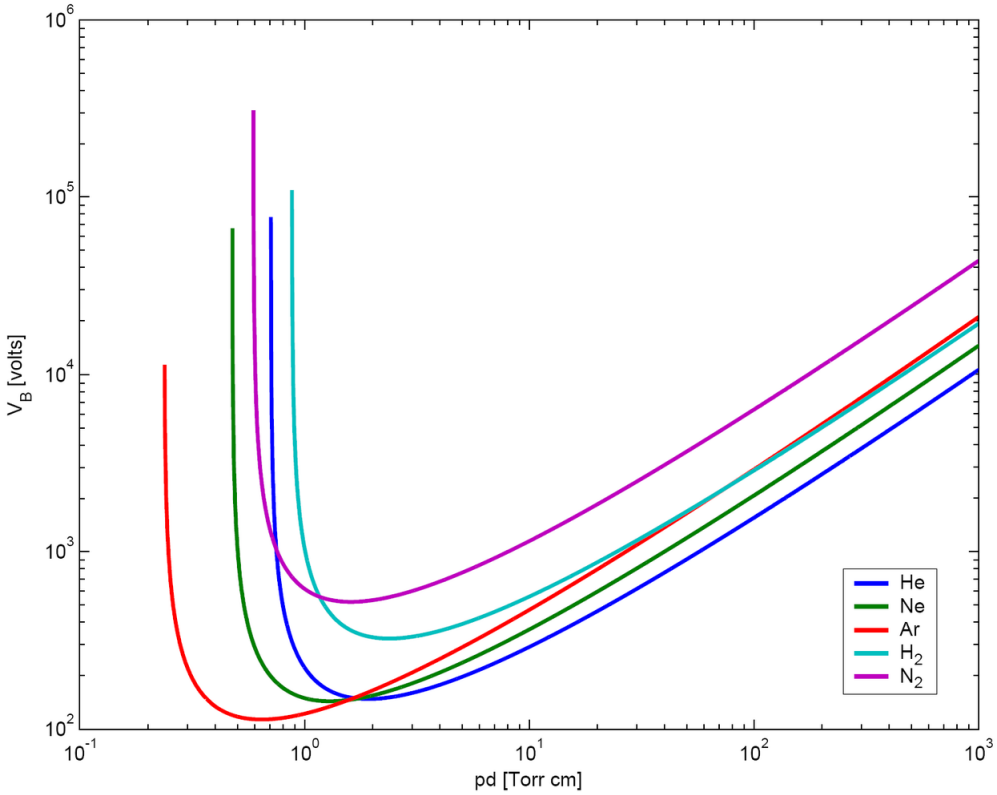

Figure 32: Paschen's Curve

In summary, the primary architecture alternative is changing the amount of redundancy in the system. Increasing the amount of redundancy will increase reliability, but will also increase weight. A trade-off study between reliability and weight will be important for the architecture selection. The next step is to consider the alternatives for the technology selection to help decrease system weight while increasing reliability by altering the performance of the system at the component level.

4.2 Technology Options

No matter which architecture is used, the system must carry out certain functions: power generation, power transmission, and power conversion. Power generation technologies have been extensively researched, so the alternatives explored will focus on power transmission and power conversion technologies. Power generation research has shown the superconducting generators and motors could provide significant weight savings and increased efficiency. The design of the superconducting machines is an ongoing area of research and limited information about the final design is currently available.

The primary components needed to fulfill the transmission and conversion functions are transmission cables, rectifiers, and inverters. A literature search will be conducted to identify upcoming technologies that could be used for the turboelectric system. The concepts behind the technologies are discussed along with their potential benefits.

4.2.0.1 Transmission Cables

One option for the transmission cables is superconducting cables. A superconducting cable has some unique properties that must be considered in its design. In order for a material to be considered "superconducting", it must distribute two properties – zero electrical resistance and perfect diamagnetism, when cooled below a critical temperature. The critical temperature is usually cryogenic (below 123 K). The zero

resistance property conveys that there are no losses when transmitting direct current [32]. The perfect diamagnetism property dictates that the material does not permit an externally applied magnetic field to penetrate into its interior [122].

The selection of transmitting in AC or DC will have a significant effect on the performance of the cables. If DC transmission is adopted, the cables will have no conduction losses [106]. Also, since high-temperature superconducting (HTS) DC cables only carry real power (there is no reactive power), there will be no significant derating of the cables [101] – meaning that the cables will not lose their ability to transmit their full power rating.

Another important superconducting cable design choice is the conductor material. The selection will have an effect on the weight of the cable and will determine the critical operating temperature which will drive the thermal management requirements for the component. A special class of man-made materials called high-temperature superconductors (HTS's) are superconducting at temperatures up to 134 K. The most widely used HTS is yttrium barium copper oxide (YBCO) [117] due to its low material cost and high critical temperature of 92 K , which is higher than the boiling point of nitrogen. The downfall of YBCO is that although the materials needed to manufacture YBCO are cheap, the manufacturing of the wire is complicated and expensive. Another widely used superconducting material is bismuth strontium calcium copper oxide (BSCCO). BSCCO has a much higher operating temperature of 110 K and is much less expensive to fabricate than YBCO wires. Anyhow, since YBCO was discovered first, it holds the majority of the market share and is the most widely used HTS material [31].

The final choice that must be made for a superconducting cable is coolant type. Popular options for cryogenic cooling are liquid hydrogen and liquid nitrogen. Hydrogen has the advantage of possibly being used as a fuel as well as a coolant, and it is extremely light [108]. But, the use of hydrogen causes safety risks. Nitrogen is an

inert gas with few safety issues, but it cannot be used as fuel.

A second cable type is carbon nanotube cables. Carbon nanotubes offer significant weight savings over copper and aluminum; for example, a 20 gauge copper wire weighs 4.6 grams per meter, while a carbon nanotube wire only weighs 0.2 grams per meter [73]. Also, with further research the resistance of the carbon nanotubes could be much lower than its copper counterpart. However, this technology is still in its infancy. Growing the carbon nanotubes is a complex task and researchers have only been able to make cables a few centimeters long [19]. Significant improvements need to be made in the fabrication of the wires to make carbon nanotubes a viable option for the N3-X.

4.2.0.2 Power Converters

Power converters are needed to transform power from AC to DC and vise versa. The goal of the power conversion is to obtain high efficiency while maintaining a reasonable system weight. A variety of options for power conversion exist which all give different efficiencies and have unique advantages and problems. The goal of this section is to investigate power conversion options and discuss their implications for a turboelectric PDS. Mostly, the power converters will be analyzed based upon a DC transmission system since power converter use will be more widespread in a DC architecture.

Rectifiers :

A rectifier is a device that converts AC power into DC power [120]. If a DC architecture is used, rectifiers will be required to convert the AC power from the generator to DC power to be supplied to the bus. The most important requirements of the rectifier are high efficiency, high power quality, and high specific power. High efficiency is needed in order to minimize losses in the propulsion system, and maintaining a high power quality will reduce instabilities in the system. High power quality is important so that the system remains stable and stays within performance limits. A high power density is needed on order to meet the component capacity requirements

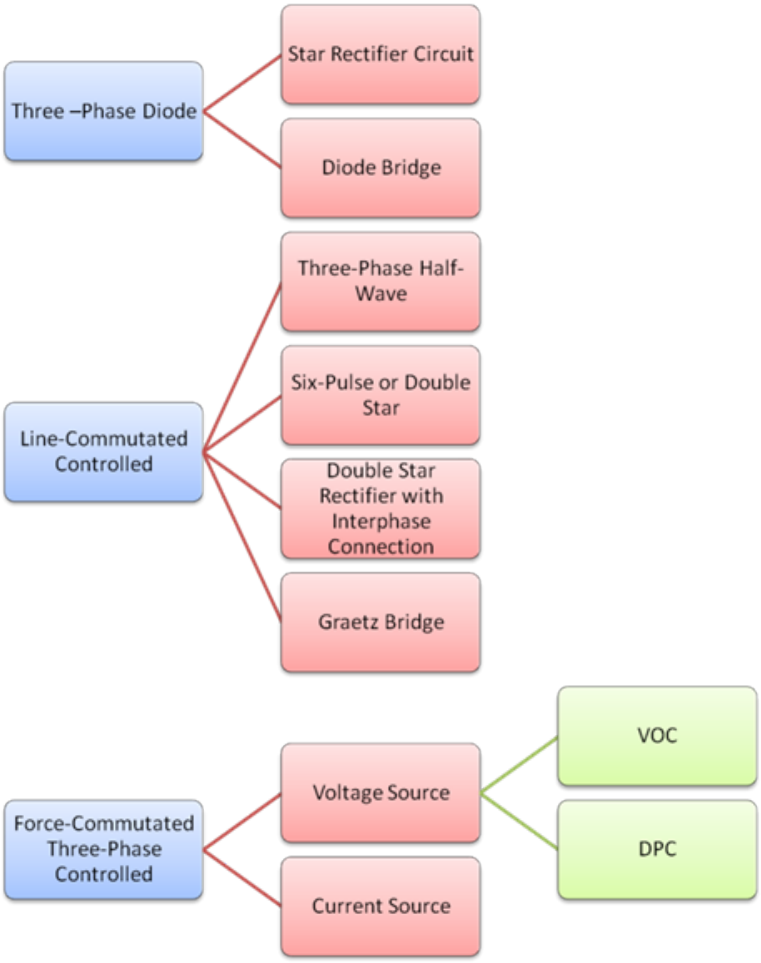

Figure 33: Rectifier design taxonomy

while minimizing component weight.

The possible three phase rectifier choices are outlined in Figure 33 [125]. The first choice is whether to use a diode rectifier or a controlled rectifier. The diode rectifier has the advantage of a simple operation scheme and less components; however, the rectifier output will contain harmonic contamination and may require the use of a filter. Also, the diode rectifier has a fixed voltage ratio between the DC voltage and the AC RMS voltage; therefore, if any change in voltage occurs at the generator, the bus voltage will be changed proportionally. Lastly, the power factor of a diode rectifier is fairly low.

In a controlled rectifier, the diodes are replaced by thyristors or an IGBT/diode

combination. Controlled rectifiers can target a given DC voltage based on the voltage requirements of the load. Depending on the control scheme selected, controlled rectifiers can provide a higher power factor than diode bridge rectifiers and the output will have less voltage ripple (which leads to higher power quality on the DC side of the rectifier). Although controlled rectifiers have many advantages, controlling the rectifier requires the addition of components such as switches, which can increase the size and complexity of the rectifier [125]; however, a diode bridge rectifier may require more filtering which will counter-act the weight problem for a controlled rectifier.

Controlled rectifiers can be broken down into two categories: line-commutated controlled rectifiers and force-commutated controlled rectifiers. Line-commutated controlled rectifiers have a similar set-up to the diode rectifiers; however, the diodes are replaced by thyristors. Line-commutated controlled rectifiers do not provide power factor correction, but they are used for some applications due to their simplicity and low cost. Figure 33 shows the different options available for line-commutated controlled rectifiers. The most popular choice is the Graetz bridge. The Graetz bridge is useful in high current situations and has less of a voltage drop than its counterparts [38].

Force-commutated controlled rectifiers actively control the opening and closing of switches to target a desired output. Actively controlling the switches allows them to be switched hundreds of times in one period, which is not possible in a line-commutated rectifier because the thyristors will only switch on and off once per cycle. The fast switching allows for the reduction of harmonics in the output voltage, controlling the power factor, and reversal of voltage at the DC link. Although the control scheme is more complicated, using this type of rectifier will give the propulsion system the highest efficiency and best power quality.

The force-commutated rectifiers can be operated as a voltage or current source. Theoretically, either selection could be used for this application; however, voltage

sources have fewer losses than current sources in power transmission applications. Losses in a voltage source application are proportional to the conductance of the insulation; while in a current source application, the losses are proportional to the conductor resistance. Generally, the conductor resistance is much greater than the insulation conductance; therefore, a voltage source rectifier was selected. In summary, the best efficiency and highest power quality will be achieved using a voltage source force-commutated controlled rectifier; however, there will be added weight to the system to realize these benefits.

For an actively controlled converter, a control strategy must be selected. For an actively controlled voltage source converter, the controller must maintain a given reference voltage for the DC link; therefore, a feedback controller is needed. Pulse width modulation (PWM) is the most commonly used control scheme because it can manage active and reactive power, which allows power factor correction [20].

PWM is used to generate a transfer function which determines which switches are on and which ones are off at any given point in time [153]. A specific type of PWM called Sinusoidal Pulse Width Modulation (SPWM) generates a transfer function by comparing a carrier signal to a control signal [81]. The carrier signal (modulated waveform) is a triangle wave that is used to create pulses which controls the switches. The control signal (unmodulated waveform) is a sinusoidal signal which is set to the frequency of the desired output waveform. Two primary types of PWM control exist; they are voltage oriented control (VOC) and direct power control (DPC). VOC uses PWM to control the DC link voltage and ensures a sinusoidal current input from the source. DPC controls the output by controlling active and reactive power. DPC determines switching states through a table based upon the sensed active and reactive power and does not directly control the current. VOC is usually used since it is more stable than DPC under highly dynamic conditions since the current draw is directly controlled.

If actively controlled power converters are used in the system, the architecture becomes a special subcategory of DC transmission called a power electronics based distribution system (PEDS). This name is derived from the fact that power electronics are used to control the power flow between components. With proper architecture design, PEDS's can offer great load regulation, good transient performance, and a high degree of fault tolerance [142]. Also, if a PEDS is optimized at the system level, it can provide cost savings and higher reliability than other types of power distribution systems. The reason that PEDS can offer these advantages is that it decouples the dynamics between sources and loads; however, designing a PEDS can be a complicated task. The controller of the power converters can be complex and will add additional weight to the system. Also, actively controlled converters can cause system stability problems since they act as a constant power load.

Inverter :

An inverter is a device that converts DC power into AC power. An inverter will be required in order to convert the DC power from the bus to AC power to drive the motors for the fans. As in the rectifier design, a high efficiency and power quality are desirable traits of the selected inverter design. Many of the same considerations from rectifier type selection apply to inverter selection. Like rectifiers, inverters can be classified as a voltage source or a current source. Voltage source inverters are the most common type of inverter. A voltage source inverter controls the output AC voltage magnitude, frequency, and phase. The motors require three-phase AC power, so a three-phase voltage source inverter is needed. As in the case of the rectifier, a control scheme is needed for the inverter. The most popular form of control is PWM. Pulse width modulation is used due to its high efficiency and fast response to transient conditions. PWM inverters also require less filtering than other inverters.

4.3 Hypothesis 2 and Experiment Plan

Based upon the literature search, several technology and architecture options are available that can significantly improve the capacity of the PDS system. The architecture analysis revealed that the primary decisions for the architecture are whether to transmit in AC or DC and the system voltage. The system voltage can be determined through analysis of the system and optimization; however, transmission type must be decided upon early in the design process. The literature search demonstrated that DC distribution has some distinct advantages over AC distribution for a turboelectric system; however, power converter type and design will greatly affect the overall system.

At the component level, many different technologies for power cables and power converters were considered. The cable technologies primarily consisted of two options – superconducting cables and carbon nanotube cables. Both options could significantly reduce system weight and improve efficiency, but superconducting cables are at a higher technology readiness level. Also, other superconducting elements such as generators will be included in the turboelectric system making them the better option for the turboelectric system.

A variety of converters will be available for the turboelectric system. Converter type is an option that will affect the system at the architecture and component level. Three categories exist for converter selection: diode bridges, line-commutated converters, and actively controlled converters. Actively controlled rectifiers have a higher weight than other rectifiers; however, they will provide higher efficiency and the possibility of added protection to the system. The main sources of losses for actively controlled power converters are switching losses and conduction losses. Both of these types of losses can be minimized by operating the device at cryogenic temperatures. Lowering the temperature to this level will significantly reduce the resistance of the materials used in the converter. The cryogenic temperatures also allow for faster

switching which will minimize switching losses [50]. By using actively controlled converters, a PEDS architecture can be achieved; this architecture will lead to an efficient and fault tolerant system. For a PEDS, VOC controlled converters will lead to the most stable and efficient design.

Using the observations about future technologies from the literature search, Hypothesis 2 is proposed:

Hypothesis 2: To meet the system design criteria the system must be comprised of superconducting technologies and must have a double redundant system (meaning that every motor can be supplied by either engine).

Double redundancy means that every motor group will have at least least one path connected to each engine. In order to test this Hypothesis 2, a virtual environment for testing and selecting PDS architectures and technologies is needed. The decisions that must be made using this process include the architecture type, the number of components, and which components should be connected. The design process is a difficult attribute to develop due to the high combinatorial nature of the problem. High level architecture decisions need to be made along with selecting component types that will lead to a light weight, reliable, and stable system. Evaluating every possible architecture and technology combination would not be feasible. So, a method for down-selecting from design combinations is needed which leads to the next step of the RAAPS methodology - down-select architectures.

CHAPTER V

ARCHITECTURE DOWN-SELECTION

When designing a PDS, both the architecture and component design must be addressed which leads to a large number of design variables and makes finding the optimal system design difficult. One way to approach the problem is to decompose the problem into two levels – architecture design and component design. Decomposition is possible if the two levels are reasonably decoupled.

5.1 Problem Decomposition

The first step in determining whether the problem can be decomposed into an architecture and component analysis is to investigate the interdependence of the two levels of the problem. One way to evaluate the interdependence is to determine the design variables for each level of analysis to see whether there is any overlap.

5.1.1 Architecture Design Variables

The architecture design variables will set the configuration of the system, which includes deciding the number and types of components in the system and the system interconnectivity. Among the most important architecture decisions is setting the number of each component and the connections between components which is illustrated in Figure 34.

As discussed in the previous chapter, the number of generators and rectifiers will be set to four. The number of motors could be either 14 (4-3-3-4 configuration) or 16 (4-4-4-4 configuration), and each motor will have its own inverter. The number of buses will vary between 3 and 4. In all cases, the number of each component is fixed or is a discrete variable.

The connections between the generator and rectifier are predetermined. Each generator will be connected to one rectifier. Also, each motor will be connected to one inverter. This is so that the converters can isolate the machines from other components in the system, which improves the fault tolerance of the system. The connections from the rectifier to the bus and from the bus to the inverters will vary. Any rectifier could be connected to each bus; however, every connection will require the use of circuit breakers to reroute power in case of a failure. Each bus can connect to any motor group. Again, protection devices will need to be used as connections are added. The connections can be treated as discrete design variables. Each possible connection location has its own variable. The variable is set to 0 if the connection is not active and is set to 1 if the connection is used. For example, consider a system with four rectifiers and four buses. A vector can be used to describe the connections, much like the use of the adjacency matrix. If each rectifier was connected to one bus, the vector would be:

c = [1000010000100001]

The first four digits are the connections from rectifier 1 to bus1, bus 2, bus 3, and bus 4. The next four digits are for rectifier 2 to the buses and this continues until all the connections from the rectifier to the buses are defined. The same notation is used for the bus to inverter/group connections.

A third type of design variables is setting the number of motors that are required to reach the critical thrust levels for the aircraft. When the baseline architecture was evaluated, the results showed that the engine-out requirement required that 12 motors be operational. When the motors were sized using the 12 motor setting for required power, the reliability analysis showed that the reliability requirement was not met. So, another study commenced in which the motors were resized such that only 8 motors out of 16 were required to meet the 20 MW requirement. With this change, the reliability of the system approached the reliability requirement. Therefore, the

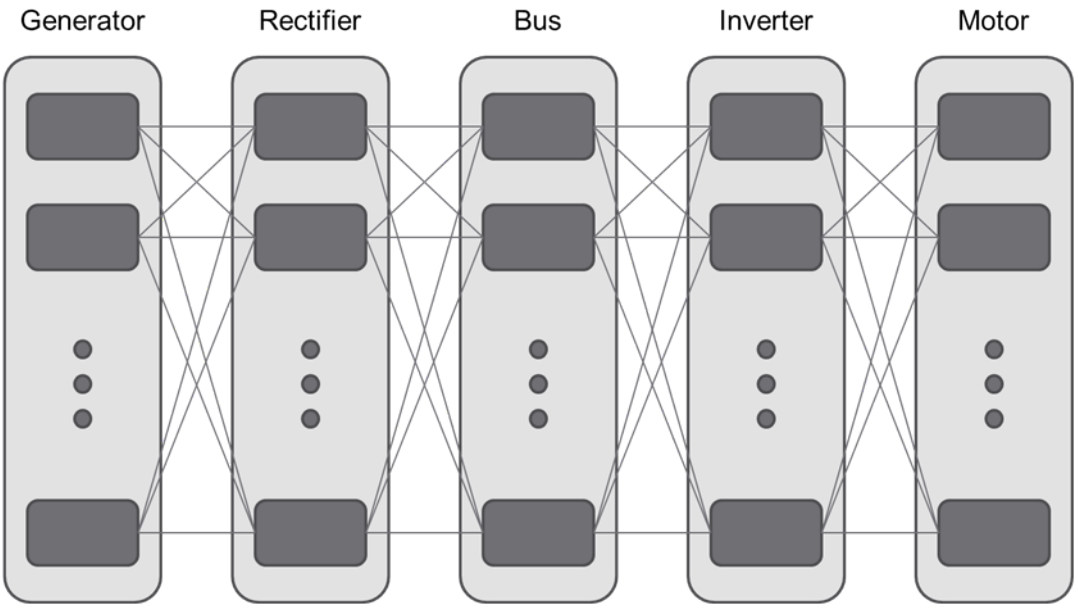

Figure 34: PEDS architecture

number of motors required to reach the power requirement is now treated as a design variable that can range from 1 motor to 16 motors.

Another important consideration is the technologies to use for each component. In the previous chapter, a number of technology options were discussed. The selection of technologies will have a great impact on system weight and reliability. Technology selection can be treated as a discrete design variable that determines the component power to weight ratio, efficiency, and failure rate. The previous chapter showed that cryogenic technologies offered significant improvements to the key performance metrics; therefore, in this study it is assumed that cryogenic components will be used.

The last variable that must be considered is system nominal voltage. Depending on the level of fidelity of the sizing method used, system nominal voltage could have an effect on component sizing. In this study, only the cables will be sized using a detailed model, so voltage will be held constant at 4,000 V. The cable weight is only a small percentage of the total system weight; consequently, a change in voltage will not have a large impact on the results.

Based upon the design considerations discussed, the architecture design variables

that will be considered are component type, number of components, and component connections. Using these design variables, the component capacities and weights can be determined, and system reliability can be calculated.

5.1.2 Component Design Variables

The component design variables will vary based upon the technologies used. Some general values that will have to be determined are component resistance, capacitance, and inductance. For the power converters, the number, type, and configuration of the switching components will have to be determined. Also, a control scheme will be required. The weight of the components will vary depending on these settings, but during the conceptual design phase little of this information will be available. The power to weight ratios used in the architecture analysis will allow the weights to be estimated, which allows a narrowing of the design space. Components can then be optimized for the selected architectures to reach a final design.

There will be some interaction between the two levels of analysis since the selection of technologies during the architecting phase will have a large impact on the component analysis stage. The use of power to weight ratios to estimate component weight helps decouple the architecture and component design process. The power to weight ratios will give an estimate of weight before detailed design. Of course, during the component design phase the updated weights should be compared to the estimates used in the architecture design phase to ensure there are no major discrepancies.

By addressing the two levels of design separately, the number of design variables for each design problem is reduced. By using this approach, the speed at which potential designs can be identified will be improved over combining the architecture and component design process. The thesis will focus on the architecture level design problem; however, some analysis on resulting architectures will be presented to demonstrate the capabilities of the methodology.

5.2 Methods for Architecture Down-selection

Now that the problem has been decomposed into an architecture and component level design problem, a method for down-selecting from the architecture design space is needed. The result of the analysis should not yield one design. Further study will be needed optimizing the components to reach a final overall system design. Nonetheless, the method should be able to identify desirable architecture attributes. Popular methods for finding the optimal design space include Design of Experiments (DOE) and optimization.

5.2.1 Design of Experiments

Design of experiments is an approach to extract information about the design problem without having to test all variable combinations. For most design problems, testing every possible configuration would be too time consuming and costly to be feasible.

Many different design of experiment approaches exist. Some design of experiments methods use orthogonal arrays to dictate design variable settings. By using orthogonal arrays, the effect of each design variable on the response can be determined. By determining the effect of the design variables, the desired settings can be determined. Other methods are simply used to explore the design space. Some methods focus on the interior of the design space and others focus on the edges. A random approach can also be used to get samples from the entire design space.

While DOE can provide guidelines for variable settings, it may not be able to locate the optimum design. Also, defining orthogonal arrays may be difficult due to the number of design variables and the interdependence of the design variables. The interdependence of the design variables will cause aliasing of the effects. In order to determine the individual effects of the variables, the number of runs would have to be increased.

Furthermore, the presence of discrete design variables limits the types of DOEs

that could be used for the problem. The only methods that can handle discrete variables and requires a feasible number of function calls are a random or latin hypercube design. The random approach may still require a large number of runs and key parts of the design space may not be evaluated. The latin hyper cube method is accurate toward the center of the design space, but has poor accuracy at the edges. If the optimal design lies in the edges of the design space, it may not be found. Based upon the shortcomings of DOE for this design problem, another approach needs to be considered.

5.2.2 Global Optimization Methods

Another option for locating potential designs is using global optimization. Global optimization procedures start with a random sample of possible designs and then manipulate those designs to meet the objectives and constraints using a variety of methods. Since global optimization methods use a random sampling to begin the process, they must be repeated multiple times to confirm a result. In some cases, the algorithms will not converge on the same design after each run which will reveal possible designs that have similar performance in regard to the objective and constraints. This attribute of global optimization methods makes them useful for this design problem. By running the global optimization multiple times, most likely a variety of designs will be produced that have similar weights and reliability, and resulting designs can be passed to the component design phase. Once the components are optimized for the architectures, a final design can be selected.

Due to the presence of discrete design variables, the optimization methods that could be used are limited. Discrete problems are best addressed using methods that rely on function calls alone. Derivative based methods would be difficult or impossible to use for the problem since the problem will contain discontinuities. The algorithms that can handle a problem with the design variables described are: genetic algorithm,

particle swarm, ant colony optimization, and simulated annealing. Each method will be discussed focusing on how it works, its pros and cons, and how it would be applied to the turboelectric PDS design problem.

5.2.2.1 Genetic Algorithm Optimization

Genetic algorithm (GA) is a zero-order optimization method that is meant to mimic the evolution of species [84]. A random population is selected in the beginning and then design variables "evolve" as better solutions are found. The following steps are used to perform a genetic search [151] [103]:

1. **Select a random population:** Each member of the population is composed of a string, often referred to as chromosomes, which corresponds to the setting of each design variable. The most popular method of creating the string is using binary numbers. The length of the string is dependent on the resolution needed for each design variable.

2. **Evaluate each member of the population using a fitness function:** The fitness of a chromosome is determined by its ability to meet the objective of the optimization process while not violating any constraints. If a member of the population violates a constraint, a "penalty" is added to the fitness function. The severity of the penalty is determined by the severity of the constraint violation.

3. **Perform the reproduction step:** The reproduction step is begun by selecting two parents out of the current population. A common method of selecting parents is called roulette selection. In this method, the fitness function of each potential parent is normalized so that the sum of the normalized fitness functions equals 1. Next, a section of the "roulette wheel" is assigned to each chromosome. Each chromosome is assigned a section of the roulette wheel which is

proportional to its normalized fitness value; then two locations on the wheel are randomly selected to determine a set of parents. This method gives the chromosomes with a high fitness value a higher chance of being selected; however, selection of some parents with poor fitness value does occasionally happen. This is important so that the algorithm does not get stuck in a local minimum. The parent selection continues until the number of pairs of parents is equal to half of the population.

4. **Perform cross-over step:** A probability of cross-over is set for the algorithm; then a number between 0 and 1 is randomly selected for each set of parents. If the random number falls between 0 and the given probability, the cross-over is performed. During the cross-over a section of the two parent chromosomes is randomly selected to be swapped. The two new chromosomes after the swap are the children and become members of the next generation.

5. **Perform mutation step:** In the mutation step, each child may be randomly mutated. The probability of the mutation occurring is set to a very low number; however, if the mutation does occur, then one bit is randomly chosen and swapped – 0 to 1 or 1 to 0.

6. **Repeat from step 2 until a termination criterion is achieved:** Common criteria that are used are a maximum number of iterations and reaching convergence. Convergence means that the highest fitness function in the population stays the same (within a given tolerance) for multiple iterations.

The advantages of the genetic algorithm are its ability to manage discrete variables and nonlinear problems. The genetic algorithm can handle discrete and continuous variables since it uses binary strings. If the variable is discrete, the string length can be set to only produce integers within a given range. For continuous variables a resolution has to be determined so that the number of bits needed to represent the

variable can be determined. The reason a GA can handle nonlinear problems well is its large population size and random selection. If a large population is initiated, it should cover the design space well. The reproduction and mutation steps slowly move the points around the design space to find the optimal solution. GA is a widely used method due to its ease of implementation and large coverage of the design space. Since it has been used in a variety of scientific fields, many variations exist to exploit certain properties of the algorithm.

Although GA has its advantages, it has a couple of problems. First of all, it is computationally inefficient. Very little information is carried between each iteration. A second problem is that it requires a high number of function calls which can be a major problem when optimizing a complex system.

The ability of the GA to handle discrete variables while optimizing using only function calls is useful for the turboelectric PDS design problem. Also, since many variations of the algorithm already exist, implementation will be easy; however, the reliability analysis used for each function evaluation can be slow if the connectivity of the system is high. The number of function calls needed to carry out a GA could be problematic.

5.2.2.2 Particle Swarm Optimization

Particle swarm is an optimization method that mimics the behavior of a flock of birds or a school of fish that has received increased attention for the design of power systems [5]. This method does not explicitly handle discrete variables, but variations of the method are available that allow the use of discrete variables. The steps in particle swarm are:

1. **Initialize particle positions and velocities**: Like the genetic algorithm, a random population is generated. The design variable settings are the position of the particle. A starting velocity for each particle is also initialized.

2. **Evaluate the fitness of particles**: Evaluate the objective function and penalty function for each member of the population.

3. **Update particle velocities based upon the "most fit" particles** (the most fit from current iteration and the most fit overall): The particle velocity will determine what direction and how far each particle will move in the iteration. The velocity is determined based upon the location of the most fit particle in the population and the best location found during all the iterations.

4. **Move particles based on time step and velocity**

5. **Repeat until converged**

Literature has shown that in general particle swarm requires less function calls to reach convergence than other zero order methods such a GA. The downside is that since more information is being carried through iterations than GA, it requires more storage space.

Particle swarm could be useful for the PDS design. While it has the capability to handle discrete variables and only relies on function calls, literature has shown that it can converge much faster than a GA [64]. Since the model of the system is complex, being able to converge in less iterations could be a distinct advantage of the particle swarm method.

5.2.2.3 Ant Colony Optimization

The ant colony optimization method is inspired by the routine that ants use to search for food. At first, ants scatter from their nest in the search for food. As they move away from the nest, they deposit pheromones that other ants can track. When a path to food is found, more ants move along the path increasing the pheromone value. The steps for ant colony optimization follow the same logic. The food is considered to be the best solution and the paths are the settings for the design variables [99]. One

major disadvantage to this method is that it can only handle discrete variables. If continuous values are needed, a range must be selected and then discretized. The steps for ant colony optimization are as follows [39]:

1. **Initialize graph** – determine the possible settings for each design variable
2. **Ant moves from vertex to vertex** – meaning the value of each design variable is selected (At each vertex the path of an ant is determined probabilistically – paths with a higher pheromone value are more likely to be selected)
3. **Evaluate the fitness of the solution using the design variable values selected in step 2**
4. **Update pheromone values based on fitness**
5. **Repeat from step 2 until converged**

The primary advantage of ant colony optimization over other zero-order methods is that it can be applied to systems that change dynamically. In the turboelectic problem, ant colony optimization could be useful for determining the system architecture since it is specifically formulated for graph problems. However, the basic method is generally used for graphs with a single source and sink. Some modifications will be needed to be able to use this method for the turboelectric design problem.

5.2.2.4 Simulated Annealing

The final method that will be discussed is simulated annealing (SA). The name for this method is inspired by the heating and cooling of materials to increase the size of their crystals and reduce their defects. The steps for simulated annealing optimization are as follows:

1. **Initialize population** (i.e. set design variable values)

2. **Perturb the placement of each point through a random move**

3. **Calculate the fitness of each original point and the point after the perturbation**

4. **Determine whether to accept the move** (Moves that produce superior points are always accepted; inferior points are accepted with a given probability.)

5. **Update and repeat from step 2**

The advantages of simulated annealing are that it guarantees convergence with enough iterations and is easy to program. One major disadvantage is that it is slow to converge. Each iteration requires two function evaluations causing it to be much slower than other zero-order methods. Also, many studies have shown that other algorithms generally produce better results than SA. Since this method is slow and has trouble converging on the optimum, it is of little use for the turboelectric PDS design problem.

5.2.3 Optimization Methods Observations

Each optimization method discussed has its advantages and disadvantages. Simulated annealing is eliminated from contention since it has difficulty finding the optimum and is slow. The other three methods could be useful and further study is needed to determine the best method for the system architecting problem. Nonetheless, due to the problem complexity and slow run time of the model, the reduced iterations for particle swarm becomes important; therefore, Hypothesis 3 is formed:

Hypothesis 3: Particle swarm can find optimal architecture and technology combinations that meet the PDS requirements with minimal iterations

In order to test Hypothesis 3, the system must be optimized using a variety of optimization methods. The first step is to initialize the optimization process for each method. This process includes identifying design variables, creating an objective function, and developing constraint functions. Next, each algorithm must be implemented. Lastly, the optimums and run times for the different optimization methods will be compared.

5.3 Requirements and Objective Evaluation

Regardless of the optimization routine used, a given system design must be evaluated based upon the system objectives and requirements. The evaluation technique used will be similar to the approach used to evaluate the baseline which is shown in Figure 35. First the system capacity will be calculated based upon the engine-out requirement. Once the capacities are set, the weight of the components will be calculated in order to determine system weight. New weight models will be needed since different technologies will be in use versus the baseline. Lastly, system reliability will be calculated and a penalty function will be evaluated.

5.3.1 Capacity Requirement

The same capacity requirement evaluation will be used that was demonstrated with the baseline system with a slight modification. If an engine fails, enough power must be available for the motors for takeoff which can be treated as an equality constraint. Now there is also a design variable that dictates how many motors need to be operational to meet the power requirement. The motor sizing will commence with the minimum of the motors required by the engine-out scenario and the motor requirement variable.

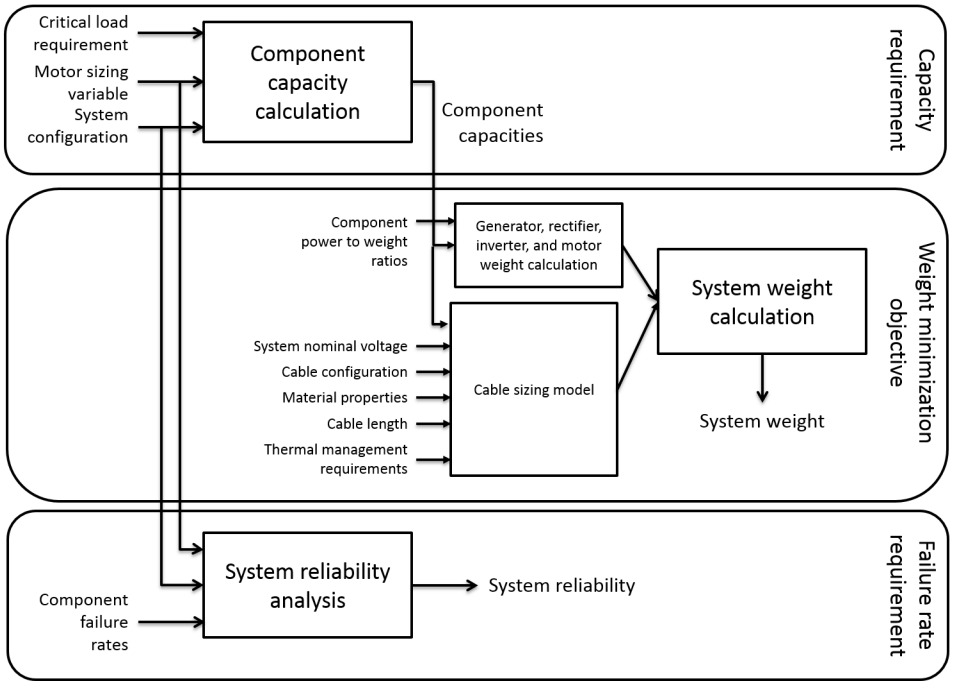

Figure 35: Modeling Environment Overview

5.3.2 Weight Calculation

Since new technologies are being considered for the system, especially cryogenic components, a new sizing model for the components will be required. Like the evaluation of the baseline, power to weight ratios are used to size the majority of the components. However, the superconducitng will be sized with a higher fidelity code to demonstrate how to incorporate this type of model into the optimization methodology. Furthermore, an approach to power converter sizing will be discussed.

5.3.2.1 Superconducting Cable Sizing

The structure of a superconducting cable is quite different from a room temperature cable. (The configuration of the HTS cable is shown in Figure 37.) First of all, the conductor is not a cylindrical core; instead, superconducting wires are made in "tapes" [106]. The structure of the tape is shown in Figure 36. In order to make the cable in a cylindrical shape, the tapes are wrapped around a former. Two layers of superconducting tape are used. The inner tape is the supply and the outer tape is

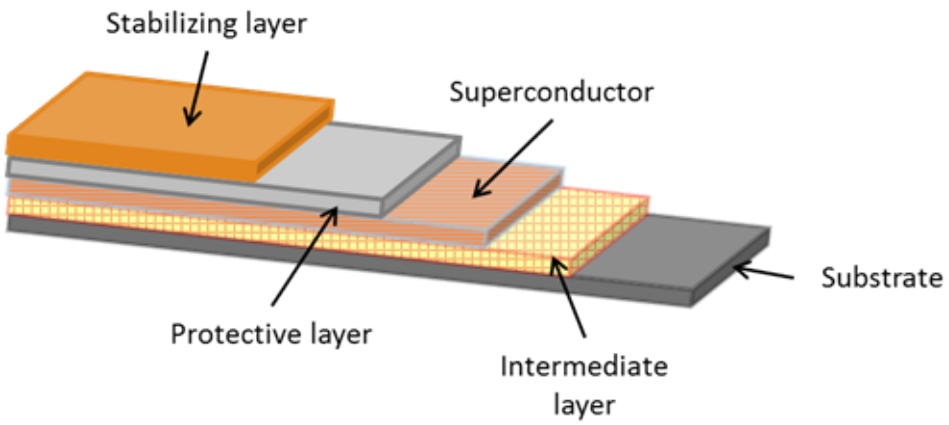

Figure 36: YBCO tape structure

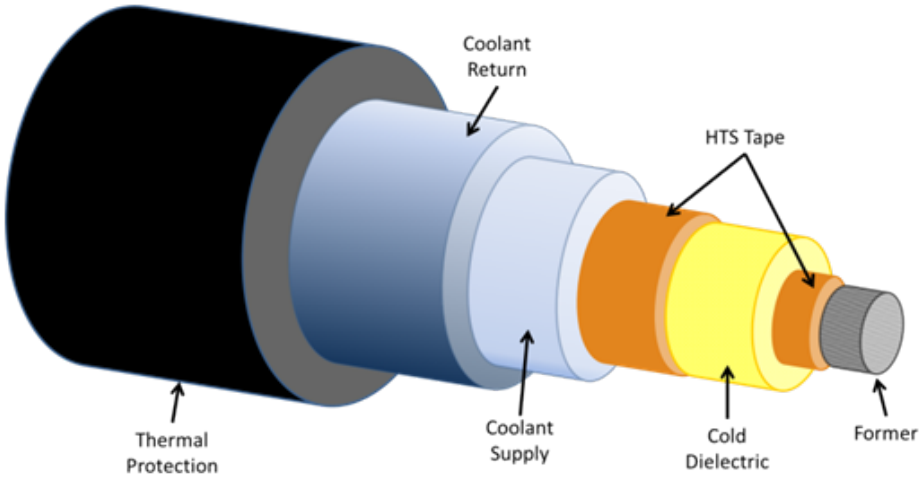

Figure 37: Simple HTS cable configuration [154]

the return. Between the two conductors is a layer of dielectric shielding. This is the only shielding required due to the perfect diamagnetism of the cable. The cryogenic coolant flows through a cooling sleeve surrounding the cable.

In order to determine the size of the wire, the following parameters must be determined: HTS tape material, HTS tape thickness, HTS tape winding pitch, dielectric thickness, coolant type, former diameter, and outer cable diameter. Based on current research, the most widely used superconducting material for this application is yttrium barium copper oxide (YBCO), which is the most cost effective option for the current carrying capacity required for this application. Studies have shown that

YBCO tapes have been created that have a critical current density of 1.4-1.5 MA/cm^2 [137] [65]. The current carrying capacity of these wires is about 400 A per cm of wire width [43]. When the wires are transmitting direct current, the amount of power that the wire can carry is proportional to the volume of the wire.

The thickness of dielectric shielding layer is dependent on the cable dimension of the former and HTS tape, the system nominal voltage, and the design stress of the insulation. The thickness is directly proportional to the voltage of the wire.

Along with the electrical tape and insulation, the cable also includes a thermal management system. The purpose of the thermal management in the wire is to keep the superconducting tape under the critical temperature. There is no heat generation in a continuous DC superconducting tape; however, in the actual system there are joints and imperfections in the cable that cause a small amount of heat production which is estimated to be around 5 W/m [21]. There is also heat invasion from the cable's surrounding environment which Hirose estimates to be about 0.7 W/m/Cable [66].

Cryogenic temperatures in the cable are maintained using a cooling sleeve as the outer layer. The cooling sleeve consists of a supply channel and a return channel. Some HTS cable designs place the coolant supply channel within the former. This design is not chosen because if supply stream is within the former, it will be at high voltage, and the high voltage of the supply stream will require the use of high voltage brushes at the refrigeration points [33]. Liquid nitrogen is chosen as a coolant because its temperature is well below the critical temperature of YBCO, even with some temperature rise over the length of the cable [1]. The diameter of the tube and the flow rate of the hydrogen are determined by the amount of heat that must be dissipated and the allowable pressure drop in the coolant channel. Once the fluid has traveled through the tube, it is returned back to a chiller through a shell inside the cable. This shell is placed as an outer layer of the cable so that the returning

hydrogen can be used as an insulator for the cable.

When designing a superconducting wire, there are three parameters that must be kept in mind: the critical temperature (T_c), the critical magnetic field (B_c), and the critical current density (J_c). If any of these three values is exceeded, the wire will "quench", i.e. no longer be superconducting. The critical temperature and critical magnetic field are properties of the wire material. The critical magnetic field is dependent on the operating temperature of the wire. The critical magnetic field can be calculated based on temperature, critical temperature, and the critical magnetic field at absolute zero ($B_c(0)$) [122].

$$B_c \approx B_c(0)[1 - (\frac{T}{T_c})^2] \tag{50}$$

Another useful parameter is the critical current [130], which is based on the critical current magnetic field [122].Using Ampere's law, the critical current is

$$I_c = \frac{2\pi B_c R}{\mu_0} \tag{51}$$

The sizing algorithm for the superconducting cable is much different than the room temperature cable since there are no transmission losses; therefore, the cable must be sized based upon critical current. The basic steps of the algorithm for HTS cable sizing are outlined in Figure 38. The first step is to determine the number of cores. Typical HTS cables have between one and three cores [121]. The critical current density is dependent on the wire design and, therefore, can be altered. The wire design is often optimized based on the desired critical current density. Typical values for critical current density of YBCO are used to begin the sizing process. Using the critical current density, critical current can be calculated. The system nominal voltage also has to be set. This value is varied in the model to determine what voltages can be used for the turboelectric application. Next, the sizes of each layer of the cable are determined. The cooling is designed such that the temperature

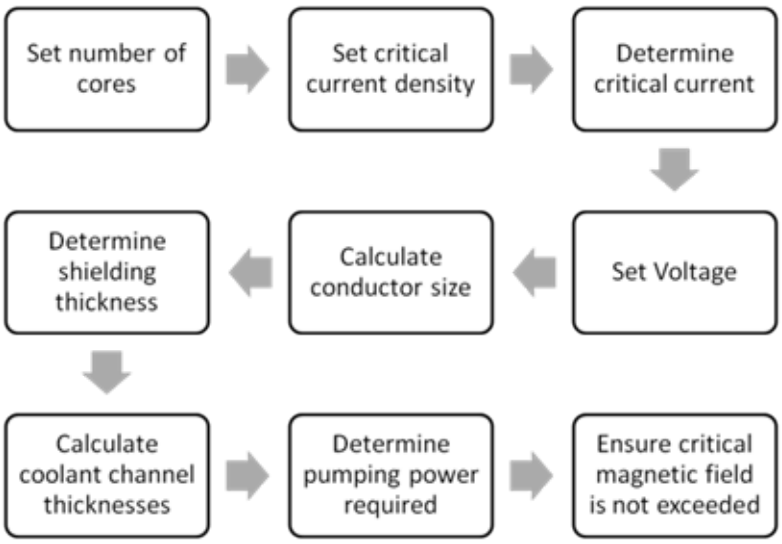

Figure 38: Superconducting cable design flowchart

Table 26: Superconducting cable parameters

Parameter	Value
Cable length	9 m
Dielectric breakdown strength	5e-8 m/V [97]
Dielectric density (PPLP w/LN2)	1000 kg/m^3 [61]
Coolant specific density (LN2)	807 kg/m^3 [47]
Coolant specific heat (LN2)	2.042 J/gK [80]
Coolant viscosity (LN2)	2 g/m*s[131]
Former density (copper)	8960 kg/m^3 [51]
Estimated power losses	5 W/m [21]
Conductor density (YBCO)	6300 kg/m^3 [105]
Thermal management pipe density (stainless steel)	8030 kg/m^3 [141]

of the cable never exceeds the critical temperature of the superconducting material. The pumping power is calculated for the thermal management system in order to determine how much more power the system will have to draw from the generator. Lastly, the cable is checked to ensure that the critical magnetic field is not exceeded.

Cable Sizing Model Validation The cable model was tested using a range of voltages from 1kV to 10kV. Power capacity was also varied from 4 MW to 40 MW. The parameters used for the model are listed in Table 26.

The results of the cable sizing models are shown in Figures 39 and 40. The coloring

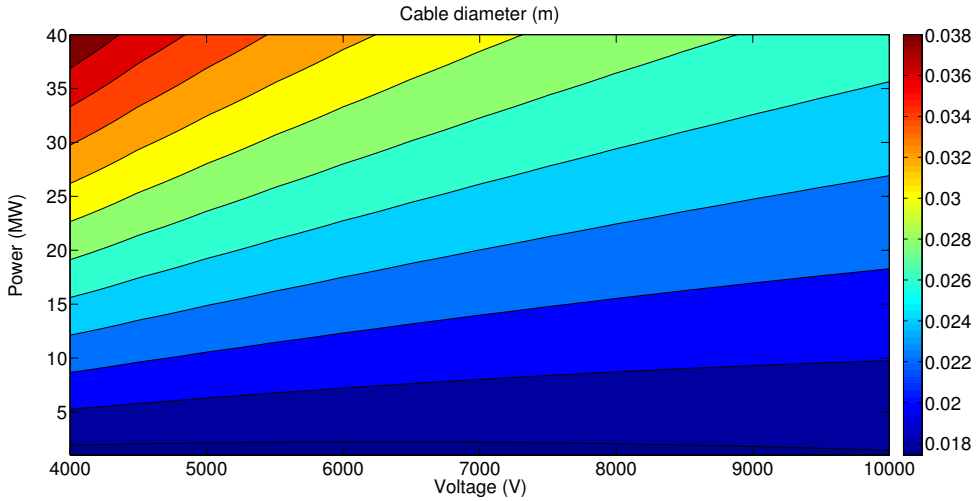

Figure 39: Superconducting cable diameter

on the plots show the effect voltage and power on cable diameter and weight. Like the room temperature case, the blue area of the graph is the region that produces that smallest cable. Similar trends are observed with the room temperature cable model, but the weight and diameter is greatly decreased. Cable diameter decreases with voltage because less conductor is needed, and in result, the current requirements are smaller. However, at high voltages, the amount of dielectric shielding increases which begins to overcome the benefit of being able to use a smaller conductor. The same trends are observed in the cable weight plot.

5.3.2.2 Power Converter Sizing

For the superconducting system, the inverters must be cryogenic in order to have an acceptable efficiency. If the efficiency is too low, then it negates the effect of using a superconducting bus. The estimated efficiency of cryogenic inverters is 98.8%. In comparison, a room-temperature inverter efficiency will be around 90%. The weight of a cryogenic inverter with a 20 MW power rating is approximately 2,450 kg [21]. The weight of a room-temperature converter would be similar; however, the cable weights will increase to make up for the lost power. The rectifier weight will be comparable

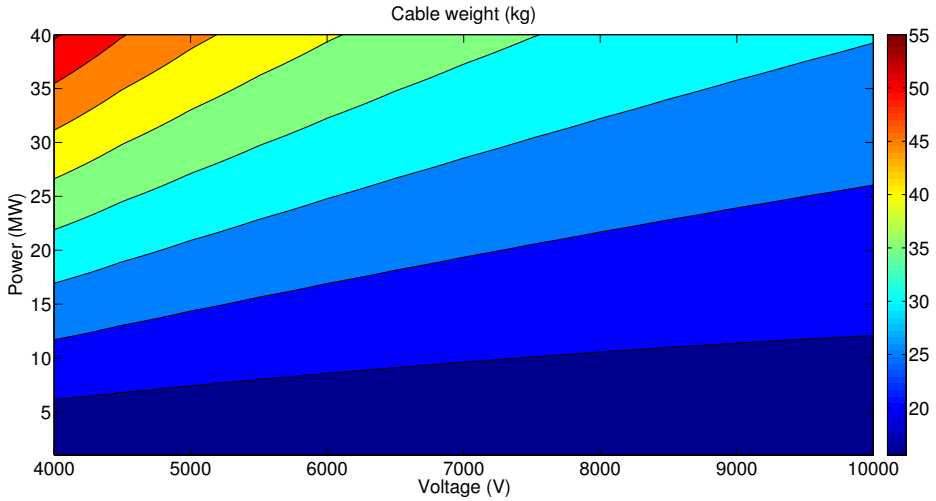

Figure 40: Superconducting cable weight

to the inverter weight. The power to weight ratio for the cryogenic power converters is about 24 kW/kg.

While it is recommended to use power to weight ratios at this stage of design in order to have reasonable computation time for the optimization, more detailed power converter sizing methods could be used. The component weights will depend on the number and size of each electrical element such as capacitors, resistors, and inductors. Two approaches exist for finding the weights. The first is to use a look-up table for each component and find the element's weight based upon its capacitance, resistance, or inductance. This approach has the advantage of being able to optimize the system using off-the-shelf parts; however, this will, most likely, limit the performance of the system. The second approach to getting the weights of each component is to calculate element weights based upon their geometry and material density. The advantage of this approach is that the optimum configuration can be found; however, the disadvantage is that most likely off-the-shelf parts will not fit the specifications given by the optimization process. Either special parts would have to be created for the system, which would be costly, or the outcome of the optimization process would have to be rounded to the nearest off-the-shelf value, which could lead to sub-optimal

performance.

For a conceptual design phase, the second approach of determining each element's weight is recommended so that the optimum configuration can be found. In later phases of the system's development, if it is determined that off-the-shelf components need to be used to maintain a reasonable system cost, then the algorithm can easily be adapted to include look-up tables.

The relationships to calculate the weight of each electrical element were adapted from the work of Chandrasekaran [29]. The first element discussed is an inductor. If the inductor can be modeled as an EE core, its weight can be estimated as the sum of the weight of the ferrite and copper used for the core and windings.

$$W_L = W_{fe} + W_{cu} \tag{52}$$

$$W_{fe} = \rho_{fe}[2 * (1 + K_2)W_w + \frac{\pi}{2}C_w]K_1C_w^2 \tag{53}$$

Where,

$$W_w = \frac{W_b}{W_{bob}K_2} \tag{54}$$

$$W_{cu} = \rho_{cu}[2F_cC_w(1 + K_1)]n_{turns}A_{cp} \tag{55}$$

Where,

$$A_{cp} = \frac{W_aF_w}{n_{turns}} \tag{56}$$

The description of each parameter is given in Table 27. The aspect ratios can be fixed and the other values are determined by the inductance.

$$L = \frac{\mu_0K_1C_w^2n_{turns}^2}{l_g} \tag{57}$$

Table 27: Component weight calculation variables

Parameter	Description
ρ_{fe}	Ferrite density
ρ_{cu}	Copper density
A_{cp}	Cross-section area of winding
C_w	Center leg width
F_c	Pitch winding factor
K_1	Aspect ratio of the center leg
K_2	Aspect ratio of window
l_g	Airgap length
n_{turns}	Number of turns
W_a	Window area
W_b	Bobbin area
W_{bob}	Thickness of bobbin wall
W_w	Window width

The weight of the capacitors can be estimated as

$$W_C = \alpha_C C V_C^2 \tag{58}$$

C is the capacitance of the capacitor and Vc is the capacitor's voltage. α_C is a coefficient that is determined based upon manufacturing data for a given capacitance.

The weight of the resistors can be calculated as

$$W_R = \alpha_R \int_0^t R \cdot i_R^2 \cdot dt \tag{59}$$

R is the resistance, i_R is the current through the resistor, t is time, and α_R is a coefficient found using resistor manufacturing data.

The resistance, capacitance, and inductance of the converter will be determined by power and stability requirements. At this point in the design, little is known about these requirements. Therefore, the optimization process will still rely on the use of power-to-weight ratios. During the component design phase, the power-to-weight assumptions used can be evaluated using the sizing approach that has been described.

5.3.2.3 Machine Sizing

The generator and motors will be sized using power to weight ratios. The expected power to weight ratio for superconducting generators is 22 kW/lb. The estimated power to weight ratio for fully superconducting motors is 10 kW/kg.

5.3.3 Reliability Requirement

As in the the study of the baseline, the stochastic flow network approach is used to evaluate system reliability. The component failure rates are updated based upon the new technologies that are being considered for the system.

Estimating the reliability of superconducting components is difficult. Some tests have revealed that the failure rate of a superconductor is less than one failure per million years [90]; however, this only applies if the superconductor remains in a superconducting state. In order to be superconducting, cryogenic temperatures must be maintained for each superconducting component, which requires the use of a cryocooler. Currently, the failure rates of cryocoolers are relatively high. Unfortunately, a failure of the thermal management of a superconducting component would result in the component quenching (that is, it will no longer be superconducting), which would severely hinder the power capacity of the component and cause the component temperature to rapidly rise. In the event of a quench, the component would have to be shut down to prevent further damage to the system thus creating the same result as a component failure.

The most reliable cryocoolers that have been built to date are small cryocoolers used for space applications. These cryocoolers use a redundant architecture that reaches a failure rate of about 3.4e-7 failures per flight hour [129]. This is the failure rate that will be used for the super conducing components because it is assumed that the cryocooler failure rate will drive the failure rate of the overall system.

In the future, more reliability testing of superconducting components will be performed and this assumption can be validated or the failure rate of the components can be updated.

5.3.4 Solution Fitness

Each solution must be evaluated based upon the objective and requirements. The best solutions will have a minimal weight while meeting the requirements. The requirements will act as constraints on the problem; however, the zero-order optimization methods that have been discussed cannot explicitly handle constraints. Therefore, "fitness" is used. Fitness is a combination of system weight and a penalty. A penalty is added when a system design violates a constraint, so the weight of the system is artificially inflated. In result, the algorithms will strive to minimize fitness rather than weight.

The capacity requirement is evaluated as an equality constraint, so it can be ignored in the fitness calculation. However, a penalty does need to be added to the fitness if the reliability of a system is less than the reliability limit. The reliability of the system is evaluated at several time points, so the penalty will be commutative across all the time points. The time points will increment at 10,000 flight hours to the lifetime of the system, t_{max}. The penalty used in all the algorithms is

$$p_t = \sum_{i=0}^{t-1000} p_i + e^{-c*100} + 1e5 \tag{60}$$

$$c = r_t - e^{-L*t}, t = 0, 1000, ..., t_{max} \tag{61}$$

p_t is the penalty incurred at time t. c is the amount the constraint was violated by at time, t. The penalty is only incurred if c is less than zero. L is the acceptable system failure rate. The penalty is evaluated for all time steps to calculate the total penalty. The total penalty is added to the system weight to get system reliability.

5.4 Down-selection Implementation and Results

The architecture will be optimized multiple times using the genetic algorithm, particle swarm, and ant colony optimization methods. The results of each method will be analyzed along with the performance of the optimization algorithms.

5.4.1 Genetic Algorithm Optimization

The first optimization routine that will be discussed is the genetic algorithm. First, the steps of the process are explained, and then the results will be discussed.

5.4.1.1 Algorithm Formulation

The first step in the process is to generate a random population. The population size that was used was 100. A smaller population may have trouble converging. Conversely, adding members to the population may help convergence, but will increase run time for each iteration. A population of 100 was the best balance found after several tests. Each member of the population is a binary string that contains the settings of each design variable. The first digit determines whether the system has 3 or 4 buses. A zero indicates 3 buses and a 1 indicates 4 buses. The second digit determines the motor group configuration. A 0 indicates a 4-3-3-4 configuration and a 1 indicates a 4-4-4-4 configuration. Next, a binary string is used to set the motor number requirement which can vary from 1 to 6. A five bit string is needed to cover the integer range.

The next portion of the design variable string determines the rectifier to bus connections. The rectifier to bus connection string is formulated by assigning each rectifier with a number of bits equal to the number of buses. A one represents that a connection between a given rectifier and bus exists. A zero means that the connection is not present in the design. For example, if the system has three buses, 12 bits will be needed to describe all the rectifier to bus connections. Bits 1-3 will show if rectifier 1 is connected to bus 1, bus 2, or bus 3. This is repeated for rectifiers 2, 3, and 4.

The same process is used to define the bus to motor group connections in which each bus will be assigned four bits (the number of motor groups).

Once the population has been initialized, the capacity constraint is evaluated for each population member. After the required capacity for each component is determined, the component weights are calculated. The weights will be the first part of the fitness of each member of the population. Next, the reliability constraint is evaluated. If the constraint is violated by a population member, then a penalty is added to the fitness of the design.

After the fitness of all the population members is known, the reproduction step begins. Reproduction consists of several steps. The first is the selection of parents. In this study, parents are selected using the roulette method. In the roulette method, each member of the population has a slice of a circle. The size of the slice is dependent on the fitness of the member. Members with a better fitness get a larger slice of the circle. Then a point on the circle is randomly selected. The point will fall within one member's "slice". That member is selected to be a parent.

The "slices" are determined by normalizing the inverse of the all the population's fitnesses. A cumulative list of the normalized inverse fitness of each member is kept. The list should range from 0 to 1. Then a number between 0 and 1 is randomly selected. This number will dictate which member is selected. Using this technique, pairs of parents are selected. (A pair consists of two parent selections.) The number total parents chosen is equal to the population size.

After the parents are selected, the cross-over step takes place. During the cross-over step, two locations in the design variable strings are selected. All bits between the two points selected are swapped between the parents. The new pair of binary strings are the children. The process is repeated (new random locations are selected) for each pair of parents.

After the cross-over step, the final part of the reproduction takes place – the

mutation step. During the mutation step, a bit has a chance of being randomly changed. However, the probability of this change is very low. For this design problem, the probability was set at 0.1%.

Once this step is completed, the children become the new population and the process loops back to the fitness evaluation step until one of the convergence criterion is met. Several criteria were used. One is a maximum number of iterations, and a second is a maximum amount of run time. The third is the number of iterations that had a percent change in the fitness of the overall best solution less than or equal to a set threshold.

The traditional GA method was having trouble converging on a solution. This is caused by the large changes in the response of the system by changing a single bit in a population member. To address this problem, the best solution found in an iteration was carried into the next iteration. So, the best solution would survive until a better solution is found. Using this method, the percent change in fitness criterion was set to zero change for 20 iterations.

5.4.1.2 Results

The genetic algorithm was repeated four times using the objective and constraints that have been described. Table 28 shows the number of components in the system and the motor requirement for each case. The table shows that the optimization tends to move to a three bus architecture and 16 motors (4-4-4-4 grouping). The motor requirement varied with a maximum of 12 motors and a minimum of 10 motors.

Table 29 shows the required capacity and resulting weight for the components in the system; it also shows the total system weight. The progression of system weight as the optimization process commenced is shown in Figure 41. The fitness values are same as the weight values because the reliability constraint was met in all cases. This occurred because a large weight penalty was applied to systems that did not meet

the reliability requirement.

The results show that the GA process has some convergence problems which is caused by the discontinuities in the design space. Changing several bits in the design variable string causes major changes to the system architecture. (The cross-over step in the GA causes the changes.)

The system reliability for each run is shown in Figure 42, and the corresponding architectures are shown in Figures 43 through 46. The architecture diagrams show the primary feeds with solid lines. These are the paths that are used in normal operation of the system. The dotted paths add redundancy to the system, but are only used in the case of a failure.

According to the weight results, the best architecture that was found during run 3 with a system weight of 23,202 pounds. Since the architecture uses only three buses, one bus must be the primary feed for two motor groups. The reliability requirement is met using this system, but approaches the limit near the end of the system lifetime. The system produced during run three has 3 buses, 16 motors, and requires 12 motors to be operational. The path redundancy found in the architecture is primarily between the buses and inverters/motor groups. By including path redundancy at this point in the system, power can be rerouted if an upstream failure occurs.

Another interesting result was that run 1 produced the system with the highest reliability. The primary driver of this result is that the motors were sized such that the aircraft can function with 11 motors. Figure 43 shows that this architecture uses path redundancy between the rectifiers and buses and also between the buses and inverters/motor groups.

The lowest reliability system was the found during run 2. The primary reason this occurred was that very little reconfigurability is available between the buses and inverters/motors.

Table 28: GA component settings

	Run 1	Run 2	Run 3	Run 4
Number of buses	3	4	3	3
Number of motors	16	16	16	14
Motor requirement	11	12	12	10

Table 29: GA component capacities and weights (lbs)

	Run 1		Run 2		Run 3		Run 4	
	Capacity	Weight	Capacity	Weight	Capacity	Weight	Capacity	Weight
G1	73	650	125	1136	100	894	110	983
G2	109	975	50	455	50	455	100	894
G3	73	650	100	894	100	894	150	1341
G4	109	975	100	894	67	596	50	715
R1	73	1300	125	2273	100	1788	110	1967
R2	109	1951	50	909	50	909	100	1788
R3	73	1300	100	1788	100	1788	150	2682
R4	109	1951	100	1788	67	1192	50	909
B1	50	250	50	250	50	250	110	550
B2	100	500	50	250	100	500	50	250
B3	73	394	75	375	100	500	100	500
B4			50	250				
Inverters	13	227	13	227	13	227	14	260
Motors	13	250	13	250	13	250	14	286
Connections		5200		6800		5800		6000
Total		23703		25703		23202		26224

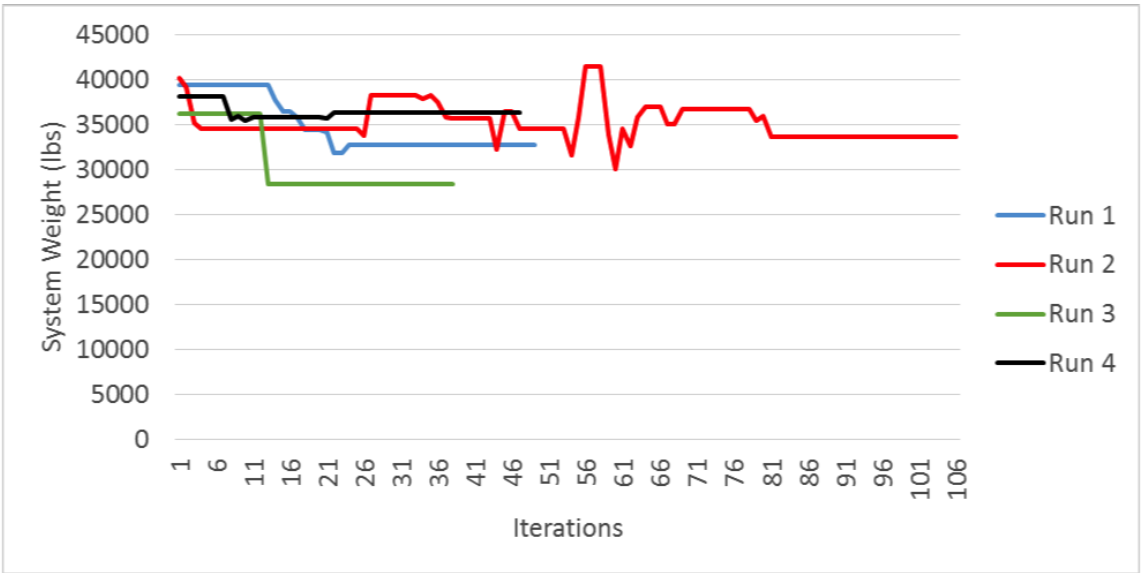

Figure 41: Genetic algorithm weight progression (iterations vs. system weight)

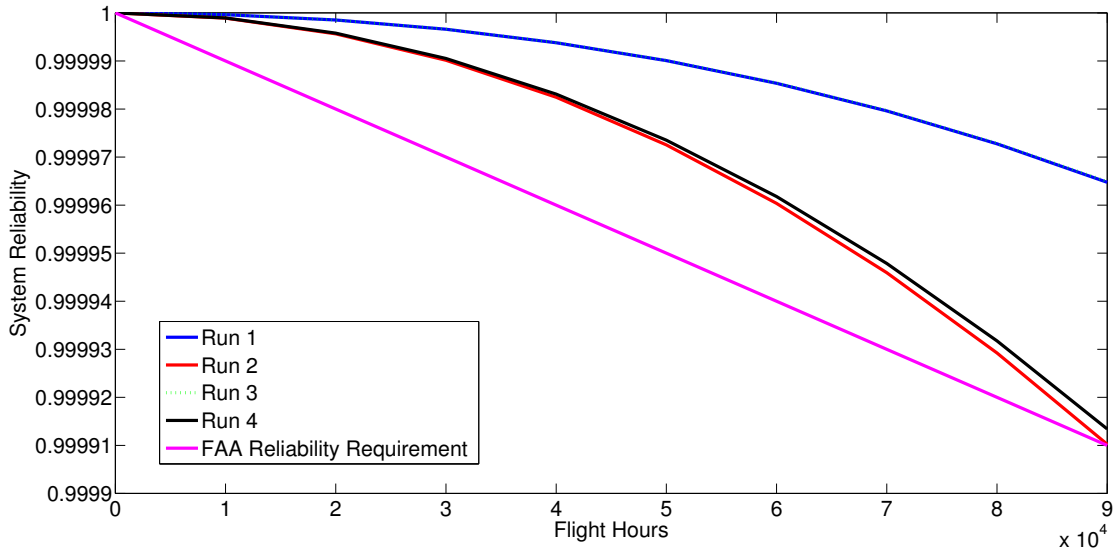

Figure 42: Genetic algorithm architecture reliablities

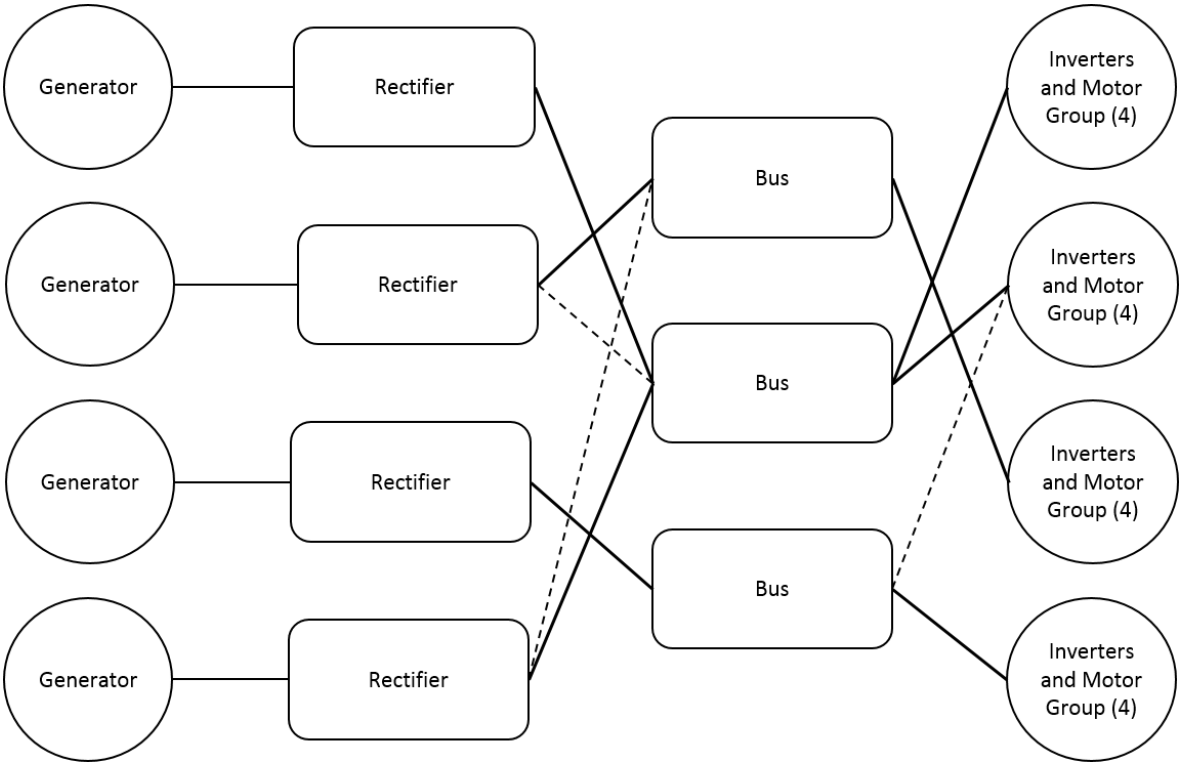

Figure 43: Genetic algorithm run 1 architecture

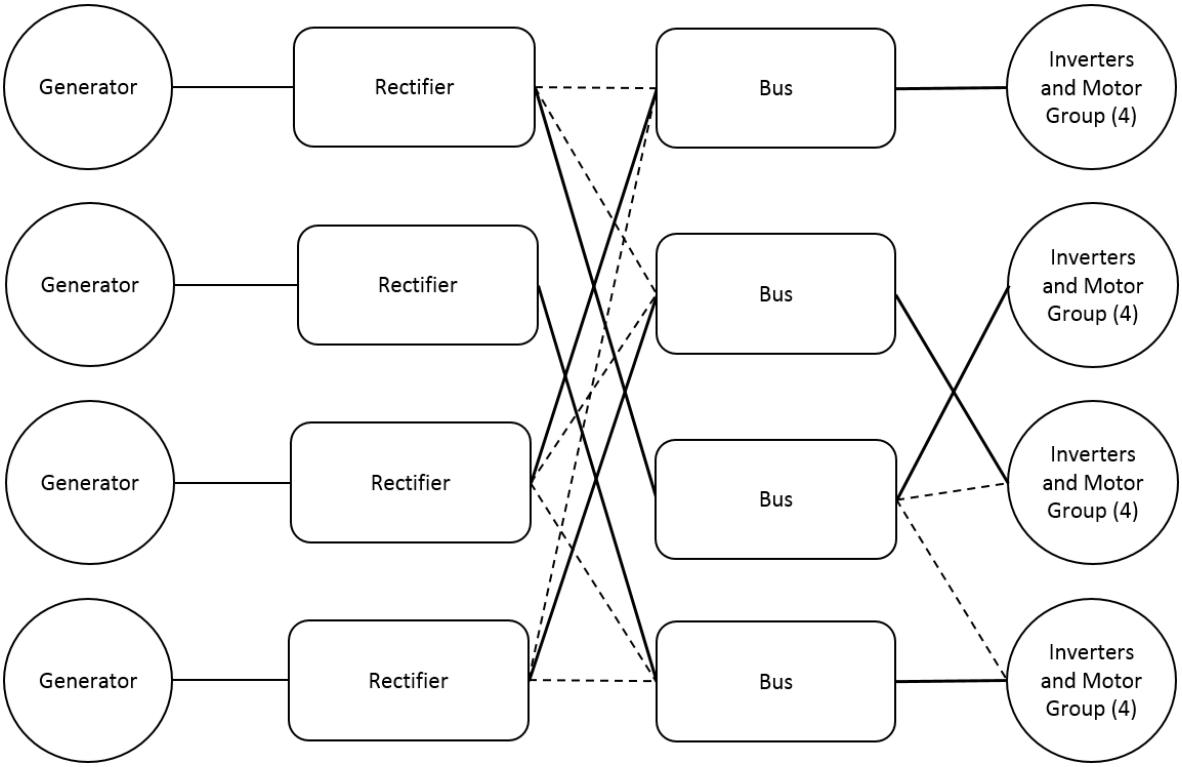

Figure 44: Genetic algorithm run 2 architecture

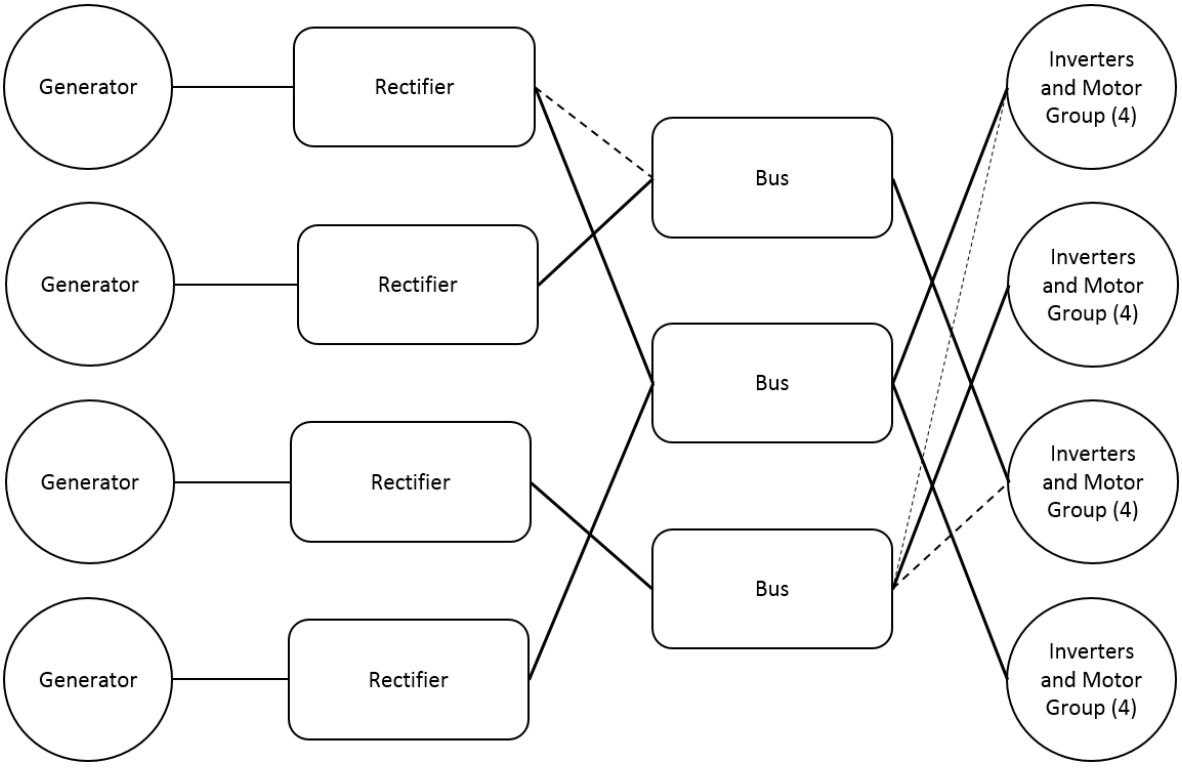

Figure 45: Genetic algorithm run 3 architecture

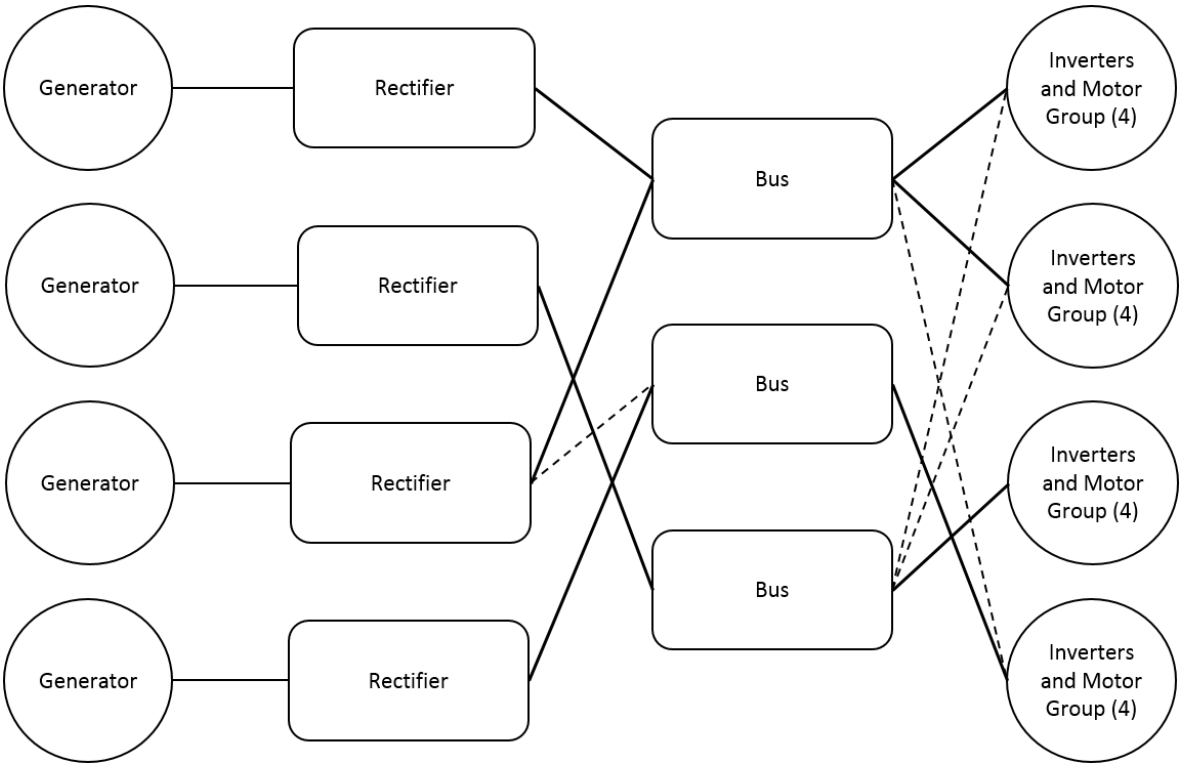

Figure 46: Genetic algorithm run 4 architecture

5.4.2 Particle Swarm Optimization

The next optimization method to be implemented was particle swarm. The approach taken to implement the methodology will be described and then the results will be presented.

5.4.2.1 Algorithm Formulation

The particle swarm optimization (PSO) algorithm starts much like the genetic algorithm. First a random population is generated. Each design is referred to as a particle. Each particle will need a position (which is represented by the design variable binary string) and a velocity.

Once the particles have been initialized, the fitness of each particle is calculated based upon its position. Again, the capacity constraint, weight calculation, and reliability calculation are used to determine the fitness of a population member.

After the fitness is calculated, the next step is to move the particles. The velocity will dictate how the particles will move iteration to iteration. The new positions of each particle are determined by the velocity and time step. The time step is set by the user. A large time step will move particles further between iterations, but may lead to convergence problems. A smaller time step will cause the algorithm to need more iterations to find the optimal solution, but is more likely to converge at a solution.

For the first iteration, all particles will be initialized by with the same velocity. The velocity is a vector equal to the particle position vector length. The velocities were all initialized at 0.5 for this optimization problem. From there, the velocities will be updated based upon the fitness of the solutions found. The velocity update used in a traditional particle swarm algorithm is formatted for continuous variables. Since discrete variables are needed for this design problem, a modified version of particle swarm is needed. Discrete PSO, like the genetic algorithm, requires the use of a binary string. All the design variables that specify a design are contained within the string. (Refer to the notation used for the GA.)

The velocity of each particle is dictated by a vector with a length equal to the length of the binary string of the particle. The velocity is updated based upon the location of the best solution from the iteration (referred to as the global solution), and the best location that has been found for a particle throughout all the iterations. The best global solution will be referenced using the subscript g, and the particle position for each particle that has been found is referenced using the subscript b.

The first step updating the velocity uses the position of the best solution that has been found overall.

$$\mathbf{V}_g = \alpha * \mathbf{P}_g + \beta * (1 - \mathbf{P}_g) \tag{62}$$

α and β are tuning parameters that dictate how fast the velocity of the particle changes. The sum of the two values should equal 1. For the simulation performed

in this thesis, α was set to 0.6 and β was set to 0.4. $\mathbf{P}_g$ is the best particle position found during the current iteration.

The next step is to create the velocity vector based upon the best positions of each particle found throughout the iterations. The equation used for the update is

$$\mathbf{V}_{b,i} = \alpha * \mathbf{P}_{b,i} + \beta * (1 - \mathbf{P}_{b,i}) \tag{63}$$

Lastly, the velocity vector for each particle, $\mathbf{V}$ is updated.

$$\mathbf{V}_{i,new} = w * \mathbf{V}_{i,old} + c_1 * \mathbf{V}_{b,i} + c_2 * \mathbf{V}_g \tag{64}$$

w is a parameter that controls the particles' tendency to remain at its current location. This was set to 0.2. c_1 and c_2 are tuning parameters that determine the influence of the best position found for a particle and the best global solution on the velocity change. Both parameters were set to 0.4.

Now that the velocity vector has been obtained, the particles can be moved. In discrete PSO, the movement of the particles is determined probabilistically. For each particle, a vector that has a length equal to the length of the velocity is generated using random numbers between 0 and 1.

Next, the value of each bit in each member's position string is determined based upon the random numbers and the velocity vectors. Each value in the velocity vectors will have a corresponding random number. If the value of the random number is greater than the corresponding velocity value, the corresponding bit in the position string will become a 1. Otherwise, the bit becomes a zero. This process is repeated for every position bit in the entire population.

Once this step is completed, all the particles have been moved. The algorithm returns to the fitness evaluation step, followed by the velocity update and particle movement until one of the convergence criterion has been met. Several criteria were used. One is a maximum number of iterations, and a second is a maximum amount

of run time. The third is the number of iterations that had a percent change in the fitness of the overall best solution less than or equal to a set threshold. The percent change threshold was set to 0. That is, the best particle position is no longer moving. If this occurred for 20 iterations in a row, the algorithm is terminated.

5.4.2.2 Results

The particle swarm optimization algorithm was repeated four times. The resulting component settings are shown in Table 30. The resulting component capacities, component weights, and system weights are shown in Table 31. The progression of system weight during the optimization process is shown in Figure 47. The figure shows that the particle swarm method was able to smoothly reach convergence with relatively few iterations. The reliability of each system found during the runs of the PSO are shown in Figure 48. The corresponding system architectures are shown in Figures 49 through 52.

Based upon system weights, the best architecture found with PSO was run 1 with a system weight of 26,551 pounds; while this system had the lowest weight, it also had the lowest reliability. However, all constraints were met, so there is no cause for concern. The system consists of four buses and 14 motors. Also, it requires the operation of 7 motors in the system. The system architecture, shown in Figure 51 shows that path redundancy exists between the rectifiers and buses and the buses and inverters/motors.

The highest reliability system found was run 2, which also uses three buses and 16 motors and has a 12 motor requirement. However, compared to the architecture from run 3, more redundant paths are available.

5.4.3 Ant Colony Optimization

The final global optimization method to be tested is ant colony optimization. The algorithm used will be described along with the modifications needed for the algorithm

Table 30: PSO component settings

	Run 1	Run 2	Run 3	Run 4
Number of buses	3	3	3	4
Number of motors	14	16	16	16
Motor requirement	7	12	12	12

Table 31: PSO component capacities and weights (lbs)

	Run 1		Run 2		Run 3		Run 4	
	Capacity	Weight	Capacity	Weight	Capacity	Weight	Capacity	Weight
G1	143	1277	167	1490	133	1192	67	596
G2	57	511	50	455	50	455	133	1192
G3	86	766	100	894	133	1192	100	894
G4	57	511	133	1192	100	894	167	1490
R1	143	2554	167	2980	133	2384	67	1192
R2	57	1022	50	909	50	909	133	2384
R3	86	1533	100	1788	133	2384	100	1788
R4	57	1022	133	2384	100	1788	167	2980
B1	57	286	100	500	100	500	100	500
B2	57	286	50	250	50	250	50	250
B3	86	429	100	500	100	500	100	500
B4							67	333
Inverters	14	260	13	227	13	227	13	227
Motors	14	286	13	250	13	250	13	250
Connections		8712		8600		8228		8400
Total		26551		29578		28312		30136

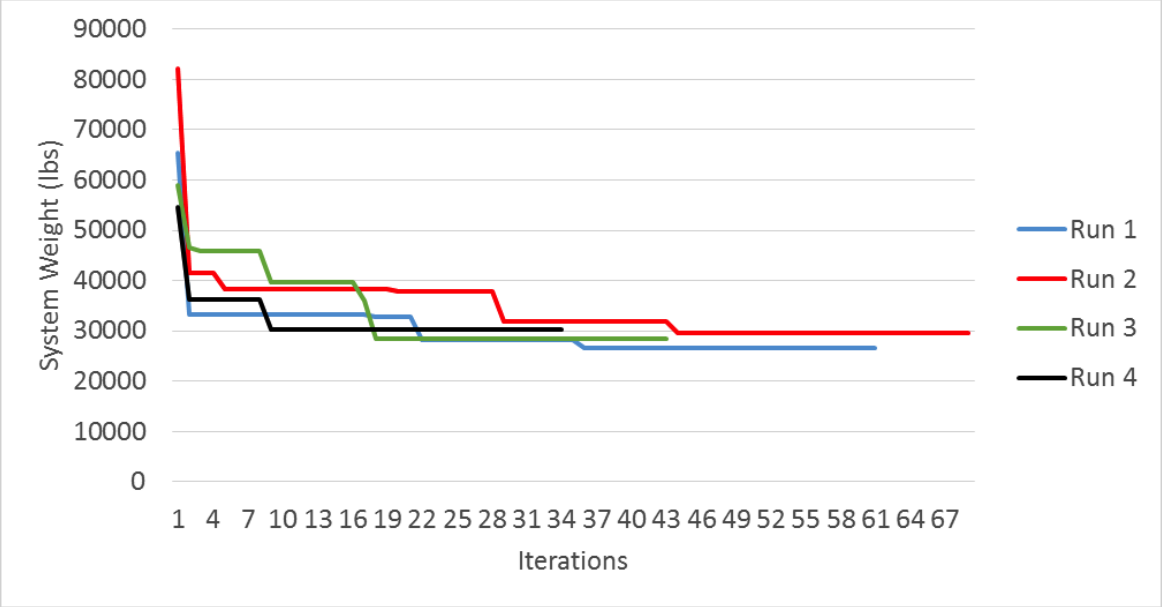

Figure 47: Particle swarm optimization weight progression (iterations vs. system weight)

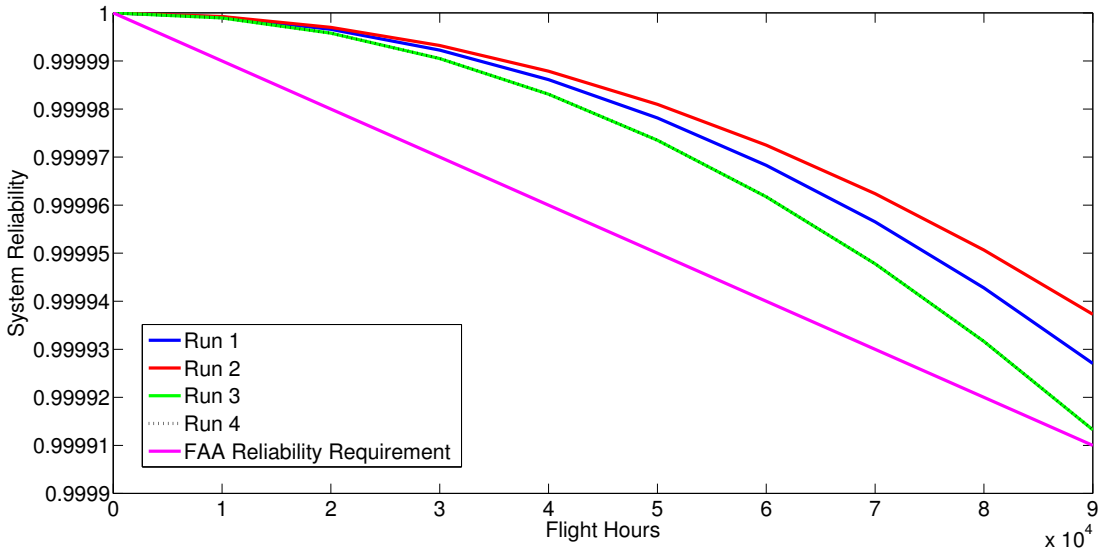

Figure 48: Discrete particle swarm optimization reliability results

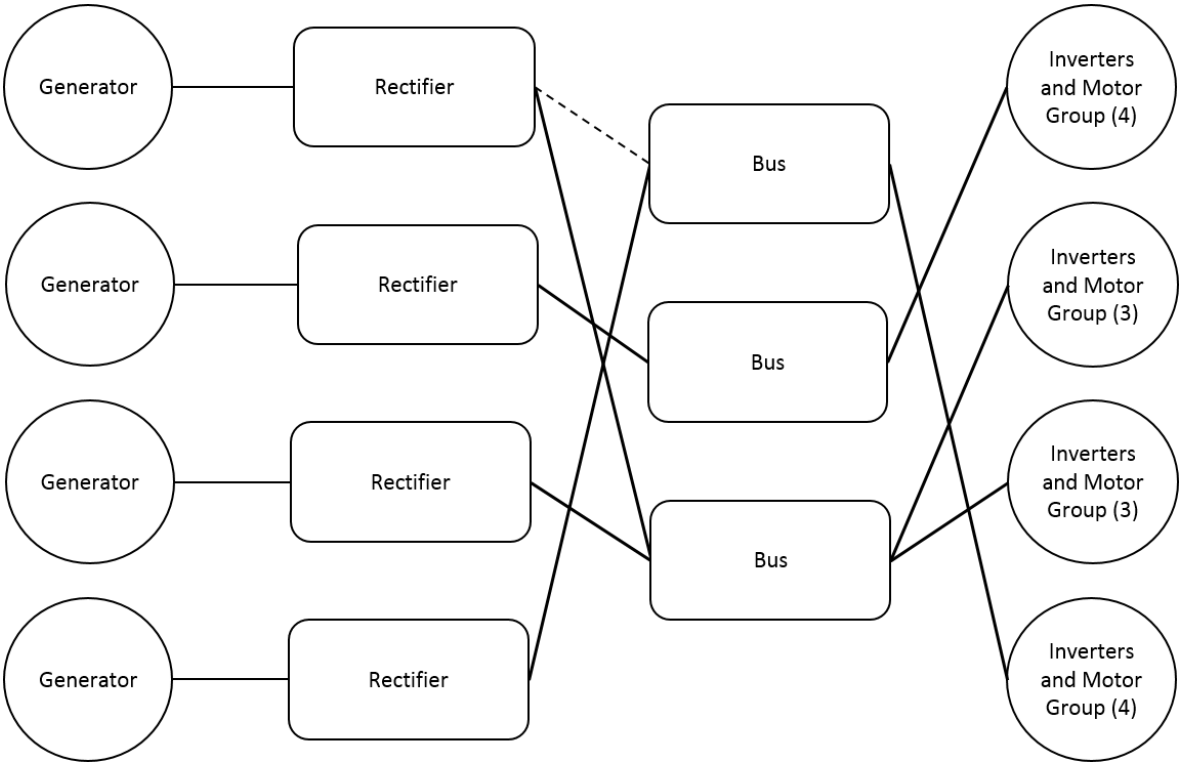

Figure 49: Discrete particle swarm run 1 architecture

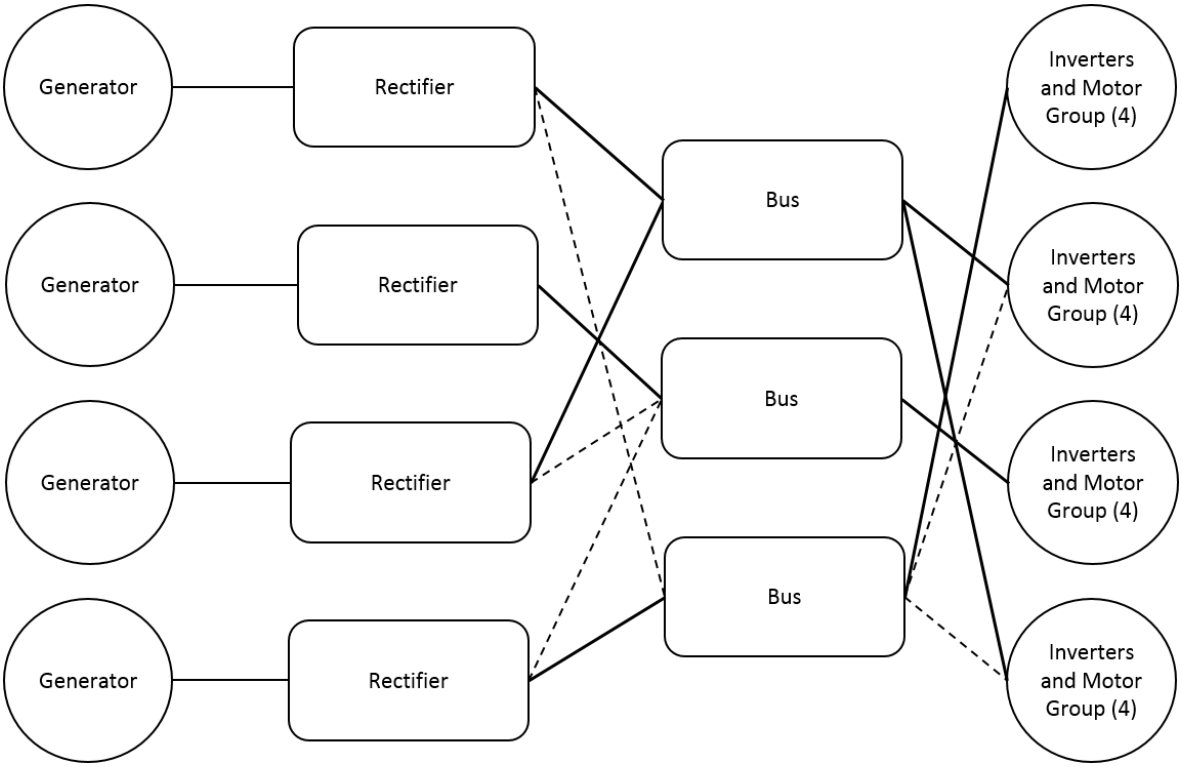

Figure 50: Discrete particle swarm run 2 architecture

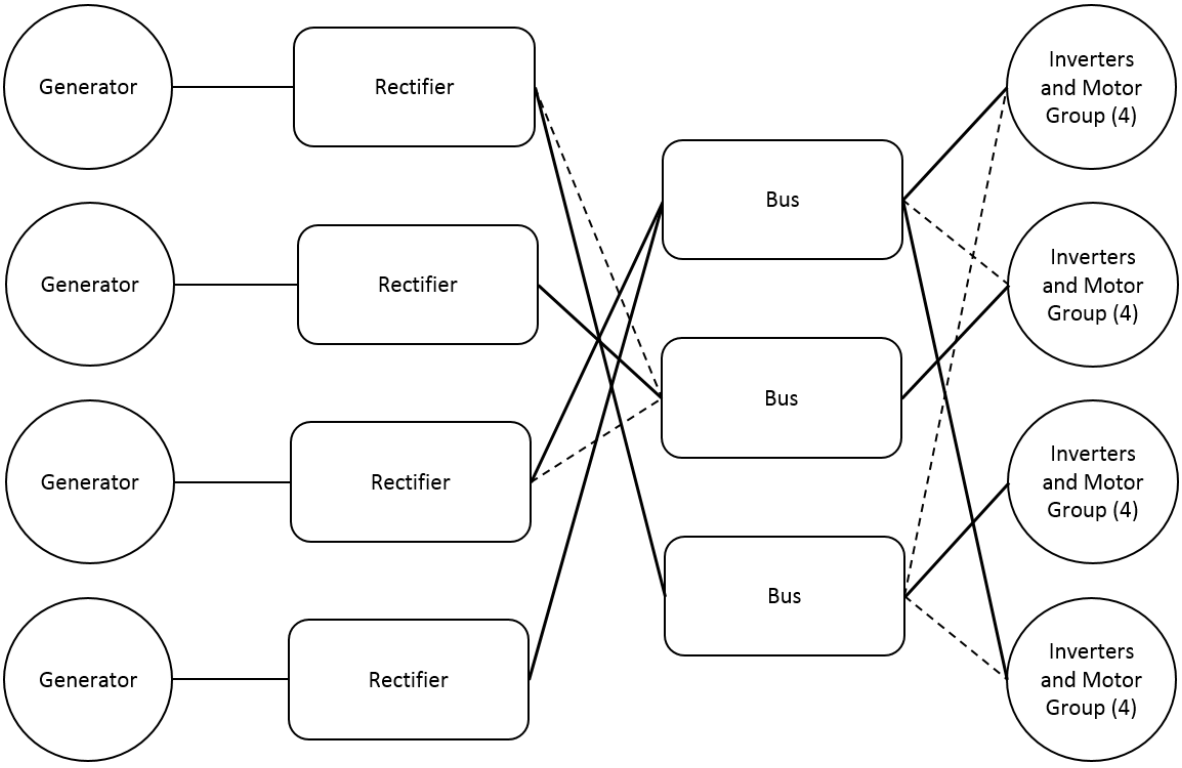

Figure 51: Discrete particle swarm run 3 architecture

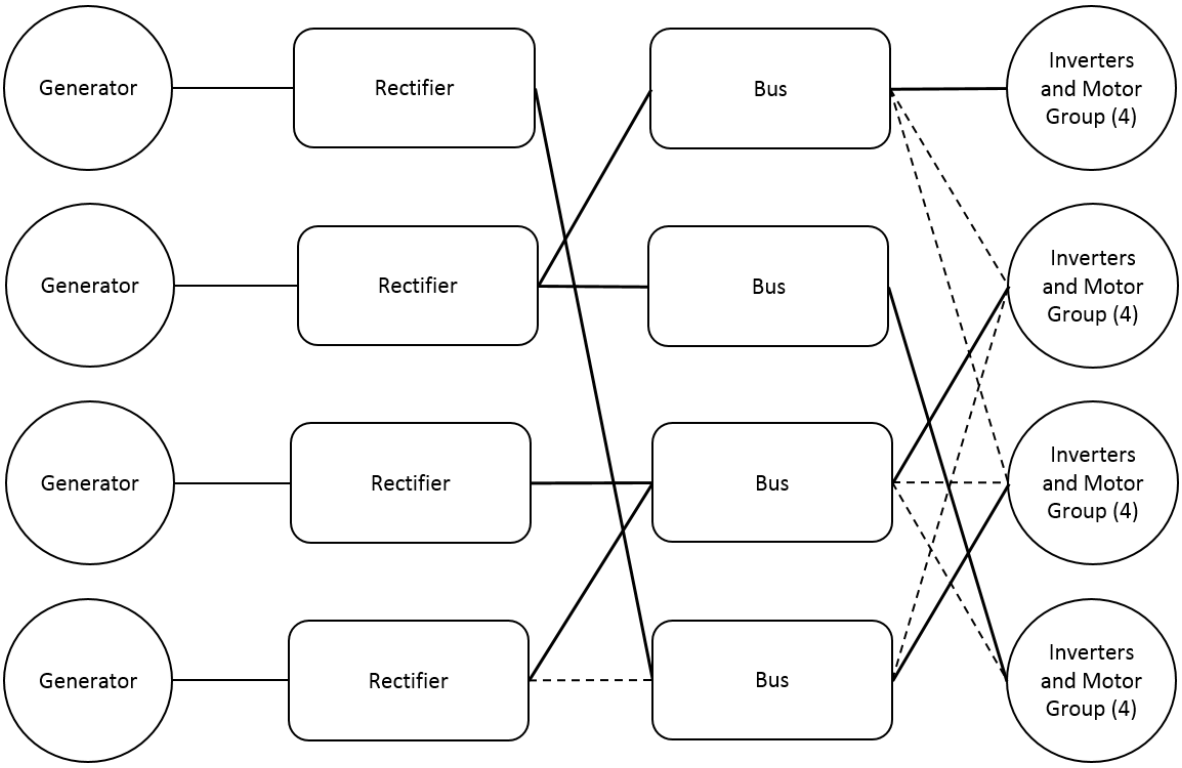

Figure 52: Discrete particle swarm run 4 architecture

to handle multiple sources and sinks. Then the results of the optimization will be presented.

5.4.3.1 Algorithm Formulation

The first step in the ant colony optimization algorithm is to initialize the graph. The graph will now not only contain the system components and connections, but it will also need nodes that define the number of buses, motor grouping selection, the number of motors required to meet the power requirement, and a starting node. Once the ants have traversed the three sets of nodes, they will proceed to the graph that describes the system components and connections. A diagram of the first section of the graph is shown in Figure 53.

Each edge in the graph will be selected with a certain probability. A pheromone value will be assigned to each edge at the beginning of the algorithm. At this point the same value is used for every edge, so, in this case, all edges were selected to have

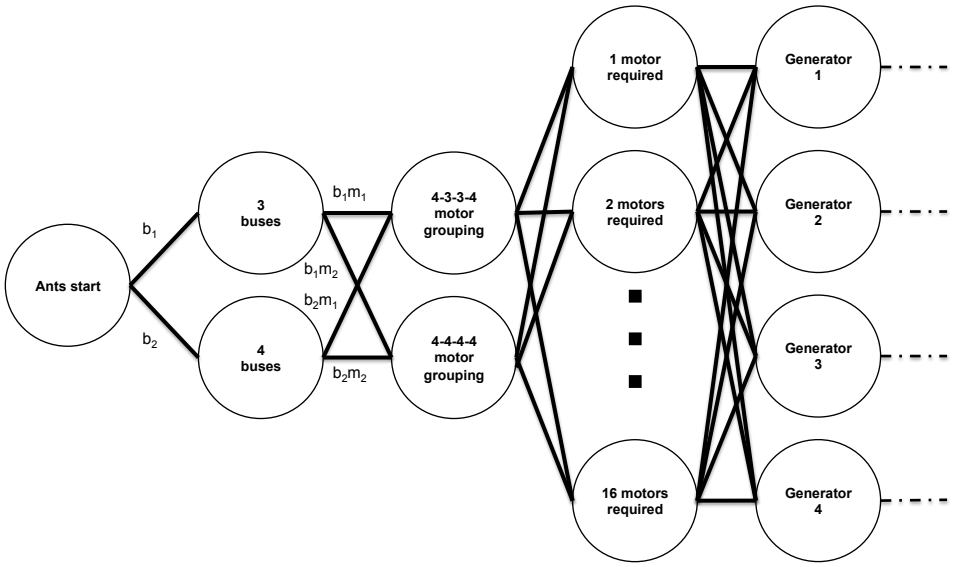

Figure 53: Ant colony graph section

a value of 1.

As previously mentioned, the basic ant colony optimization approach is formulated for graphs with a single source and sink. The turboelectric problem has four sources and four sinks, so the method needed to be adapted for this problem.

The modification begins by redefining an "ant". Normally a single ant will traverse the graph on its own. Now an "ant" will be referred to as a group of ants. The ants will move together through the first three sets of vertices that define the number of buses, motor grouping, and motor requirement. After that point, the group of ants will be split. An equal number of ants is sent to each generator. Each group of ants at each generator will have to be equal to the total number of possible paths from a generator to the motor groups. For a 4-4-4-4 system, each group will need 16 ants (4 possible selections from a rectifier to the buses and 4 edges from a bus to motor groups – 16 total combinations). The same number will be used for the 4-3-3-4 configuration to simplify the algorithm. After each generator has 16 ants, the ants will transverse the system on their own.

The movement of the ants through the graph is determined probabilistically. Each

edge will have a probability of being chosen based upon the value that has been assigned to it. The probabilities of the edges from one node to the next set of nodes (one design variable to the next design variable settings) must add to one. That is, the ant must move to the next set of nodes in the graph which sets a value for a design variable.

As stated, in the beginning all the edges have a pheromone value of 1. Those values must be normalized so that the sum of the values of the edges extending from a node equals 1. Examine the graph shown in Figure 53. At the ant start node, two edges (b_1 and b_2) extend from it to the set of nodes that set the number of buses. The value of each edge is 1. The values are normalized by dividing each edge by the sum of the edges.

$$p_{b_1} = \frac{b_1}{\sum_{i=1}^{n} b_n}, n = 1, 2 \tag{65}$$

$$p_{b_1} = p_{b_2} = \frac{1}{2} = 0.5 \tag{66}$$

The probability of each edge getting selection is 0.5. For the group of ants, a number between 0 and 1 is randomly selected. If the number is less than or equal to 0.5, the ants move to the 3 buses node. Otherwise, the ants move to the 4 buses node.

After the number of buses has been selected, the next movement of the ants will determine the motor grouping configuration (reference Figure 53). If the ants are at the 3 buses node, they have two possible edges to move along – b_1m_1 and b_1m_2. Once more, the edge values are normalized and each edge has a 50% chance of being selected. The same is true if the ants are located at the 4 buses node. Again, a random number between 0 and 1 is generated for the group of ants. If it is less than or equal to 0.5, the ants will move to the 4-3-3-4 configuration node. Otherwise, they will move to the 4-4-4-4 configuration node.

The next movement of the ants determines the number of motors that must be operational to meet the critical power requirement. Again, all the ants will move together to one vertex. There are 16 possible moves for the ants. (The number of critical motors can range from 1 to 16.) At the beginning, each path has an equal probability of being selected.

Now that the ants have reached a motor requirement node, they must be evenly divided amongst the generator nodes. Each generator node will receive 16 ants (one-fourth of the total ants in the group). Probabilities are not used in this case and the paths of the ants are forced. This is because enough ants are needed at each generator node to explore all possible paths from the generators to the motor groups. After the ants have arrived at the generators, they are moved to their generator's corresponding rectifier.

Each rectifier will have 16 ants and have four possible moves (given that there are 4 buses). For example, consider rectifier 1. 16 ants will be at that location. The ants can move to bus 1, bus 2, bus 3, or bus 4. Again, in the beginning, each edge has a value of 1. There are four edges extending from each rectifier, so when the values are normalized, each edge has a 25% chance of being selected. A random number between 0 and 1 is selected for each ant, and based upon the probability it will move to a bus. For example, if the random number is 0.25 or less, an ant from rectifier 1 will move to bus 1. If the random number is between 0.25 and 0.5, an ant from rectifier 1 will move to bus 2. This continues through bus 4. Then the processes is repeated for the rest of the rectifiers. When a connection between a rectifier and bus is used, the design variable that defines that connection is switched from 0 to 1.

At this point, the ants will be at the bus nodes. Each bus node will have some amount of ants (it is important to track how many ants moved to each bus). Now the ants will move from the buses to the motor groups. Like the rectifier example, begin with bus 1. Bus 1 will have some amount of ants that moved there from the

rectifiers. For each ant, a random number between 0 and 1 is selected. The ants at bus 1 have four possible edges to move along. In the beginning, each edge has a 25% chance of being selected. Like the rectifier to bus connections, if a connection between a bus and motor group is used, the design variable that describes that connection is switched from 0 to 1.

Once all the ants have moved through the graph, one member of the population has been defined. The population member fitness is evaluated using the capacity constraint, weight calculation, and reliability calculation. Since the probabilities of the component connections are equal at the beginning, most early designs will include all connections. Computational time can be saved by saving the fitness evaluation for the configurations found early in the process since they will likely be repeated by following ants. The algorithm checks whether a population member has one of the configurations that has already been explored. If so, the fitness of that member is set without needing to repeat the capacity, weight, and reliability calculations.

The next step is to update the pheromone values for each edge. The pheromone update used after each group of ants transverses the graph is called the online update. The online update encourages following ants to use a different path than the previous ant. This gives the algorithm the capability to have good coverage of the design space. The pheromone update is performed as follows:

$$p_{i,new} = \rho_{ant} * p_{i,old} + \frac{1}{A_i}, n = 1, 2, ..., \text{number of edges} \tag{67}$$

p_i is the pheromone level of edge i. A_i is the number of ants that transversed edge i when the group of ants moved through the graph. ρ_{ant} is a tuning variables that determines the degree of change in the pheromone values. During testing of the algorithm, it was found that 0.2 was the optimal setting for ρ.

Once the online pheromone update is complete, the next group of ants is sent through the graph. This continues until a number of groups equal to the population

size has been sent through the graph. After the design variable configuration for each member of the population has been evaluated, the second type of pheromone update, called the offline update, commences. This update changes the pheromone values to encourage the ants to use paths that led to the best solutions. As the ants transversed the edges of the graph, each ant added pheromones to the edges it moved along. The pheromones are then updated by evaporation. The best fitting solutions have a slower pheromone evaporation rate. The pheromones on the paths that led to the poorest solution will evaporate faster. Two values are used when determining the evaporation rate for each edge. One is the fitness of the best solution found throughout all iterations (An iteration being that the entire population of ants has transversed the graph). The best overall solution will be donated by the subscript o. The second is the best solution found during that iteration. The iteration best solution will be denoted by the subscript s.

The step of the update is performed using the overall best solution.

$$p_{i,new} = \rho_{ant} * p_{i,old} + (1 - \rho) * \frac{10e4}{f_o * A_{i,o}} \tag{68}$$

p_i is the pheromone level of edge i. ρ_{ant} is a tuning parameter that controls the rate of pheromone evaporation. f_o is the fitness of the overall best solution. $A_{i,o}$ is the number of ants that transversed edge i when the overall best solution was found. After this step, a second part of the offline update is performed based upon the iteration best solution.

$$p_{i,new} = \rho_{ant} * p_{i,old} + (1 - \rho) * \frac{10e4}{f_s * A_{i,s}} \tag{69}$$

f_s is the fitness of the best solution found during the iteration, and $A_{i,s}$ is the number of ants that transversed edge i when the best solution of the iteration was found.

Once the offline pheromone update is complete, the convergence criteria are checked.

Several criteria were used. One is a maximum number of iterations, and a second is a maximum amount of run time. The third is the number of iterations that had a percent change in the fitness of the overall best solution less than or equal to a set threshold. In the case of ant colony optimization, the percent change threshold was set to zero. This is because eventually the pheromone levels will send ants along the same path. This will create identical best solutions through the iterations. If the number of times that the best solution remains unchanged is equal to the threshold, then the algorithm is terminated.

If none of the criteria are met, the previous population of ants will "die" and a new population will be formed by moving groups of ants through the graph. This will continue until one of the convergence criterion has been met.

5.4.3.2 Results

The ant colony optimization was repeated four times. The resulting architecture settings are shown in Tables 32 and 33. The progression of the system weight through the iterations of the algorithm is shown in Figure 54, and the reliability of the architectures is shown in Figure 55. The architectures are shown in Figures 56 through 59.

The weight progression graph shows that the best architecture changes several times before convergence. The reliability plot, shown in Figure 55, shows that the ant colony algorithm converged on overly conservative designs. This is why the weights of the architectures were high. The architecture diagrams show that the algorithm converged on designs with a high amount of path redundancy between the rectifiers and the buses. While this did provide increased system reliability, it added more redundancy than was needed to meet the requirement and drove up system weight.

All the architectures used a three bus configuration; however, there was a mix of 14 and 16 motors. If 14 motors were used, the takeoff requirement dictates that 10

Table 32: Ant colony component settings

	Run 1	Run 2	Run 3	Run 4
Number of buses	3	3	3	3
Number of motors	14	16	16	14
Motor requirement	10	12	12	10

Table 33: Ant colony component capacities and weights (lbs)

	Run 1		Run 2		Run 3		Run 4	
	Capacity	Weight	Capacity	Weight	Capacity	Weight	Capacity	Weight
G1	60	536	100	894	50	455	100	894
G2	110	983	133	1192	133	1192	240	2146
G3	170	1520	167	1490	167	1490	110	983
G4	100	894	167	1490	133	1192	110	983
R1	60	1073	100	1788	50	909	100	1788
R2	110	1967	133	2384	133	2384	240	4291
R3	170	3040	167	2980	167	2980	110	1967
R4	100	1788	167	2980	133	2384	110	1967
B1	50	250	100	500	100	500	50	250
B2	100	500	100	500	50	250	100	500
B3	110	550	50	250	67	333	110	550
Inverters	14	260	13	227	13	227	14	260
Motors	14	250	13	286	13	286	14	250
Connections		17601		16200		16200		19423
Total		38346		40284		37905		43386

motors must be operational. If 16 motors are used, then the aircraft can function on 12 motors.

5.5 Down-selection Observations

While the optimization methods produced varying results, they all demonstrated certain characteristics. One being that path redundancy is needed between both the rectifiers and buses and the buses and motor groups. Redundancy can be concentrated at either location due to the high bus reliability. In other words, placement of path redundancy is not as important as the amount of redundancy. This occurs due to the high reliability of the bus. Since its reliability is so high, it is unlikely that it will be the failure point in the system.

Another outcome of the down-selection was that the aircraft needs to be able to function even if three motors have failed. The only way to overcome a motor failure is

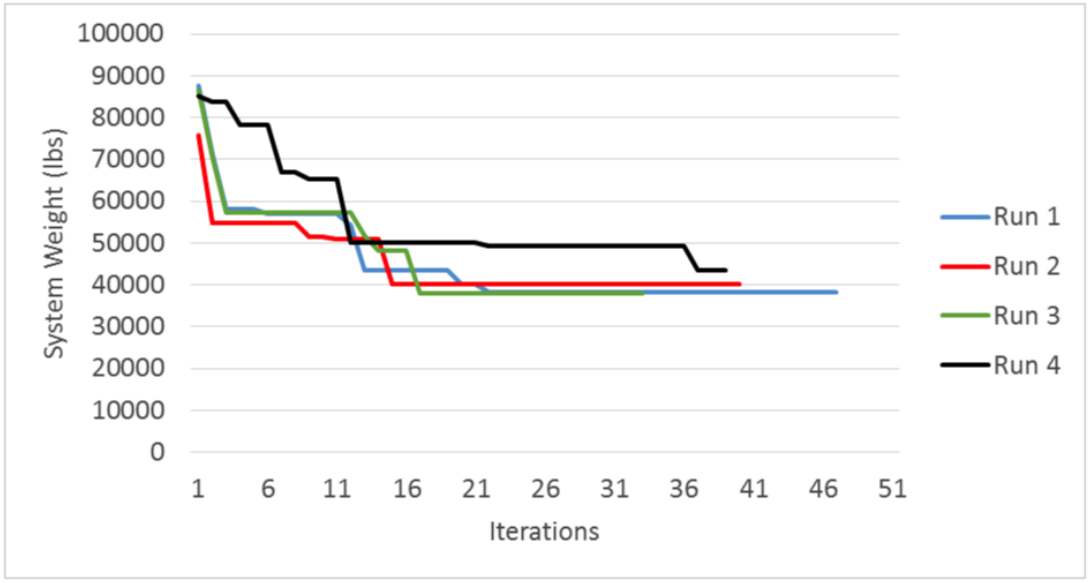

Figure 54: Ant colony optimization weight progression (iterations vs. system weight)

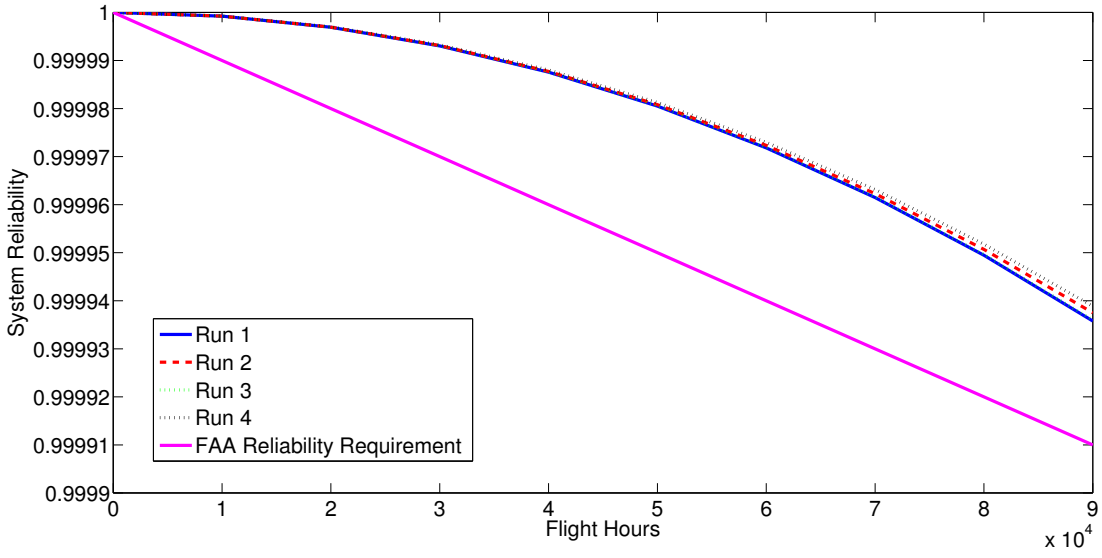

Figure 55: Ant colony optimization reliability results

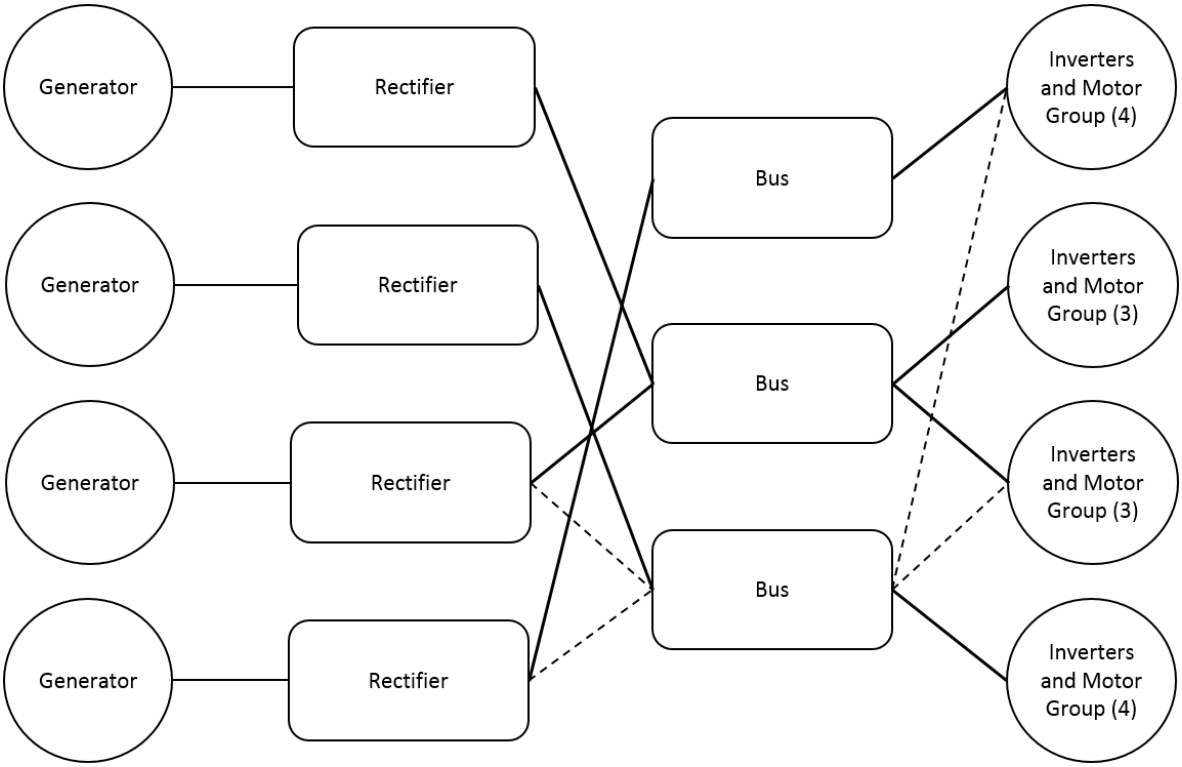

Figure 56: Ant colony run 1 architecture

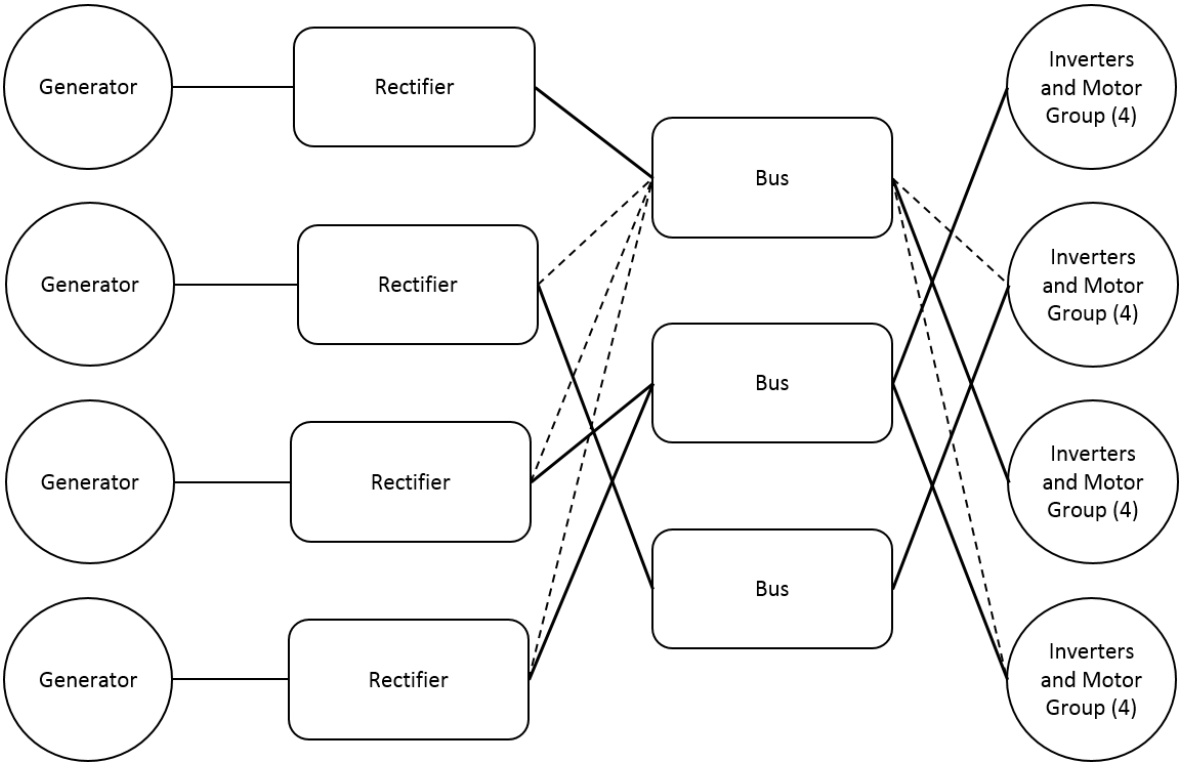

Figure 57: Ant colony run 2 architecture

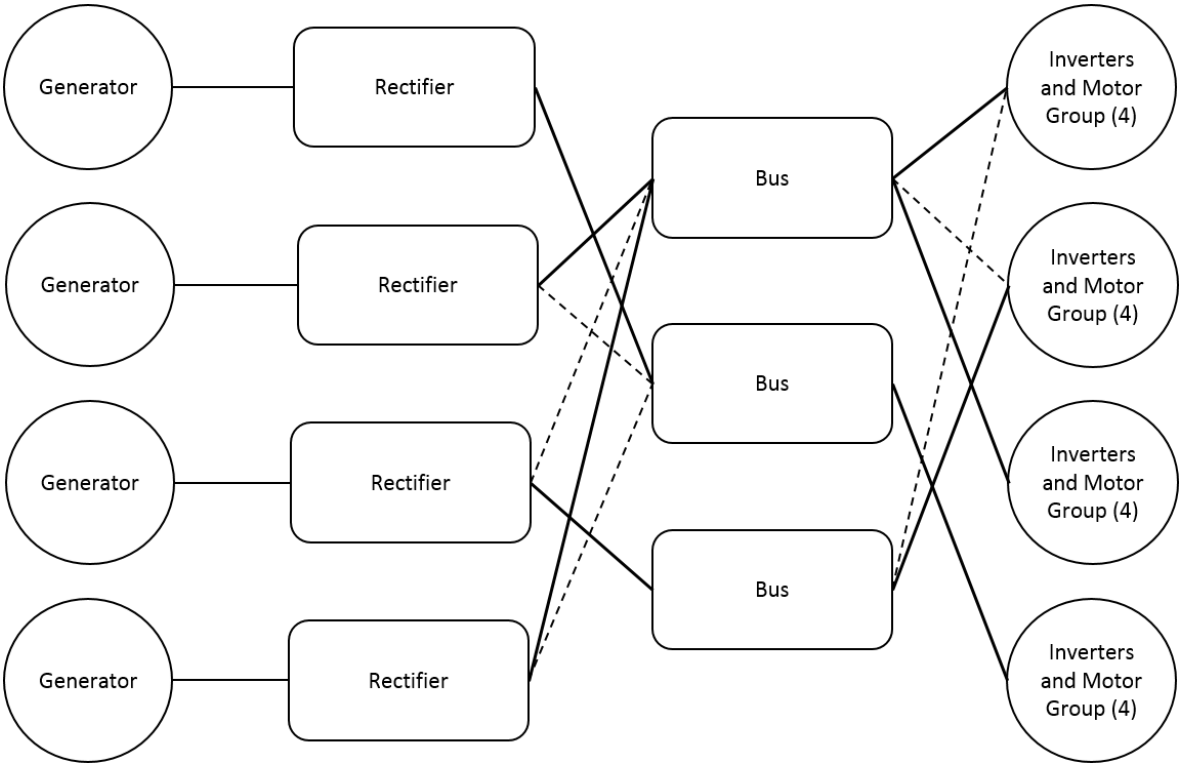

Figure 58: Ant colony run 3 architecture

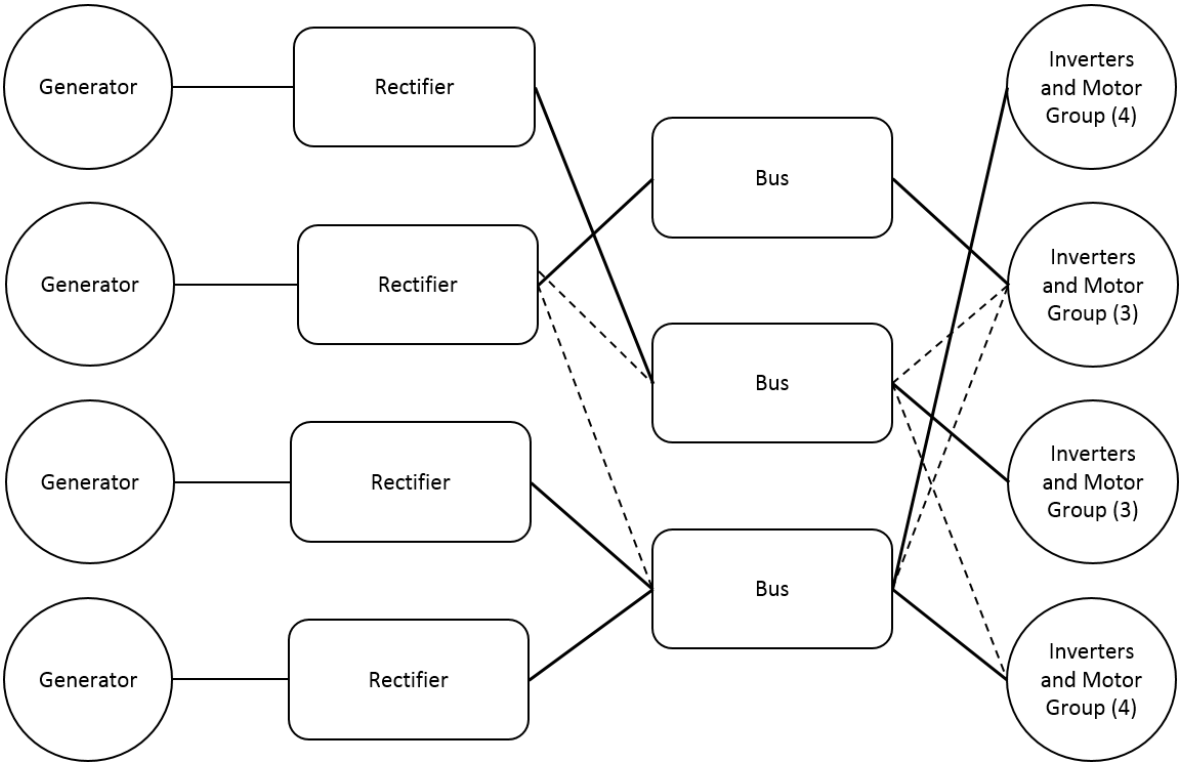

Figure 59: Ant colony run 4 architecture

Table 34: Outcome of optimization methods

Optimization method	Average number of iterations	Average best fitness (lbs)	Average best weight (lbs)
Genetic Algorithm	60	24,707	24,707
Particle Swarm	53	28,644	28,644
Ant Colony	48	39,980	39,980

to increase motor redundancy by increasing the size of the motors so that the system can reach the critical power requirement with less motors being operational. This led to the trend observed about the number of motors requirement that emerged.

A third observed trend is that the optimization primarily led to three bus architectures. This occurred since the reliability of the system is highly dependent on the motor requirement. The addition of a bus increased system weight without significantly changing system reliability.

Lastly, the optimization showed that a 16 motor architecture was generally better than a 14 motor architecture. Again, this is due to the system reliability being highly dependent on motor requirement. Using a 16 motor architecture led to smaller motor sizes and increased redundancy at the most critical point in the architecture.

5.5.1 Optimization Method Comparison

The optimization processes were compared based upon the average number of iterations before convergence, the average best fitness found, and the average best weight found. The results are displayed in Table 34.

The comparison of the methods produces some interesting trade-offs. First of all, the genetic algorithm weight progressions that were shown in Figure 41 showed that the genetic algorithm had some convergence problems; also, the genetic algorithm needed more iterations to converge than either of the other methods. However, in the end, the genetic algorithm produced the lowest weight architecture while still meeting the reliability constraint.

The particle swarm method converged with less iterations than the genetic algorithm and required less run time than any of the methods. However, it tends to converge before finding an optimal solution. The ant colony method converged in the fewest number of iterations, but converged on overly conservative designs. The designs produced by the ant colony algorithm were the heaviest, but had the highest reliability.

Based upon the outcome of the optimization methods, the genetic algorithm is the best suited for the power distribution design problem. Switching the bits led to longer convergence time, but also provided good coverage of the design space so that the best designs could be found.

5.5.2 Selected Architectures

The genetic algorithm optimization method produced the lightest weight system that met the reliability constraint. The three best architectures from all the runs were selected to continue to the next phase of analysis. The architectures selected are shown in Figures 60, 61, and 62. The motor requirement and weight of each architecture are shown in Table 35.

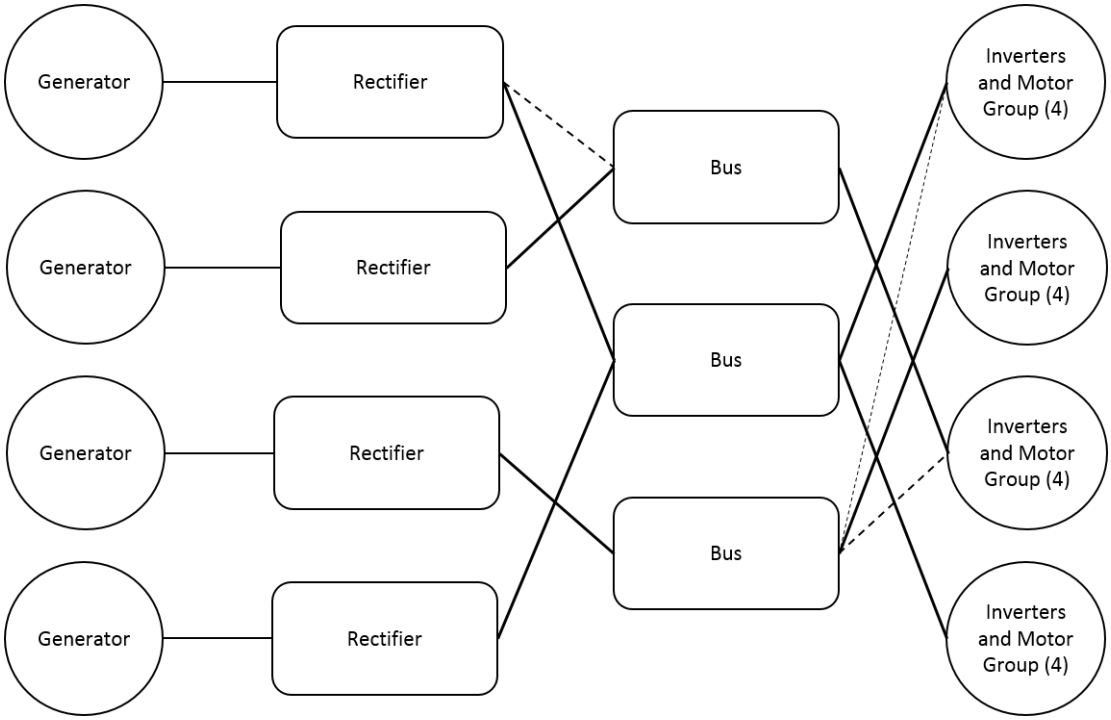

Figure 60: Architecture 1

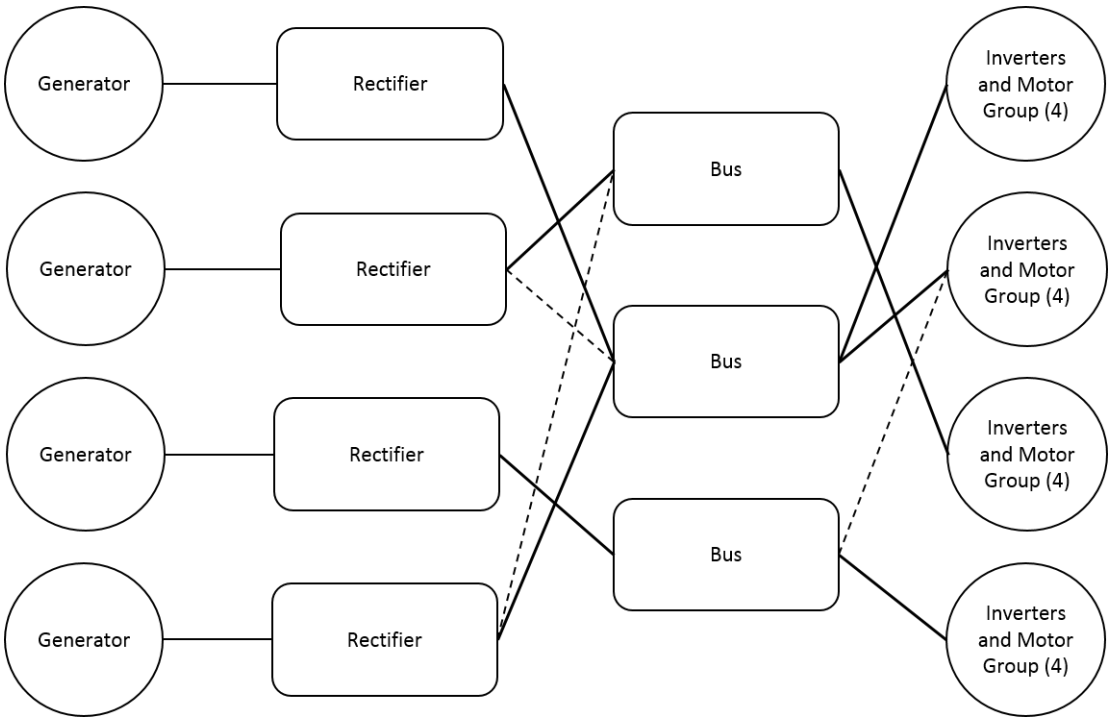

Figure 61: Architecture 2

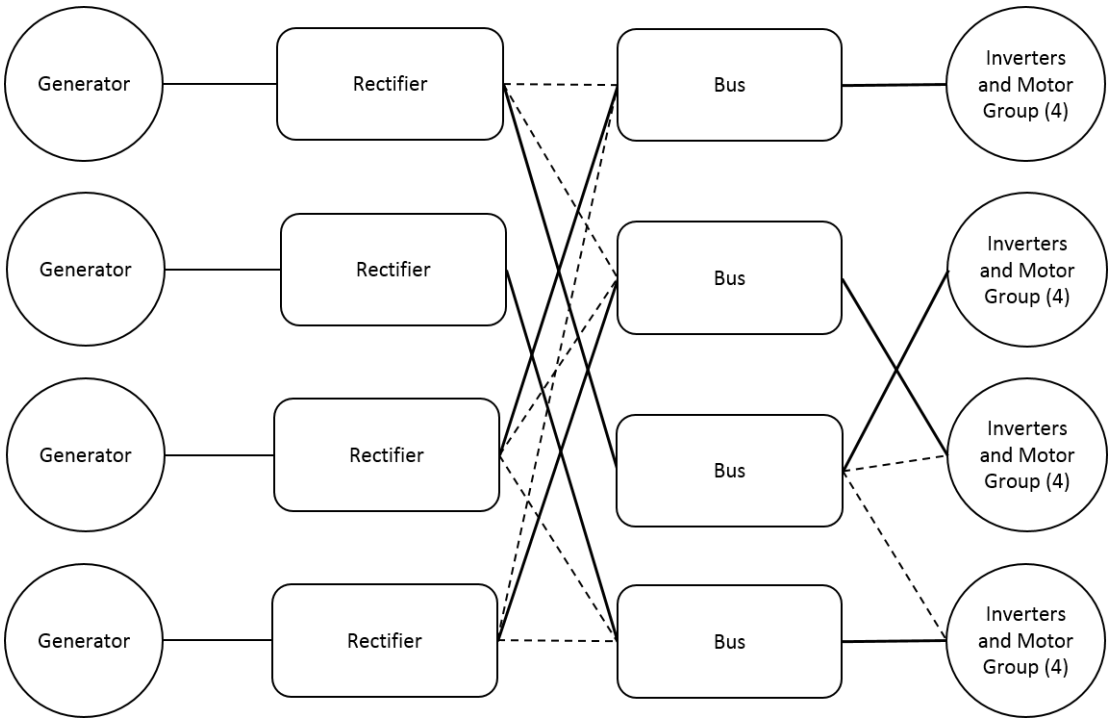

Figure 62: Architecture 3

All the architectures selected use 16 motors. This shows that having a greater number of small, light motors leads to a better overall architecture weight than fewer, larger motors. Table 35 shows that all the architectures require either 11 or 12 motors to be operational for a successful takeoff for the aircraft. Architectures 1 and 2 use a three bus design, while Architecture 3 uses a four bus structure.

Table 35: Architecture motor requirement and weight

	Architecture 1	Architecture 2	Architecture 3
Motor requirement	12	11	12
System weight (kg)	23,202	23,703	25,698

A sensitivity analysis was performed to see which components drove system reliability for each architecture. The results also show how robust each architecture is to a change in a component failure rate. For all cases, failure rate was varied by one order of magnitude. The results for architecture 1 are shown in Figures 63 through

67. The results for architecture 2 are shown in Figures 68 through 72. The results for architecture 3 are shown in Figures 73 through 77.

The architecture 1 results show that the architecture is highly sensitive to the generator and rectifier failure rates. This is because of the redundancy that is included at the inverters and motors by requiring less than all motors to be operational to reach takeoff power. Architecture 1 is least sensitive to the bus. Like the sensitivity analysis of the baseline from Chapter 3, this occurs because the bus reliability is very high.

Similar sensitivity trends are observed for the other two architectures. Architecture 3 is slightly less sensitive to changes in component failure rate. This occurs since the architecture uses 4 buses rather than 3. Since there is increased redundancy, architecture 3 is the most robust architecture.

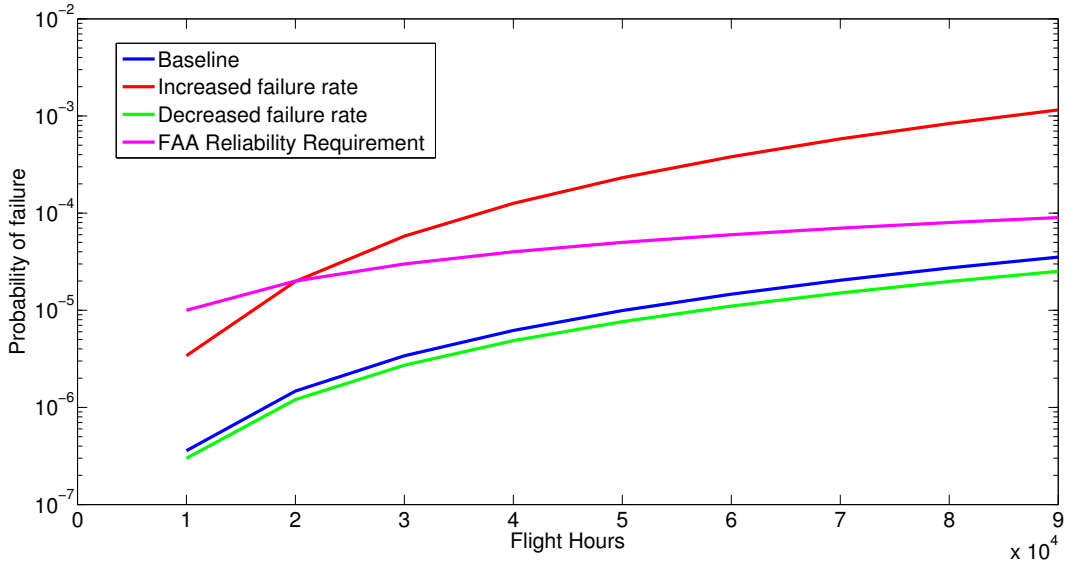

Figure 63: Architecture 1 reliability sensitivity relative to generator failure rate

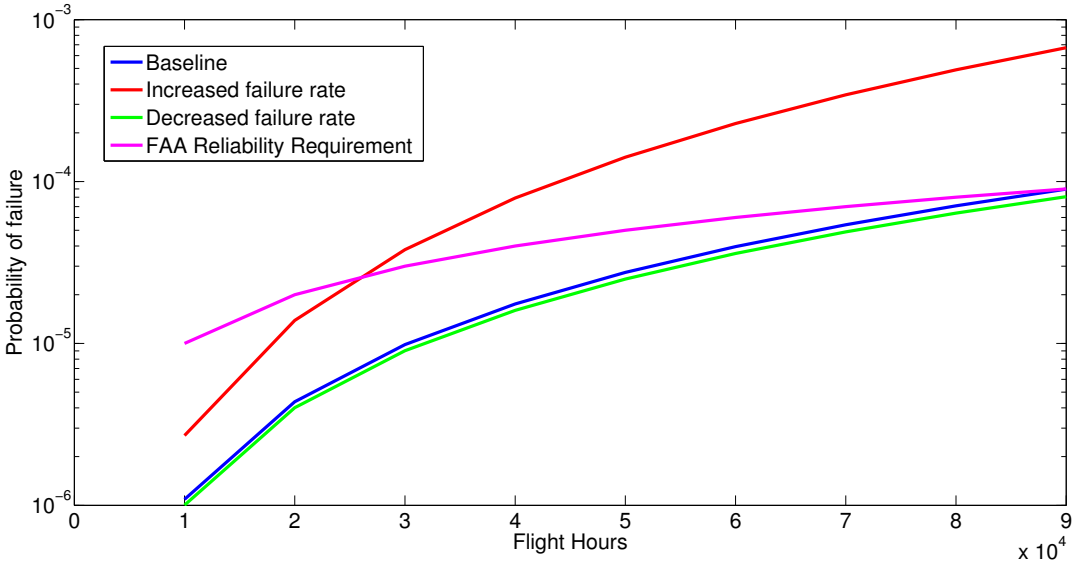

Figure 64: Architecture 1 reliability sensitivity relative to rectifier failure rate

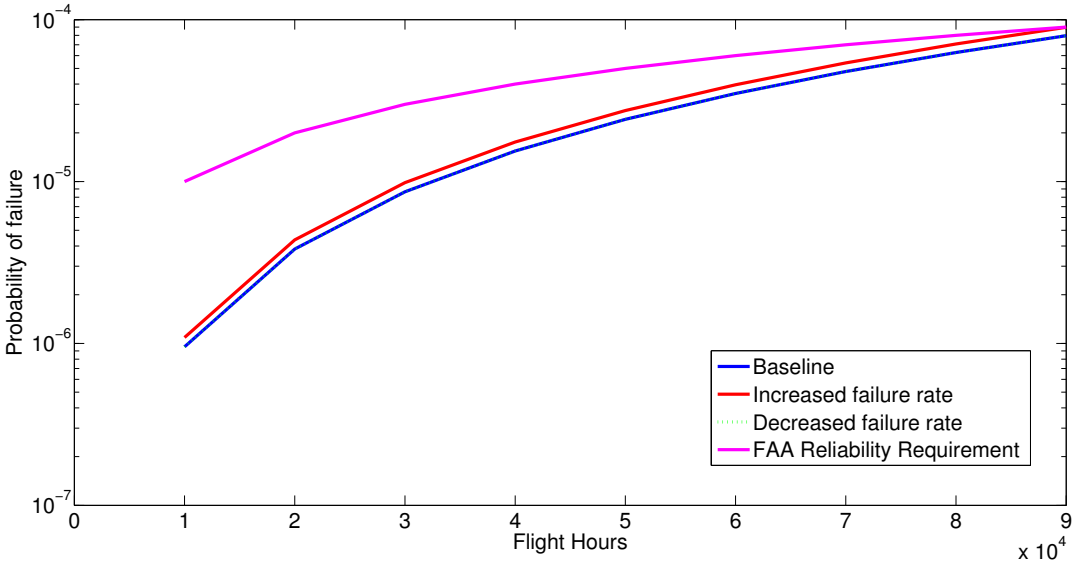

Figure 65: Architecture 1 reliability sensitivity relative to bus failure rate

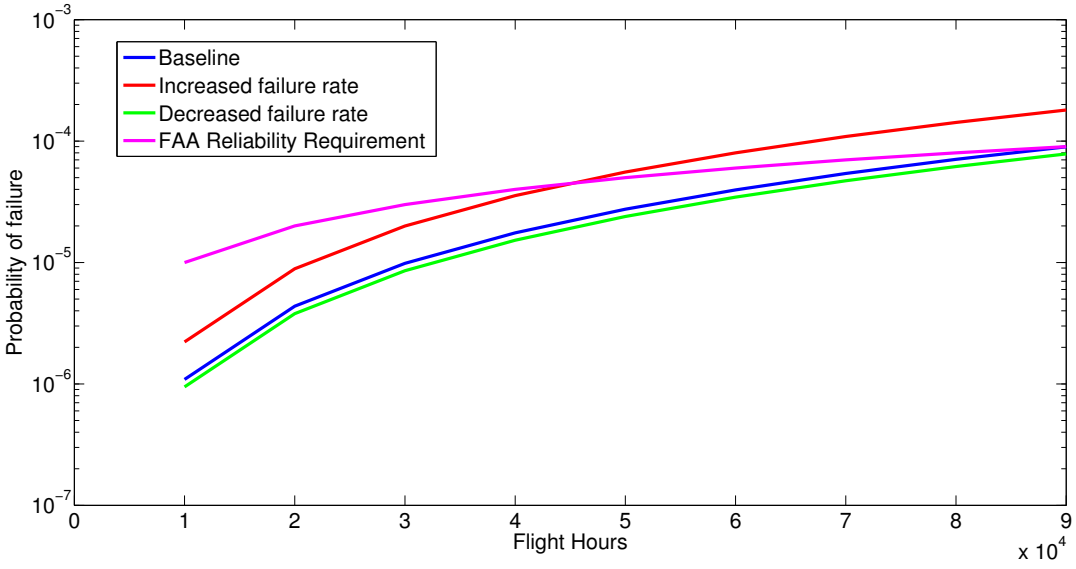

Figure 66: Architecture 1 reliability sensitivity relative to inverter failure rate

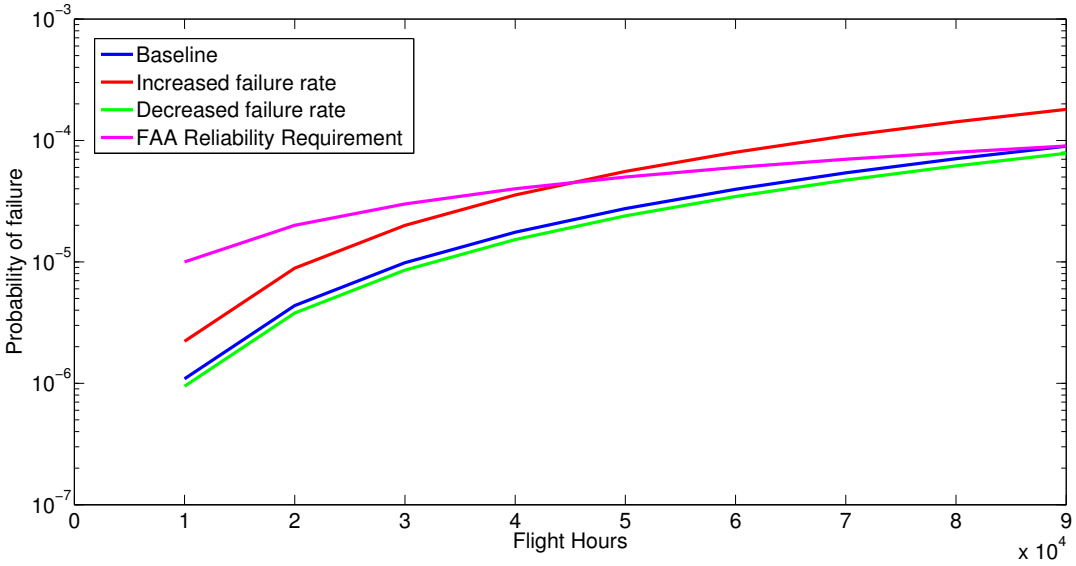

Figure 67: Architecture 1 reliability sensitivity relative to motor failure rate

The system weights and robustness are important factors to consider when selecting an architecture. However, the system performance and stability will need to be studied to make a final decision. The next chapter will provide a further evaluation of each architecture in order to make a final architecture decision.

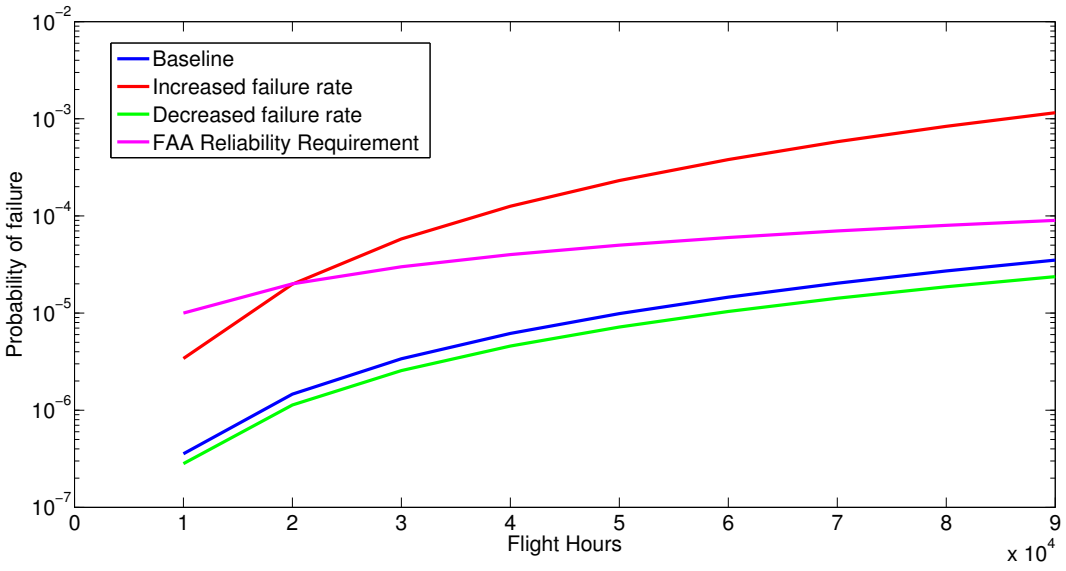

Figure 68: Architecture 2 reliability sensitivity relative to generator failure rate

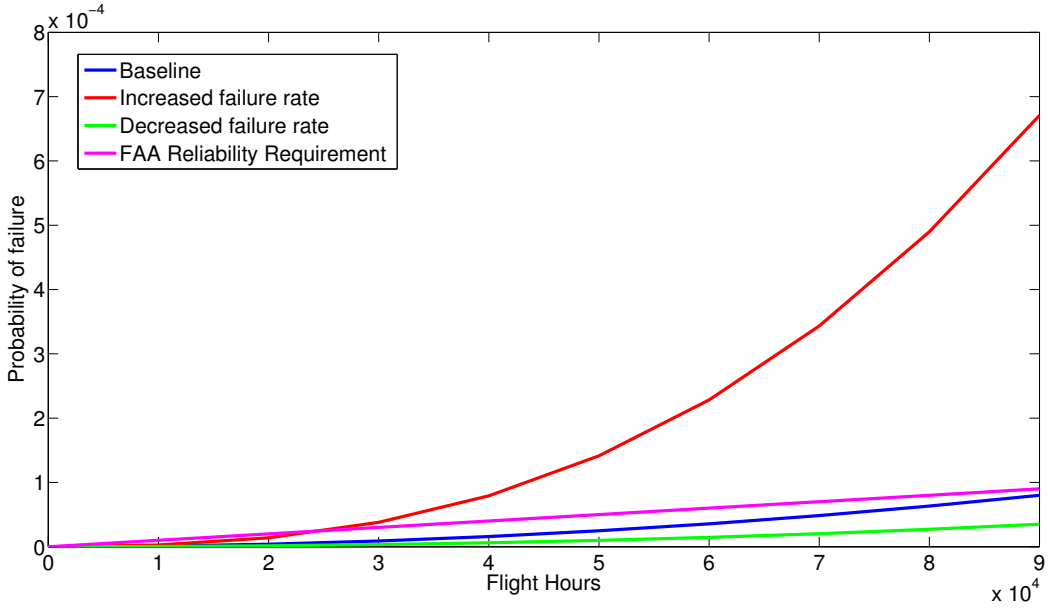

Figure 69: Architecture 2 reliability sensitivity relative to rectifier failure rate

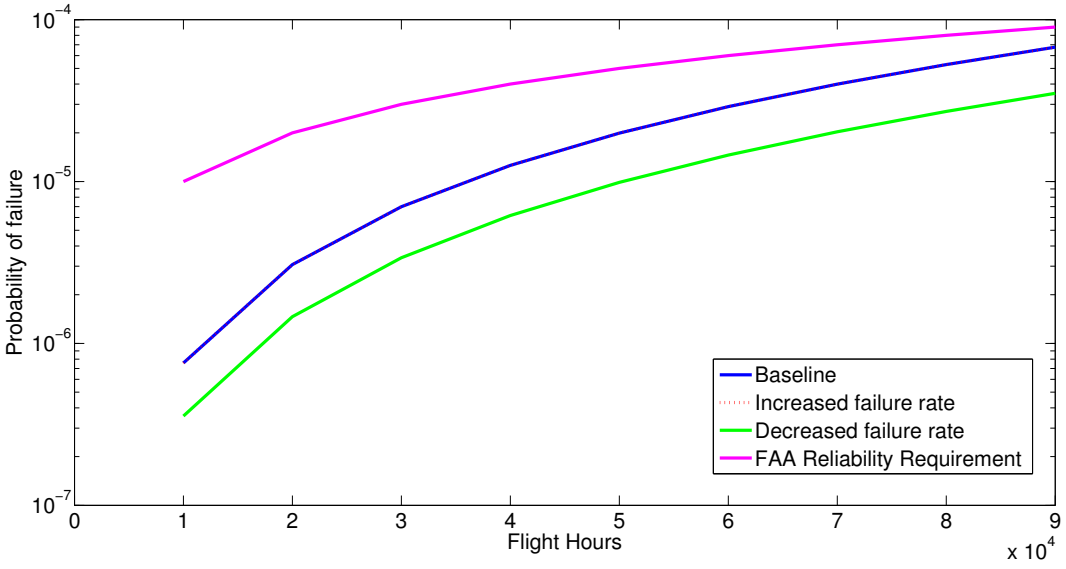

Figure 70: Architecture 2 reliability sensitivity relative to bus failure rate

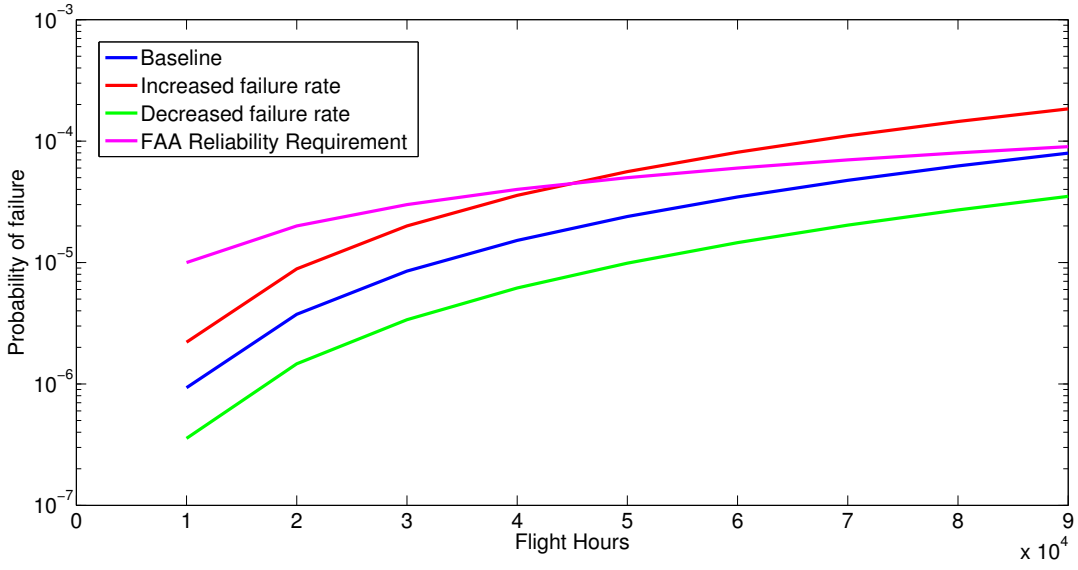

Figure 71: Architecture 2 reliability sensitivity relative to inverter failure rate

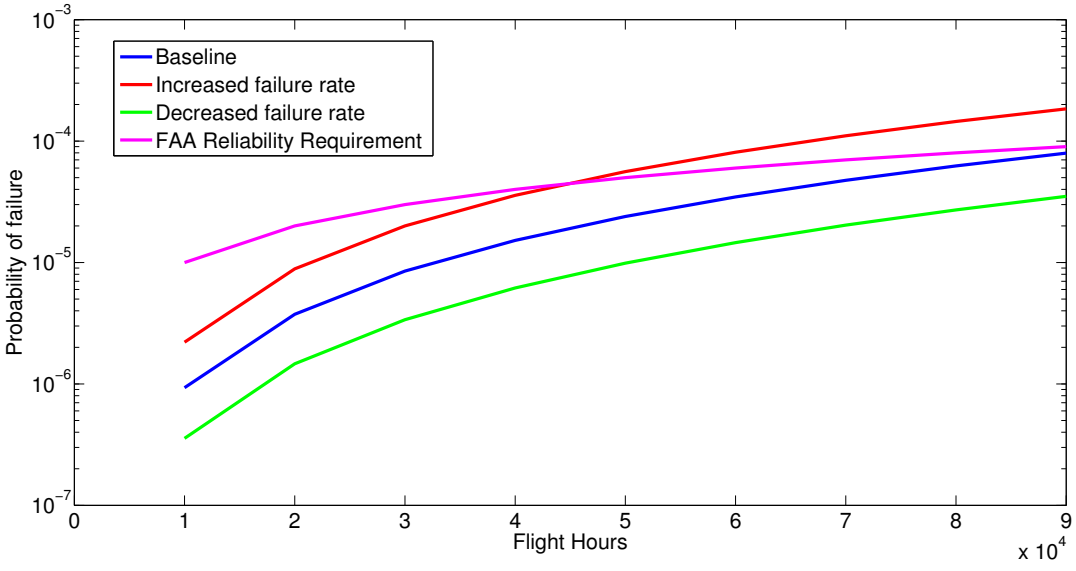

Figure 72: Architecture 2 reliability sensitivity relative to motor failure rate

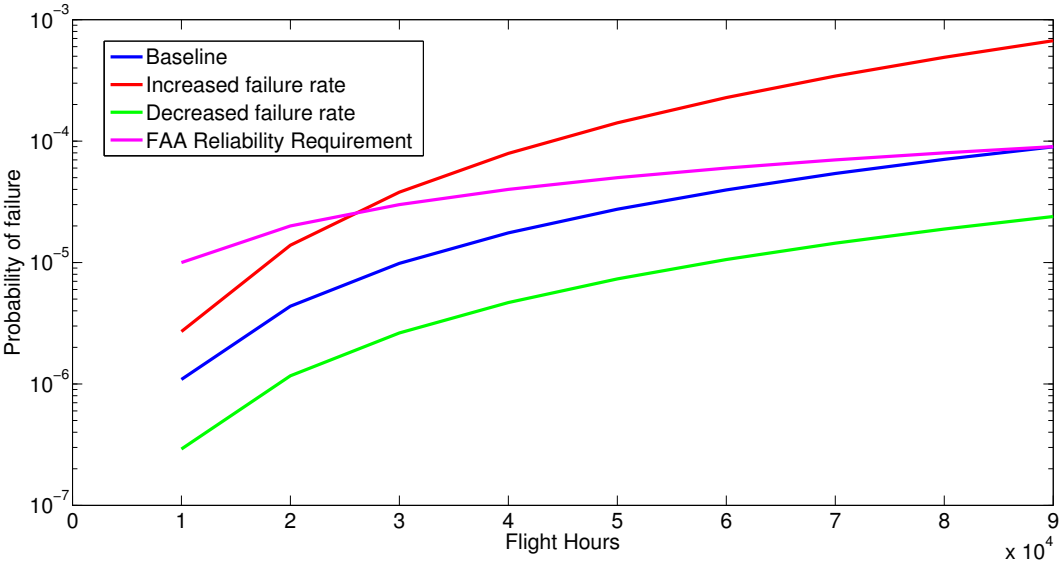

Figure 73: Architecture 3 reliability sensitivity relative to generator failure rate

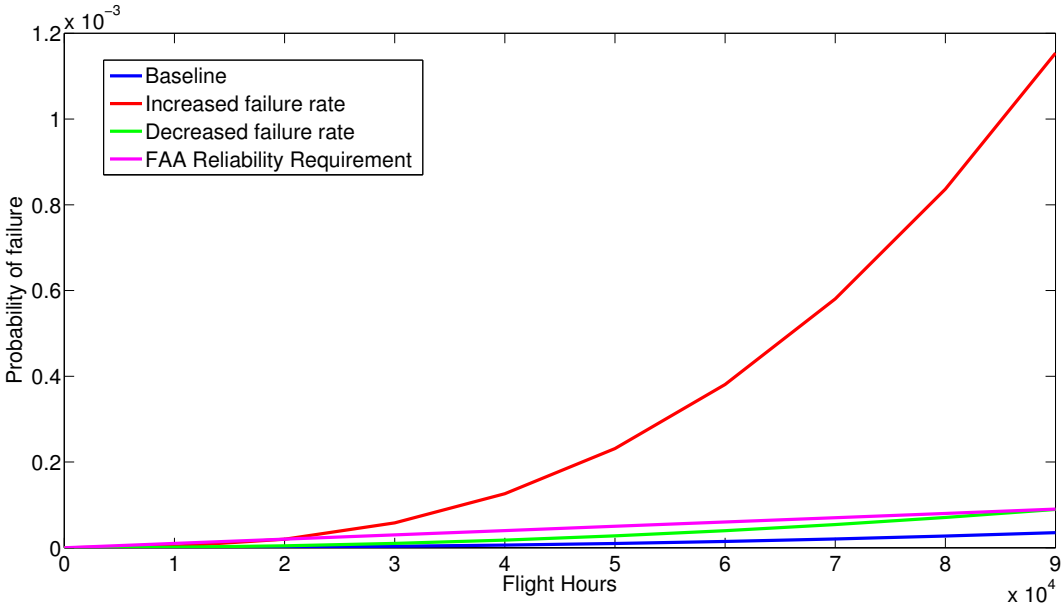

Figure 74: Architecture 3 reliability sensitivity relative to rectifier failure rate

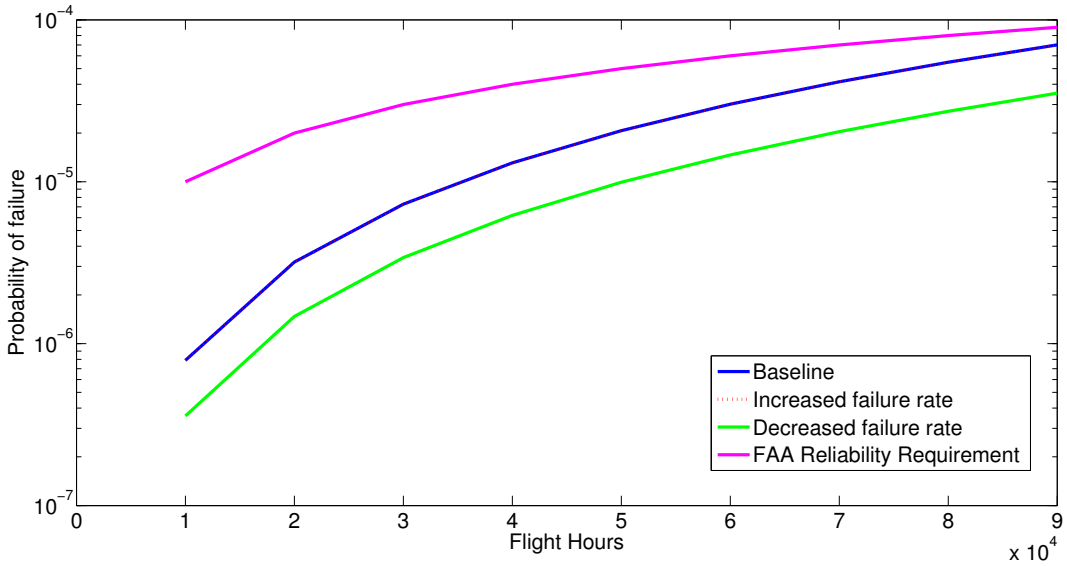

Figure 75: Architecture 3 reliability sensitivity relative to bus failure rate

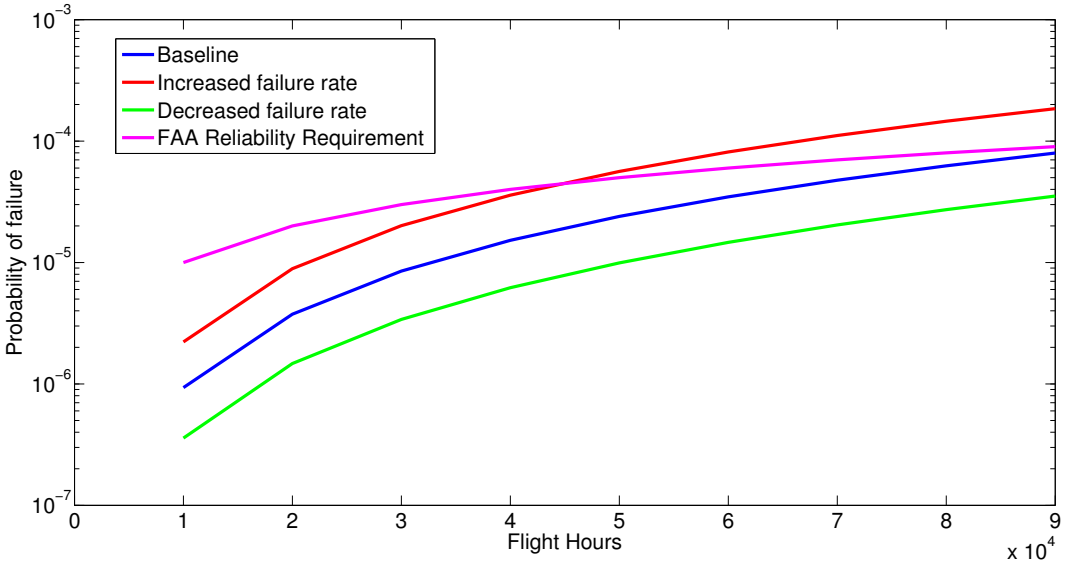

Figure 76: Architecture 3 reliability sensitivity relative to inverter failure rate

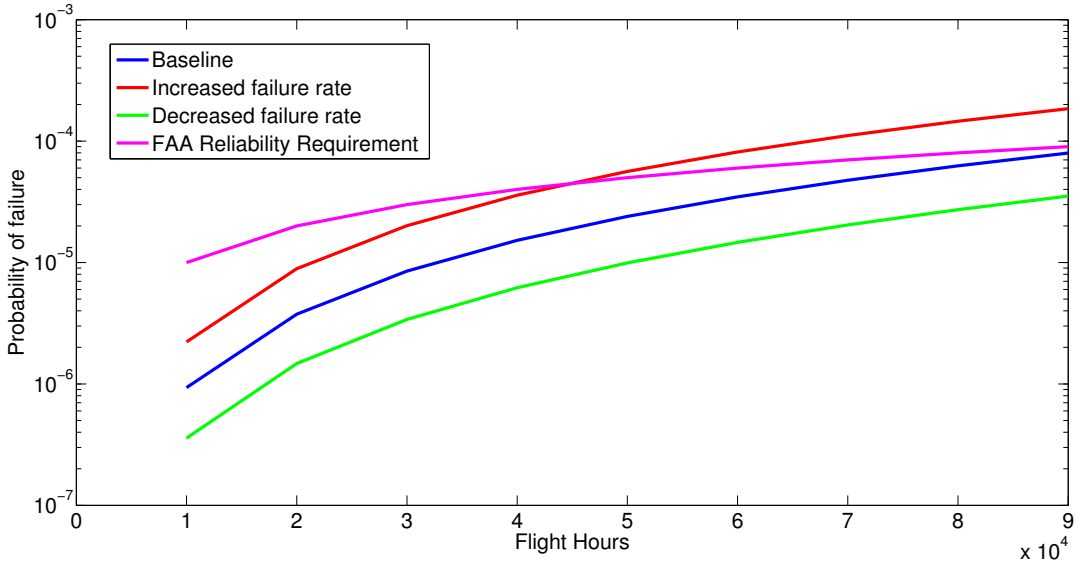

Figure 77: Architecture 3 reliability sensitivity relative to motor failure rate

CHAPTER VI

ARCHITECTURE EVALUATION

The optimization process provided system configurations that are light weight and meet the reliability constraint. The next step is to perform a more detailed analysis on the options to determine the proper system design. To learn more about the system, dynamic modeling is needed. Dynamic modeling will allow the system performance to be studied under a variety of conditions. Furthermore, the modeling will facilitate stability analysis. As discussed in the alternatives chapter, one of the technologies used is actively controlled (or force-commutated) power converters which provides the system with the efficiency needed to reduce overall system weight. However, they are prone to causing instabilities in the system. The stability analysis will help determine if any of the system designs are prone to instability. The first part of the chapter will describe the dynamic models created for the system components. The next section will describe the integration of the component models to provide system models. The final part of the chapter will describe how the system models are used to calculate system stability.

6.1 Component Dynamic Modeling

The first step in modeling each architecture is to create models of the system components. The approach to building each component model will be described and the capabilities of each model will be demonstrated.

6.1.1 Rectifier Model

During the identify technology alternatives phase, voltage-oriented-controlled, voltage-source rectifiers were chosen for the architecture. This rectifier topology was modeled

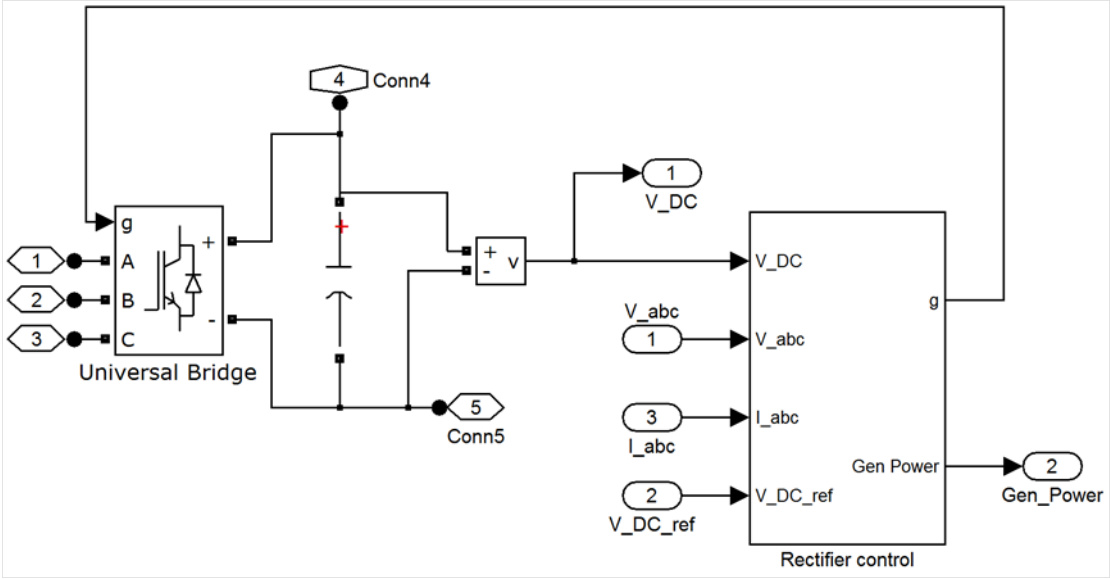

Figure 78: rectifier model

and then simulated to better understand the rectifier's performance.

6.1.1.1 Rectifier Modeling Approach

The model of a voltage source, voltage oriented controlled rectifier is created using the SimPowerSystems toolbox in Simulink. The model is shown in Figure 78. A 3-phase IGBT/diode bridge is connected to the three phase output of a generator, and a capacitor is placed across the output terminals of the bridge. The switches of the bridge are controlled by a decoupled VOC controller.

The decoupled controller block is shown in Figure 79. The inputs into the block are the three-phase voltage from the generator, the three-phase current from the generator, the output DC voltage of the rectifier, and the reference bus voltage. When using this type of rectifier, there is an important limitation that must be recognized; in order to maintain control of the rectifier, the DC voltage must be higher than the peak voltage generated in the diodes in the rectifier. If this condition is not met, the polarization on the diodes will not be correct and the rectifier cannot be controlled [125]. To ensure that this problem does not occur, the DC bus voltage must satisfy

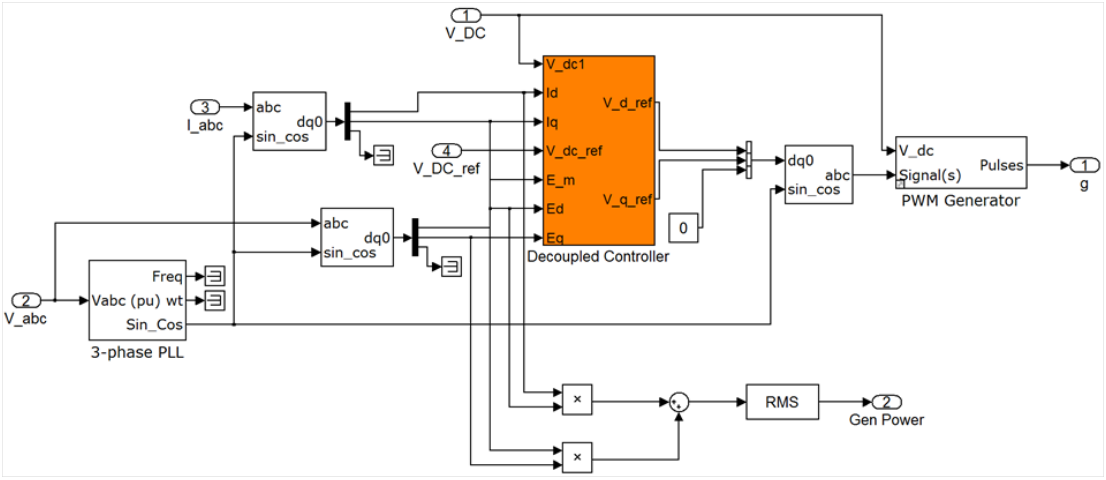

Figure 79: Rectifier controller

the following condition [133]:

$$V_{DC} > \sqrt{3[E_m^2 + (\omega L i_D)^2]} \tag{70}$$

where, i_D is the DC current supplied to the load of the rectifier.

The VOC scheme selected for this rectifier uses the stationary dq reference frame. In order to use this reference frame, a coordinate transformation is required. The equations used to transform the coordinates are [133] [93]:

$$\begin{bmatrix} \alpha \\ \beta \end{bmatrix} = \begin{bmatrix} \frac{2}{3} & -\frac{1}{3} & -\frac{1}{3} \\ 0 & \frac{1}{\sqrt{3}} & -\frac{1}{\sqrt{3}} \end{bmatrix} \begin{bmatrix} a \\ b \\ c \end{bmatrix} \tag{71}$$

$$\begin{bmatrix} a \\ b \\ c \end{bmatrix} = \begin{bmatrix} 1 & 0 \\ -\frac{1}{2} & \frac{\sqrt{3}}{2} \\ -\frac{1}{2} & -\frac{\sqrt{3}}{2} \end{bmatrix} \begin{bmatrix} \alpha \\ \beta \end{bmatrix} \tag{72}$$

$$\begin{bmatrix} d \\ q \end{bmatrix} = \begin{bmatrix} cos(\theta) & sin(\theta) \\ -sin(\theta) & cos(\theta) \end{bmatrix} \begin{bmatrix} \alpha \\ \beta \end{bmatrix} \tag{73}$$

$$\begin{bmatrix} \alpha \\ \beta \end{bmatrix} = \begin{bmatrix} cos(\theta) & -sin(\theta) \\ \sin(\theta) & cos(\theta) \end{bmatrix} \begin{bmatrix} d \\ q \end{bmatrix} \tag{74}$$

Theta is the voltage angle which is found using a phase-locked loop (PLL). A PLL is a feedback controller which "locks" two waveforms to the same frequency [87]. This controller also has the ability to determine the frequency of a wave and find the phase between waveforms [120].

Once the coordinate transformation has taken place, the voltage and current signals are sent to the decoupled controller which is shown in Figure 80. As shown in the diagram, three PI controllers are required, two of which are current controllers [30] [62]. The proportional (kip) and integral (kii) coefficients of the current PI controllers are

$$k_{ip} < \frac{2\pi F_s}{10} L; k_{ii} < \frac{2\pi F_s}{10} R \tag{75}$$

where, F_s is the PWM switching frequency.

The proportional (kvp) and integral (kvi) coefficients for the PI voltage controller are

$$k_{vp} < \frac{2\pi F_s C}{30 E_m}; k_{vi} = 0.001 \tag{76}$$

The integral portion of the PI voltage controller has almost no effect on the outcome of the model, which is why a small coefficient is arbitrarily chosen. The proportional coefficient for the voltage controller has a very strong influence on the performance of the controller. A large proportional coefficient will cause large voltage oscillations on the bus and hinder convergence. Using a small proportional coefficient will reduce the magnitude of the oscillations; however, a higher frequency harmonic distortion will be present on the bus.

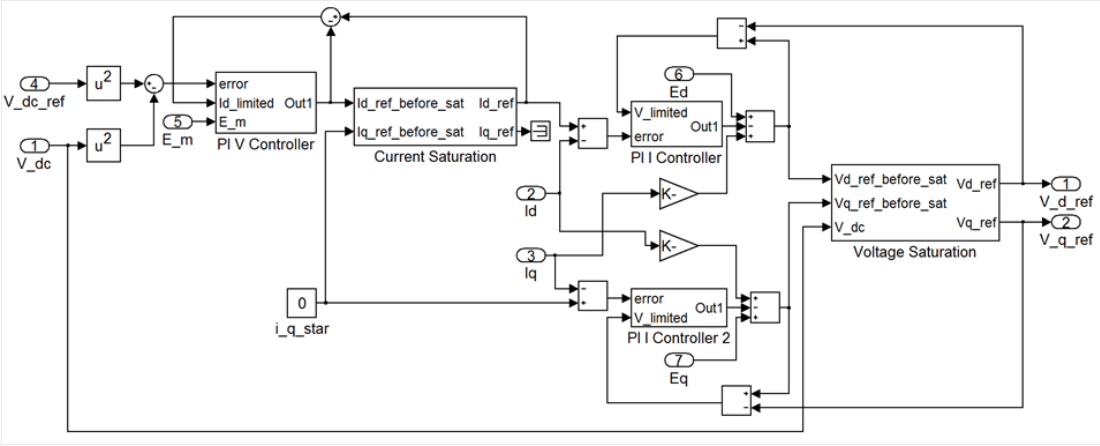

Figure 80: Rectifier decoupled controller

In some cases, a large step in the reference voltage may occur which will cause the controller to demand a higher voltage than the rectifier can supply; therefore, a saturation block needs be added to the current controller to ensure that the reference voltage does not exceed the maximum voltage output of the rectifier. This issue can also arise for the voltage controller, so a saturation block is also used in conjunction with it. Although using saturation fixes the problem of demanding too large of a voltage or current, it introduces another problem. When the voltage or current is limited, a phenomenon called integrator wind-up can occur which causes an overshoot in the response of the PI controller and the controller error will increase. In order to correct this problem, the error input into the current controller should become

$$\bar{\varepsilon} = \varepsilon + \frac{\bar{v} - v}{k_p} \tag{77}$$

where, $\bar{\varepsilon}$ is the limited error and $\bar{v}$ is the limited voltage. The same principle can be applied to the voltage controller.

6.1.1.2 Rectifier Model Validation

The rectifier model was tested to ensure it is properly representing the component. The inputs into the model are selected based upon literature and to represent values

Table 36: Rectifier design variable settings

Rectifier Parameter	Value
Snubber resistance	1e5 Ω
Snubber capacitance	infinite
Internal resistance	0.001 Ω
Capacitance	0.02 F
Inductance	0.01 H
Switching frequency	18,000 Hz
Reference voltage	700 V

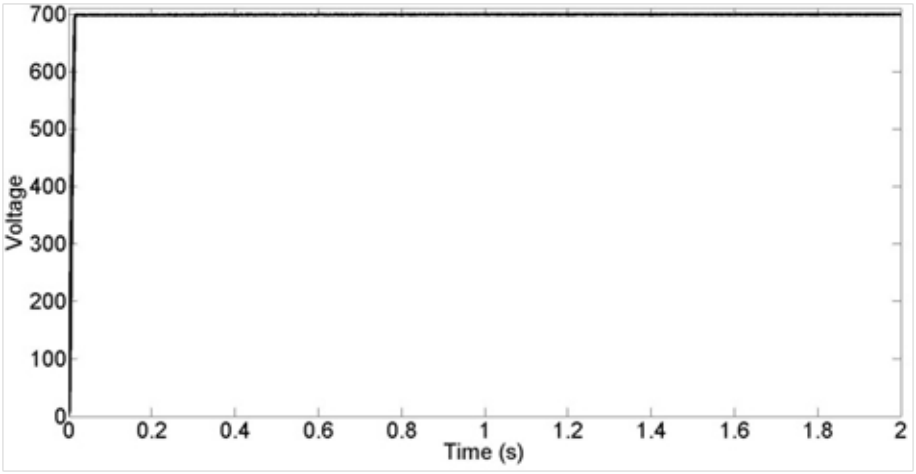

Figure 81: Rectifier model DC bus voltage

that may be used in the final system design.

The rectifier model is tested by connecting it to a simple generator model and a RLC load. The generator model consists of an ideal three-phase voltage source with a series resistance and inductance. For this test, the generator voltage is set to 800 Volts, and the resistance and inductance are 0.2 Ω and 6 X 10^4 H, respectively. The rectifier parameters are set to the values listed in Table 36. The RLC load has an active power draw of 100 kW, inductive reactive power of 100 W, and capacitive reactive power of 100 W.

The rectifier output is shown in Figures 81 through 84. The DC bus voltage reaches the 700 V target set. The zoomed view of the voltage, Figure 82, demonstrates some harmonic interference in the voltage output signal. Figures 83 and 84 show the

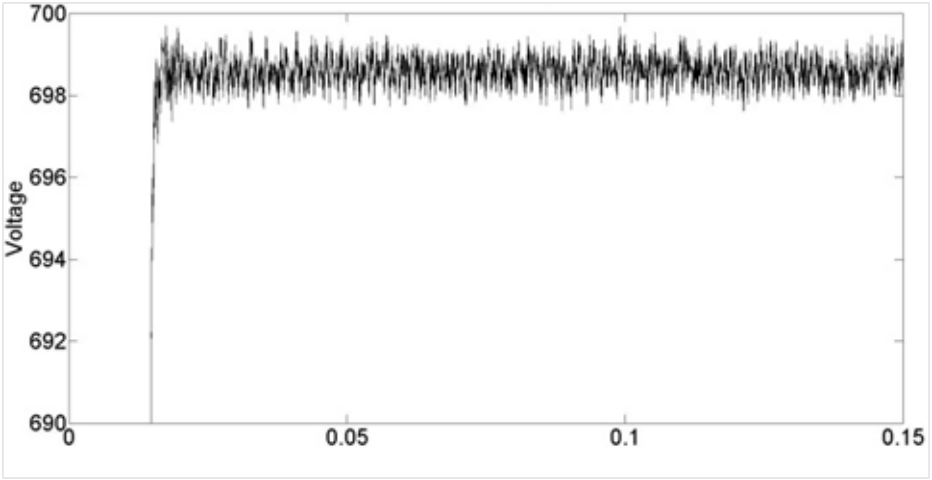

Figure 82: Rectifier model DC bus voltage close-up

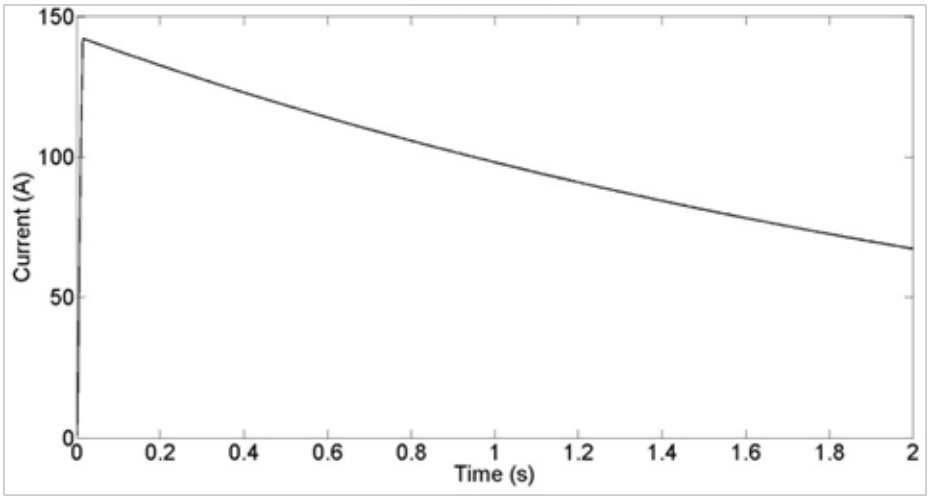

Figure 83: Rectifier model DC bus current

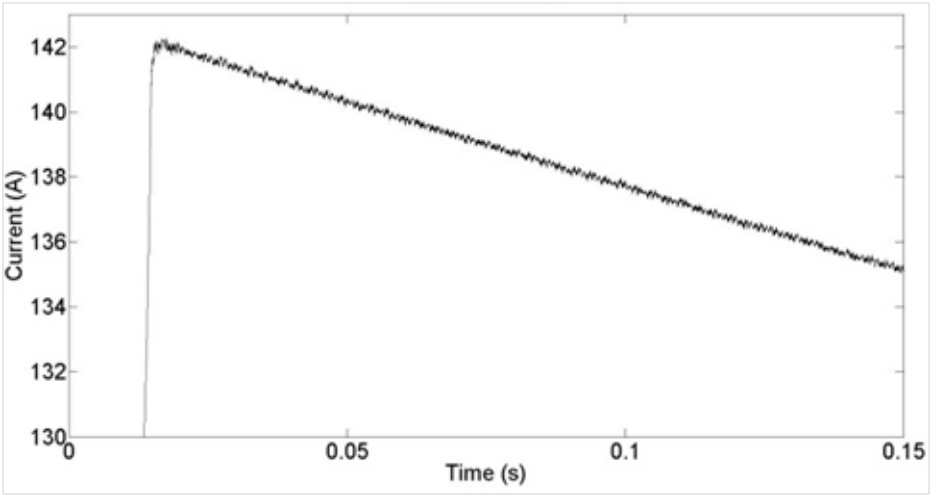

Figure 84: Rectifier model DC bus current close-up

DC bus current draw spikes in the beginning of the simulation as the motor is being started from rest; then, the current decreases and begins to level. The same harmonics shown in the voltage output are also found in the current output. Filters can be added to the rectifier in order to reduce the harmonic contamination in the output.

6.1.2 Inverter Model

The selected technology for the inverter is a pulse-width modulated, voltage source inverter. The inverter is the same circuit as the rectifier; however, current flow is reversed and the control scheme is different.

6.1.2.1 Inverter Modeling Approach

The Simulink system used for the inverter modeling is shown in Figure 85. The inverter is supplied by an ideal DC voltage source and is connected to a permanent magnet synchronous machine to simulate a similar type of load that would be found in a turboelectric propulsion system.

The inverter block is shown in Figure 86. The inverter model consists of a capacitor connected across the terminals of a three phase IGBT/diode bridge [24]. The pulses to control the switches are created using a PWM generator. The PWM signals are

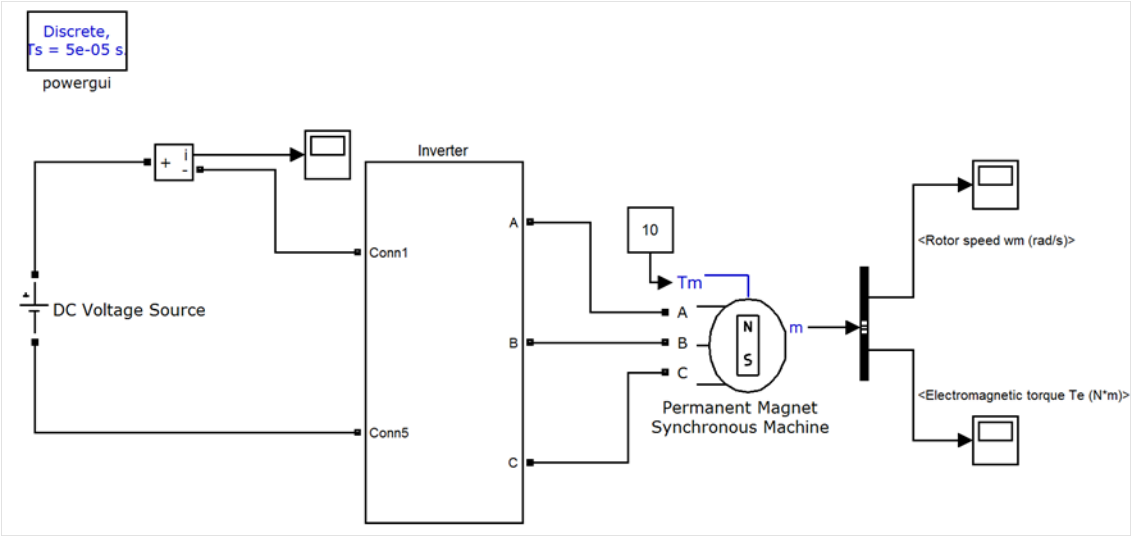

Figure 85: Model for inverter testing

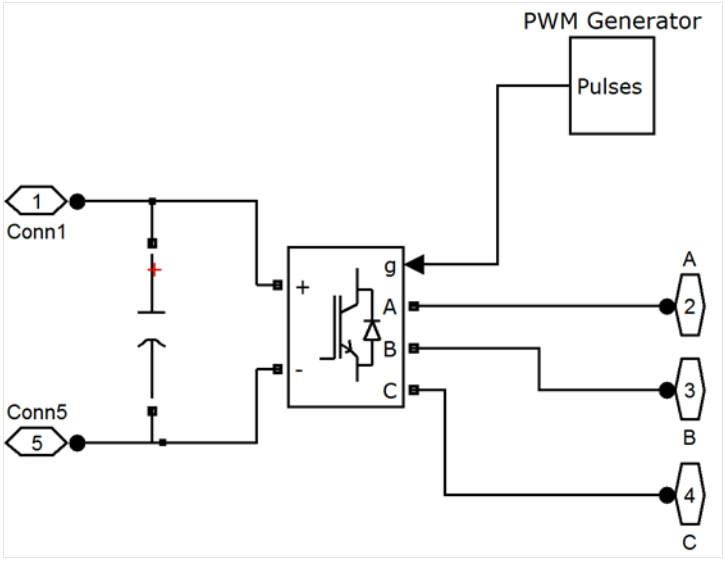

Figure 86: Inverter model

constructed by comparing a carrier signal to a control signal. The carrier signal is a triangle wave that is set to a high frequency. The control signal is a sinusoidal signal at the desired output frequency. A 20 kHz carrier signal and control signal are shown in Figure 87. The blue signal is the carrier signal and the green signal is the control signal. The magnitude of the carrier signal corresponds to the modulation index [11]. The modulation index determines the amplitude of the output voltage of the inverter. The amplitude of the control signal should not be greater than that of the carrier signal to ensure that overmodulation does not occur. The pulses sent to the switches are created by comparing the carrier signal to the control signal. Based upon this comparison, the signal is set to 0 or 1. For each arm of the bridge, two signals are sent. These signals should be opposite of each other. An example of the pulses is shown in Figure 88. A set of pulses is generated for each of the three arms of the inverter.

After the power flows through the inverter, it is sent to the permanent magnet motor. A SimPowerSystems pre-built model was used to simulate the motor. The motor model requires a value for mechanical torque that is applied to the motor. The sign associated with this torque decides whether the machine is in motor or generator mode. The motor is connected to the three-phase output of the converter.

6.1.2.2 Inverter Model Validation

The inverter is tested with the same inputs that are used by Lee and Ehansani [81]. An ideal DC voltage source of 300 V is supplied to the inverter, and the inverter has a load with 20 mH of inductance and 5 Ohms of resistance. The switching frequency of the inverter is 1 kHz and the output frequency is set at 60 Hz. The resulting output three-phase AC current is shown in Figure 89, and the inverter phase voltage (for a single phase) is shown in Figure 90. The results of the experiment are identical to those present in Lee and Ehasani's paper [81].

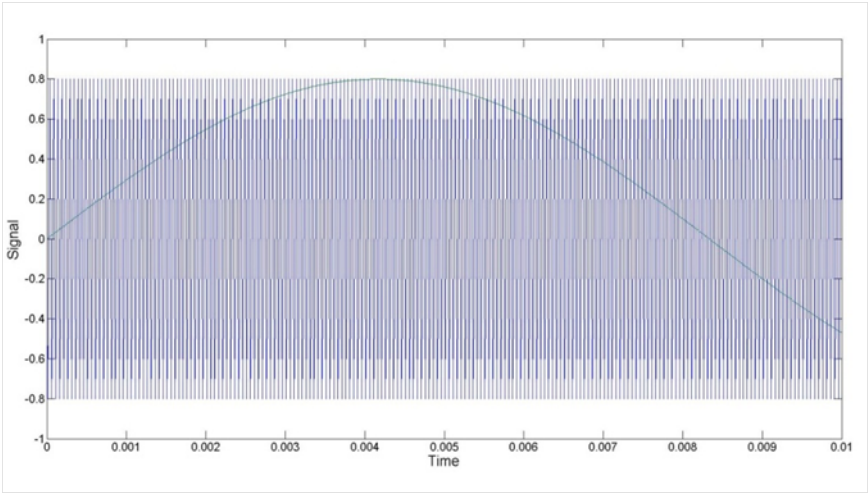

Figure 87: PWM control and carrier signals

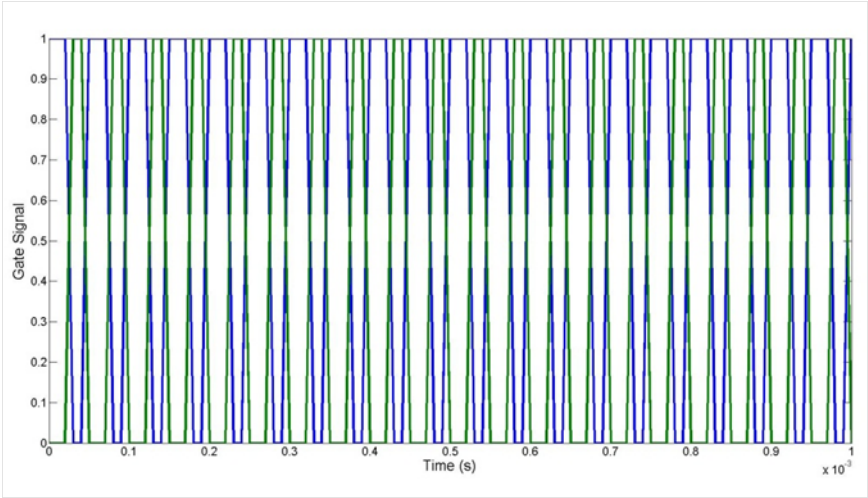

Figure 88: PWM switching pulses

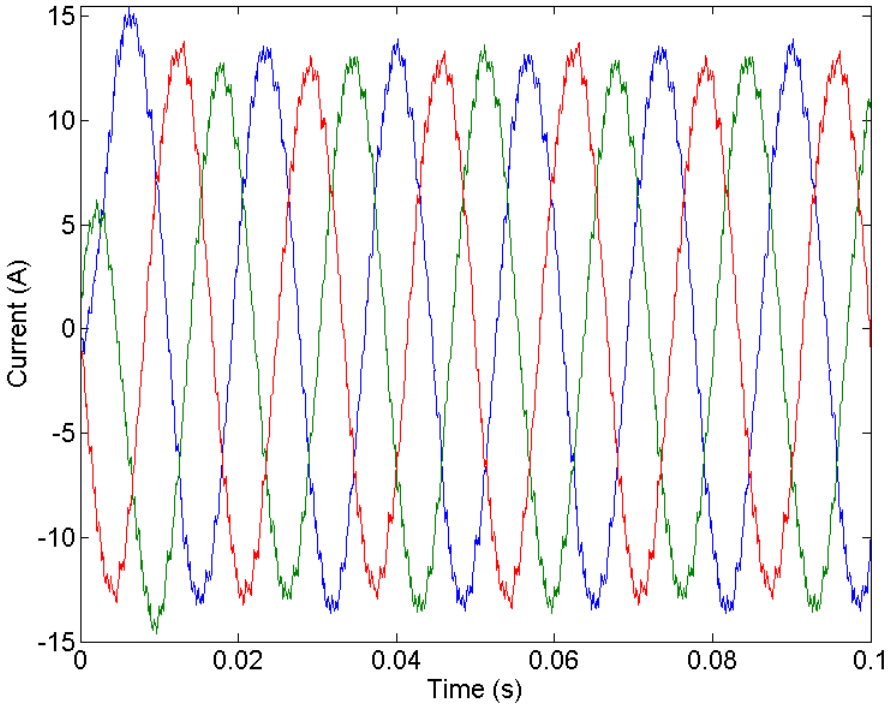

Figure 89: Inverter output current

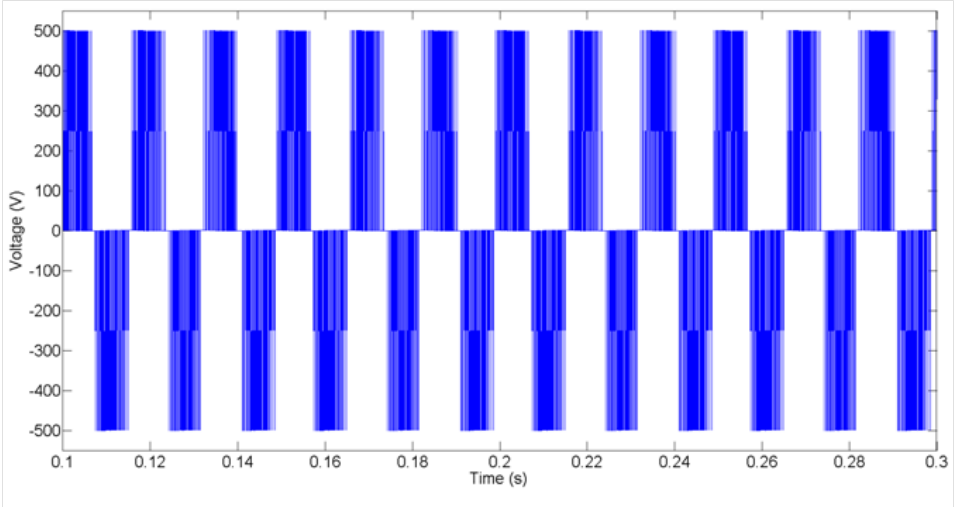

Figure 90: Inverter phase voltage

6.1.3 Cable Modeling

The performance model of the cable is relatively simple. If superconducting cables are used, only minimal losses will occur. Essentially, all power is transmitted through the cable from start to end. Some losses will occur at joints in the cable as discussed in the sizing model section. A small amount of additional power will be needed from the generators to compensate for the loss, and, proportionally, a small voltage drop will occur.

The cable was modeled based upon SimPowerSystem's pi section line which consists of a resistor, inductor, and capacitor. The value for each element is set based upon expected values for the cable [135].

6.1.4 Machine Modeling

Since detailed information on the design of the machines is not available at this point in the design process, simple models were used for the machines. The generator was modeled using an ideal three-phase AC voltage source with a series resistance and inductance. The motors were modeled using the pre-built SimPowerSystems permanent magnet machine model. The machine model parameters were updated to correspond with the superconducting motor that is presented by Masson et al [94].

6.2 System Dynamic Modeling

Once all the component models are finished, system modeling commences. Five system models are created. The first is a single motor model. This model consists of one of each component: generator, rectifier, bus, inverter, motor. This model is built to ensure that the component models could be successfully integrated. The next model built is the baseline system which was built to determine whether the full system model could be successfully constructed. After the baseline system is

completed, each of the three architectures selected in the previous chapter are modeled. The creation of each model will be discussed. The steady-state performance is analyzed for the one motor, baseline, and architecture 1 models. Since the baseline and architecture 1 systems have many attributes in common with the architecture 2 and 3 system during normal operation, architectures 2 and 3 are simulated using an engine-out scenario.

6.2.1 One Motor Model

The system tested with one permanent magnet motor is shown in Figure 91. The generator acts as a three-phase voltage source. The output of the generator is then rectified and sent to the DC bus. The DC bus is modeled using a pi section line. The pi section line models the resistance, inductance, and capacitance of a transmission line. The power on the DC bus is transmitted to the inverter. The three-phase output of the inverter is then used to drive the motor. Each component requires a set of design variables to be initialized in order to run the model. The values selected for the design variables are shown in Table 37; these were selected so that the system remains stable. The target bus voltage is selected to be equivalent to the baseline. The resistance, inductance, and capacitance parameters for the transmission line are set to mimic a superconducting cable, and the inverter values are selected based upon information found in literature. The input values for the motor are the most difficult to define. A small perturbation to one of these inputs will have a dramatic impact on the motor power draw and rotor speed. The settings for the motor were selected based upon published superconducting motor design data.

The results of this study are shown in Figures 92 through 97. The generator output voltage is shown in Figure 92. The output is a smooth sinusoidal signal since an ideal voltage source is used to model the generator. The generator output current is illustrated in 93. The current draw spikes in the beginning as the system starts up

Table 37: Single motor system model design variables

Component	Parameter	Value
Generator	Voltage Amplitude	12,000 V
	Voltage Phase	0
	Frequency	60 Hz
	Resistance	0.2 Ω
	Inductance	0.0006 H
Rectifier	Snubber Resistance	1e5 Ω
	Snubber Capacitance	infinite
	Resistance	0.01 Ω
	Capacitance	0.02 F
	Inductance	0.01 H
	Switching Frequency	20,000 Hz
	Reference Voltage	4,000 V
	Current Controller Bandwidth Coefficient	0.05
	Voltage Controller Bandwidth Coefficient	0.003333
Transmission Line	Resistance per km	0.01273 Ω
	Inductance per km	0.09337 H
	Capacitance per km	12.74e-10 F
	Length	0.1 km
Inverter	Capacitance	1e-6 F
	Modulation Index	0.8
	Output Frequency	60 Hz
	Switching Frequency	10,000 Hz
Motor	Speed	2000 RPM
	Rotor Type	Round
	Stator Phase Resistance	0.18 Ω
	Armature Inductance	0.000835 H
	Torque Constant	0.21435 $\mathrm{N \cdot m/A}_{peak}$
	Inertia	0.00112 $\mathrm{J(kg \cdot m^2)}$
	Viscous Damping	0.1035 $\mathrm{F(N \cdot m \cdot s)}$
	Pole Pairs	2
	Static Friction	0 $\mathrm{Tf(N \cdot m)}$

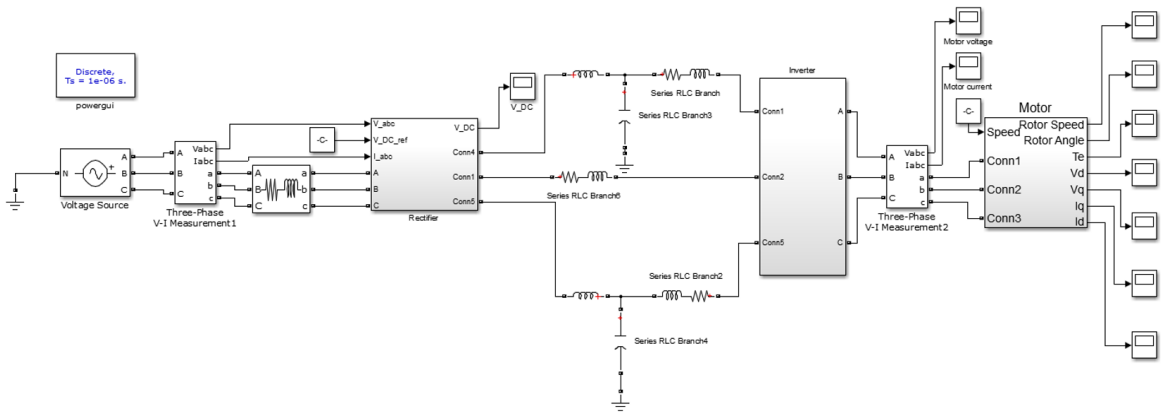

Figure 91: One motor system model

from rest; as the motor reaches steady state, the generator output current becomes constant.

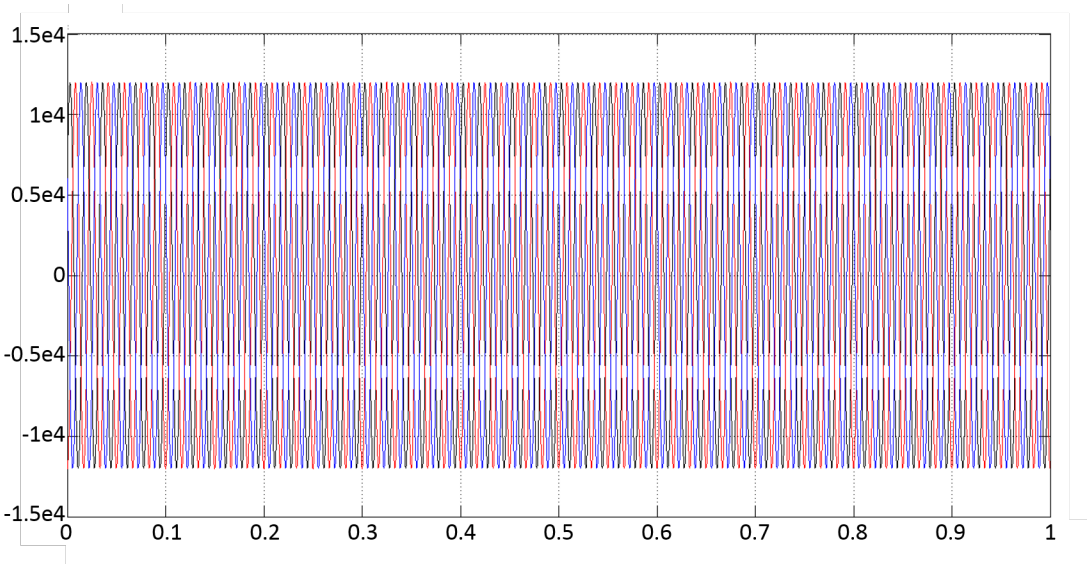

Figure 92: Generator output voltage

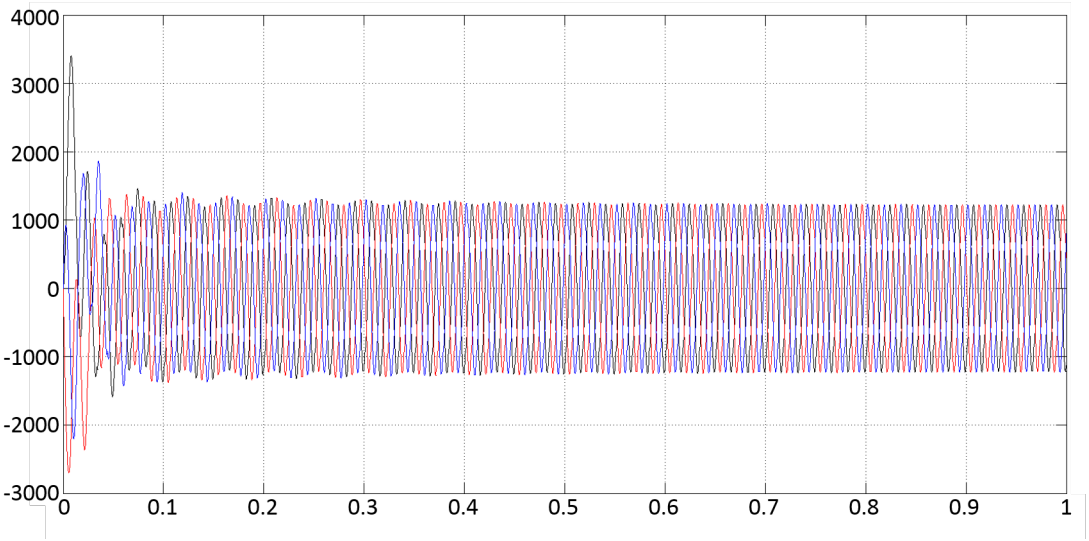

Figure 93: Generator output current

The rectifier output voltage is revealed in Figure 94, and its output current is shown in Figure 95. The DC bus voltage reaches the 4000 V target set by the inputs. The current is also well maintained with some harmonic interference. Filtering can be used to produce a smoother output. Given the voltage and current levels on the bus, around 2.3 MW of power will be delivered to the inverter.

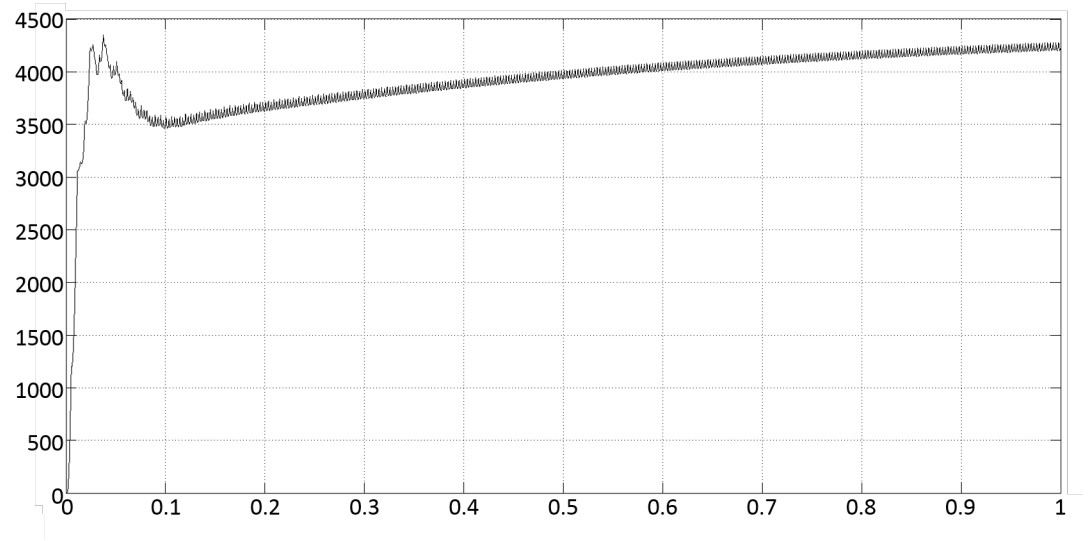

Figure 94: DC bus voltage

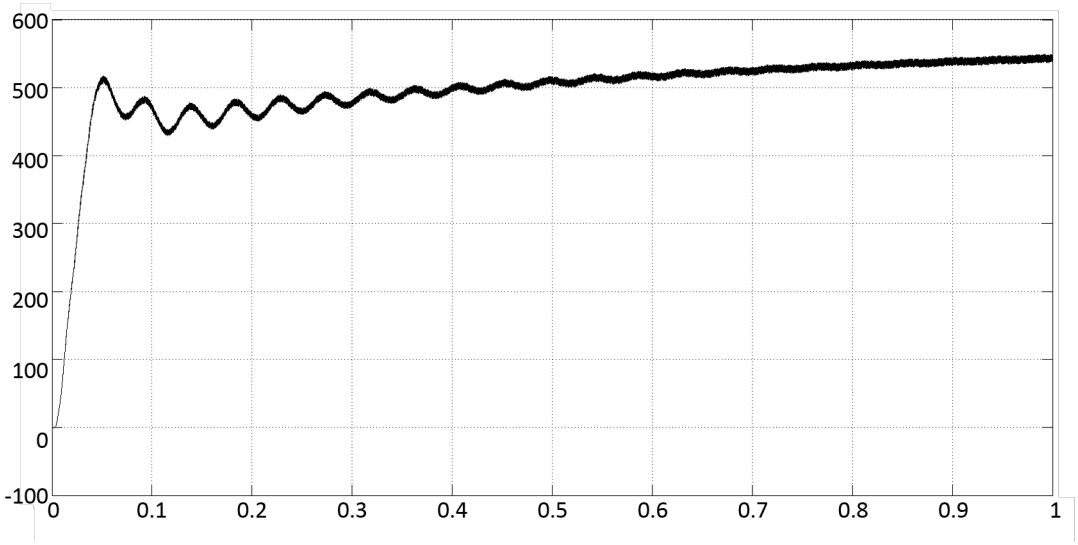

Figure 95: DC bus current

The inverter output current going to the motor, and the inverter output voltage to the motor are shown in Figure 96 and Figure 97, respectively. Figure 96 demonstrates that the inverter provides a smooth sinusoidal current signal to the motor; however Figure 97 shows that the voltage output of the inverter is not a smooth signal. (A zoomed view of the plot is shown in Figure 98.) The signal consists of high voltage spikes which are caused by the PWM control of the inverter.

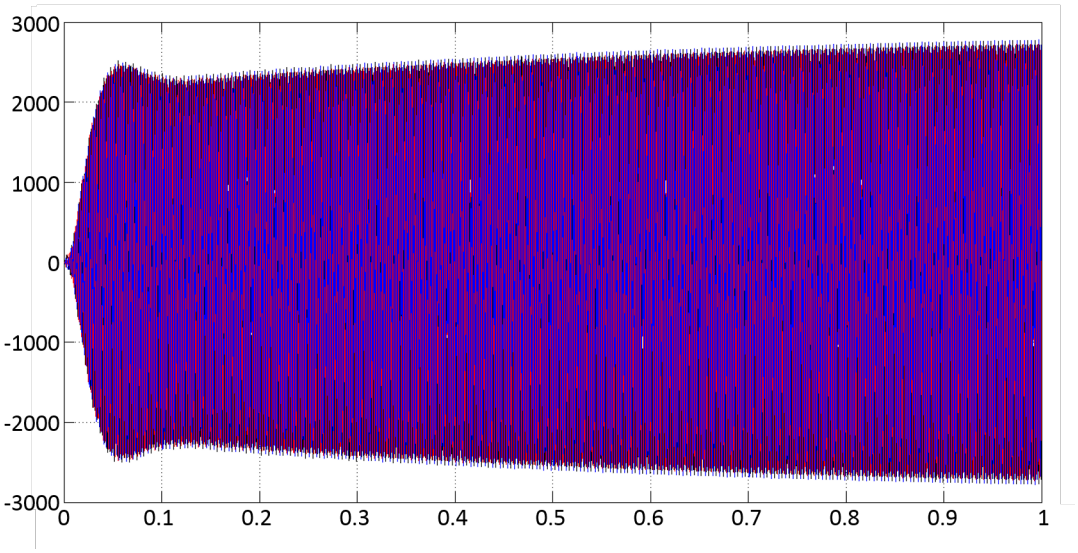

Figure 96: Inverter output current

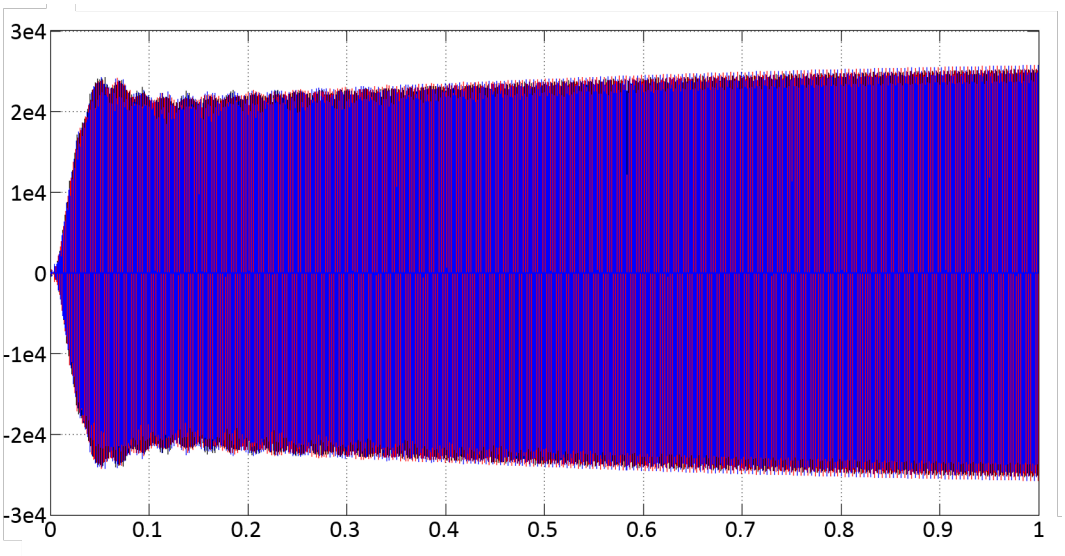

Figure 97: Inverter output voltage

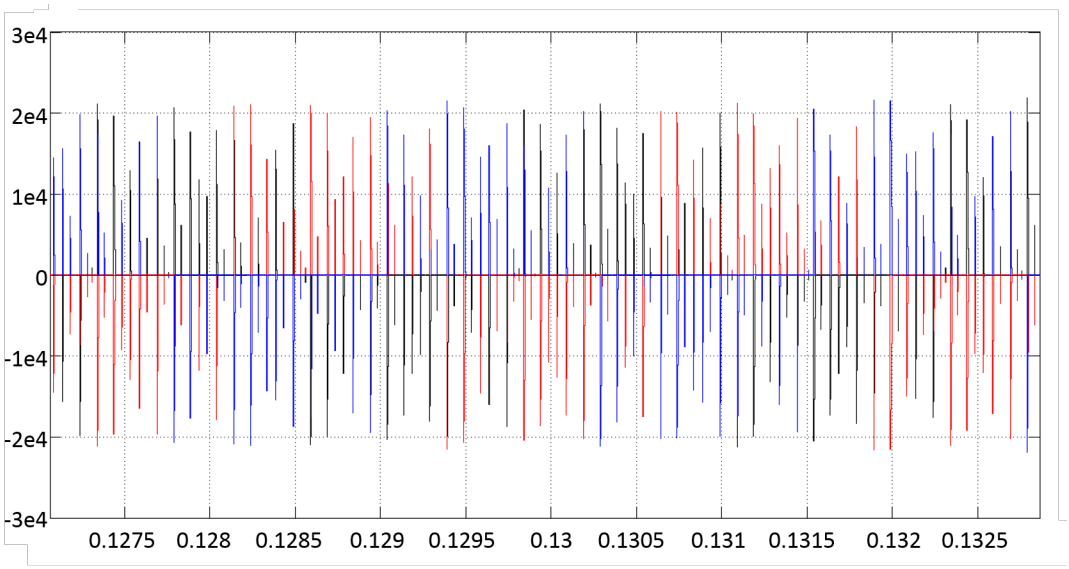

Figure 98: Inverter output voltage zoomed view

As demonstrated by Figure 97, the output voltage of the inverter going into the motor is contaminated with the PWM switching harmonics. The motor input voltage can be smoothed into a sinusoidal signal by using a low-pass RC filter between the inverter and motor. The filter resistance is set at 1 Ohm and the capacitance is set to 0.01 F. The filtered input voltage for the motor is shown in Figure 99. the filter smooths the output voltage of the inverter into a smooth sinusoidal signal.

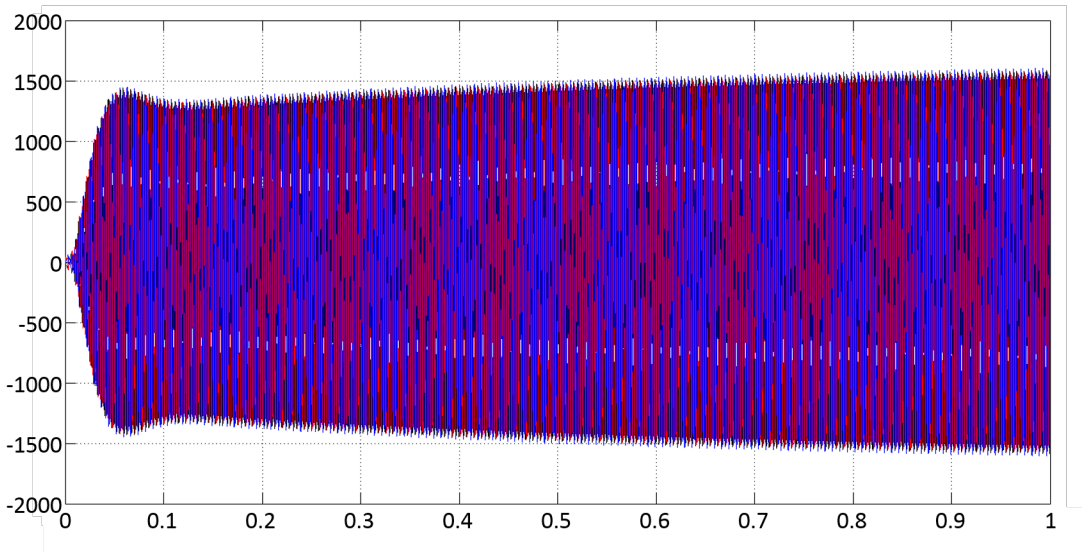

Figure 99: Inverter output voltage with filter

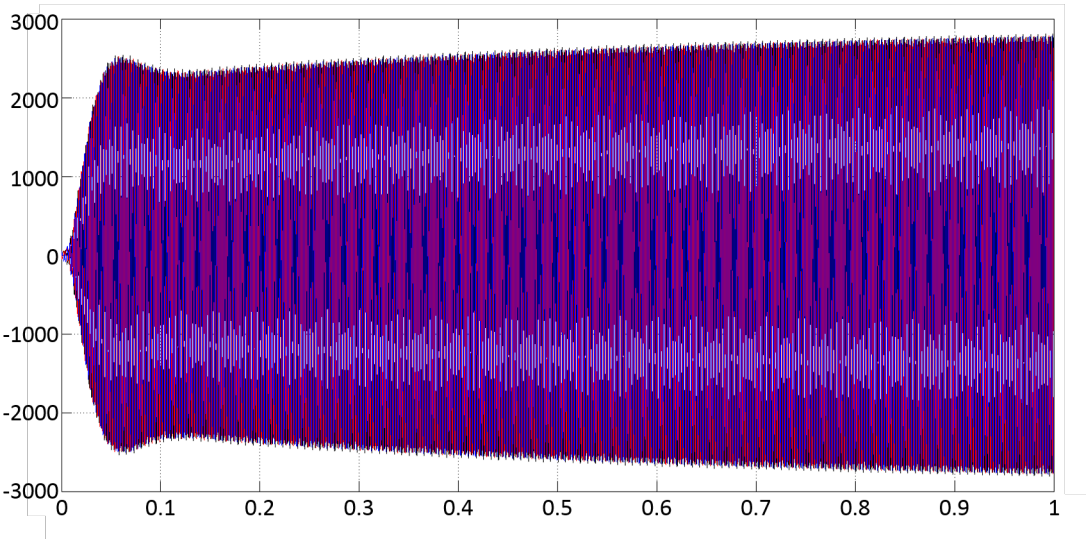

Figure 100: Motor power consumption with filter

6.2.2 Baseline System Model

After the successful test of a system with one motor, a model of the baseline system was built which is shown in Figure 101. The component models were integrated into the model and connected based upon the architecture diagram. The component models are found under the masks shown in the system model figure. The masked

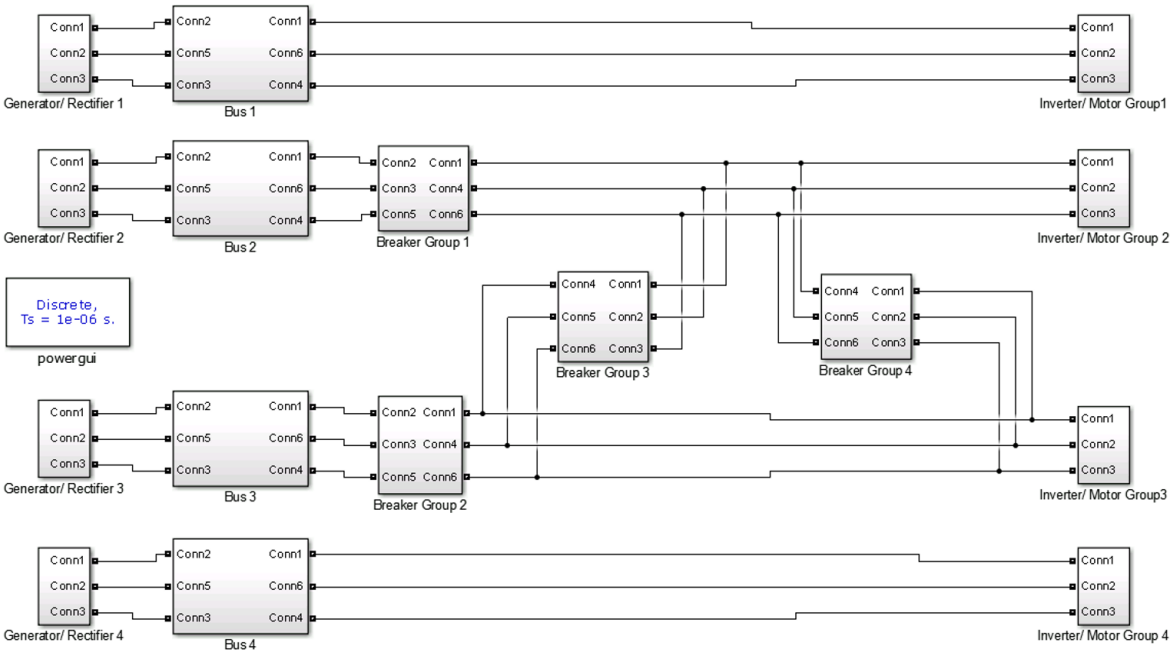

Figure 101: Baseline system model

component models are shown in Figures 102, 103, and 104. Figure 102 shows the generator and rectifier models. The generator is represented using an ideal voltage source with a series inductance and resistance. The rectifier model is the same model that was described during the component model section. Figure 102 also shows that output inductors were used; they were included to filter the current output of the rectifier. Figure 103 shows the bus model. The resistance, inductance, and capacitance values were set to be representative of a superconducting cable. Figure 104 shows the inverters and motors. The inverter model is the model described in the component modeling section. The motors are represented using a prebuilt permanent magnet machine model the was available through the Simulink SimPowerSystems toolbox. Along with the component models that were described, circuit breakers are included to reroute power during a failure.

The settings for the design variables are shown in Table 38. The model was run to simulate 0.5 seconds. The run time to complete the simulation is about 45 minutes. The state variables (current and voltage) were tracked through the model, and the

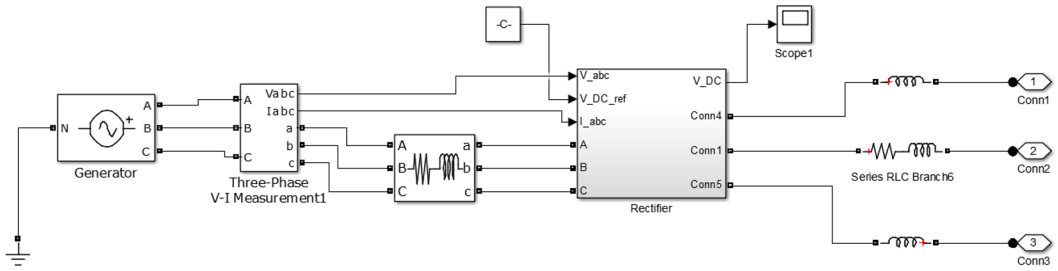

Figure 102: Generator and rectifier masked model

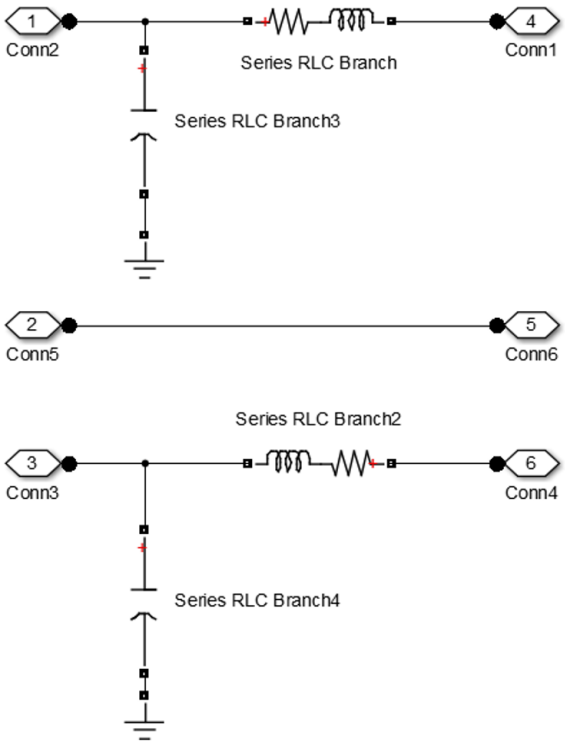

Figure 103: Bus masked model

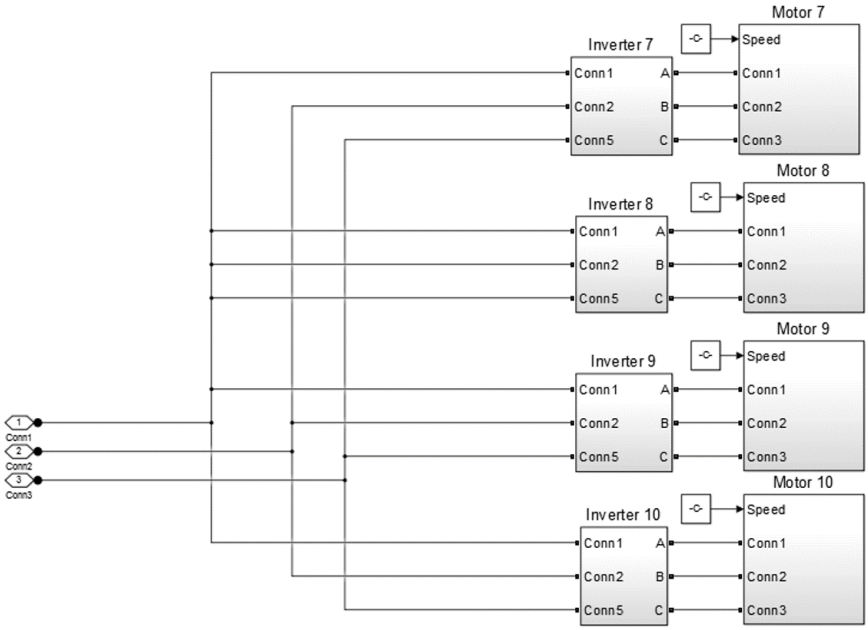

Figure 104: Inverter and motor masked model

results are shown in Figures 105 through 110.

The generator voltage shown in Figure 105 shows a smooth response which occurs because an ideal voltage source is used to model the generator. The generator output current, shown in Figure 106, shows a slight imbalance between the phases. The stability analysis will be important to determine if the imbalance causes a stability problem.

Table 38: Baseline system model design variables

Component	Parameter	Value
Generator	Voltage Amplitude	30,000 V
	Voltage Phase	0
	Frequency	60 Hz
	Resistance	.001 Ω
	Inductance	.01 H
Rectifier	Snubber Resistance	1e5 Ω
	Snubber Capacitance	infinite
	Resistance	0.01 Ω
	Capacitance	0.017 F
	Inductance	.0006 H
	Switching Frequency	20,000 Hz
	Reference Voltage	4,500 V
	Current Controller Bandwidth Coefficient	10,0000
	Voltage Controller Bandwidth Coefficient	10,000
Transmission Line	Resistance per km	.0001 Ω
	Inductance per km	0.15e-5 H
	Capacitance per km	150e-11 F
	Length	0.1 km
Inverter	Capacitance	.001 F
	Modulation Index	0.8
	Output Frequency	400 Hz
	Switching Frequency	10,000 Hz
Motor	Rotor Speed	2,000 RPM
	Rotor Type	Round
	Stator Phase Resistance	0.2 Ω
	Armature Inductance	0.000102 H
	Torque Constant	0.044335 $N \cdot m/A_{peak}$
	Inertia	0.00112 $J(kg \cdot m^2)$
	Viscous Damping	0.1035 $F(N \cdot m \cdot s)$
	Pole Pairs	4
	Static Friction	0 $Tf(N \cdot m)$

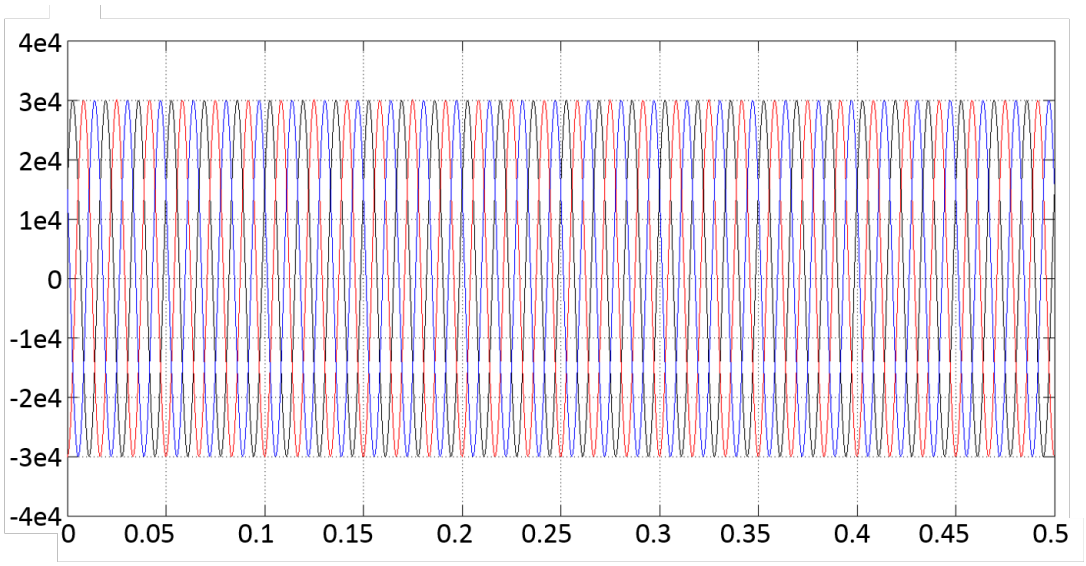

Figure 105: Baseline generator voltage

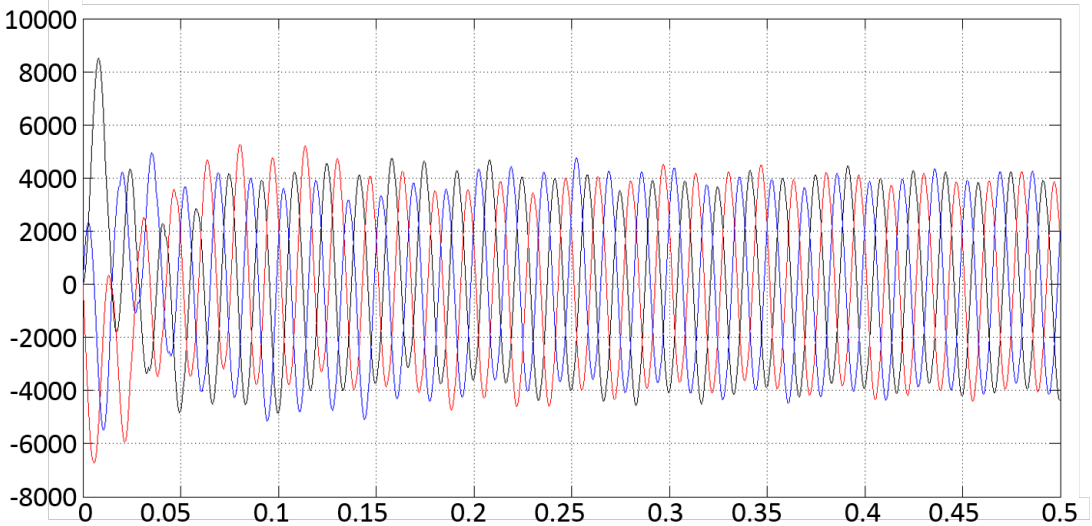

Figure 106: Baseline generator current

The bus voltage shown in Figure 107 shows that the bus reaches steady-state after about 0.5 seconds, and the peak current at start up of the system reaches about 10 kV. It is important to design the cables to be able to handle the peak load. The bus voltage also contains a ripple caused by the switching of the converter. A filter could be added to the system to mitigate this problem, or the bus capacitance could be

increased. Figure 108 shows that the bus current is fairly smooth. To achieve this trend, an inductance was added to the output of the rectifier.

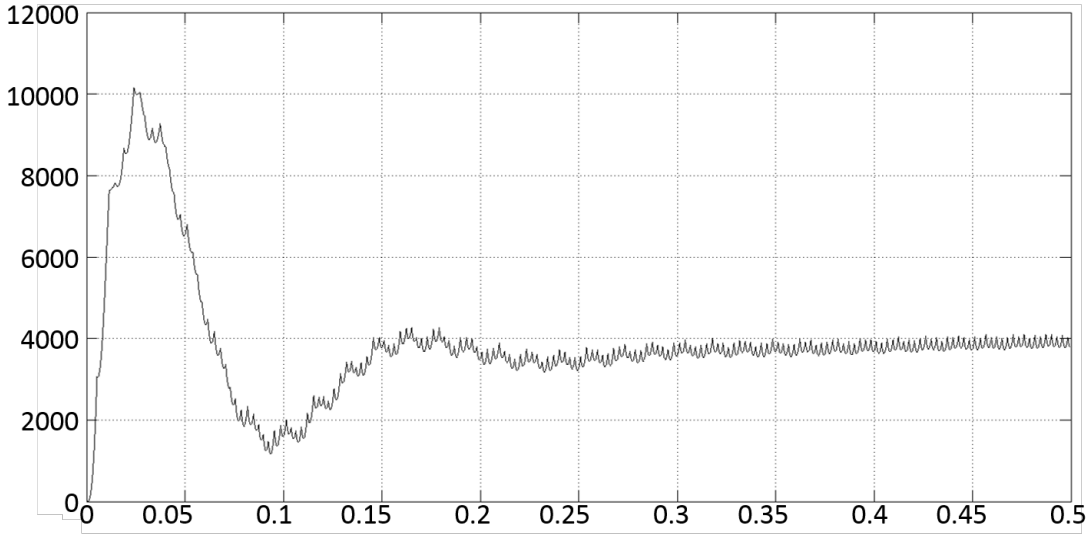

Figure 107: Baseline bus voltage

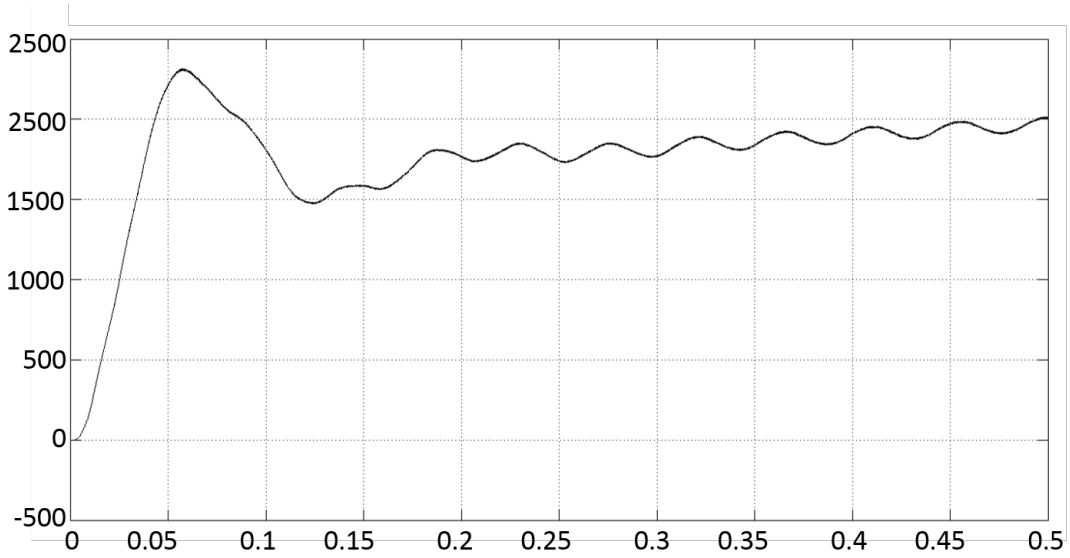

Figure 108: Baseline bus current

The input voltage and current for the motor are shown in Figures 109 and 110. The figures show that the motor also takes about 0.5 to reach steady-state. The

response is fairly smooth, but contains some harmonics caused by the switching of the inverter. A R-C filter can be used at the output of the inverter to smooth the motor input power. The dynamics between the inverter and motor have the potential to cause a stability problem, so stability analysis will be important to identify potential problems.

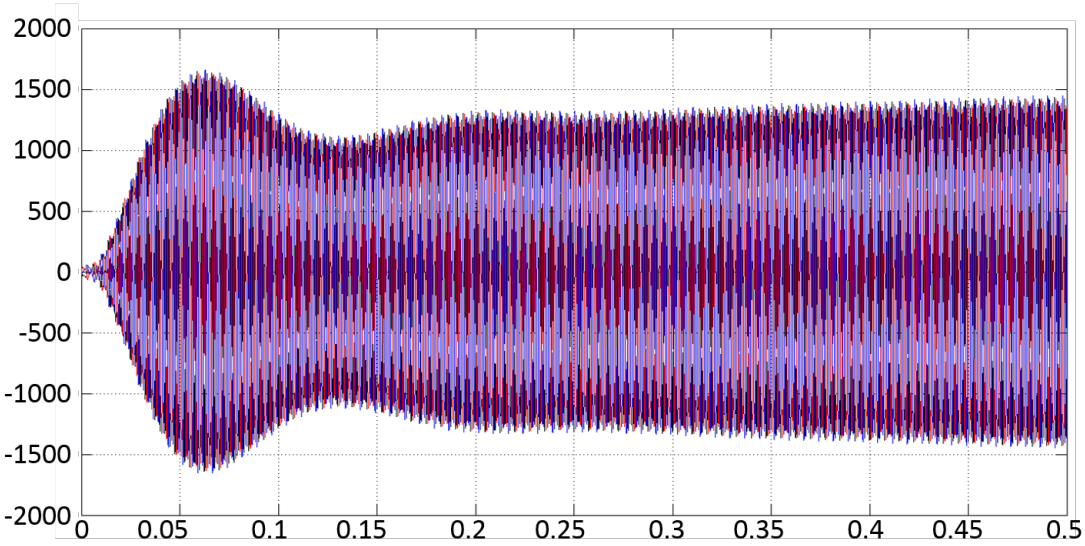

Figure 109: Baseline motor voltage

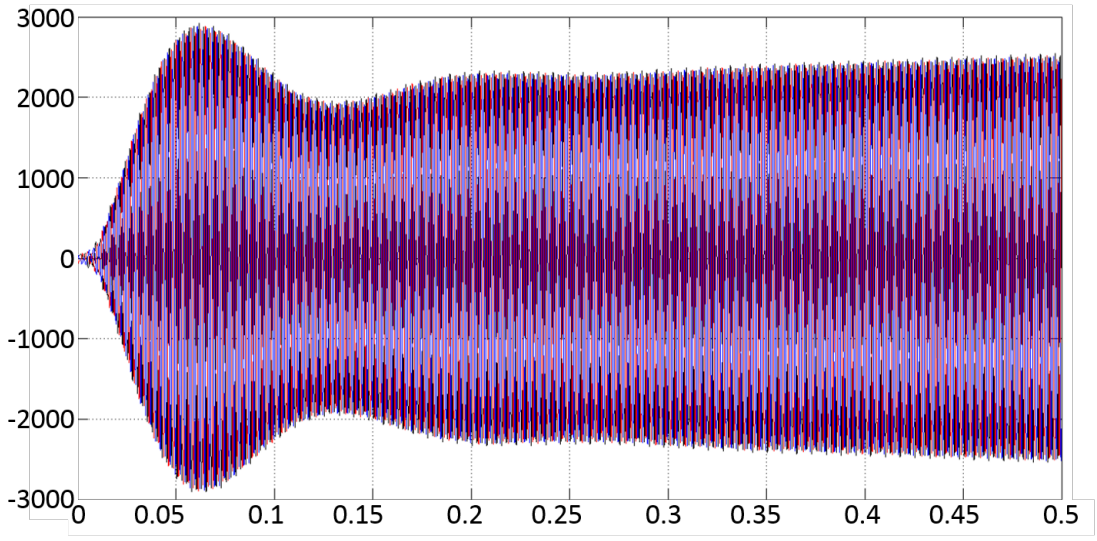

Figure 110: Baseline motor current

6.2.3 Architecture 1 Steady-State Results

The next system to be modeled was architecture 1, which was selected in the previous chapter. The same component models were used as the baseline system, and circuit breakers were included to reroute power during a failure.

A review of the architecture is shown in Figure 111. During normal operation, power flows along the connections represented by the solid lines in the architecture diagram. During a failure, connections represented by the dotted lines are used. The model is shown in Figure 112.

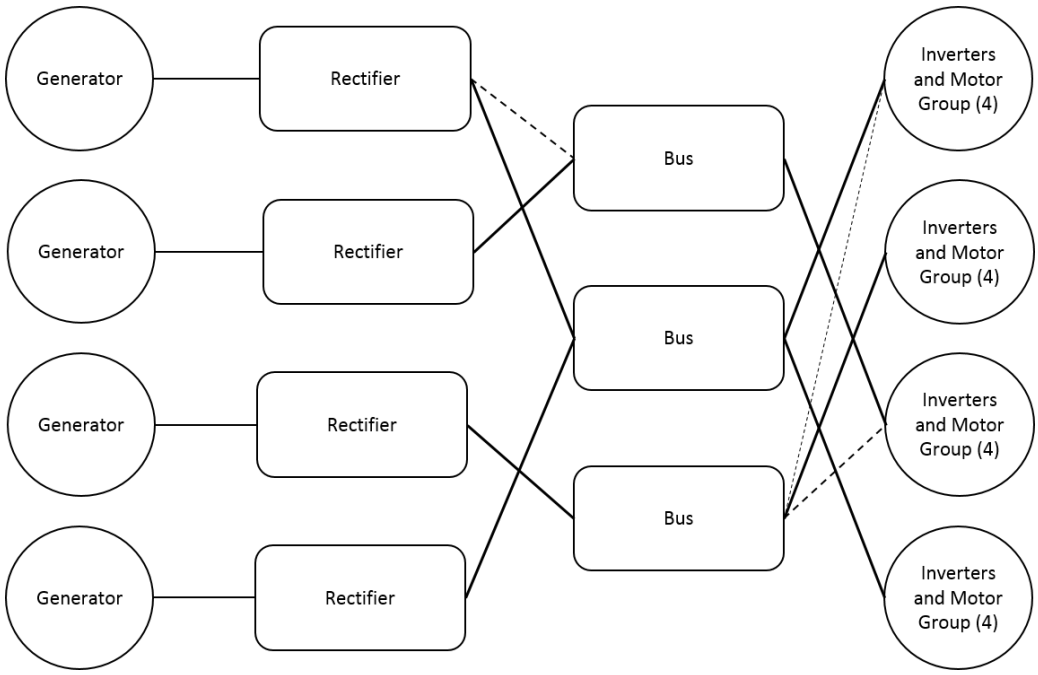

Figure 111: Architecture 1 diagram

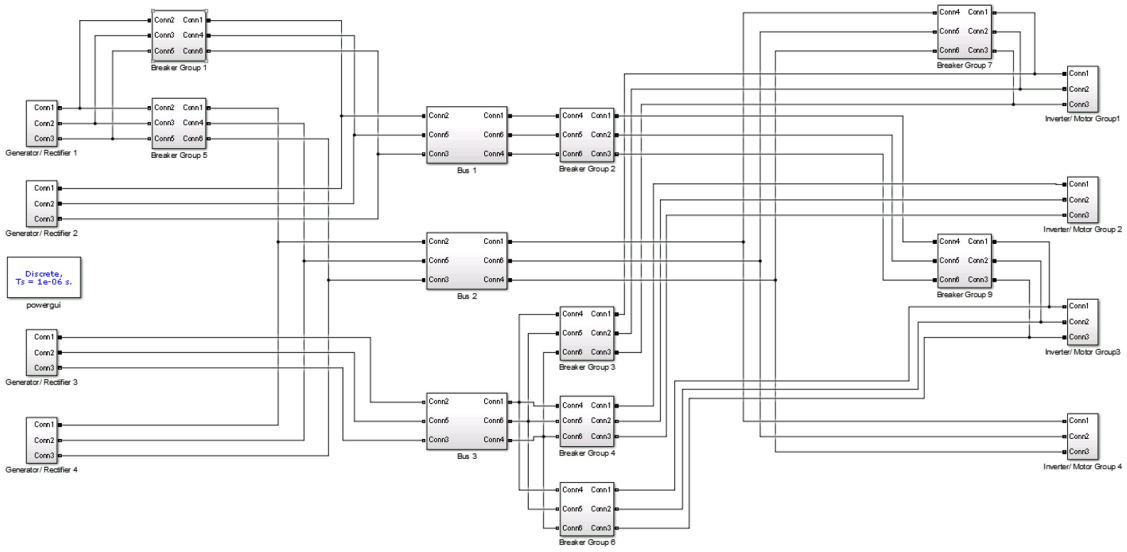

Figure 112: Architecture 1 dynamic model

During normal operation, the architecture has two branches that consist of one generator, one rectifier, one bus, and one inverter/motor group. These are the branches that stem from generator 2 and generator 3. Generator/rectifier 1 and 4 share a bus during normal operation. Branches 2 and 3 should behave identically since they do not share any components with other branches. So, bus performance is only studied for bus 1 and bus 2 since bus 3 performance should be identical to bus 1.

The model was simulated for 0.5 second using the same parameters as the baseline simulation. The results are shown in Figures 113 through 119. Figures 113 and 114 show the generator voltage and current. The figures show that the generator response is similar to that observed with the baseline. This occurs because the actively controlled rectifier shields the generator from configuration changes downstream.

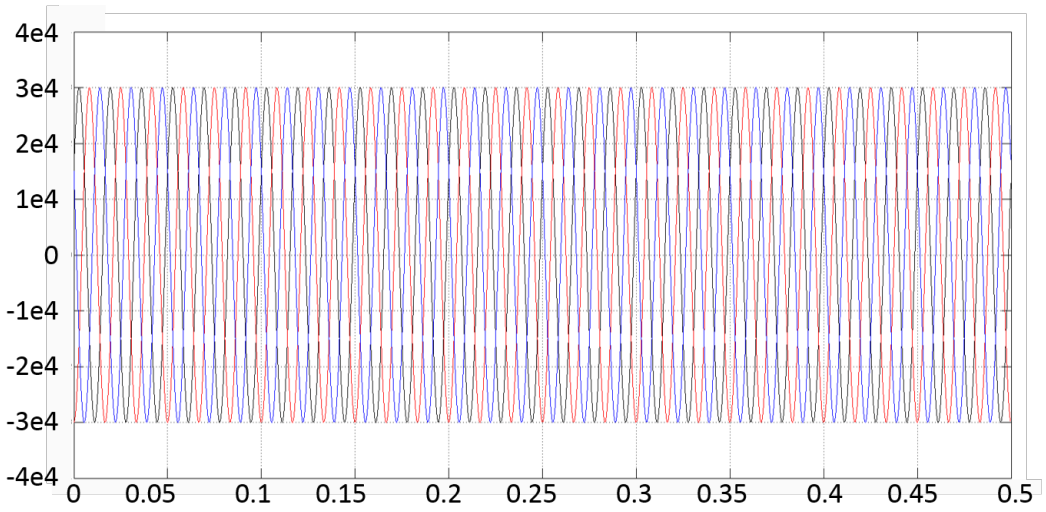

Figure 113: Architecture 1 generator voltage

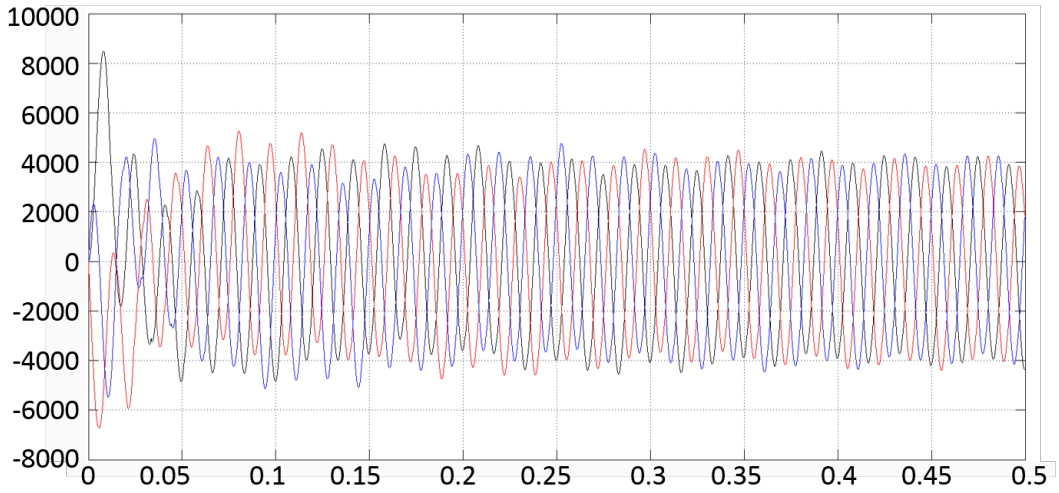

Figure 114: Architecture 1 generator current

Figure 115 demonstrates that the actively controlled rectifier maintains the targeted 4000 V bus voltage. Figure 117 shows that the current on bus 2 is about double of the current on buses 1 and 3 (shown in Figure 116). This occurs because bus 2 supplies two motor groups rather than one. Figures 118 and 119 show the current and voltage supplied to the motor. Given the current and voltage response, the required power for the motors is available.

In general, the system has a smooth response. There is some oscillation in the rectifier output voltage that is caused by the control scheme selected for the rectifier. It will be important to later check whether the oscillation causes any stability concerns.

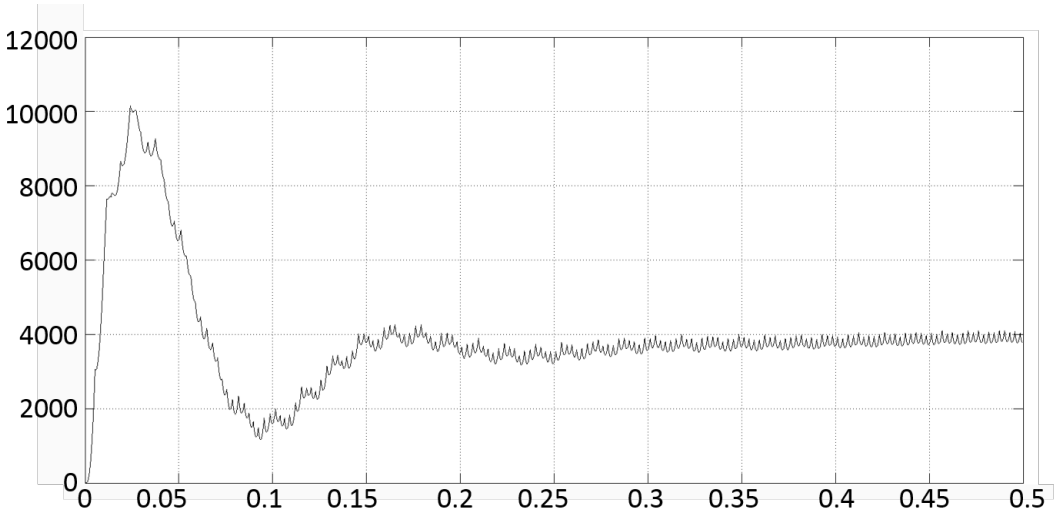

Figure 115: Architecture 1 rectifier voltage

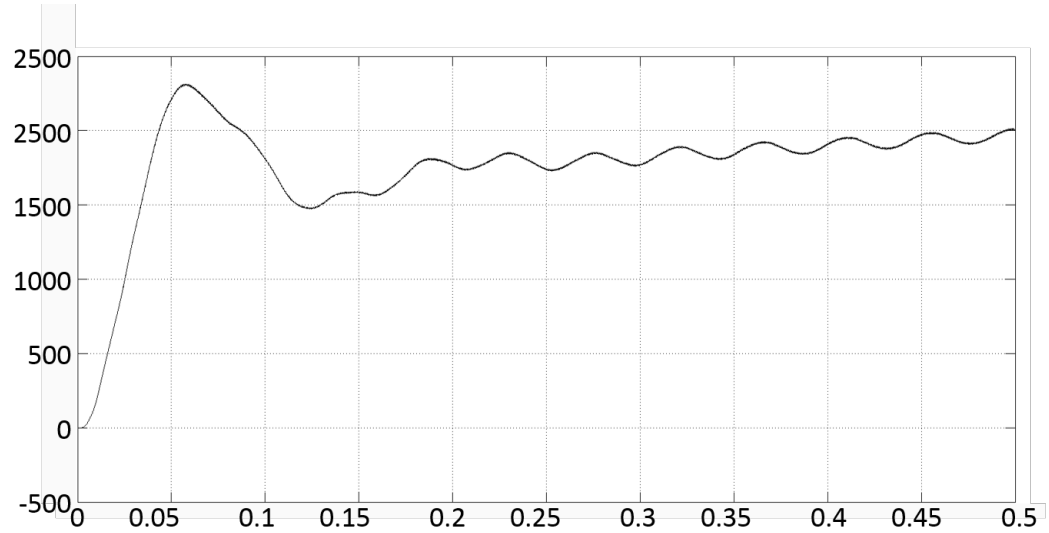

Figure 116: Architecture 1 bus 1 and bus 3 current

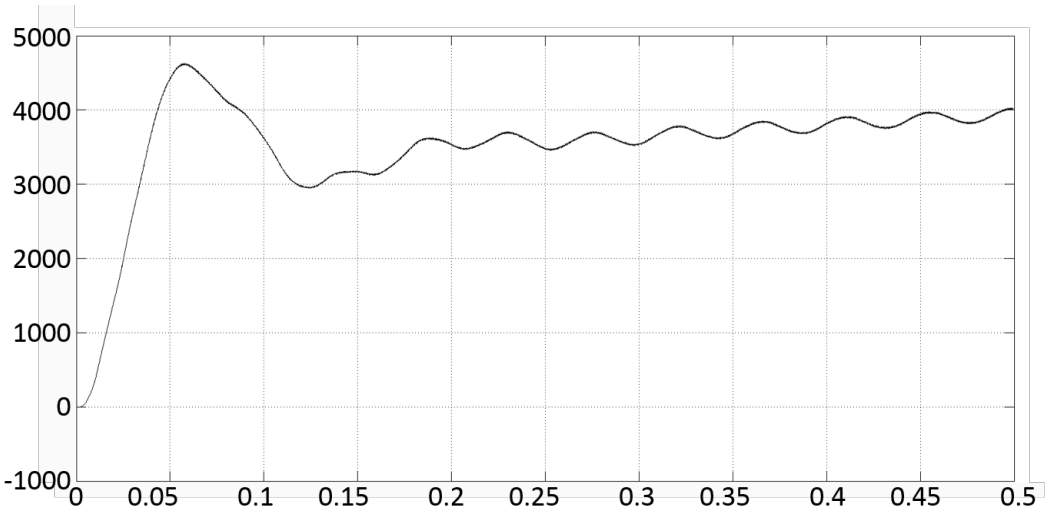

Figure 117: Architecture 1 bus 2 current

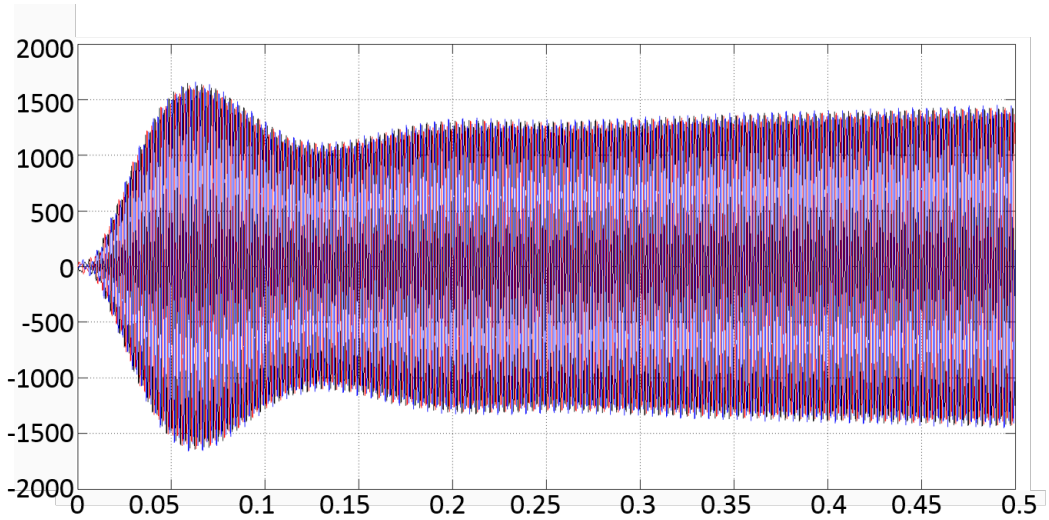

Figure 118: Architecture 1 motor voltage

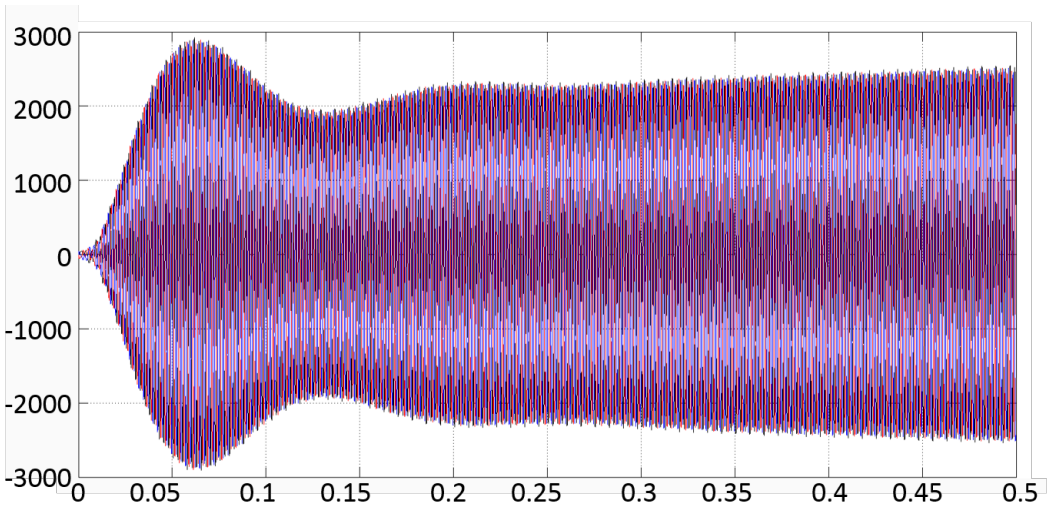

Figure 119: Architecture 1 current voltage

6.2.4 Architecture 2 Engine 1 Failure Results

Under normal operation, architecture 2 should have the same performance as architecture 1; therefore, the architecture 2 model was used to simulate an engine-out condition. The configuration of the system during an engine-out scenario is shown in Figure 120 . The lines in red are connections that have failed due to the engine failure. The green dotted lines show connections that are activated due to the failure. The model used to simulate architecture two under an engine-out scenario is shown in Figure 121.

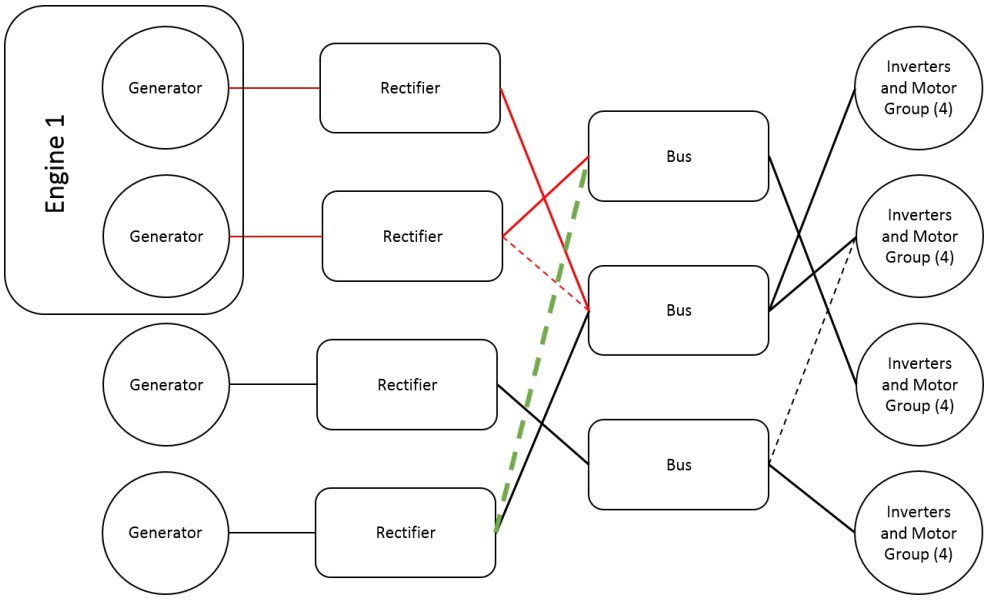

Figure 120: Architecture 2 operation during engine 1 failure

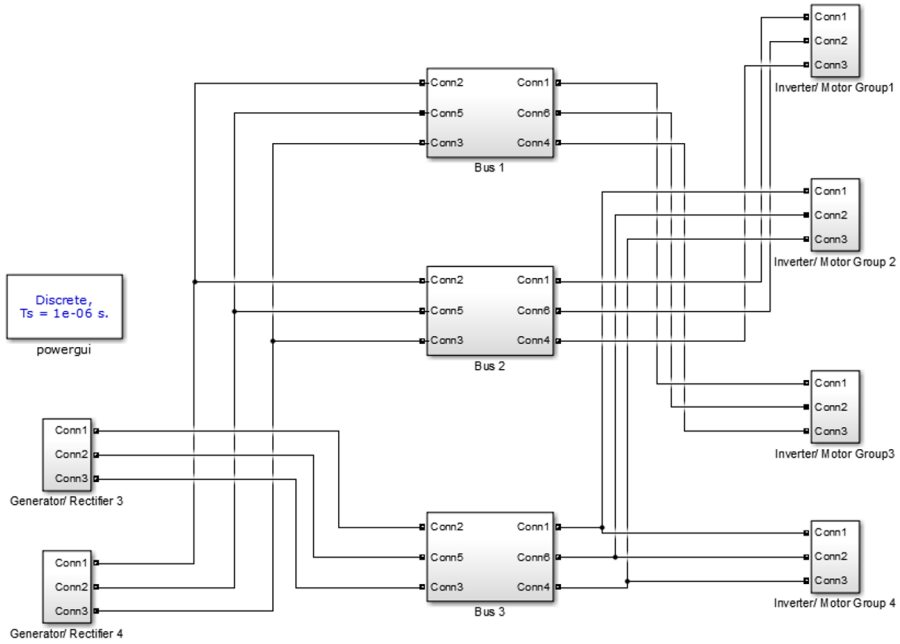

Figure 121: Architecture 2 engine failure model

Figures 122 and 123 show the current for each generator. The generator current for the generator 3 has some low frequency oscillation. This may occur since the bus to which it is connected feeds multiple motors. The stability analysis will be

important to ensure that the generator to rectifier connection is stable.

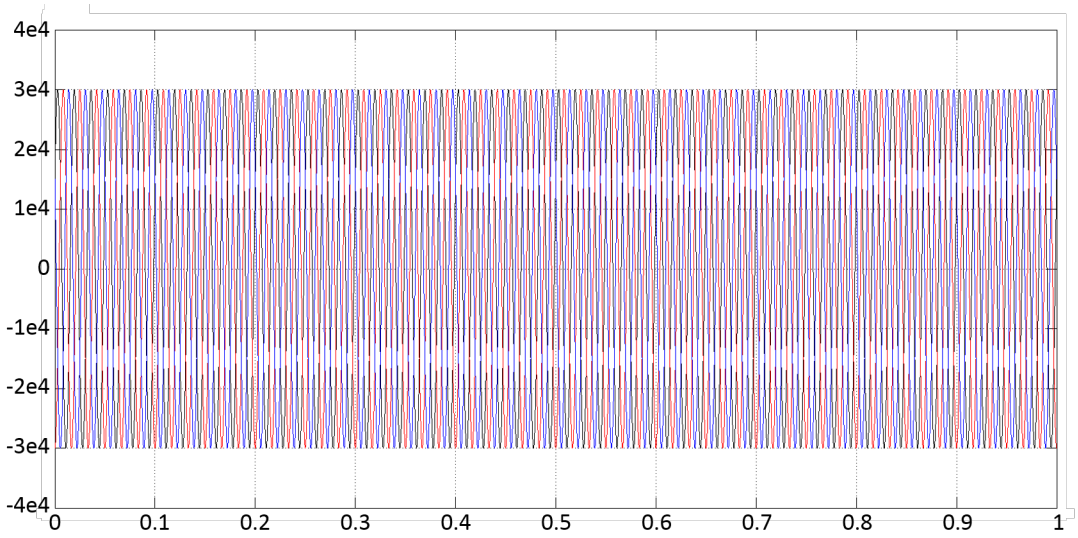

Figure 122: Architecture 2 generator voltage

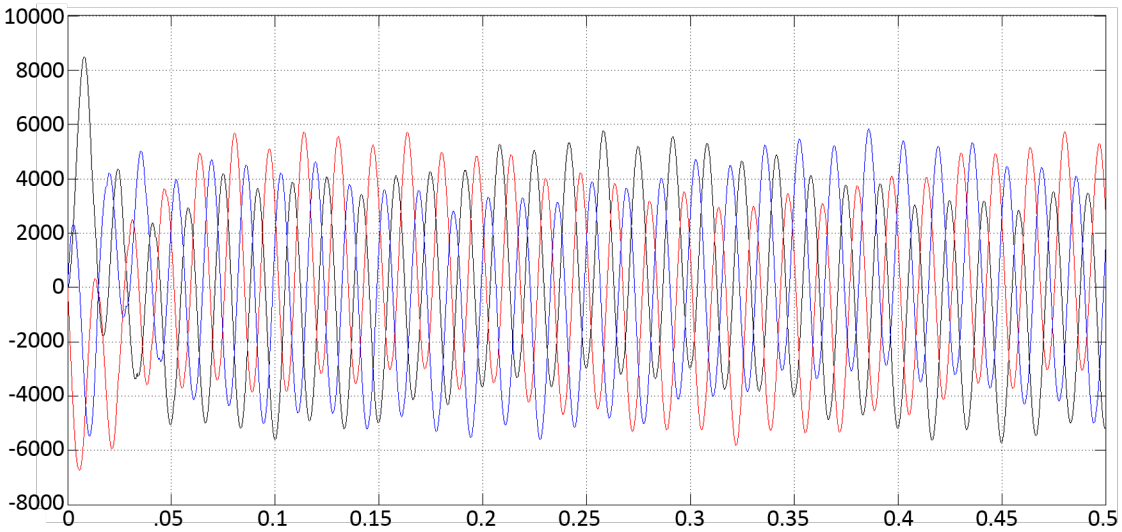

Figure 123: Architecture 2 generator 3 current

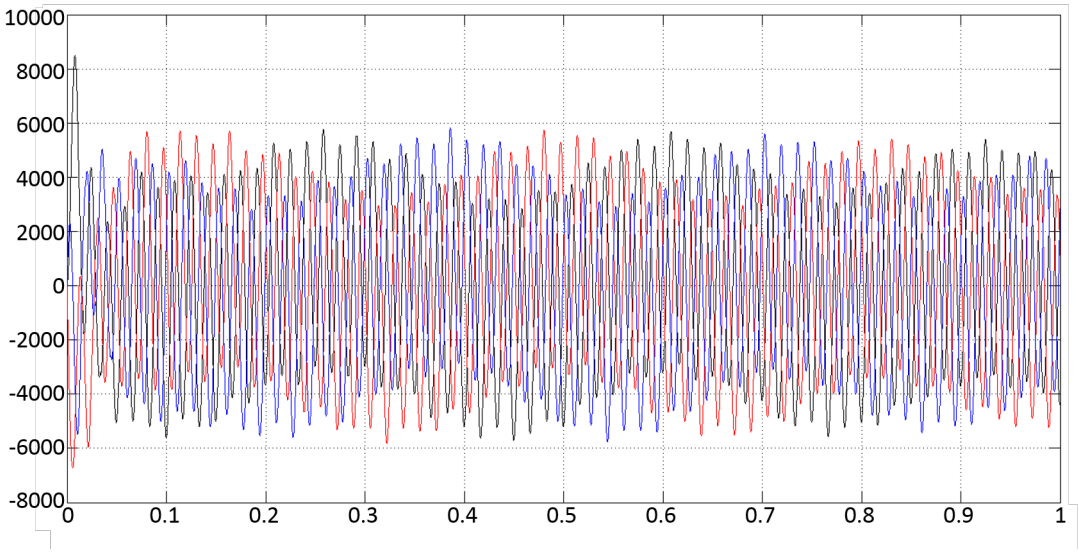

Figure 124: Architecture 2 generator 4 current

Figure 125 shows that the rectifier output voltage was not able to reach the specified level; this may occur because the power demand from the loads is greater than what the generator can provide. Figures 126 and 127 show the current of each bus. The current for buses 1 and 2 reach the expected value based upon the results of architecture 1. The current draw for bus 3 is high. Again, this is most likely because multiple motors are being fed by the bus.

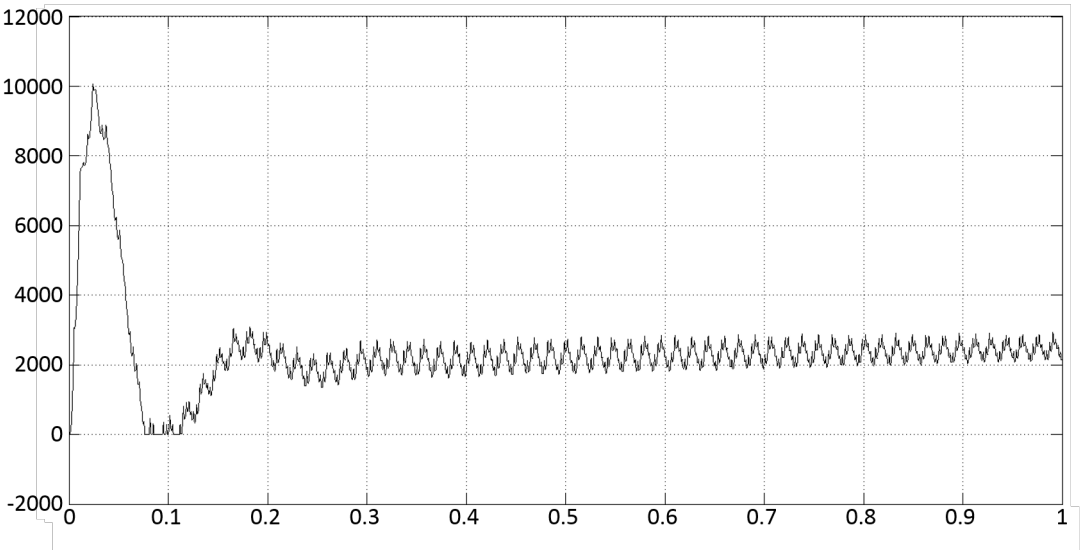

Figure 125: Architecture 2 rectifier voltage

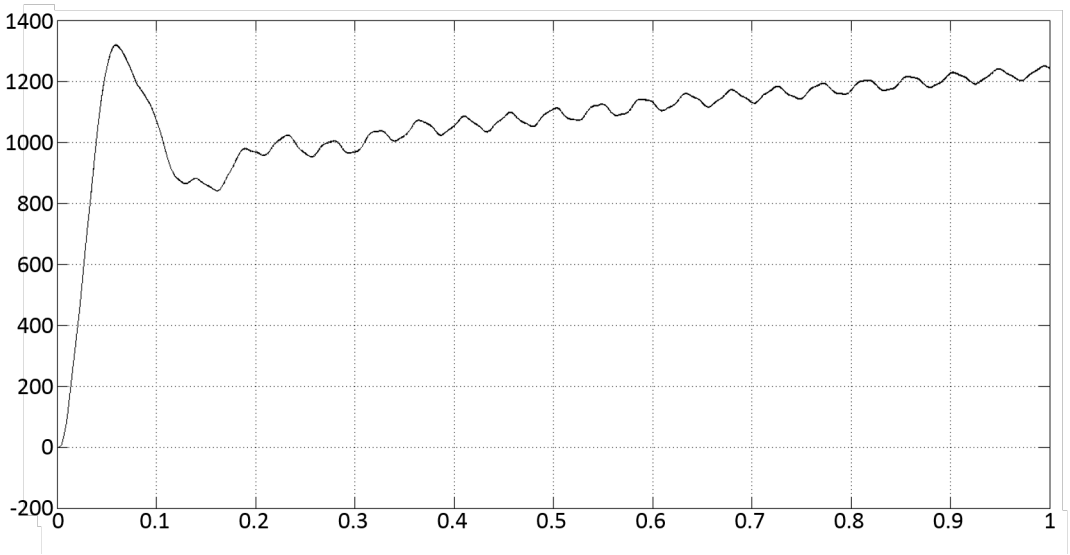

Figure 126: Architecture 2 bus 1 and 2 current

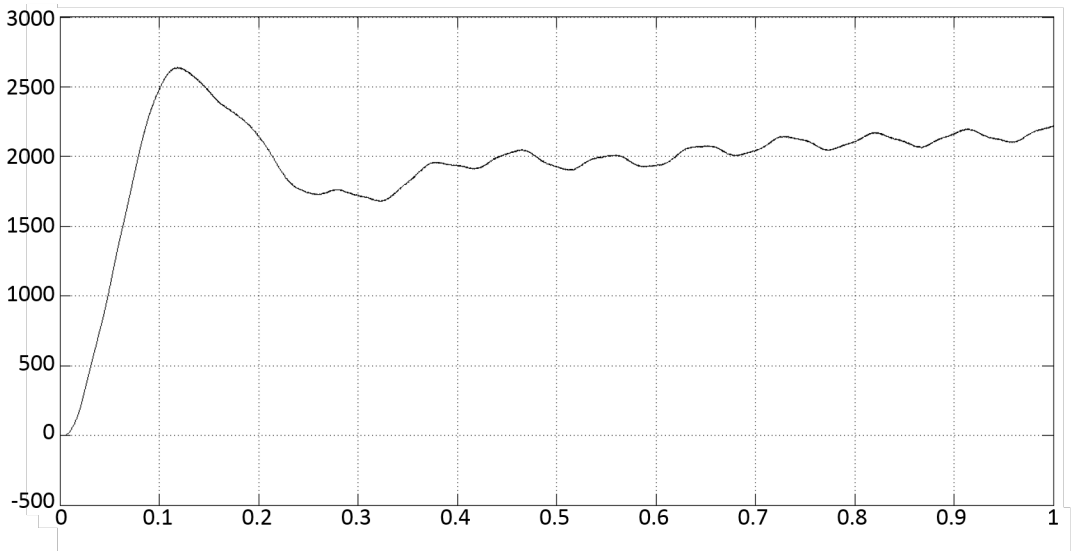

Figure 127: Architecture 2 bus 3 current

Figures 128 and 129 show the motor current. The values are less than shown for architecture 1. This occurs because the two generators that are left after the engine failure are having difficulty supplying all the loads.

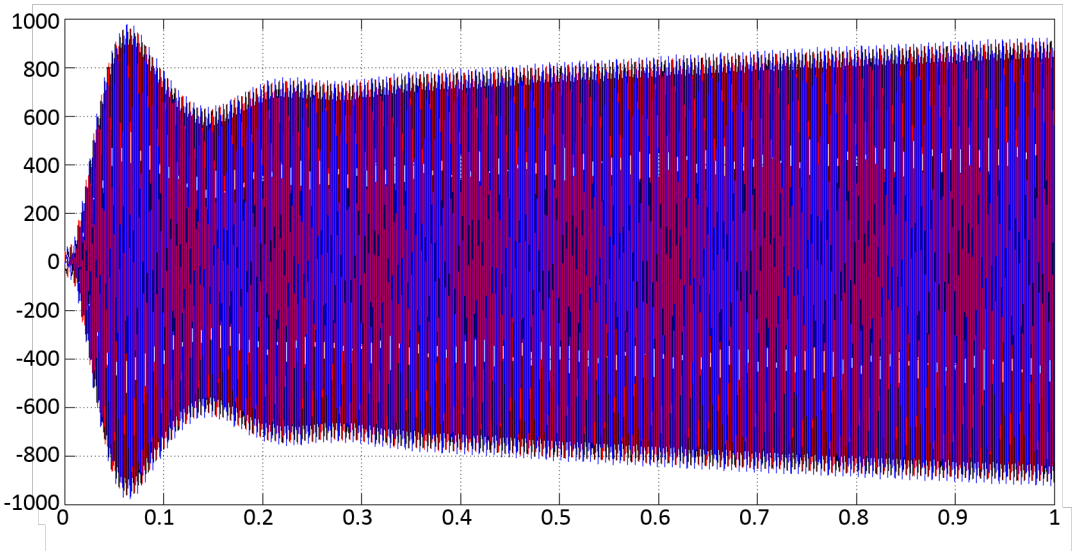

Figure 128: Architecture 2 motor voltage

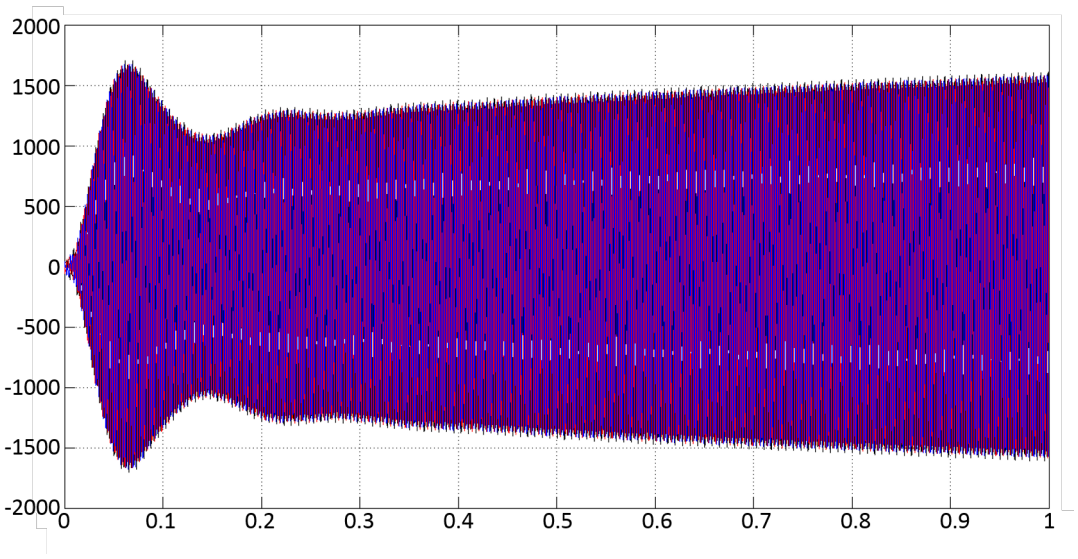

Figure 129: Architecture 2 motor current

6.2.5 Architecture 3 Engine 2 Failure Results

Like architecture 2, architecture 3 would have the same performance as architecture 1 under normal operating conditions. However, if engine 2 fails in architecture 3, a different system configuration is reached. The new configuration is shown in Figure 130. The model of an engine 2 failure for architecture 3 is shown in Figure 131.

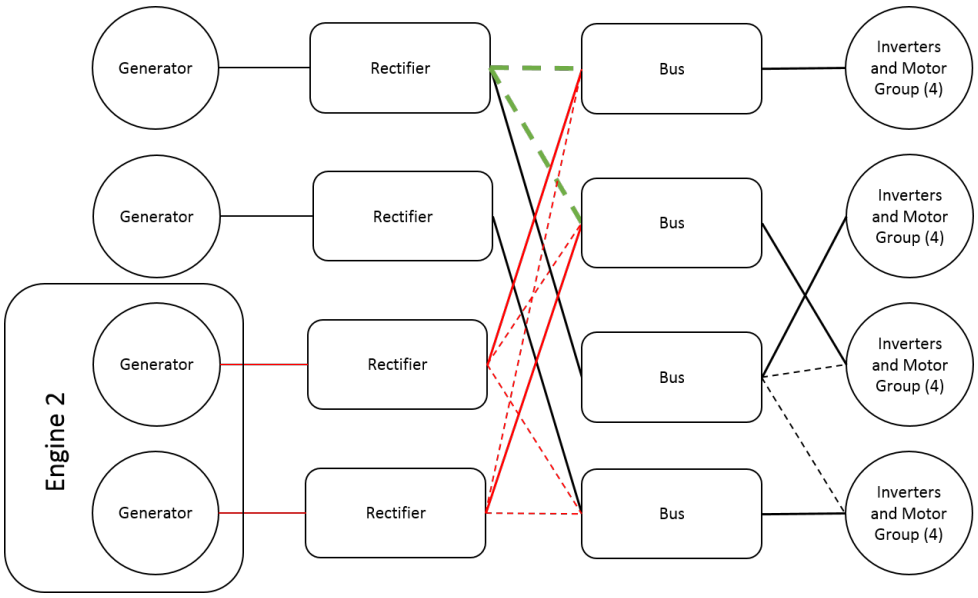

Figure 130: Architecture 3 operation during engine 2 failure

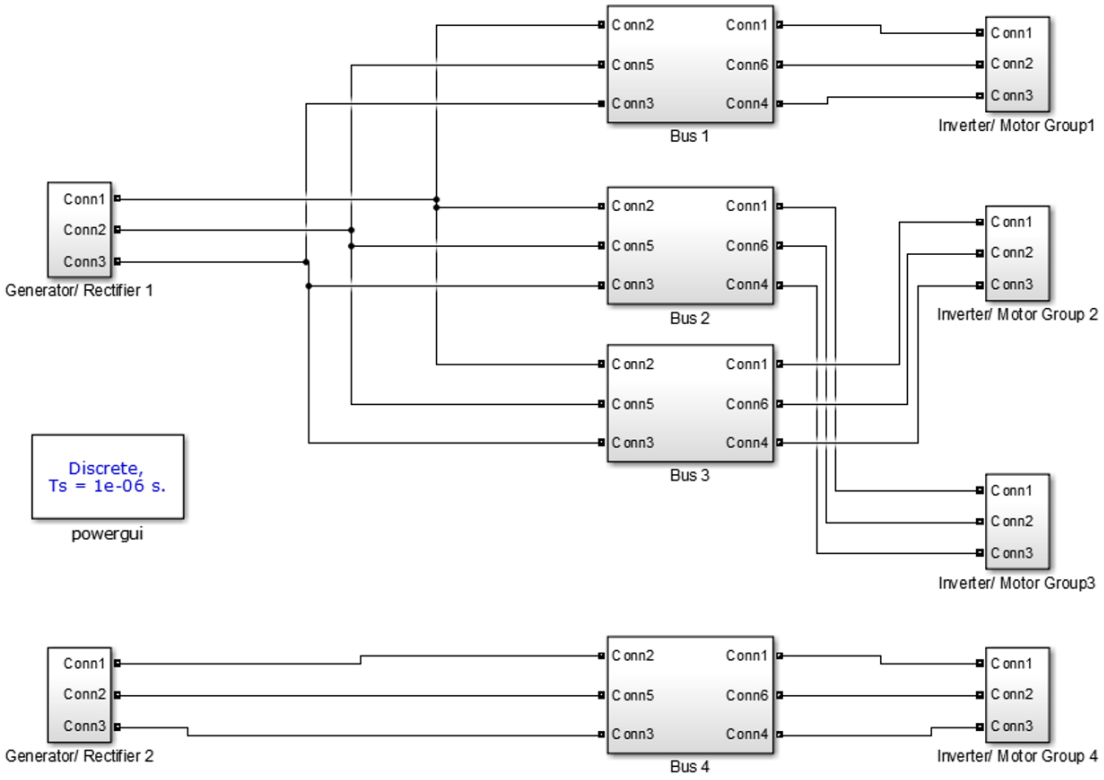

Figure 131: Architecture 3 engine 2 failure model

The state-variables for architecture 3 are shown in Figures 132 through 139. The results are similar to those observed with architecture 2. For example, the generator/rectifier combination that was supplying multiple buses presented some low frequency harmonic interference (as shown in Figures 132, 133, and 134).

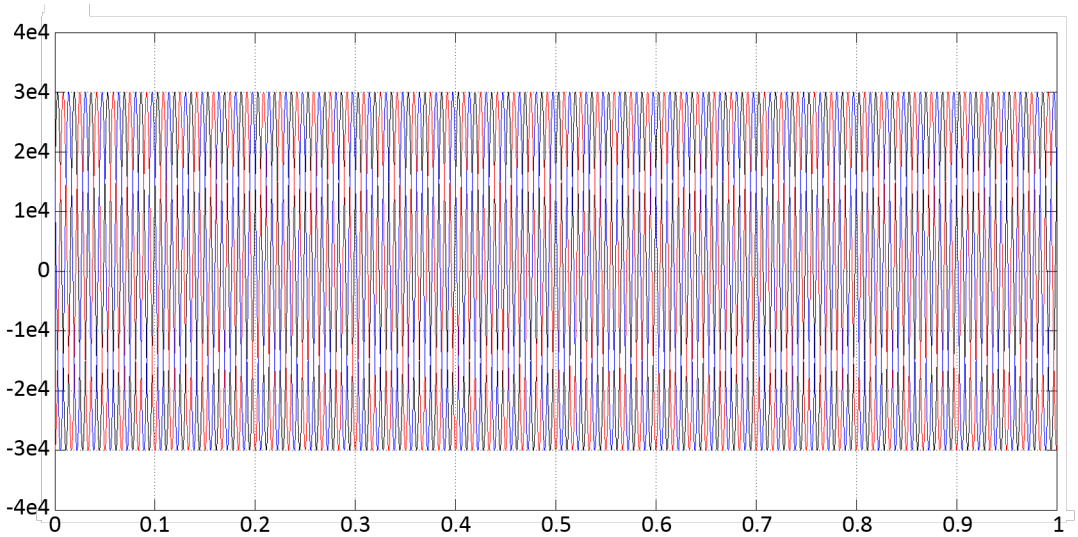

Figure 132: Architecture 3 generator voltage

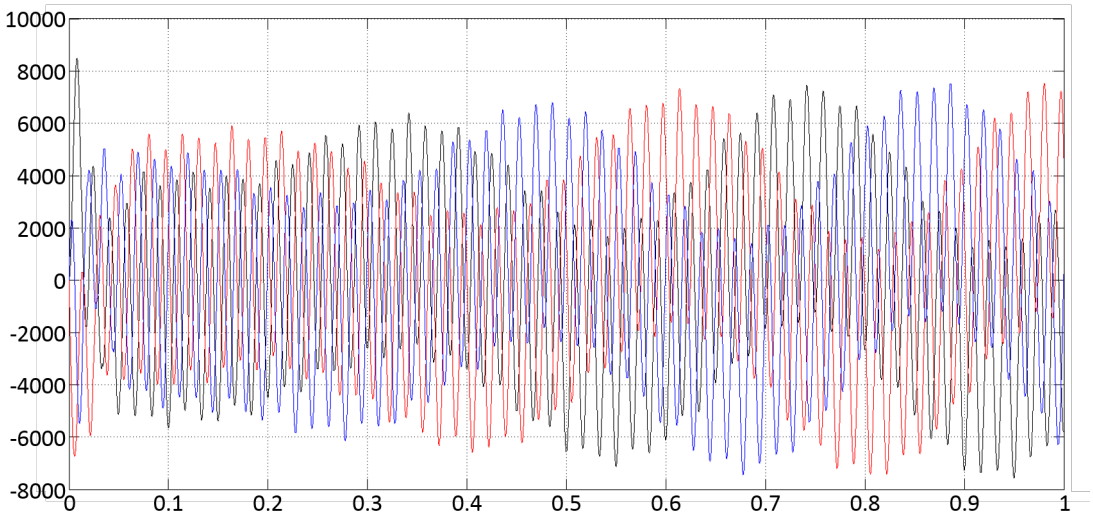

Figure 133: Architecture 3 generator 1 current

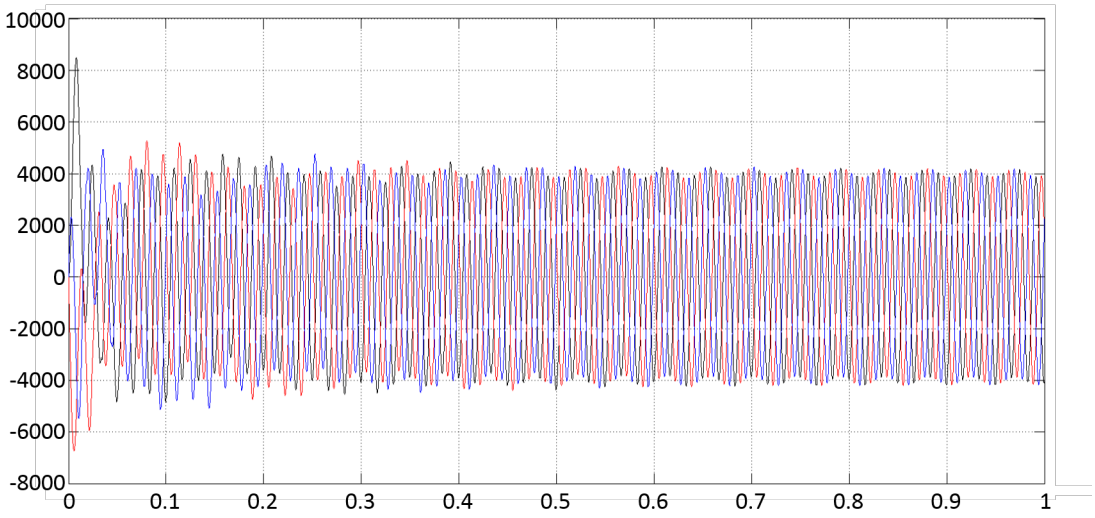

Figure 134: Architecture 3 generator 2 current

Figure 135 demonstrates that rectifier 1 had difficulty reaching the 4000 V target. Rectifier 4 was able to reach the target since it is only feeding a single bus and inverter/motor group (as shown in Figure 136). The bus currents are shown in Figure 137. The current falls well short of the bus currents of the other architectures, meaning that the system is failing to meet the load demand. Furthermore, like architecture 2, the motor current and voltage (shown in Figures 138 and 139) was low since the two remaining generators had difficulty supplying enough power to all the loads.

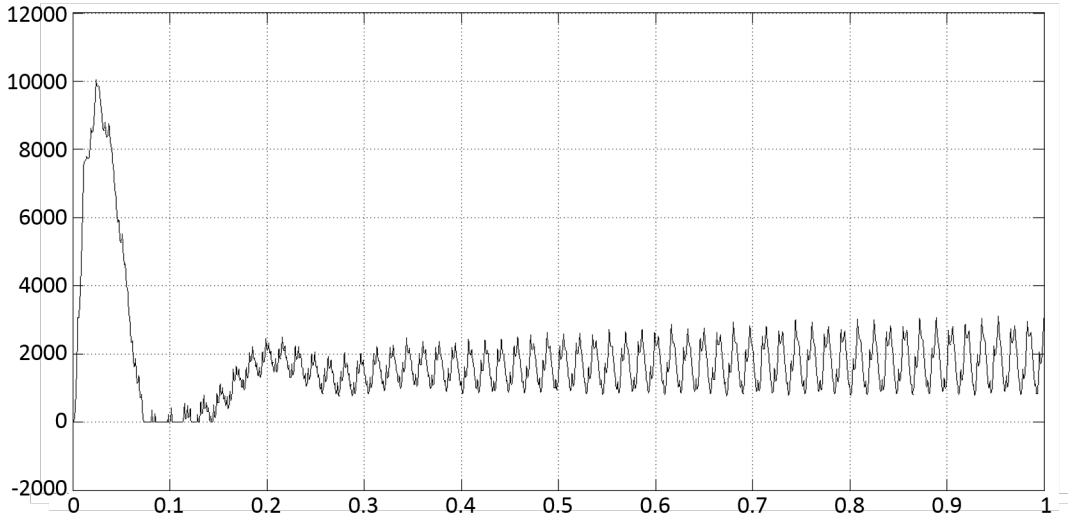

Figure 135: Architecture 3 rectifier 1 voltage

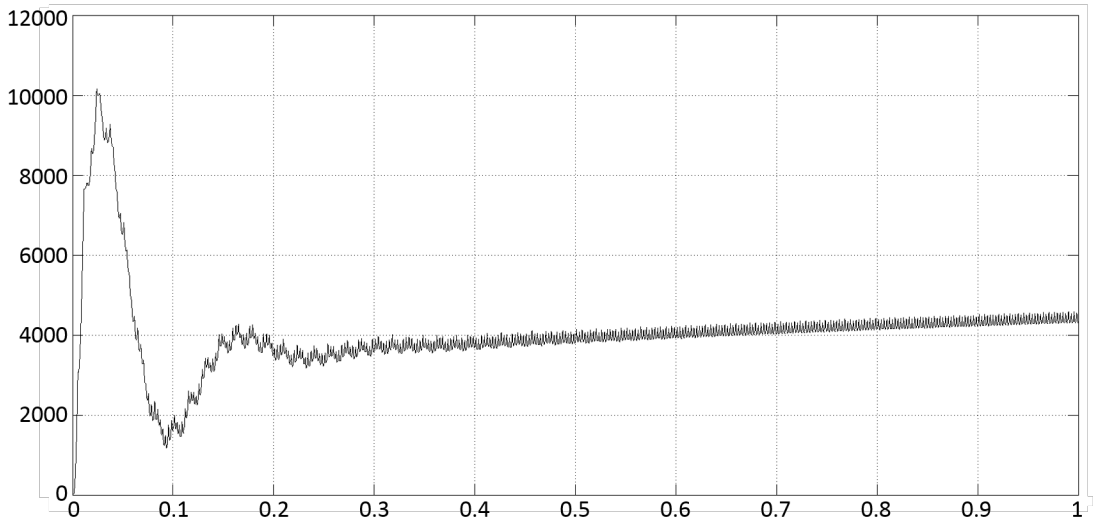

Figure 136: Architecture 3 rectifier 2 voltage

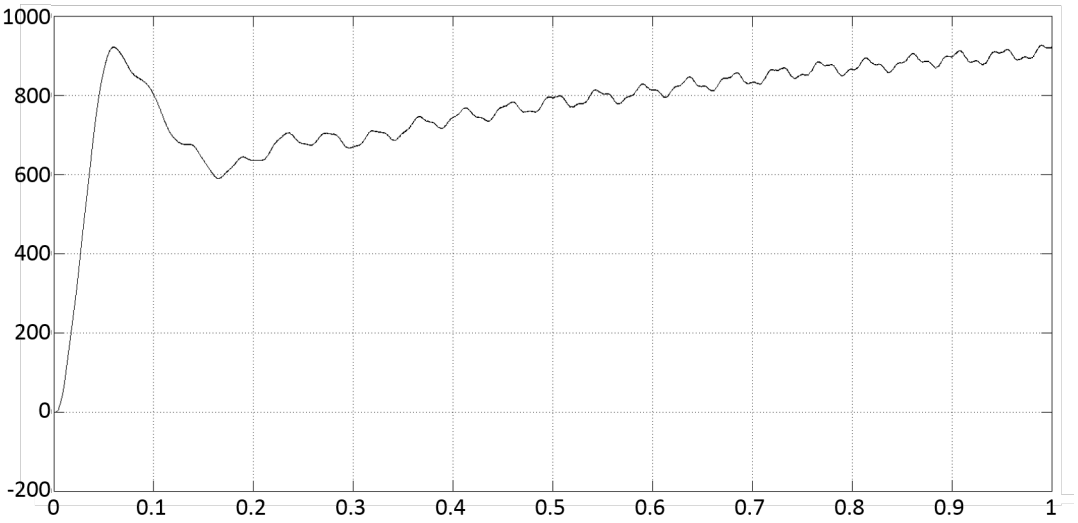

Figure 137: Architecture 3 bus current

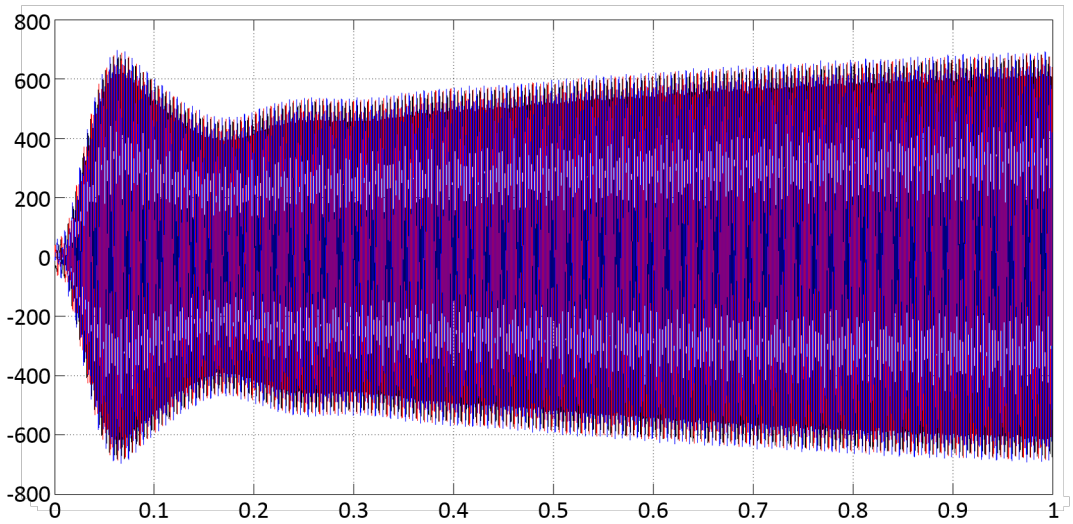

Figure 138: Architecture 3 motor voltage

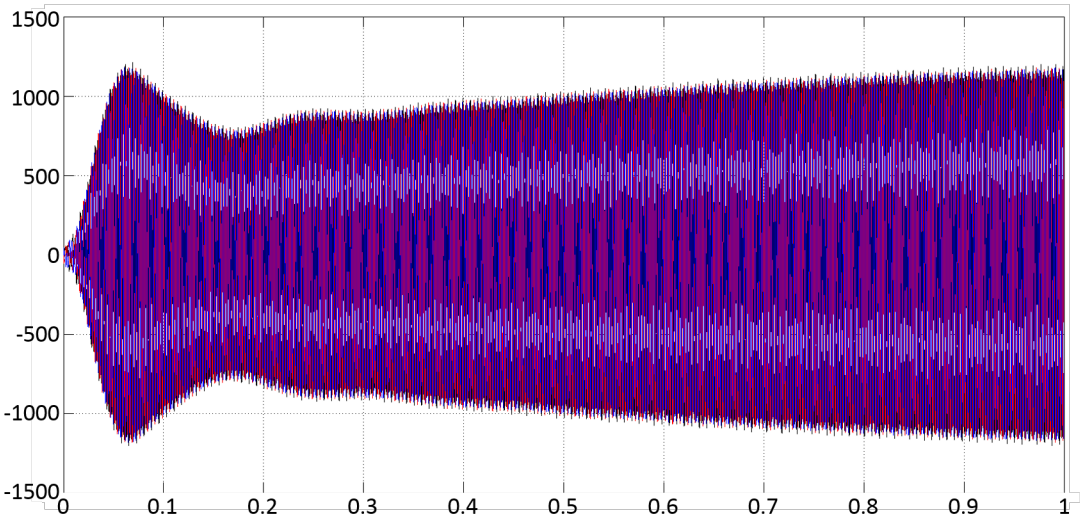

Figure 139: Architecture 3 motor current

6.2.6 Performance Model Observations

Dynamic performance models were created for each architecture being considered. In general the models presented similar behavior. One trend that emerged was that buses that had multiple sources had a tendency to not reach the specified voltage. Also, if a bus needs to supply multiple loads, the current level will increase. The engine failure scenarios showed that the generators had difficulty meeting the demands of the loads. Therefore, the sizing of the generators may need to be revisited.

6.3 Decreasing Model Runtime

The SimPowerSystem models are high fidelity, and, in turn, are slow. A literature search was performed to explore options for increasing the speed of the simulation so that the architectures can be analyzed in a reasonable amount of time. Based upon the information found in the literature search, a method for reducing model run time is selected and the process of implementing the method will be discussed.

6.3.1 Literature Search

The method selected for altering the model must significantly reduce run time, yet retain enough fidelity to depict the transient attributes of the system. If the fidelity of the system is too low, events may not be captured that affect the stability of the system. The literature search revealed two potential solutions: surrogate models and linearized models.

6.3.1.1 Surrogate Model

Surrogate models approximate the behavior of a higher fidelity model by using rapid and cheap function calls. A variety of methods exists for creating surrogate models using data from higher fidelity models. Some of the most popular methods are response surface, Kriging, and artificial neural networks [54] [58].

Polynomial Response Surface Methodology :

Response surface methodology is the most widely used surrogate modeling technique. In this method, a polynomial is fit to data points from the original model. The general form for a second order response surface equation (RSE), y, is:

$$y = \beta_0 + \sum_{j=1}^{k} \beta_i x_i + \sum_{j=1}^{k} \beta_{ii} x_i^2 + \sum_{j=1}^{k-1} \sum_{j=i+1}^{k} \beta_{ij} x_i x_j \tag{78}$$

The β's are the regression coefficients, and the x's are the design variables. The ε is the variability in the response that is not captured by the model. To create the surrogate model, the regression coefficients and error must be estimated using a method such as least squares approximation [107] [92].

The advantage of this method is that once the response surface function is found, function evaluations are quick. Short falls of RSE's is that estimating the error can be difficult, and the equation is only valid in the range of the data used to train the model [158]. Also, RSE's tend to have difficulty capturing highly nonlinear, not

well-behaved functions.

Kriging :

Kriging works on the basis that an unknown point should be the average of two nearby points weighted by their distance to the unknown point. The Kriging model is a true unknown function that is modeled as the sum of a fixed and known trend function, B(x), and a departure function known as a Gaussian random function, Z(x), with a mean of zero and non-zero variance σ^2 [54].

The primary advantage of Kriging is that a surrogate model is a better representation of the actual response than a RSE [77]. On the other hand, although Kriging models will be significantly faster than the high fidelity models, studies have shown that the function evaluations are not as fast as those achieved by response surface methodology [139]. Also, Kriging models are much more difficult to implement than RSE's.

Time-based Artificial Neural Network :

A time-based artificial neural network is a surrogate modeling technique which is useful for nonlinear systems that are changing in time. Artificial neural networks mimic the processes of a brain and work by creating a mapping of inputs to outputs. The mapping (often referred to as the hidden layer) consists of neurons and synapses. The neurons contain simple mathematical operations, and the synapses are weightings that determine the effect of each neuron on the output. As the weightings change, certain mathematical operations will have a larger effect on the output and some will have less of an impact on the output. These weightings are adjusted to find a mapping that properly represents the original model. One major advantage of neural networks over other modeling techniques is that they have the ability to learn. As a user supplies more example inputs and outputs to the neural net that was generated by the original model, the weightings (synapses) are updated. The downfall of the

neural net is that creating and training can be time consuming. Also, there is no guarantee that the new model will capture all the behaviors of the system.

6.3.1.2 Linearized Model

The primary reason that the models are slow is that a very small time-step is used to capture the switching of the power converters. A popular area of research in power converter modeling is linearized models [42]. The linearized models do not capture all transient events that occur within the converters, but generally represent the behavior of the converters well. There are two primary methods for linearizing power converter models: state-space averaging (SSA) and DQ transformation theory [28] [110].

In the SimPowerSystems model, every resistor, diode, capacitor, etc. is simulated in detail to create the component model. In a linearized model, the detailed simulations of each element is replaced by a set of differential equations that describe the behavior of the circuit. By using the set of equations, the model can be run with a much larger time-step and the equations can be solved in a fraction of the time needed for the SimPowerSystems model. In order to gain this amount of speed, model fidelity is sacrificed; many of the transient effects in the system will be lost when using an averaged model. Although the general behavior will still be the same, losing the transient effects could affect the results of the stability study which will be discussed in a later chapter.

State-space Averaged Model :

The SSA method was created by Middlebrook and Cuk in 1976 [100]. A SSA model works by averaging state-space variables over a switching period to obtain a time-continuous model. A state-variable or vector is averaged over a switching period, T_c, using the following equation [59]:

$$x_a(t) = \frac{1}{T_c} \int_{t-T_c}^{t} x(\tau) d\tau \tag{79}$$

The averaged state-space variables are then used in conjunction with the circuit equations to model the response of the system.

Since its development, SSA has been applied to a variety of converter types and power systems and studies have shown that the SSA model is a good representation of the behavior of a power converter [91]. The major drawback of the SSA method is that it cannot be used for converters that are vector-controlled. (Currently, vector-control is not used, so this is not an issue.)

DQ Transformation Model The DQ transformation model uses a change in reference frame to model the system. Essentially, power is divided into its active and reactive components. The advantage of the DQ model is that it can be used with any type of converter control. Also, DQ power converter models can easily be combined with models of other components with rotating reference frames such as generators [28]. One problem is that DQ transformation models have not been throughly researched, so little validation data is available to determine how well they represent the behavior of an actual system.

6.3.2 Model Alteration Approach

Two basic approaches to increasing model speed were presented: surrogate models and linearized models. The surrogate models will provide approximate models with fast function calls. However, the surrogate model must be trained using data from the high fidelity model, and there is no guarantee that the surrogate model will properly represent the behavior of the highly nonlinear PDS. In contrast the linearized models will capture the behavior of the system well since they are based on the circuit equations. Based upon the literature search, the effects of using SSA have been throughly researched in the literature and can easily be applied to the PDS design problem. Since SSA is a proven linearization method that is guaranteed to capture the general behavior of the system, it was selected to create a new model of

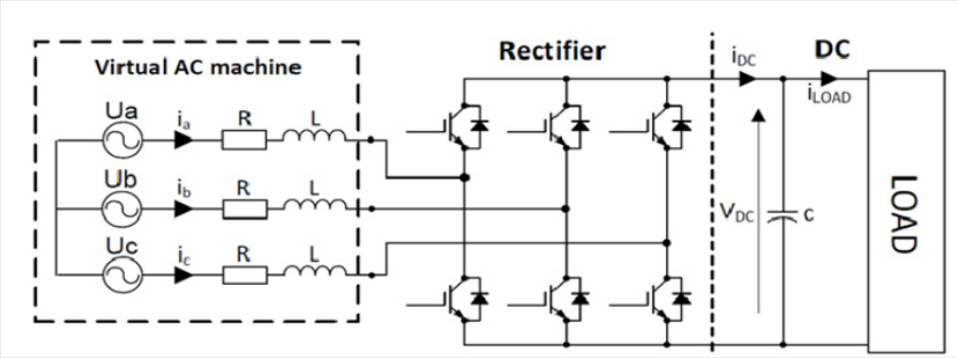

Figure 140: Rectifier circuit

the system.

Of course this approach comes with the problem of needing to replace the SimPowerSystems models, but the SimPowerSystems models will still be useful for validating the state-space averaged models. The procedure for building the averaged state-space models is described in the following subsections.

6.3.2.1 Rectifier State-Space Averaged Model

A state-space model of the rectifier can be created using the rectifier circuit equations. The circuit representation of the rectifier being modeled is shown in Figure 140.

A mathematical model of this circuit can be created using the following equations [93] [155] [70]. The three-phase line voltage is calculated as:

$$u_a = E_m cos(\omega t) \tag{80}$$

$$u_b = E_m cos(\omega t - \frac{2\pi}{3}) \tag{81}$$

$$u_c = E_m cos(\omega t - \frac{4\pi}{3}) \tag{82}$$

Where E_m is the line voltage amplitude and ω is the angular frequency of the power source. The line current going into the rectifier can be calculated using the

following equation:

$$\frac{1}{2}C\frac{d(V_{dc}^2)}{dt} = (u_a i_a + u_b i_b + u_c i_c) - \frac{V_{dc}^2}{R_{load}} \tag{83}$$

R_{load} is the resistance of the load to which the rectifier is connected, and C is the capacitance of the DC bus to which the rectifier is connected.

When applying these equations, there is an important limitation that must be recognized. There is a minimum DC voltage that must be obtained in order to obtain undistorted current waveforms. In order to maintain control of the rectifier, the DC voltage must be higher than the peak voltage generated in the diodes in the rectifier. In order for this condition to be satisfied, the DC voltage must satisfy the condition:

$$V_{dc} > \sqrt{3[E_m^2 + (\omega L i_D)^2]} \tag{84}$$

Where i_D is the DC current supplied to the load of the rectifier.

Using the previous equations, a state-space model of the rectifier could be created. In the state-space model, the SimPowerSystems elements from the previous model are replaced with the circuit equations. The same control scheme is used as the SimPowerSystems model. An overview of the state-space model created in Simulink is shown in Figure 141. The inputs into the model are the amplitude of the output voltage of the generator, the resistance of the rectifier's load, the DC bus capacitance, the incoming line inductance, the incoming line resistance, the targeted DC bus voltage, the switching frequency, and the power source frequency. The outputs of the model are the incoming line currents and the actual DC bus voltage.

Moving left to right, the first block in the model is the voltage measurement (green block). The inner workings of this block are shown in Figure 142. This block is responsible for simulating the voltage waveforms that would be output by the generator and fed into the rectifier. These waveforms are dependent of the generator voltage amplitude and the frequency of the power. The voltage waveform is translated

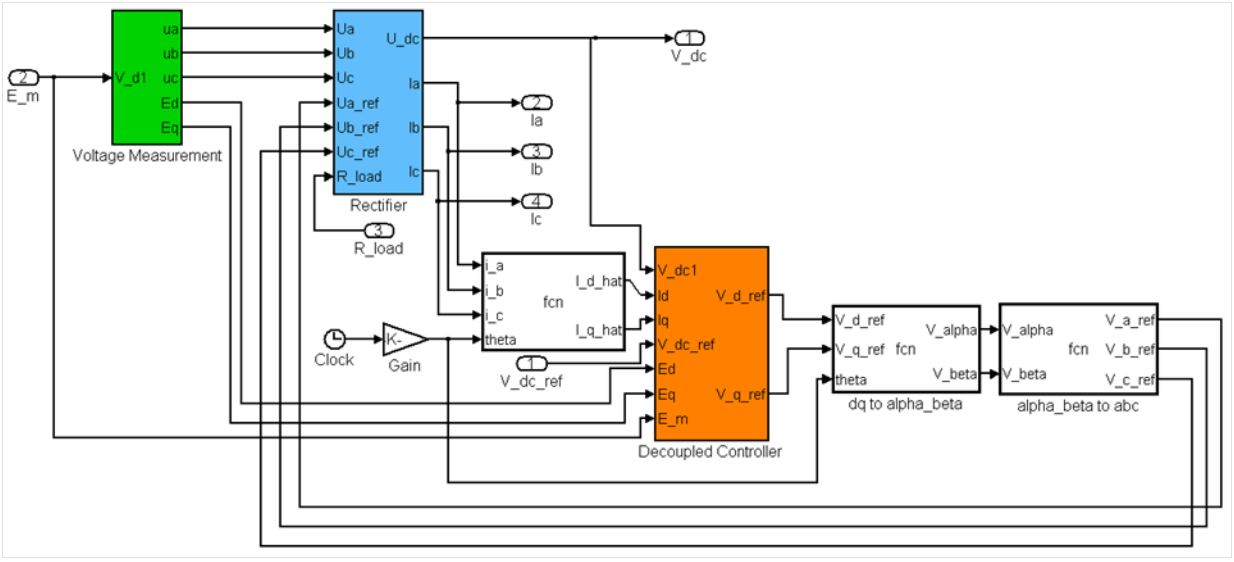

Figure 141: Rectifier state-space model

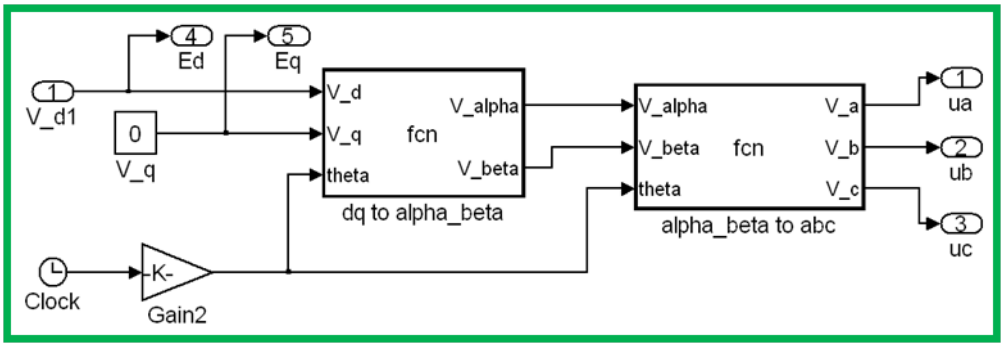

Figure 142: Rectifier voltage measurement

into three reference frames in order to be used by the rectifier mathematical model and the decoupled controller.

The next block in the model is the mathematical representation of the rectifier. This is the blue box in Figure 141, and it shown in detail in Figure 143.

The third block (white block) in Figure 141 simply transforms the line current from the abc reference frame to the rotating reference frame through the use of equations 72 and 74. The fourth block is the decoupled controller (orange block). The orange block in Figure 141 is the rectifier controller. This is the same controller used in the SimPowerSystems model and can be seen in Figure 80.

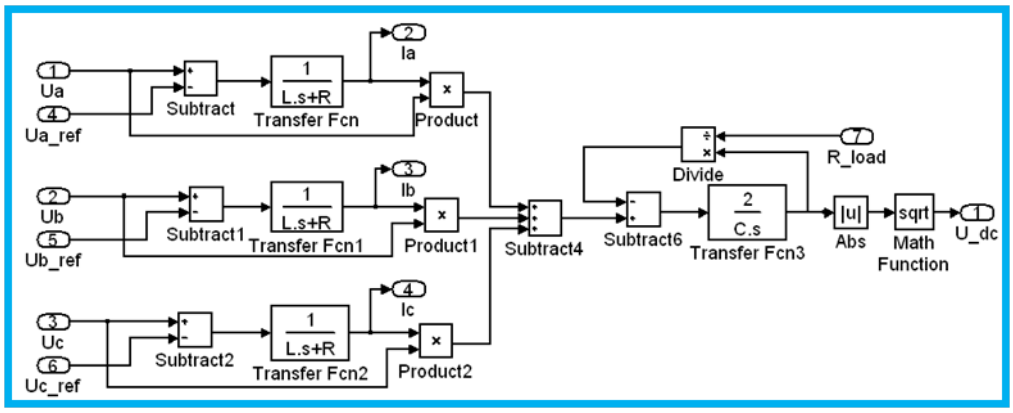

Figure 143: Model of rectifier state equations

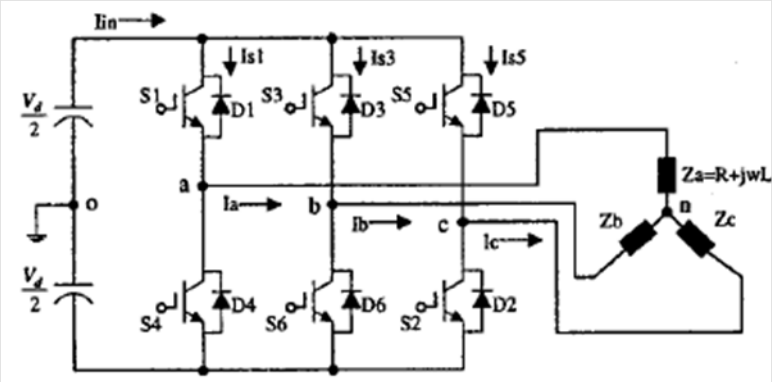

Figure 144: Inverter circuit

6.3.2.2 Inverter State-Space Averaged Model

In order to model the inverter, the state equations based on the circuit configuration are needed. The circuit representation of this model is shown in Figure 144.

Pulse Width Modulation (PWM) is used to generate a transfer function that will be used to calculate the independent variables of the model. The PWM signals are similar to those used in the SimPowerSystem model; however, unlike the SimPowerSystems switching pulses that only range from 0 to 1, one set of switching pulses will range from -1 to 1. These modified signals are shown in Figure 145. The first graph in Figure 145 shows the modulated and unmodulated waveforms. Using these signals, the transfer function is defined as:

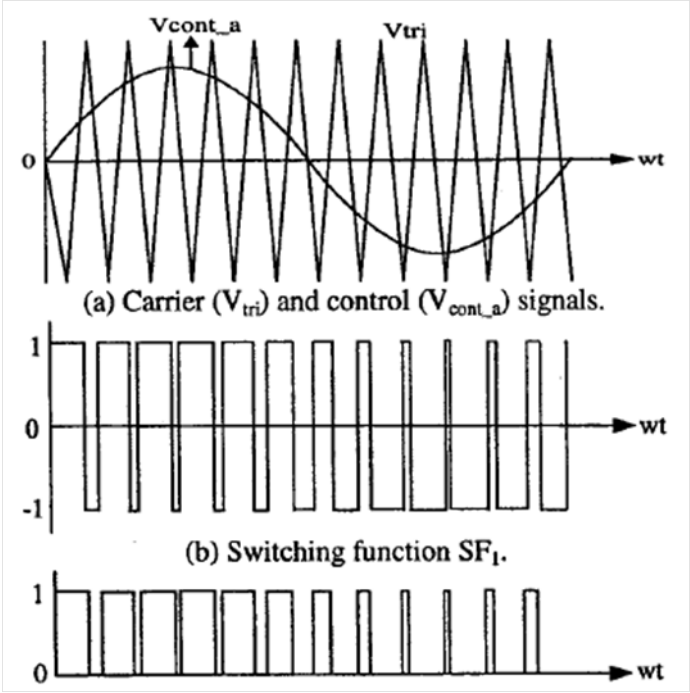

Figure 145: Inverter state-space PWM

$$TransferFunction = \frac{UnmodulatedWaveform}{ModulatedWaveform} \tag{85}$$

The middle graph in Figure 145 is the switching function for the voltages, SF_1. The bottom graph in Figure 145 is the switching function for the current, SF_2.

This transfer function is used to define the relationships between the inputs and outputs of the inverter model.

$$[V_{ab}, V_{bc}, V_{ca}] = TF \cdot V_d \tag{86}$$

$$I_{in} = TF \cdot [I_a, I_b, I_c]^T \tag{87}$$

Where TF is the transfer function; V_{ab}, V_{bc}, and V_{ca} are the output voltages of the inverter; V_d is the input voltage into the inverter; I_{in} is the input current into the inverter; and I_a, I_b, and I_c are the output currents from the inverter.

The inverter line-to-line voltages are calculated as

$$V_{ab} = \frac{V_d}{2} \cdot SF_{1a} - \frac{V_d}{2} \cdot SF_{1b} \tag{88}$$

$$V_{bc} = \frac{V_d}{2} \cdot SF_{1b} - \frac{V_d}{2} \cdot SF_{1c} \tag{89}$$

$$V_{ca} = \frac{V_d}{2} \cdot SF_{1c} - \frac{V_d}{2} \cdot SF_{1a} \tag{90}$$

The DC current into the inverter is calculated as

$$I_{in} = I_{S1} + I_{S3} + I_{S5} \tag{91}$$

Where,

$$I_{S1} = I_a \cdot SF_{2a} \tag{92}$$

$$I_{S3} = I_b \cdot SF_{2b} \tag{93}$$

$$I_{S5} = I_c \cdot SF_{2c} \tag{94}$$

The output currents are calculated based on the load to which the rectifier is attached. In this case the motor that the rectifier supplies can be modeled as a resistive-inductive (R-L) load. Based on those values, the output currents are calculated as

$$I_a = \frac{V_{an}}{R + j\omega L} \tag{95}$$

$$I_b = \frac{V_{bn}}{R + j\omega L} \tag{96}$$

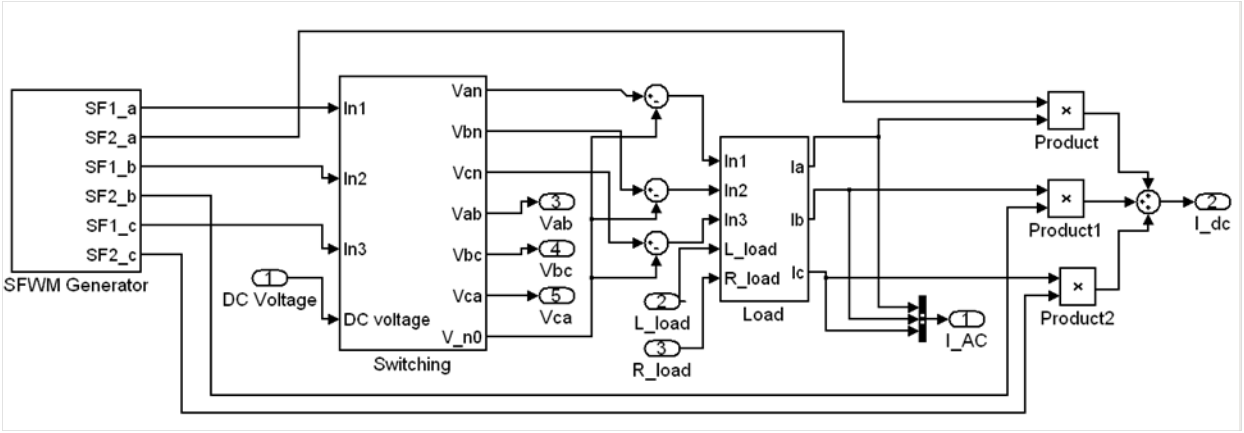

Figure 146: Inverter state-space model

$$I_c = \frac{V_{cn}}{R + j\omega L} \tag{97}$$

Where the phase voltages (V_{an}, V_{bn}, and V_{cn}) are calculated as

$$V_{an} = \frac{V_d}{2} \cdot SF_{1a} - \frac{1}{3}(\frac{V_d}{2} \cdot SF_{1a} + \frac{V_d}{2} \cdot SF_{1b} + \frac{V_d}{2} \cdot SF_{1c}) \tag{98}$$

$$V_{bn} = \frac{V_d}{2} \cdot SF_{1b} - \frac{1}{3}(\frac{V_d}{2} \cdot SF_{1a} + \frac{V_d}{2} \cdot SF_{1b} + \frac{V_d}{2} \cdot SF_{1c}) \tag{99}$$

$$V_{cn} = \frac{V_d}{2} \cdot SF_{1c} - \frac{1}{3}(\frac{V_d}{2} \cdot SF_{1a} + \frac{V_d}{2} \cdot SF_{1b} + \frac{V_d}{2} \cdot SF_{1c}) \tag{100}$$

The model of the inverter was created using Simulink. In this model the independent/input variables are the DC voltage supplied from the transmission line and a R-L load representing a motor load. The dependent/output variables are the DC current that must be supplied to the inverter and the output voltage of the inverter. The complete inverter model is shown in Figure 146.

The PWM control was simulated using sine wave generators for the control signals and a repeating signal generator for the carrier signal. For the first transfer function, SF_1, a pulse up to 1, is created whenever the carrier signal is below the control signal. The pulse goes to -1 for the opposite case. The second transfer function, SF_2, is

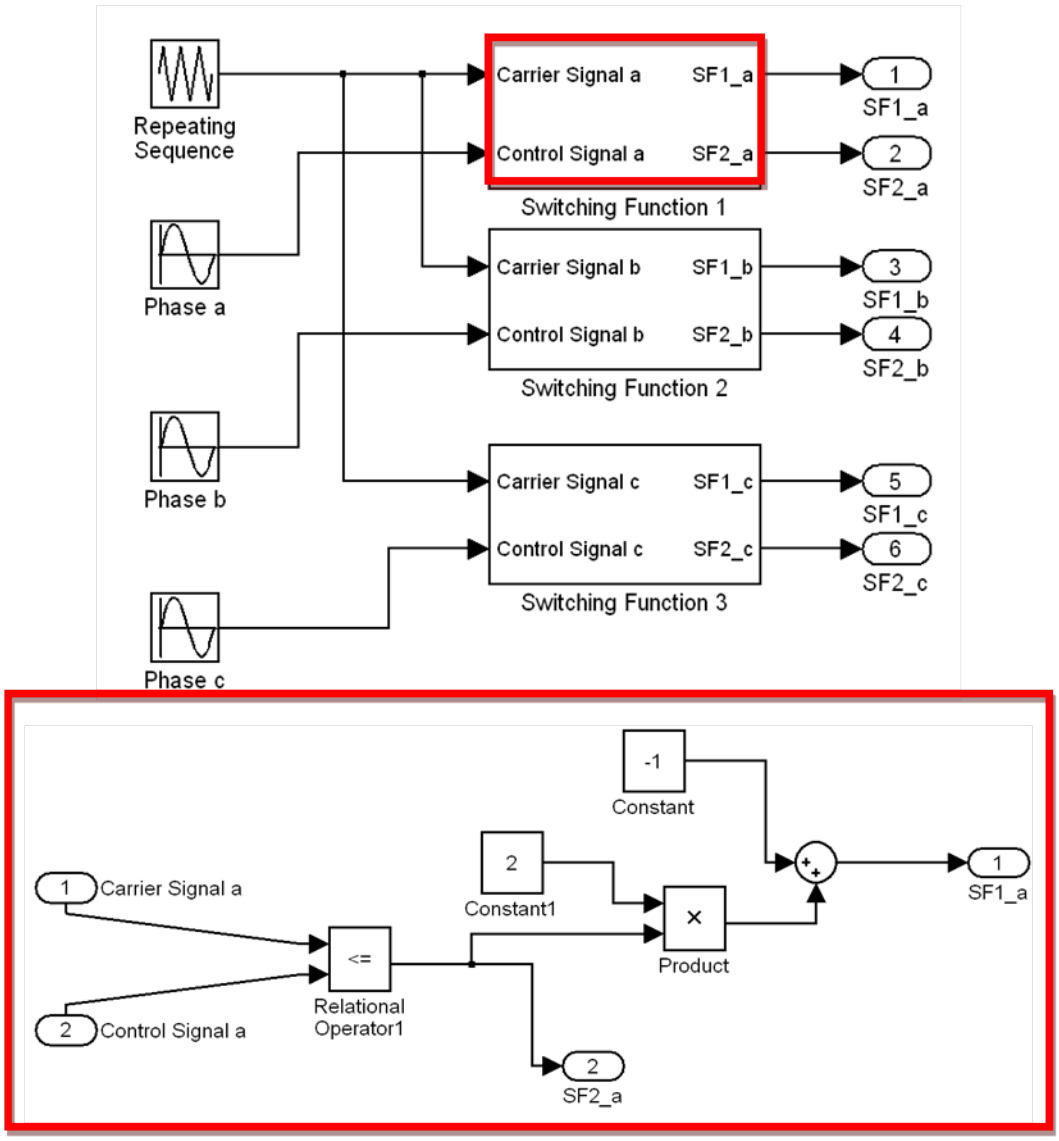

Figure 147: Inverter state-space model PWM control

similar in nature; the only difference is it goes to 0 instead of negative one when the carrier function is greater than the control function. The model of the PWM control is shown in Figure 147.

The switching block determines the output voltage of the inverter. Within the block, equations 88 through 90 and 98 through 100 are applied. The load block determines the output current of the inverter. This block is responsible for implementing equations 92 through 94.

6.3.2.3 Machine Models

The SimPowerSystems models of the machines must also be replaced. The generator model simply sets the input voltage for the rectifier. This is done using a sine wave generator with a frequency and amplitude that matches the output of the SimPowerSystem generator emulation.

The motor model was replaced using a DQ transformation model. The model consists of two parts – an electrical model and a mechanical model. The set of equations that define each model were implemented into Simulink to create the model. The electrical response of the machine can be described by three equations.

$$\frac{d}{dt}i_d = \frac{1}{L_d}v_d - \frac{R}{L_d}i_d + \frac{L_q}{L_d}p\omega_m i_q \tag{101}$$

$$\frac{d}{dt}i + q = \frac{1}{L_q}v_q - \frac{R}{L_q}i_q - \frac{L_d}{L_q}p\omega_m i_d - \frac{\lambda p\omega_m}{L_q} \tag{102}$$

$$T_e = 1.5p[\lambda i_q + (L_d - L_q)i_d i_q] \tag{103}$$

The mechanical performance of the machines is governed by the following two equations:

$$\frac{d}{dt}\omega_r = \frac{1}{J}(T_e - T_f - F\omega_m - T_m) \tag{104}$$

$$\frac{d\theta}{dt} = \omega_m \tag{105}$$

The variables for the electrical and mechanical equations are listed in Table 39.

6.3.2.4 State-space system model

The power converter and machine models were combined to create a state-space model of a single motor system. The results of the model are shown in Figures

Table 39: DQ motor model parameters

L_q, L_d	q and d axis inductances
R	Resistance of the stator windings
i_q, i_d	q and d axis currents
v_q, v_d	q and d axis voltages
ω_m	Angular velocity of the rotor
λ	Amplitude of the flux induced by the permanent magnets of the rotor in the stator phase
p	Number of pole pairs
T_e	Electromagnetic torque
J	Combined inertia of rotor and load
F	Combined viscous friction of rotor and load
θ	Rotor angular position
T_m	Shaft mechanical torque
T_f	Shaft static friction torque

148 through 152. While the state-space models provide some of the same trends as the high fidelity SimPowerSystems model, there are some discrepancies. In general, the current is much higher throughout the state-space model (shown in Figures 148, 149, and 151); this occurs because some losses in the buses and filters have been ignored by the model. As a result, the rectifier recognizes the extra current and attempts to block current which results in the dramatic drop-off in generator current shown in Figure 148. While the currents are high, the voltage throughout the system is similar to the SimPowerSystems model. Figure 150 shows that the bus voltage perfectly meets the 4,000 V target. The primary difference is the voltage ripple observed using the SimPowerSystems model is not present in the state-space model. Lastly, the motor voltage observed in Figure 152 is slightly higher than that of the SimPowerSystems model and does not portray all the startup dynamics that are seen in the SimPowerSystems model.

The state-space models quickly provide an estimate of system performance. The state-space model can simulate the system in 1/28,800 % of the time required for the high fidelity model. However, in the process, some of the high frequency harmonics in the system are lost which will be important for the stability analysis. Therefore, it

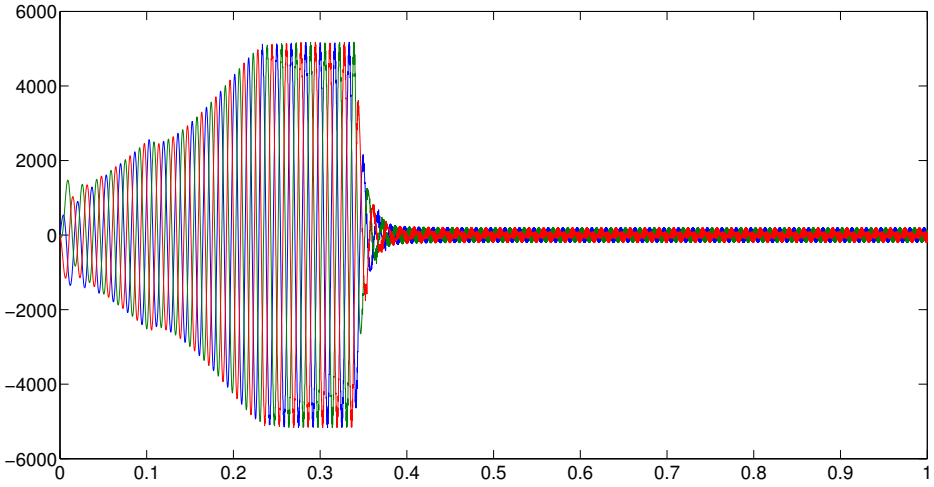

Figure 148: State-space system model generator current

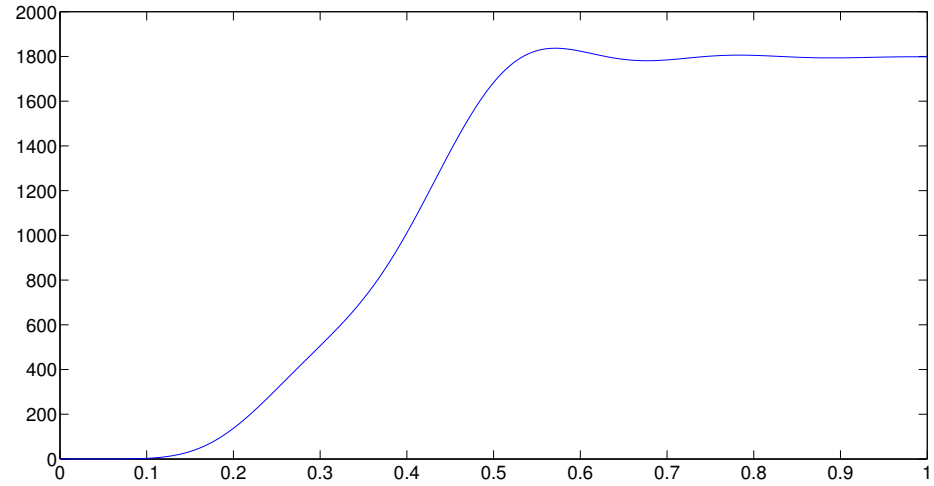

Figure 149: State-space system model bus current

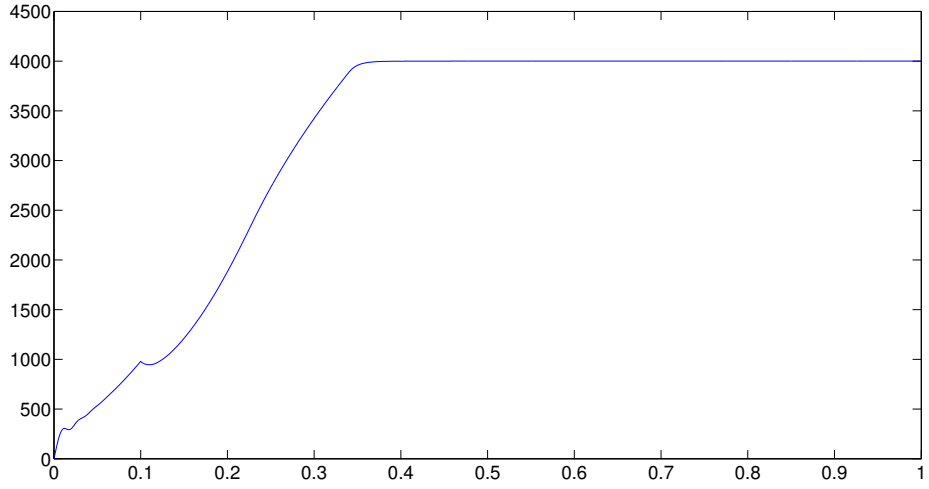

Figure 150: State-space system model bus voltage

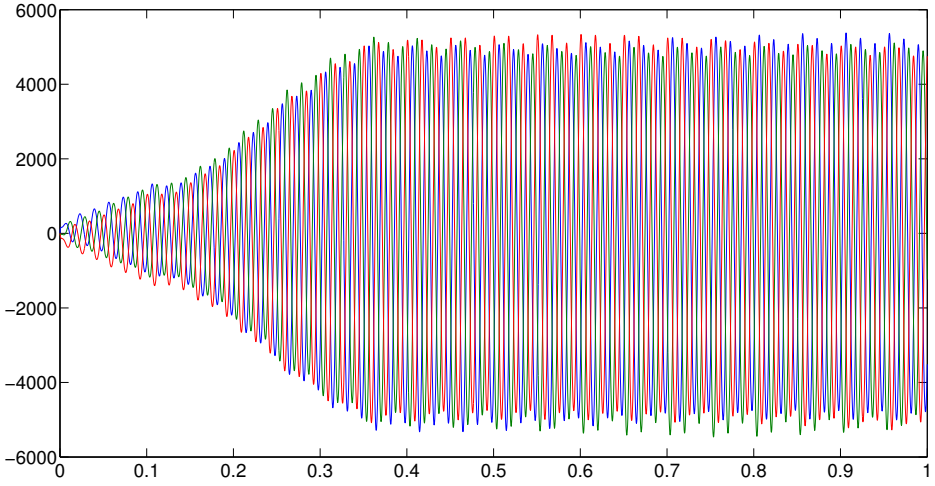

Figure 151: State-space system model motor current

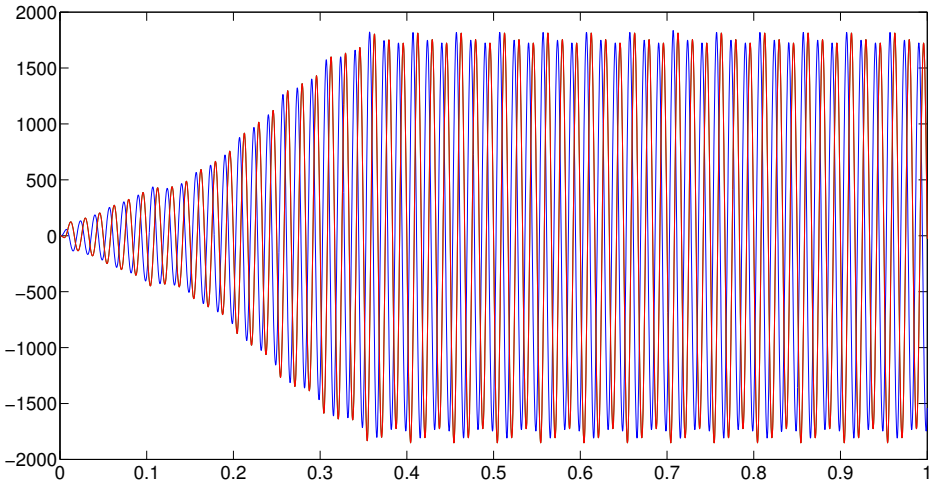

Figure 152: State-space system model motor voltage

is recommended that the state-space models only be used to quickly evaluate steady-state performance, but should not be used for detailed analysis such as determining system stability.

6.4 Stability Analysis

Another major concern when designing the PDS is stability. A system is considered stable when it can return to equilibrium after a disturbance. If the PDS becomes unstable, multiple problems can arise. In some cases, the system will not be able to provide the required amount of power or the power quality may not be sufficient. In other instances, surges may occur causing problems like arcing or burnout of a component. In either case, stability cannot be reached unless the system is shut down, and sometimes the system will need to be repaired [152].

In PDS systems today, stability is usually not a problem since only passive components are used; however, in the PDS for the turboelectric system, stability is a major concern due to the presence of active converters. Active converters can cause instabilities because they act as a constant power load (CPL) [27]. The V-I graph for a CPL is shown in Figure 153. In Figure 154, the CPL curve is displayed with

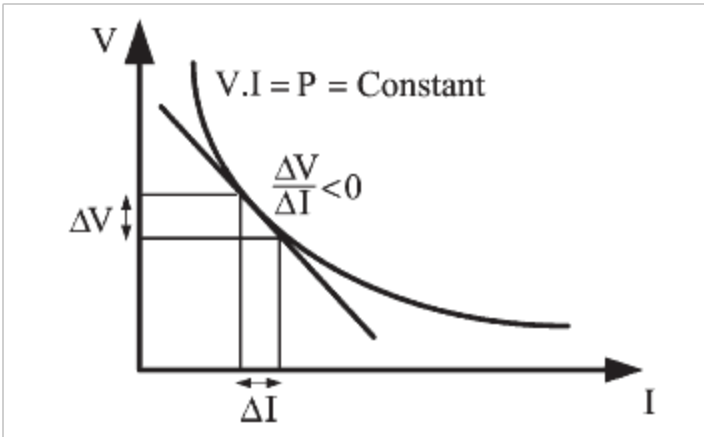

Figure 153: Constant power load [41]

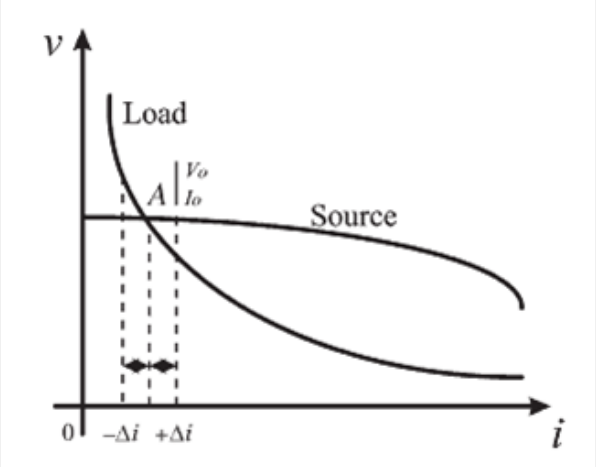

Figure 154: Constant power load and source [41]

the power curve of a source. At point A on the graph, the system is stable. Suppose that current is decreased; this will cause the voltage of the load to be greater than the voltage of the source, so the load will demand a decrease in current. This will cause the system to move further from the equilibrium point A causing asymptotic instability.

The first step in determining whether a given system is stable is to understand how to calculate stability. The stability of a system is based upon component impedance and admittance values. A challenge is that these attributes are calculated in the frequency domain rather than the time domain. All of the models are built using

the time domain; therefore, a Fourier transform is needed to convert the data to the frequency domain for stability analysis [67].

Stability analysis can be broken into two categories – small signal and large signal stability [123]. Small signal stability determines whether a given operating point is stable. (It can also guarantee that the point is stable with small perturbations.) Large signal stability analysis defines a region for which an operating point is stable. This region defines the magnitude of perturbations that the system can withstand and return to equilibrium. In this problem only small signal stability will be considered. Large signal stability analysis can be performed after the design is selected to determine the bounds of its operation.

6.4.1 Stability Analysis Approaches

A variety of stability analysis methods have been developed. They vary in how conservative the approach is and what stability regime that it addresses. In this study, small signal stability and voltage ripple are addressed. Large signal stability would be studied later in the design process to determine operation limits for the system.

6.4.1.1 Small Signal Stability

Small signal stability is often studied by multiplying impedance and admittance values at an interaction point and then plotting the result on a Nyquist plot [143]. The system is stable if the (-1,0) point on the Nyquist plot is not encircled. The typical stability constraint used in this type of system is the Middlebrook criterion. The Middlebrook criterion dictates that the product of the impedance and admittance should fall within the unit circle on a Nyquist plot. While this criterion ensures that system is stable, it can lead to artificially conservative designs because part of the forbidden plane has little effect on stability.

Other approaches for ensuring system stability are implementation of the Gain

and Phase Margin Criterion or the Opposing Component Criterion. Both of these approaches can lead to less conservative designs than those obtained using the Middlebrook criterion. The primary downfall of these approaches is that in order to get less conservative designs, the circuit must be rearranged for the calculation. Also, these methods do not explicitly include uncertainty, parameter variation, or nonlinearities. These aspects of system design can only be included in the analysis direct assignment of gain and phase margins. If the designer does not properly select these values, instability may occur.

The fourth option for a stability criterion is Admittance Space Stability Analysis [142]. The admittance space stability design process can be used to find specifications of the system that will keep the system stable while incorporating uncertainty, a wide range of operating points, and reconfigurability. Nyquist plots demonstrating each of the four criteria are shown in Figure 155. Admittance space stability analysis will be used in this study since it has proven to ensure system stability while not being overly conservative.

6.4.2 Admittance Space Stability Criterion

The admittance space stability analysis consists of several steps. The first is to capture the impedance and admittance data from the models. After the data is collected, the criterion is used to determine whether the system is stable. Each step of the analysis will be described for both AC and DC applications.

6.4.2.1 Impedance/Admittance Measurement

There are two ways to calculate impedance/admittance. One is an analytical method in which the circuit equations are solved which is difficult to do in the presence of switching elements. The second is using simulation. With this method, an AC current is injected into the system at the point of interest, and the magnitude of the disturbance on the current and voltage in the system is measured. Current injection

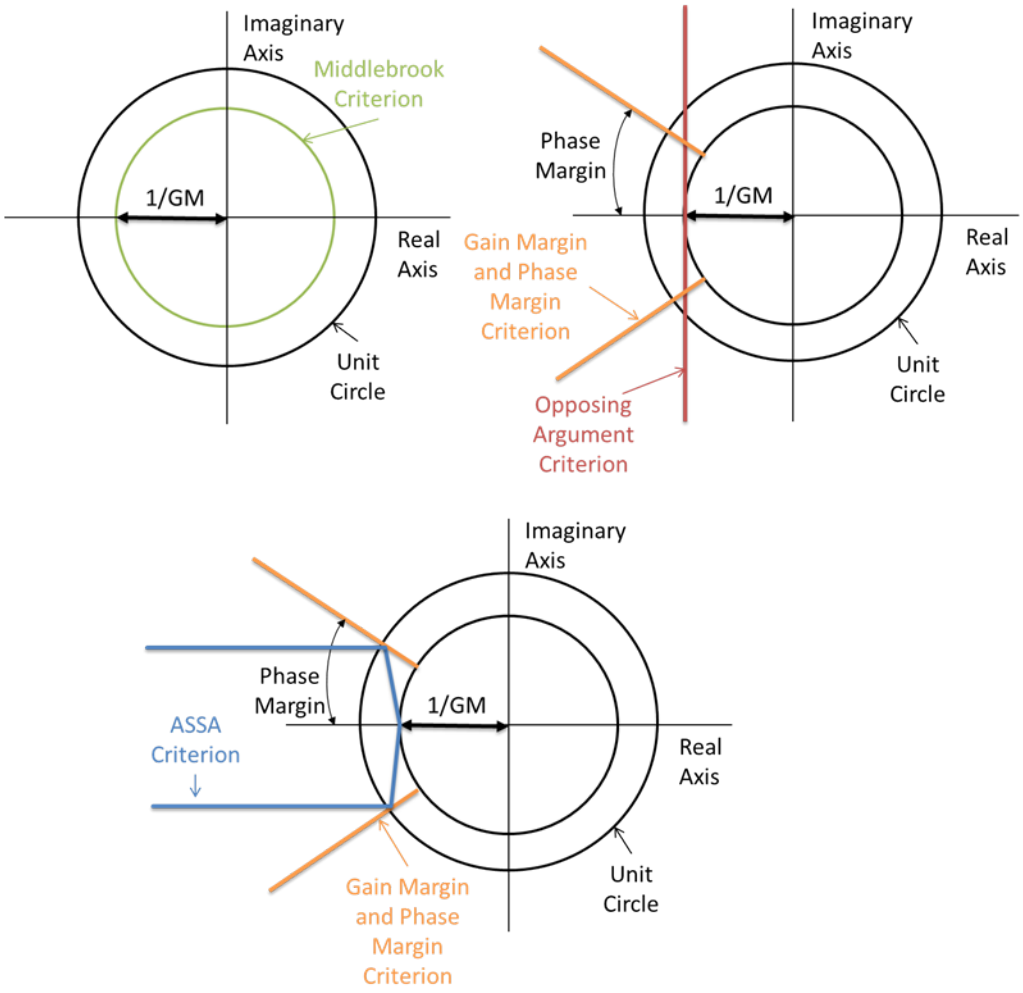

Figure 155: Stability constraint nyquist plots

will be the method used for impedance measurement in this study due to the presence of the switching elements. The method in which impedance is calculated is slightly different depending on whether the measurement is for a DC or AC point in the system.

DC Impedance Measurement The DC impedance measurement is needed to determine the stability of the bus. The first step in the measurement process is to inject a current from pole-to-pole at the frequency being measured. The magnitude of the current should be relatively small compared to the existing bus current. (The current amplitude used in this study was 10 Amps and was injected using an ideal current source.)

The system is simulated for a small amount of time (given the system begins at steady-state) and the voltage and current time domain data is collected upstream and downstream of the injected current. The upstream data is denoted with the subscript S, and the downstream data is denoted with the subscript L.

Once the time domain data has been captured, a Fourier transform is performed to obtain voltage and current in the frequency domain. (The MATLAB fft function was used to perform the transform.) Next, impedance can be calculated using the data.

$$Z_S = \frac{V_S(s)}{I_S(s)} \tag{106}$$

The admittance of the load is calculated as:

$$Y_L = \frac{1}{\frac{V_L(s)}{I_L(s)}} \tag{107}$$

The current injection and impedance/admittance calculation is then repeated for each frequency of interest.

AC Impedance Measurement The AC impedance measurement is needed to determine the stability of the generator to rectifier connection and the inverter to motor connection. The AC impedance measurement begins similar to the DC impedance measurement method. Similarly, a current is injected into the system; however, the measurement requires two linearly independent injections. In this case, the current is injected between the b and c phases. The frequency used for the first injection is:

$$\omega_i = |\omega_s + \omega_e| \tag{108}$$

ω_s is the frequency being measured. ω_e is the fundamental electrical frequency of the system. During the current injection, the time domain data (i_a, i_b, i_c, v_a, v_b, v_c) on both sides of the injection is captured. Next, a Park's transformation is performed to transform the time domain data captured to a rotating reference frame, (The data becomes i_d, i_q, v_d, and v_q.) which is the same technique that was used for the rectifier control scheme.

$$\begin{bmatrix} \alpha \\ \beta \end{bmatrix} = \begin{bmatrix} \frac{2}{3} & -\frac{1}{3} & -\frac{1}{3} \\ 0 & \frac{1}{\sqrt{3}} & -\frac{1}{\sqrt{3}} \end{bmatrix} \begin{bmatrix} a \\ b \\ c \end{bmatrix} \tag{109}$$

$$\begin{bmatrix} d \\ q \end{bmatrix} = \begin{bmatrix} cos(\theta) & sin(\theta) \\ -sin(\theta) & cos(\theta) \end{bmatrix} \begin{bmatrix} \alpha \\ \beta \end{bmatrix} \tag{110}$$

Where θ is equal to ω_e.

After the Park's transformation, a Fourier transformation is used to move the data from the time domain to the frequency domain, which produces i_{d1}, i_{q1}, v_{d1}, and v_{q1}.

Next, the process is repeated, but now the current is injected at:

$$\omega_i = |\omega_s - \omega_e| \tag{111}$$

The Park's transformation and Fourier transformation when completed produce: i_{d2}, i_{q1}, v_{d2}, and v_{q2}.

The final step is to calculate the impedance and admittance values:

$$\mathbf{Z_{Sdq}}(s) = \begin{bmatrix} v_{d1}(s) & v_{d2}(s) \\ v_{q1}(s) & v_{q2}(s) \end{bmatrix} \begin{bmatrix} i_{Sd1}(s) & i_{Sd2}(s) \\ i_{Sq1}(s) & i_{Sq2}(s) \end{bmatrix}^{-1} \tag{112}$$

$$\mathbf{Z_{Ldq}}(s) = \begin{bmatrix} v_{d1}(s) & v_{d2}(s) \\ v_{q1}(s) & v_{q2}(s) \end{bmatrix} \begin{bmatrix} i_{Ld1}(s) & i_{Ld2}(s) \\ i_{Lq1}(s) & i_{Lq2}(s) \end{bmatrix}^{-1} \tag{113}$$

6.4.2.2 Admittance Space Stability Criterion

The admittance space stability criterion determines system stability by defining a forbidden and acceptable region for load admittance. The bounds of the forbidden region are determined based upon the source impedance which is depicted in Figure 156.

The bounds of the forbidden region are determined by three parameters. One is gain margin (GM) which is a value less than 1. The criterion intersects the real axis at 1/GM. The second parameter used is s_c. This defines the criterion distance from the x-axis and how far the criterion extends along the negative x-axis. The values chosen were 5 away from the x-axis and extended to -10e5. The last parameter used to define the criterion bounds is phase margin (PM), which defines that angle of the line that connects the real axis intersection and the line defined by s_c. The phase margin chosen was 60 degrees. The lines that are defined are then mirrored over the real axis.

The admittance space criterion works by defining a forbidden region for which load admittance cannot intersect. The bounds of the region must be calculated for every frequency of interest using the following equation:

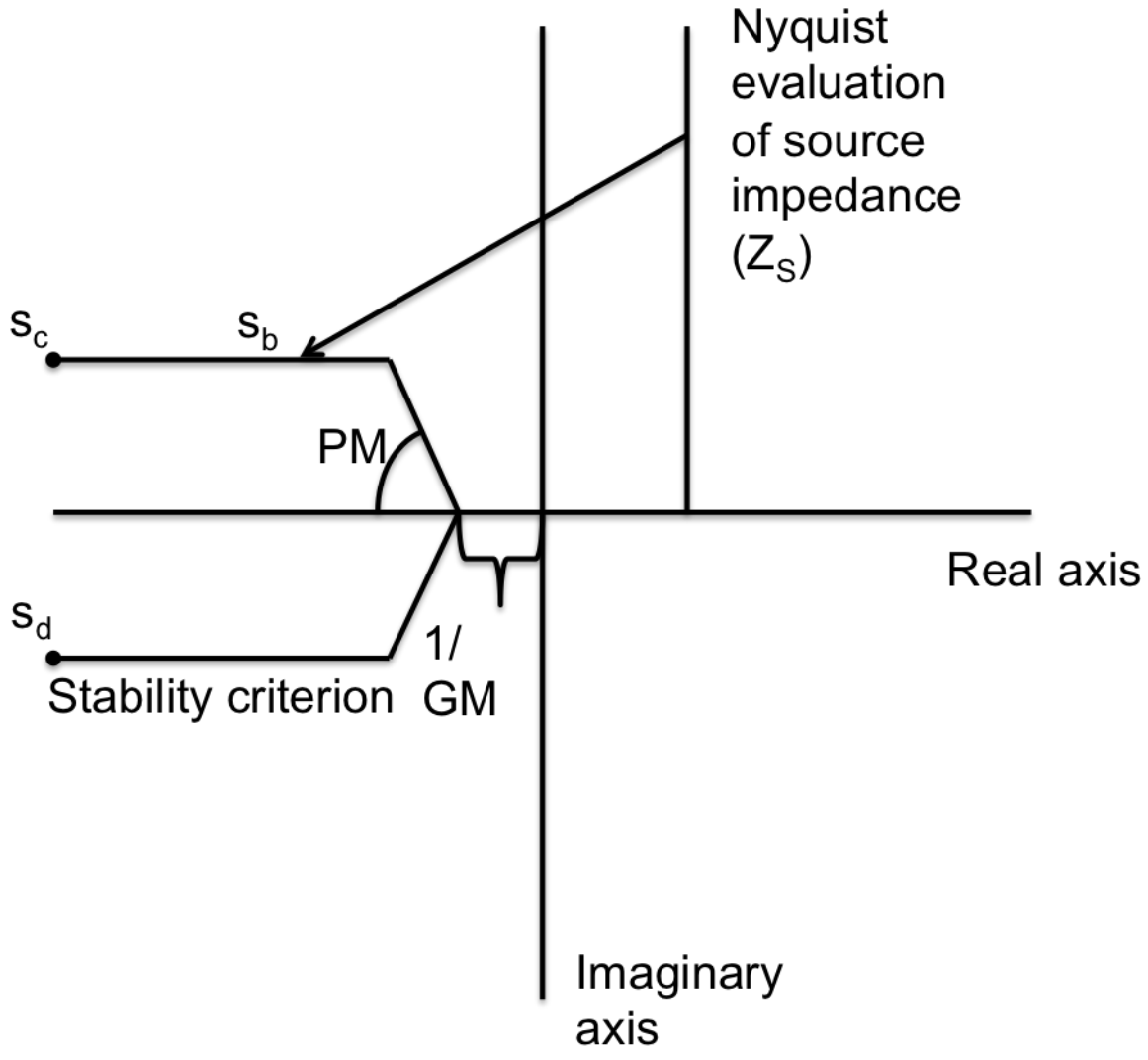

Figure 156: Admittance space stability criterion

$$Y_{L,b} = \frac{s_b}{Z_S} \tag{114}$$

$Y_{L,b}$ is the bound of acceptable load admittance at frequency b. s_b is a parameter that is swept across the stability criterion shown in Figure 156. By sweeping s_b a forbidden region is defined at frequency b. This process must be repeated for all frequencies. Once the forbidden region has been defined for all frequencies of interest, the forbidden region and measured load admittance values are plotted.

6.5 Stability Analysis Results

The stability analysis was performed for the buses, generator to rectifier connections, and inverter to motor connections for each architecture. If there were identical branches in the architectures, the stability analysis was only performed once since an identical configuration would have the same response.

The admittance space and the load impedance are plotted in three-dimensions: frequency, phase, and magnitude. The admittance space stability criterion will determine what regions of the plot are forbidden. In each plot the forbidden region is shown in red. The forbidden region was plotted for each frequency that source impedance was measured. The region appears to be discontinuous since impedance measurements were made at discrete frequency points. The region was extrapolated between measured frequencies.

The load admittance values for each frequency are also plotted on the diagram. If none of the load admittance points fall within the forbidden region, then the system is stable. If any of the points do fall within the forbidden region, the component designs and control schemes need to be revisited. Also, for points in the stable region, the distance of the point from the forbidden region (referred to as stability margin) determines how conservative a given design is. Designs with load admittance points close to the forbidden region are considered to be more risky compared to designs

that have load admittance values that are far from the forbidden region; that is, for designs with a low stability margin, the chance of a disturbance moving the system to an unstable point is higher. The stability margin of a system design should be considered when making a final architecture decision.

6.5.1 DC Stability Analysis Results

The DC analysis was performed first to show the stability of the buses in each architecture. The results of each analysis will be presented and discussed.

6.5.1.1 Architecture 1 DC Stability Results

The bus stability for architecture 1 is shown in Figures 157 and 158. Since the branches containing bus 1 and 3 are identical, only one plot is needed. In both cases, all the load admittance values fall outside of the forbidden region – meaning that the bus is stable. Figure 157 shows that around 3,000 Hz is one load admittance point close to the forbidden region. Figure 158 shows that the stability margin is the smallest for bus 2 at low frequencies, so there is some risk associated with the design.

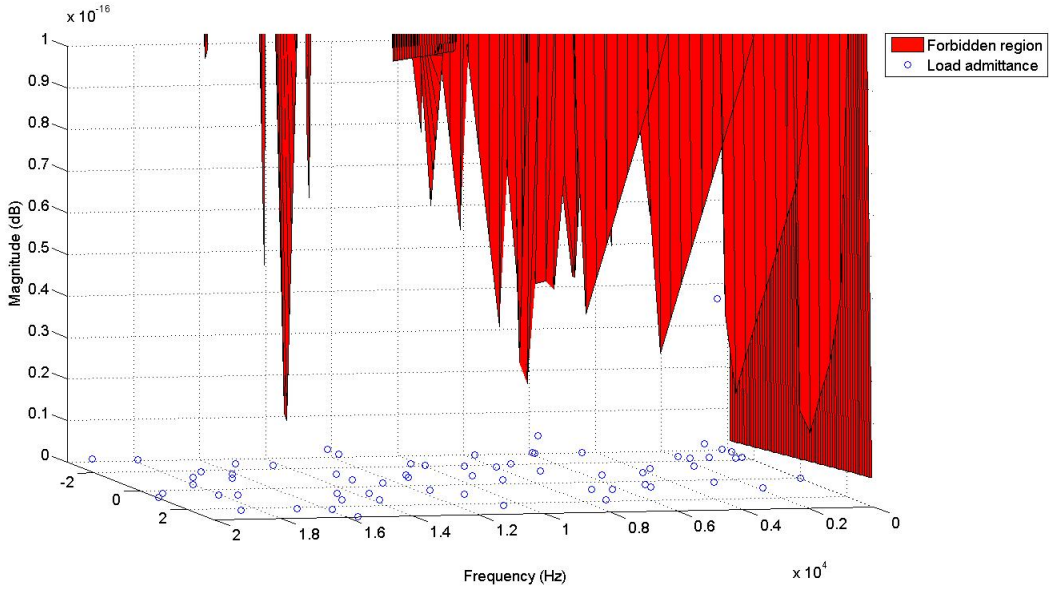

Figure 157: Architecture 1 bus 1/3 stability

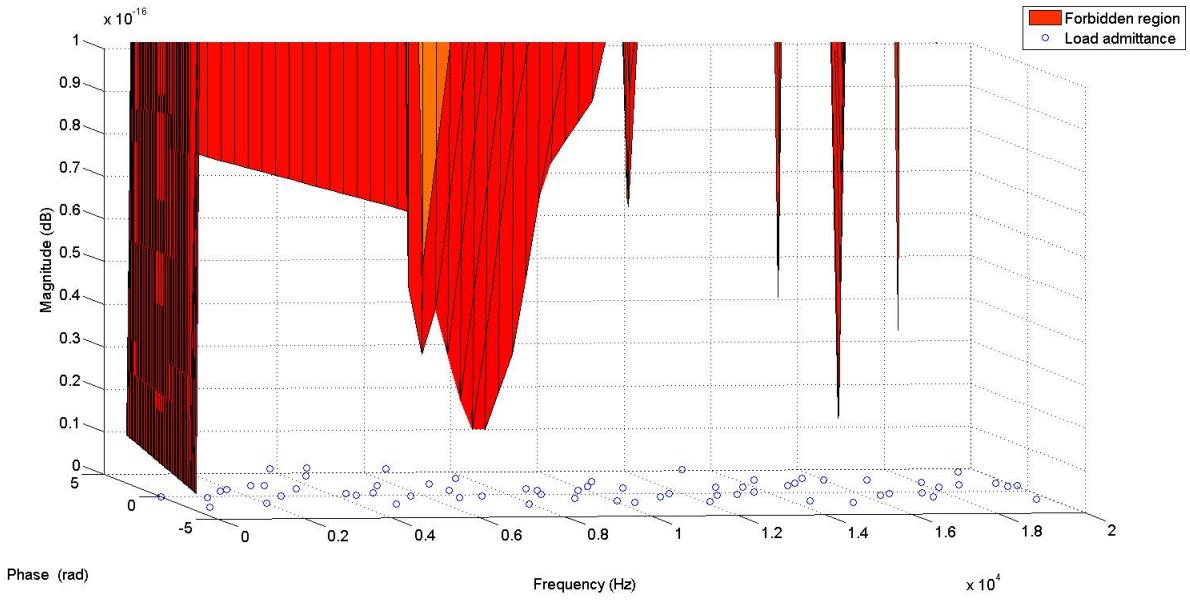

Figure 158: Architecture 1 bus 2 stability

6.5.1.2 Architecture 2 DC Stability Results

The stability of the architecture 2 buses is shown in Figures 159, 160, and 161. The figures show that all three buses are stable in the architecture. Figure 159 shows that the stability margin for bus 1 shrinks around 15,000 Hz – meaning that a disturbance at that frequency may push the system toward an unstable operating point. Figure 160 shows that bus 2 is stable over the spectrum of frequencies. Furthermore, the magnitude of the load admittance values is fairly constant. Lastly, Figure 161 shows that bus 3 has the smallest stability margin in the architecture. The load admittance value magnitude is fairly constant, but the forbidden region approaches the load admittance points. This means that bus 3 has the highest risk of moving to an unstable point compared to the other buses in the architecture.

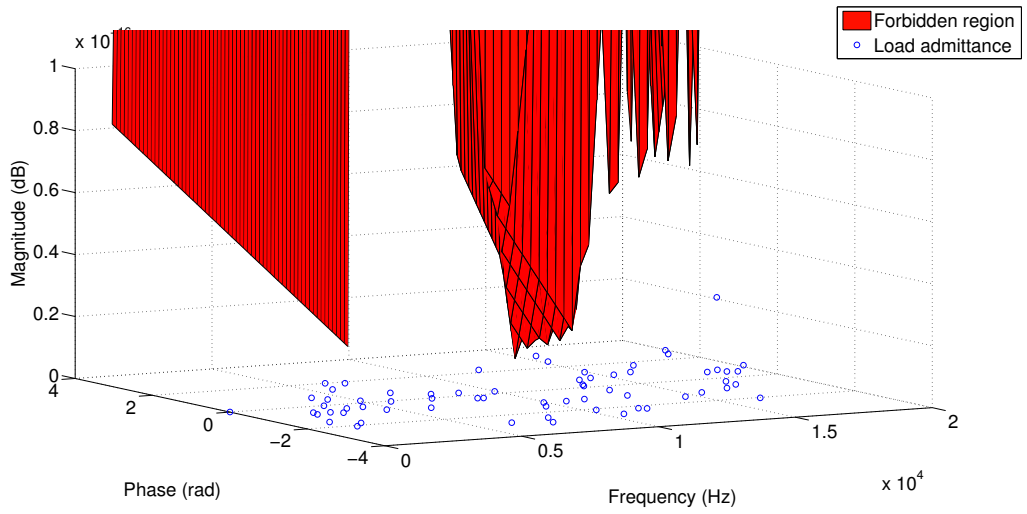

Figure 159: Architecture 2 bus 1 stability

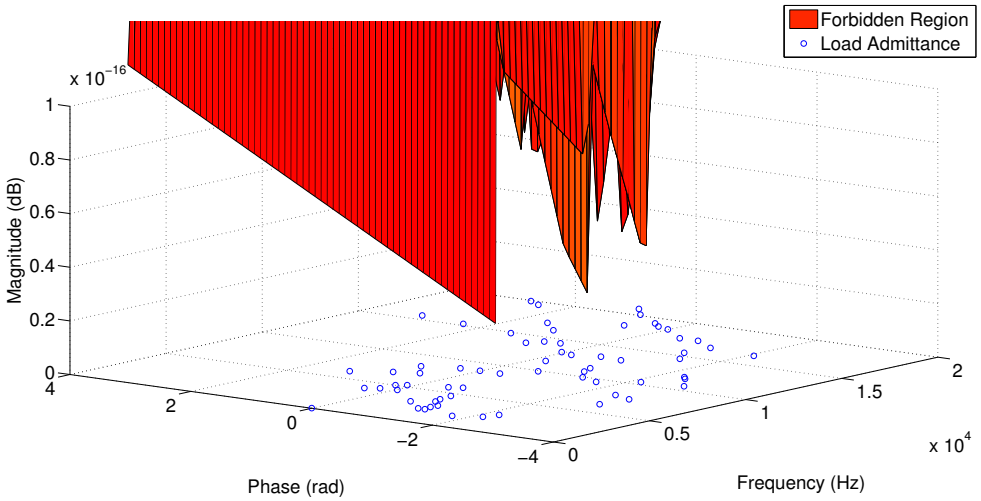

Figure 160: Architecture 2 bus 2 stability

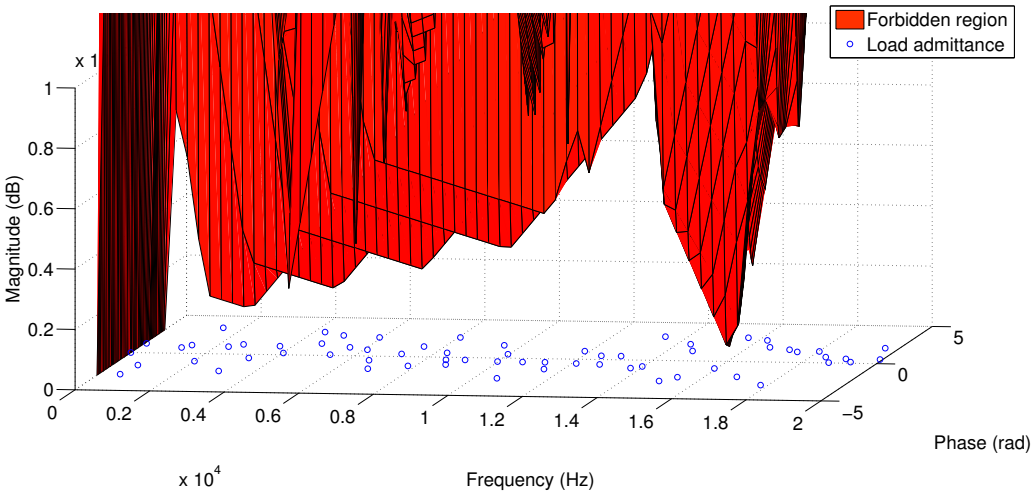

Figure 161: Architecture 2 bus 3 stability

6.5.1.3 Architecture 3 DC Stability Results

The stability of the architecture 3 buses is shown in Figures 162, 163, and 164. The figures show that all the buses are stable at the operating point tested. In fact, the load admittance values are even further from the forbidden region than the architecture 2 case. Therefore, architecture 3 is a more conservative design and is more likely to remain stable.

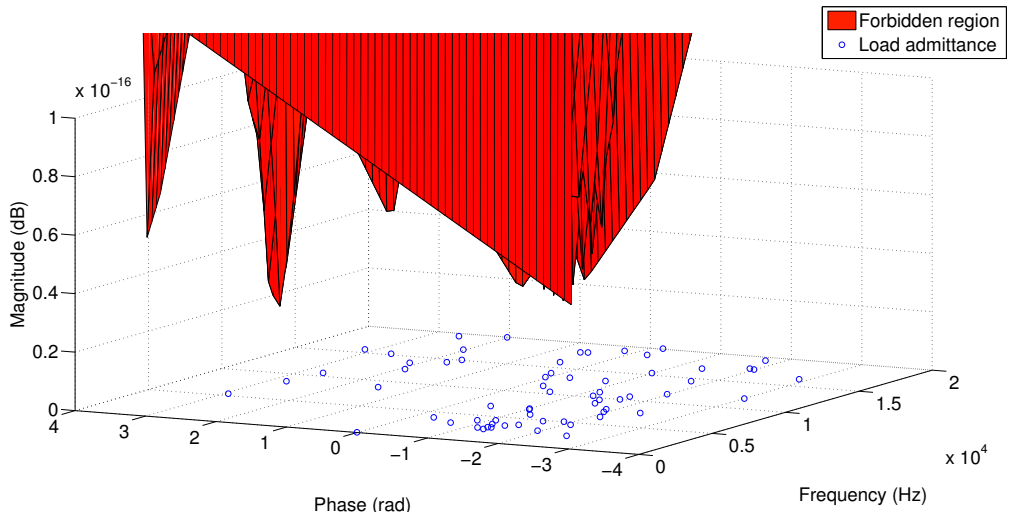

Figure 162: Architecture 3 bus 1 stability

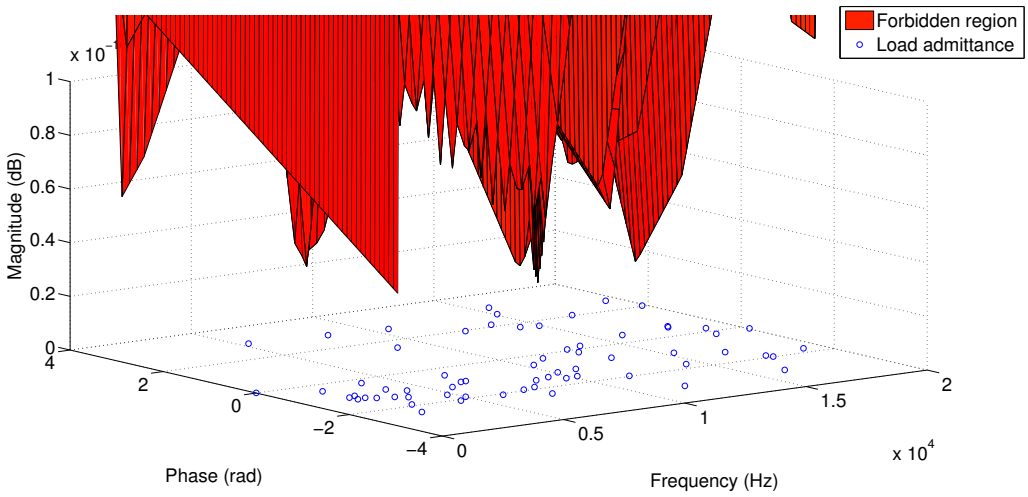

Figure 163: Architecture 3 bus 2 stability

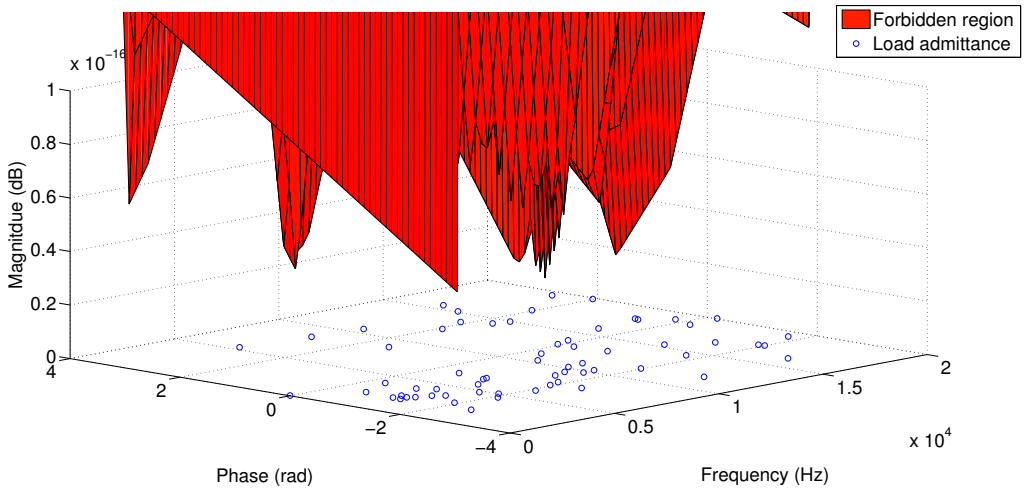

Figure 164: Architecture 3 bus 3 stability

6.5.2 AC Stability Analysis Results

The next step in the stability analysis is to study the stability of the AC connections; that is, determine the stability of the generator to rectifier connections and the inverter to motor connections. For each connection, four stability conditions must be checked since impedance is measured in 4 regimes: dd, dq, qd, and qq. A few examples of results will be shown for each architecture. The remaining results can be

found in Appendix A.

6.5.2.1 Architecture 1 AC Stability

Some examples of the architecture 1 AC plots are shown in Figures 165 though 170. Figures 165 though 167 show the stability results for the generator to rectifier connections for the dd, dq, and qq regimes. Figure 165 shows that the connection has a low stability margin in the dd regime at high frequencies. Figure 166 shows the the stability margin in the dq regime is fairly constant. Figure 167 shows that only a small stability margin is available around 7,000 Hz. For frequencies with a small stability margin, a variation in the steady-state performance of the system could push it into an unstable operating point.

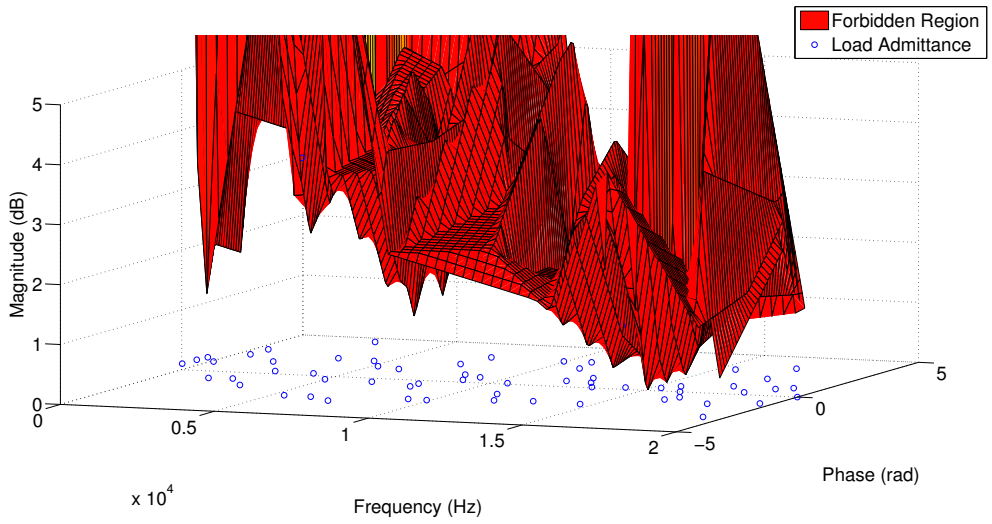

Figure 165: Architecture 1 generator 1 to rectifier 1 connection stability (dd)

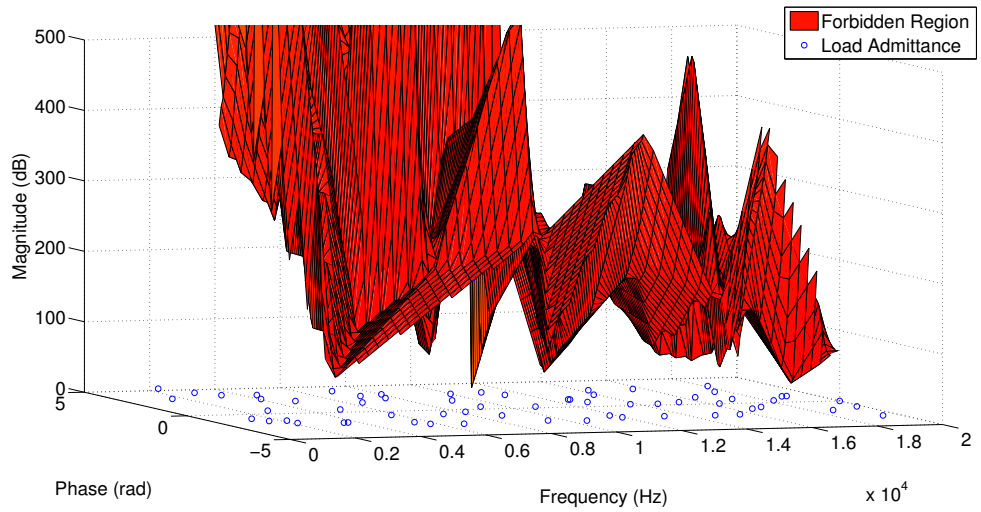

Figure 166: Architecture 1 generator 1 to rectifier 1 connection stability (dq)

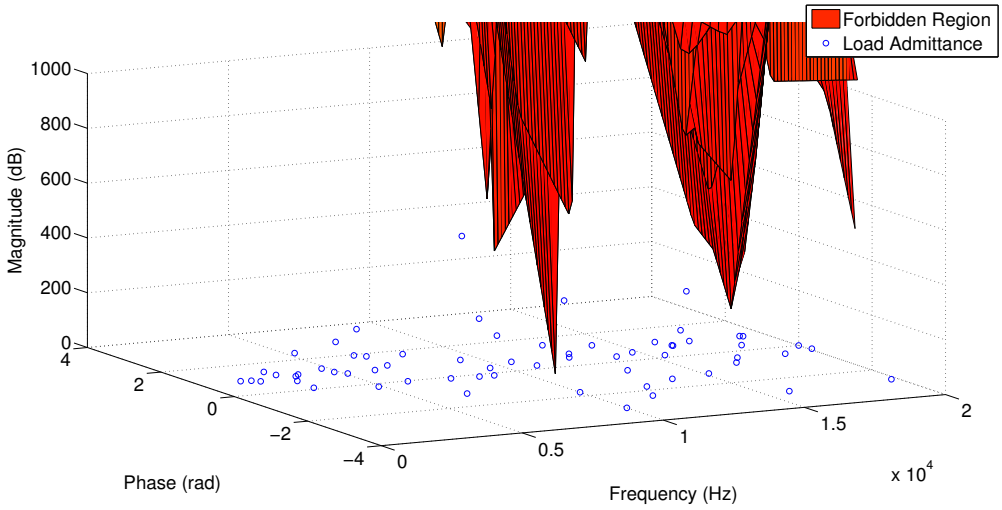

Figure 167: Architecture 1 generator 1 to rectifier 1 connection stability (qq)

Figures 168 through 170 show that the inverter to motor stability surrounds the forbidden region in the dd, dq, and qq regimes. Figure 168 shows that at frequencies around 7,000 Hz and 17,000 Hz, the load admittance magnitudes in the dd regime float above the forbidden region. While the points are stable, movement between frequencies that have load admittance points that are above and below the forbidden region, may cause a system instability. The same trend is observed in Figure 169

for the dq regime; however, in this case, the load admittance points that are above the forbidden region occur at frequencies greater than 10,000 Hz. Lastly, Figure 170 shows that load admittance falls above the forbidden region in the qq regime around 12,000 Hz. In all cases, the motor control will be important in ensuring that the system remains stable.

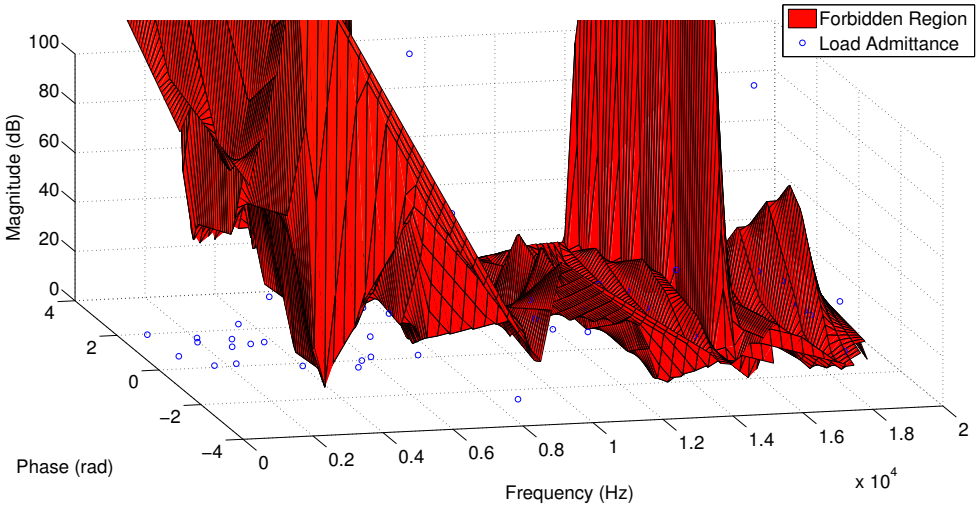

Figure 168: Architecture 1 inverter to motor connection stability (motor group 1) (dd)

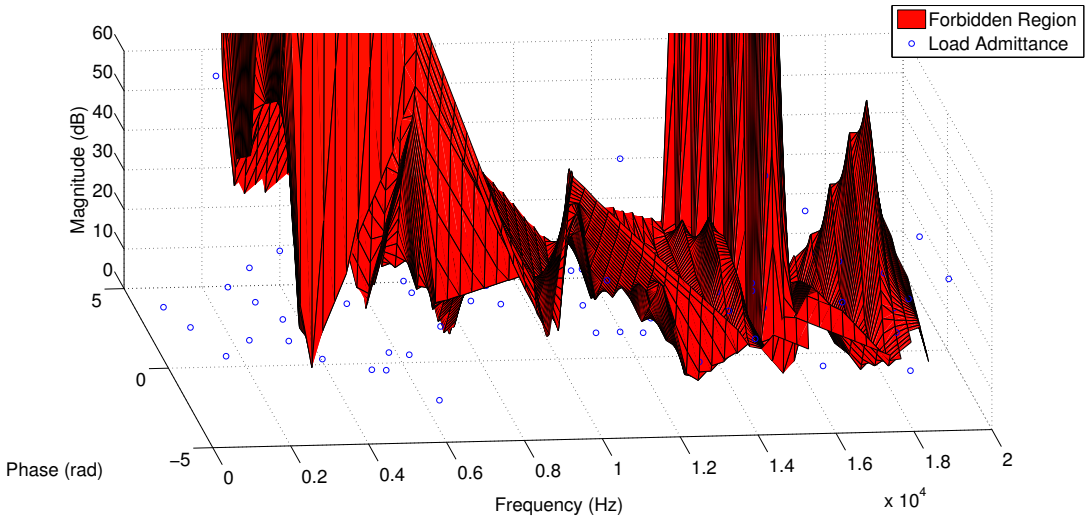

Figure 169: Architecture 1 inverter to motor connection stability (motor group 1) (dq)

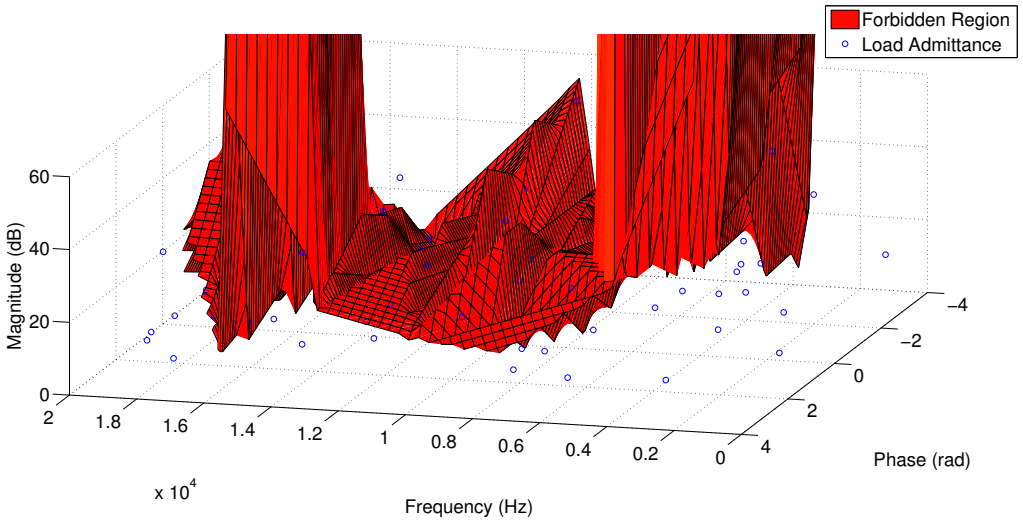

Figure 170: Architecture 1 inverter to motor connection stability (motor group 1) (qq)

6.5.2.2 Architecture 2 AC Stability

Some results of the AC stability study for architecture 2 are shown in Figures 171 through 173. (The remaining results can be found in Appendix A.) The results of the generator 3 to rectifier 3 stability (shown in Figures 171 through 173) show

that the connection is stable. Figure 171 shows that the load admittance points in the dd regime had a fairly constant magnitude. However, at high frequencies the forbidden region began to approach the load admittance values which shrunk the stability margin. Figure 172 demonstrates that the connection is stable in the dq regime, but has a small stability margin at frequencies near 8,000 Hz and 14,000 Hz. As shown in Figure 173, a large stability margin is available in the qq regime, except for around 15,000 Hz. The results show that the generator to rectifier connections are stable; however, stability margin is generally smaller at high frequencies.

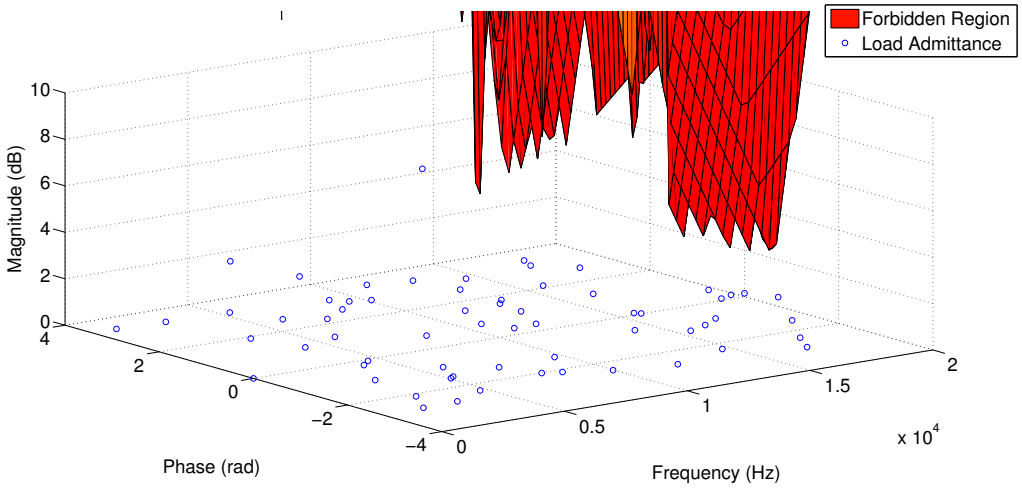

Figure 171: Architecture 2 generator 3 to rectifier 3 connection stability (dd)

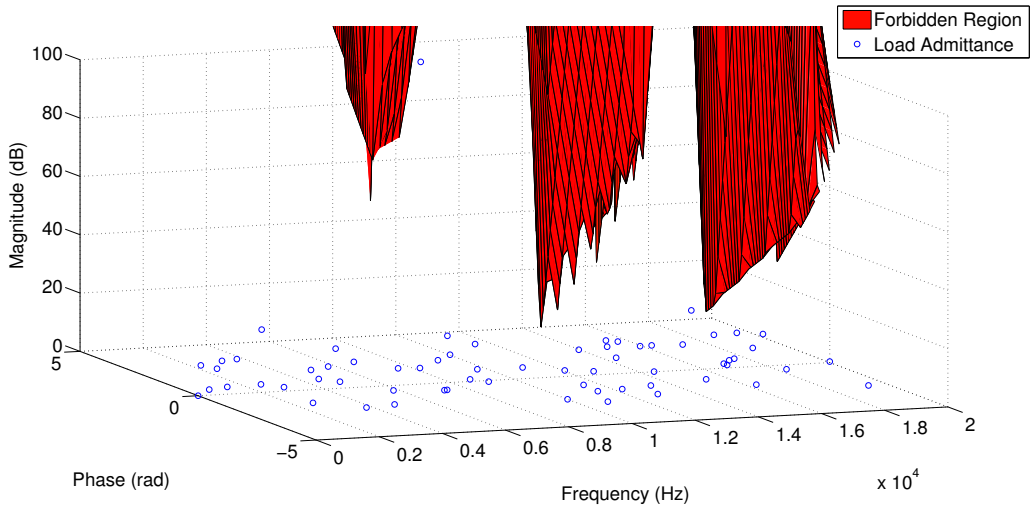

Figure 172: Architecture 2 generator 3 to rectifier 3 connection stability (dq)

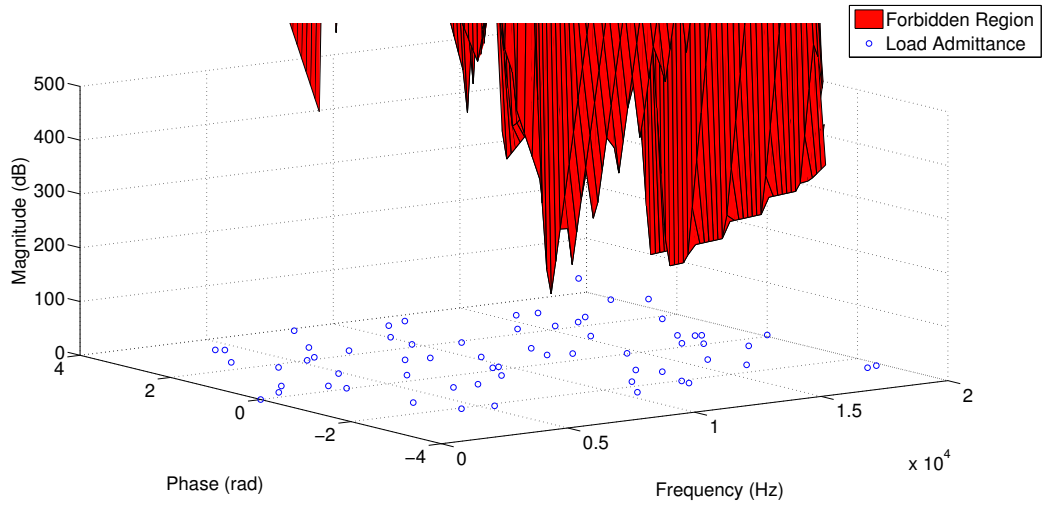

Figure 173: Architecture 2 generator 3 to rectifier 3 connection stability (qq)

The inverter to motor connection stability figures (Figures 174 through 176) show that the inverter to motor connection is stable as well. Compared to the architecture 1 inverter to motor connections, architecture 2 appears to be more stable. Figure 174 shows that the magnitudes of the load admittance values in the dd regime are mostly constant, and stability margin only has a small amount of fluctuation in the frequency spectrum that is examined. Figure 175 shows that the load admittance values in the

dq regime have a phase that is on either side of the forbidden region. Care must be taken to ensure that the forbidden region is not violated at frequencies between the frequencies measured. Lastly, Figure 176 demonstrates that the stability margin in the qq regime is low at frequencies around 1,000 Hz. Therefore, if a disturbance occurs at this frequency, the stability of the system may be compromised.

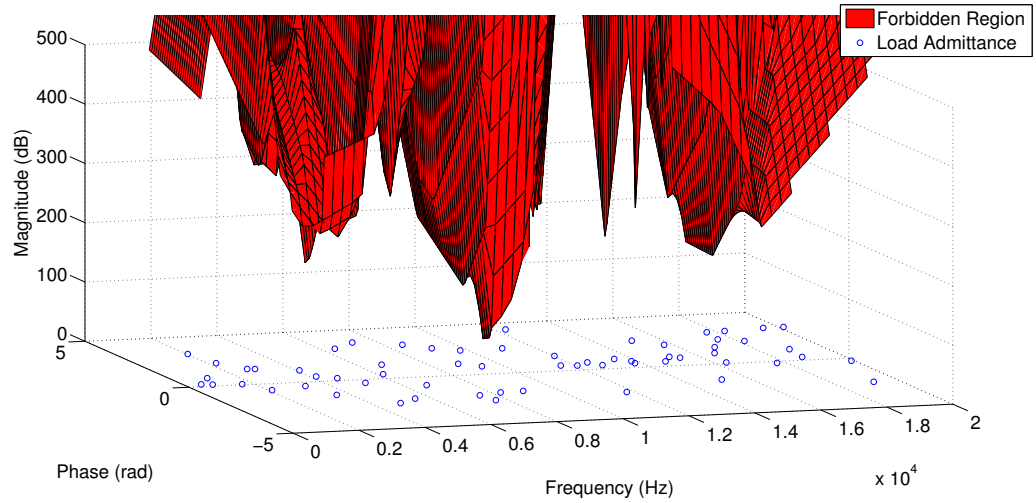

Figure 174: Architecture 2 inverter to motor connection stability (motor group)(dd)

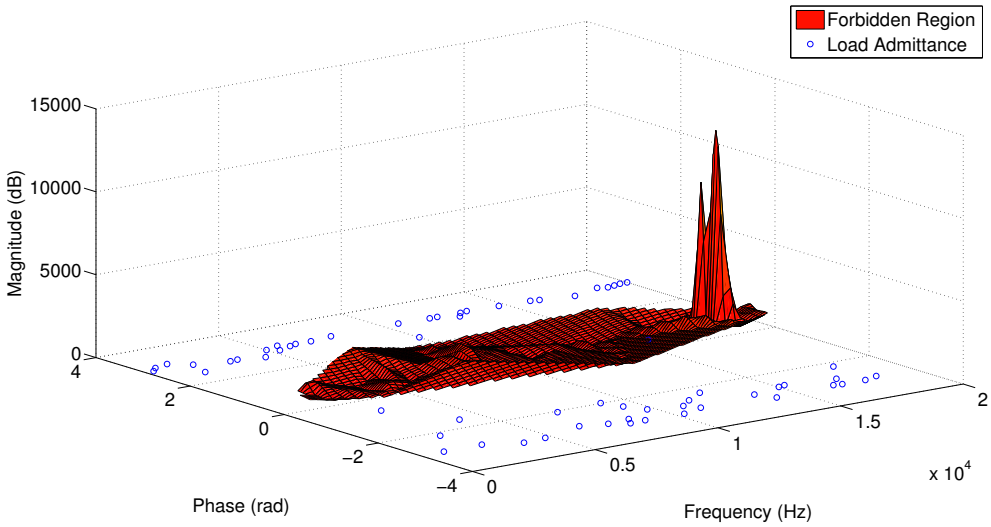

Figure 175: Architecture 2 inverter to motor connection stability (motor group)(dq)

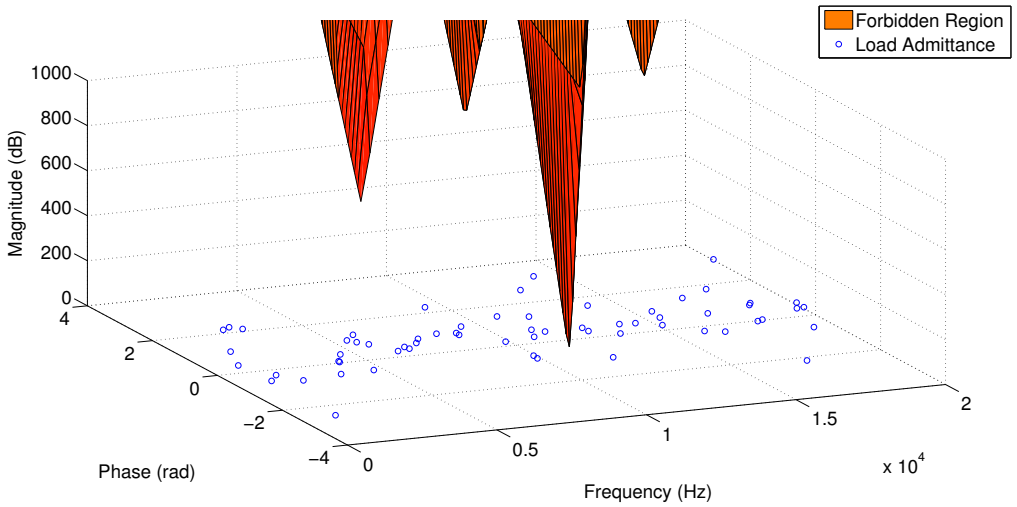

Figure 176: Architecture 2 inverter to motor connection stability (motor group)(qq)

6.5.2.3 Architecture 3 AC Stability

The results of the AC stability study for architecture 3 are shown in Figures 177 through 184. The plots for the generator to rectifier connection stability (Figures 177, 178, 179, and 180) show that the design is stable; however, the forbidden plane extends further down along the magnitude axis than other designs, bringing the forbidden region closer to the load admittance points. The plots show that at high frequencies only a small stability margin is available. Therefore, architecture 3 is a more risky design than the other two architectures. This most likely occurs because three rectifiers serve a single bus during an engine-out scenario with this architecture.

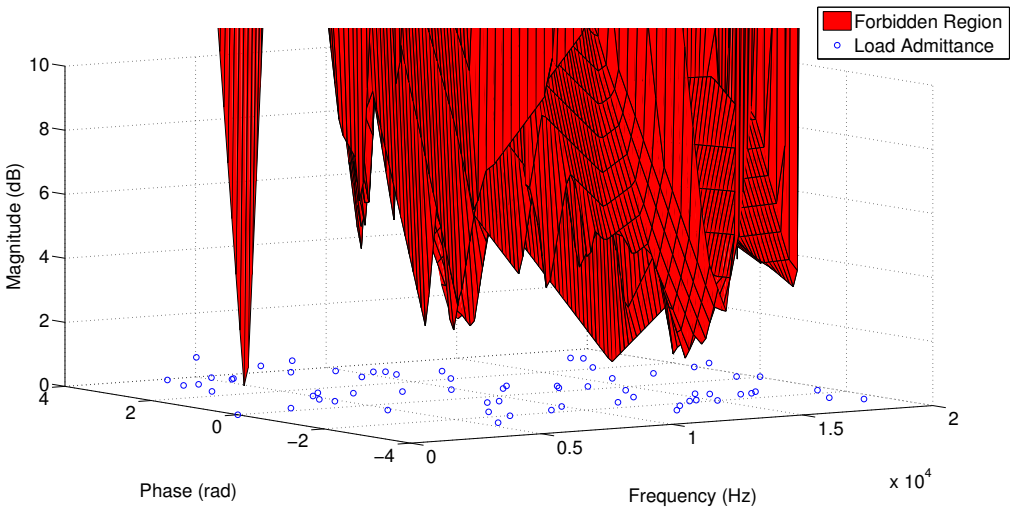

Figure 177: Architecture 3 generator 1 to rectifier 1 connection stability (dd)

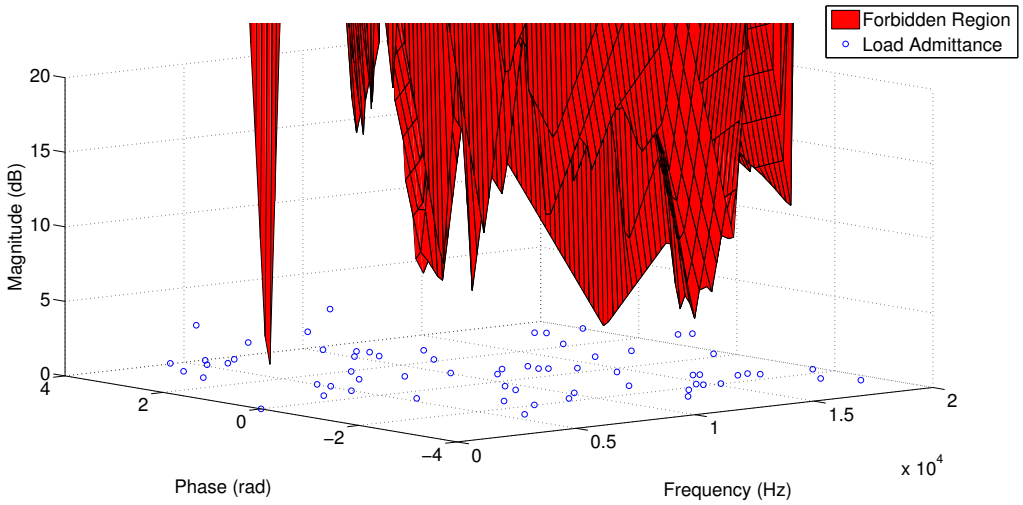

Figure 178: Architecture 3 generator 1 to rectifier 1 connection stability (dq)

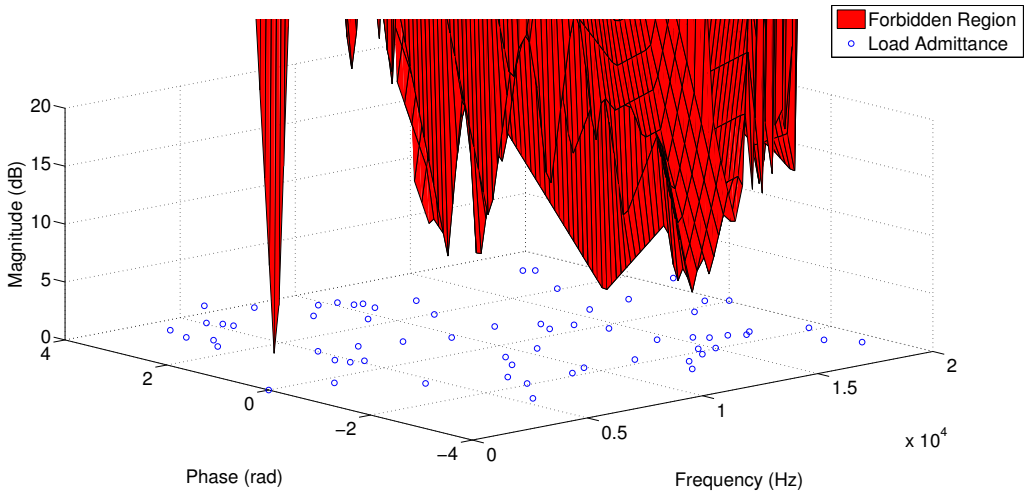

Figure 179: Architecture 3 generator 1 to rectifier 1 connection stability (qd)

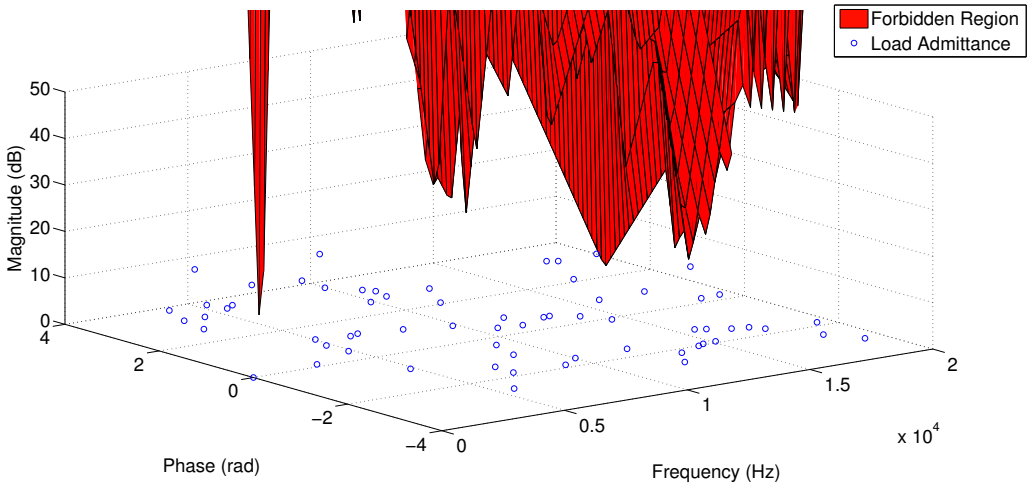

Figure 180: Architecture 3 generator 1 to rectifier 1 connection stability (qq)

The inverter to motor connection plots (Figures 181, 182, 183, and 184) again show that the forbidden plane is close to the load admittance values. This is especially true at low frequencies. Therefore, a low frequency disturbance in the system could move the system operating point to an unstable region.

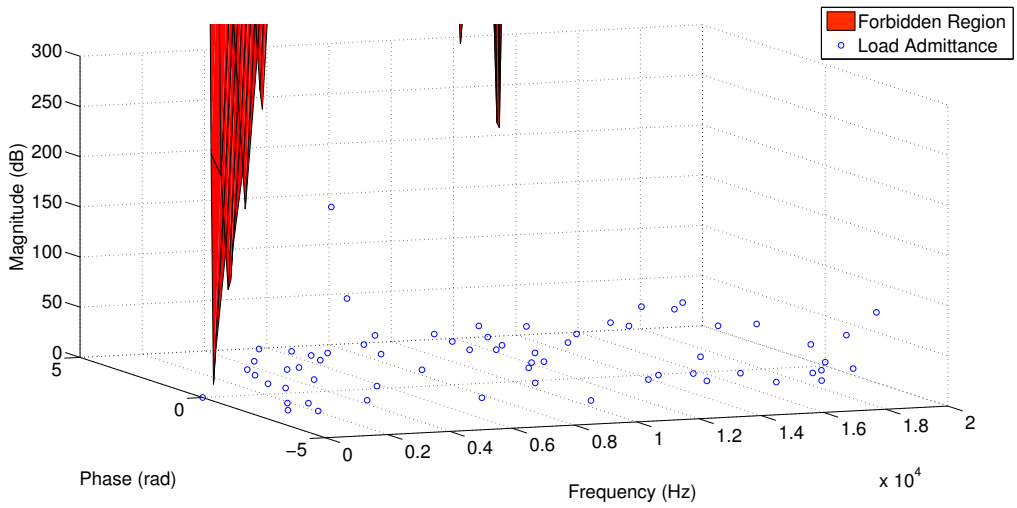

Figure 181: Architecture 3 inverter to motor connection stability (motor group 1) (dd)

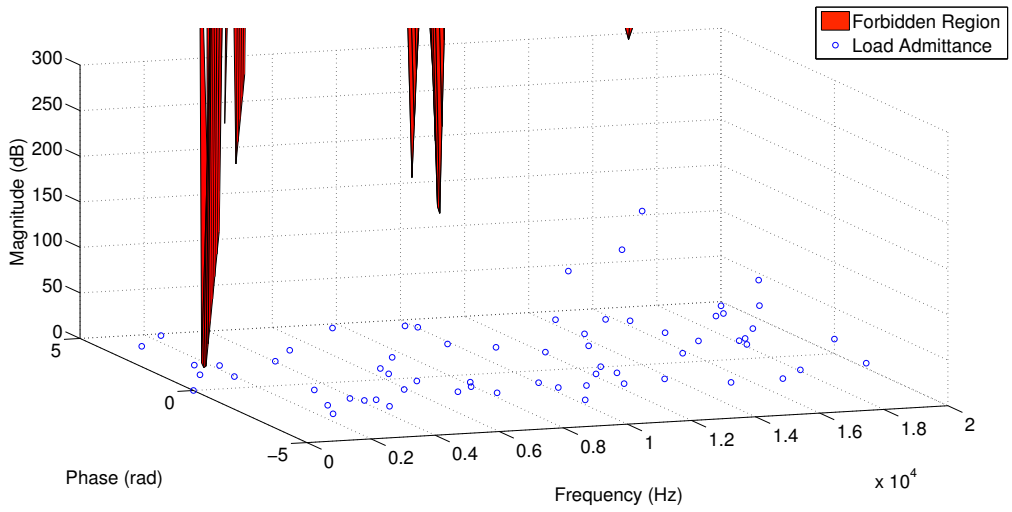

Figure 182: Architecture 3 inverter to motor connection stability (motor group 1) (dq)

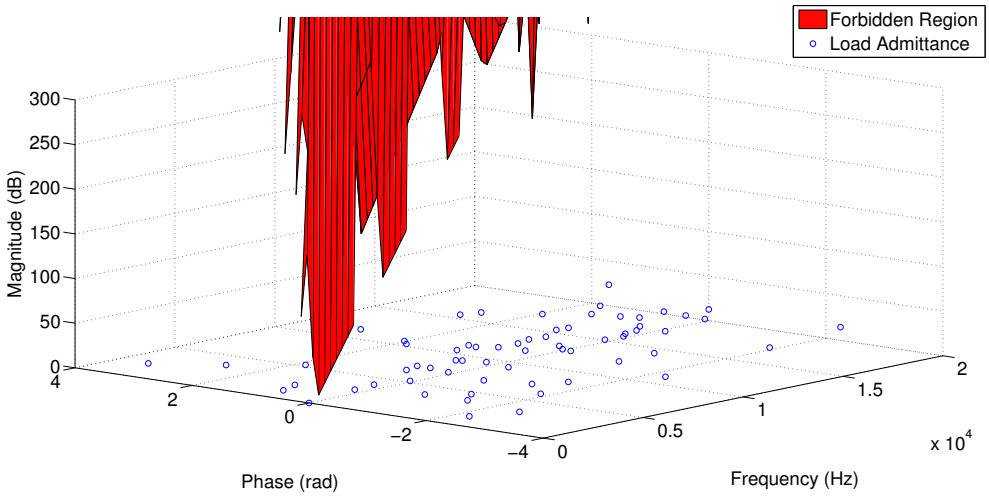

Figure 183: Architecture 3 inverter to motor connection stability (motor group 1) (qd)

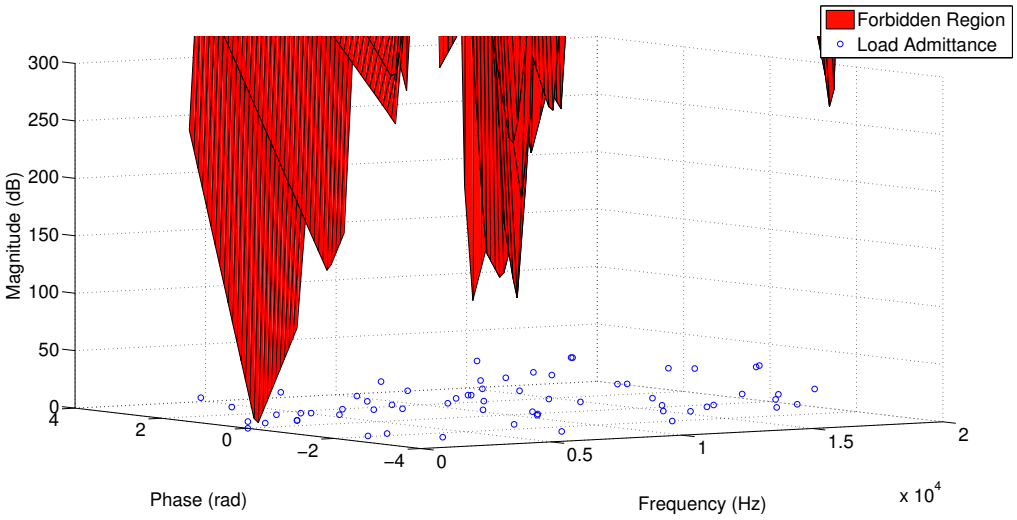

Figure 184: Architecture 3 inverter to motor connection stability (motor group 1) (qq)

6.5.3 Stability Analysis Observations

The stability analysis provided insight into the stability of the AC and DC connections in the system. The results showed that the designs are stable; however, some are more risky than others. In particular, the load admittance points for the architecture

3 during an engine failure were close to the forbidden plane which occurs because during the failure scenario, three rectifiers supply a single bus. For architectures 1 and 2, an engine-out scenario would not cause this scenario. In all situations, the maximum number of rectifiers that supply a bus is two, so the interaction effects between components are minimized. Based upon the outcome of the stability study, it is recommended that architecture 1 or 2 be selected.

6.6 Architecture Evaluation Observations

During the architecture evaluation step, a number of methods for evaluating system performance and stability were presented. The studies provided new insights into the feasibility and risk of each architecture that was being studied. The performance results showed that architectures that required multiple generator/rectifier combinations to feed a single bus cause some harmonic interference which means that the number of multiple sources on a bus should be minimized. The stability study also confirmed this notion. Since architecture 3 had multiple sources on a bus, the load admittance values were close to the forbidden region. Therefore, the architecture evaluation stage revealed that architecture 1 and architecture 2 had preferable attributes to architecture 3. The results of the performance models and stability models are factors that should be examined during the final architecture selection which is presented in the following chapter.

CHAPTER VII

ARCHITECTURE SELECTION AND CONCLUSIONS

Through this thesis a methodology for redundancy allocation for TeDP power system. In this chapter the information gathered from each step of the methodology will be reviewed. Next, a final system architecture will be selected. Following the architecture selection, the hypotheses that were postulated during the thesis will be discussed. Afterwards, the contributions of this thesis will be discussed. Lastly, future studies that could be performed based upon the work of this thesis will be postulated.

7.1 Methodology Review

The methodology that was developed was applied to architecting the power distribution system of the NASA N-3x turboelectric distributed propulsion system. An overview of the methodology is shown in Figure 185.

The first step of the methodology was to define the system requirements. The primary requirements considered in this study were system capacity and reliability. Under normal operating conditions, the system needed to deliver 40 MW of power from the generators to the motors, and the system is required to deliver 20 MW of power to the motors if an engine has failed. Also, the failure rate of the system over the lifetime of the aircraft cannot exceed one catastrophic failure per billion flight hours.

The next step of the methodology was to define the system objectives. Two objectives were discussed – minimizing weight and maximizing efficiency. For this preliminary study, efficiency was addressed through a weight penalty.

After the requirements and objectives were set, a baseline system was selected to determine whether current technologies and architectures could meet the system

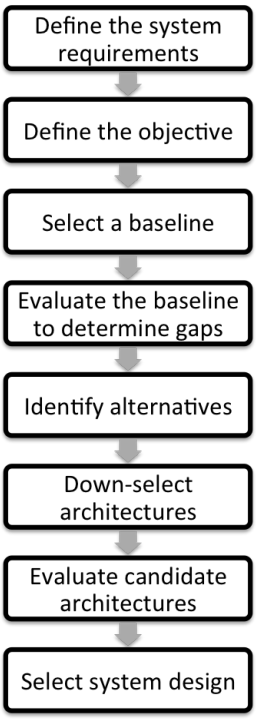

Figure 185: Methodology

requirements. The baseline was created after a literature search was performed on state-of-the-art power distribution architectures and technologies.

Once the baseline had been established, the next step was to evaluate the baseline to determine gaps between its performance and the system requirements and objectives. To accomplish this task a number of evaluation tools were created. The first model created determined the required capacity of every component in the system based upon the capacity requirement and engine-out scenario. The next model that was created sized all the components in the system based upon the capacities that were calculated by the previous model. Lastly, a model was built using stochastic flow networks to calculate system reliability.

The baseline model evaluation revealed that the reliability requirement could not be met with a reasonable weight using current technologies and architectures; therefore, the analysis proceeded to the next step of the methodology which was to identify alternatives. During this step, low TRL technologies that could offer the weight and

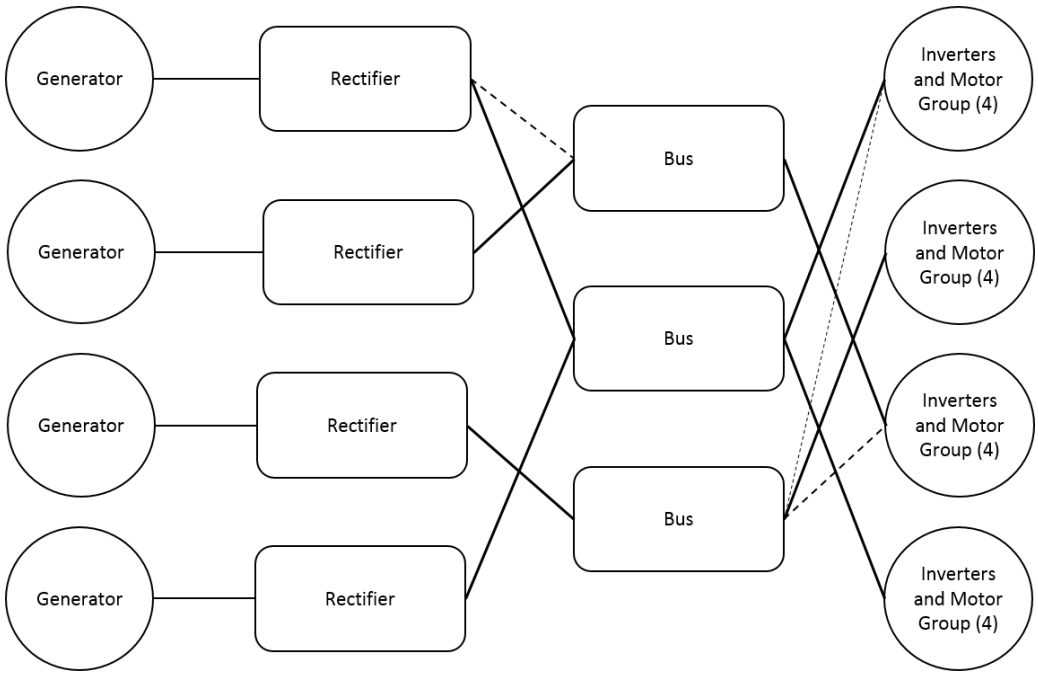

Figure 186: Architecture 1

reliability performance needed to reach a feasible architecture were explored.

The number of possible technology and architecture combinations was too large to evaluate each possibility individually, so the next step of the methodology, down-select architectures, commenced. In this step global optimization was used in order to locate architectures that meet the requirements and objectives. During this step, three candidate architectures were identified. The architectures that were selected are shown in Figures 186 through 188.

At this point, estimates for component weights and capacities, system weight, and system reliability for each architecture were available; however, more information about the performance and stability of each system was needed in order to make a final architecture selection. This led to the "evaluate candidate architectures" step of the methodology. During this step, dynamic models of each architecture were created and admittance space stability analysis was used to determine the stability of the systems. Now that each architecture has been evaluated, the final step of the methodology, "select system design", commences.

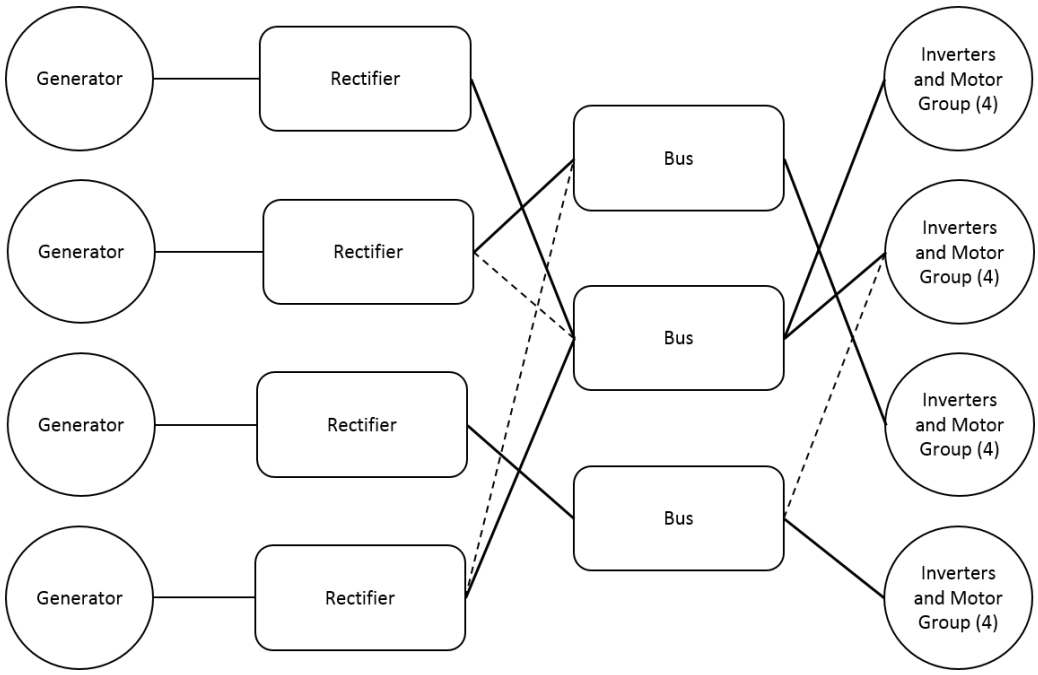

Figure 187: Architecture 2

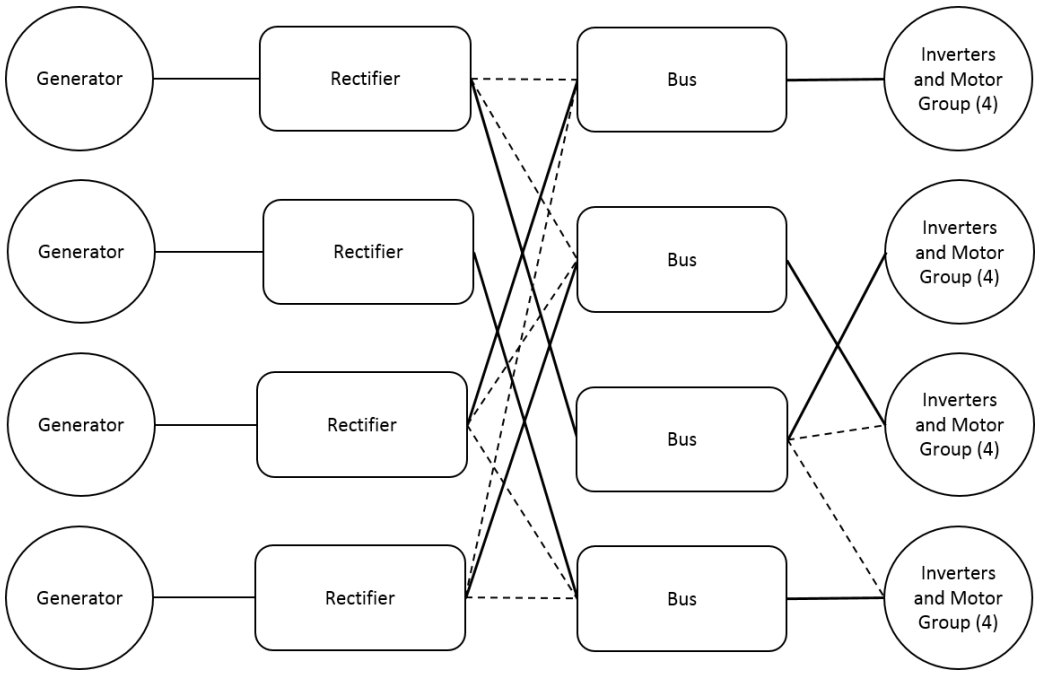

Figure 188: Architecture 3

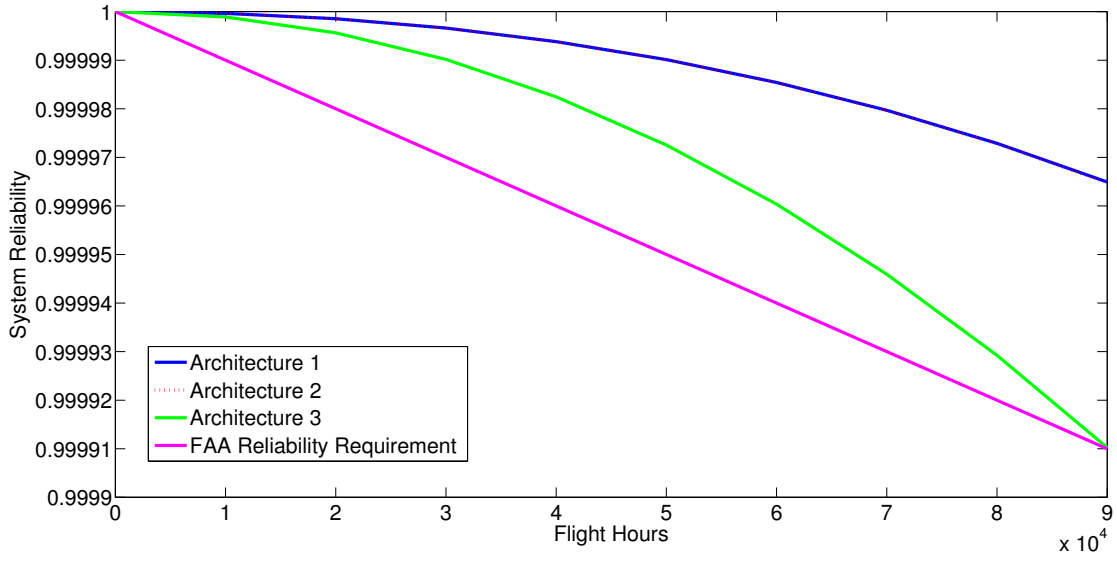

Figure 189: Architecture reliability

7.2 Selected Architecture

When selecting a final architecture, all the information that was gathered about each architecture should be considered including: system weight, reliability, dynamic performance, and stability. The analysis begins using information from the architecture selection step which showed that the system with the lightest weight was architecture 1 with a weight of 23,202 pounds. The weight of architecture 1 was about 500 pounds lighter than the next best option, architecture 2, at 23,703 pounds.

Another important factor is reliability. Figure 189 shows the reliability of each architecture option. The plots show that architecture 1 and architecture 2 have identical reliabilities and are more reliable than architecture 3.

Furthermore, the sensitivity of the system reliability to changes in component reliability should be considered. The sensitivity study was presented in the architecture selection chapter which found that architecture 3 was more robust to changes in component reliability than the other two architectures. Therefore, in this case, there is a trade-off between reliability robustness and reliability. Since architecture

1 and architecture 2 well exceeded the reliability requirement, they are superior to architecture 3 since some reliability could be lost while still meeting the reliability requirement.

The performance and stability studies also showed that architecture 1 and architecture 2 were the best options. Most performance and stability problems arose when multiple sources are used to supply a single bus. While this cannot be always avoided, architecture 3 had a bus that was supplied by three sources during an engine-out scenario, which caused the stability margin for architecture 3 to be small compared to the other two architectures.

Based upon on the factors that have been discussed, architecture 1 is the best option for the electric distribution system for the N3-X. First of all, it had the best weight out of all the options while still meeting the reliability requirement. Also, the performance and stability results showed that architecture 1 was as good as architecture 2 and better than architecture 3.

7.2.1 Detailed Design Considerations

Now that a system architecture has been chosen the next step is to perform detailed design which includes selecting designs for the components in the system. During the design process, estimates about the component designs were made for the analysis. For example, the motor parameters, such as stator resistance and inductance, were predicted. During the detailed design phase, exact settings for the component parameters will be determined. It is important to ensure that the architecture evaluation be performed again once the parameters have been set. This is especially true for designs that had small stability margins since small changes to a component could push the load admittance into the forbidden region.

Also, during the details design phase, component weight will be more accurately predicted. The updated component weights should be compared to the estimates used

during the architecture optimization phase to ensure that no major discrepancies have occurred. If the component weights have change drastically, the architecture selection should be revisited.

7.3 Hypotheses Review

The thesis consisted of three hypotheses. The first was regarding the performance of the baseline system. The hypothesis postulated was:

Hypothesis 1: The amount of redundancy required to meet the reliability requirement will result in an unacceptable system weight if current technologies are used.

The hypothesis was tested by building the capacity, weight, and reliability analysis tools to evaluate a baseline architecture. The first test showed that the weight of the architecture was large and missed the reliability requirement by a large amount. A sensitivity study revealed that the reliability of the system was largely dependent of the reliability of the motors. In an attempt to meet the requirement, the motors were resized so that the aircraft could function if half the motors had failed. The weight of the system was greatly increased by this change, and, while system reliability was greatly improved, it still fell short of the reliability requirement. Thus, Hypothesis 1 was confirmed.

The second hypothesis stated the expected attributes of a system that would meet the system requirements and objectives. The hypothesis was:

Hypothesis 2: To meet the system design criteria the system must be comprised of superconducting technologies and must have a double redundant system (meaning that every motor can be supplied by either engine).

Hypothesis 2 was nullified based upon the results of the architecture selection. In fact, the hypothesis was overly conservative. During the baseline study, the sensitivity analysis revealed that the motors were the most critical point in the architecture; therefore, a new design variable was created that changed the sizing of the motors so that the aircraft could function on less than the total number of motors. The architecture found that rather than every motor needing power under an engine-out scenario, only the number of motors dictated by the design variable that set motor sizing needed power; therefore, architecture 1, the selected architecture, meets the reliability requirement since 12 motors are supplied power under either engine-out scenario.

The final hypothesis addressed the expected performance of the optimization methods that were tested. Hypothesis 3 was:

Hypothesis 3: Particle swarm can find architecture and technology combinations that meet the turboelectric PDS requirements with minimal iterations in comparison with other zero-order methods.

Hypothesis 3 was tested by using three different global optimization methods for the design problem. In all cases, the same objective and constraint functions were used. The results showed that genetic algorithm optimization performance was superior to the particle swarm or ant colony optimization; thus, hypothesis 3 is nullified. While it was true that particle swarm converged faster than the genetic algorithm, it converged before reaching the optimal design space after every test. The reason that genetic algorithm was able to outperform the other methods was that it had better coverage of the design space. For this design problem the design space contained many discontinuities causing the particle swarm and ant colony methods to converge on local minimums.

7.4 Contributions

To develop the methodology a number of advancements were made regarding power system architecting and architecture evaluation. The contributions range from the framework of the methodology to the system evaluation tools that were created.

7.4.1 Methodology Framework

The primary contribution made by this thesis is the development of the methodology. The methodology provides a series of steps to follow to address redundancy allocation during power system architecting. Furthermore, recommendations for best practices for each steps were provided. The methodology was demonstrated by architecting the electrical distribution system of the NASA N-3x; however, the general methodology can be applied to an array of power system design problems that require multiple sources and loads.

7.4.2 Capacity Evaluation Method

To assess the baseline architecture, a number of system evaluation tools were created including the component capacity evaluation method. The method that was presented provides the user with the capability to rapidly determine required capacities for any component in the system architecture. While it was applied to the turboelectric design problem, it could easily be applied to any power distribution network that can represented by an adjacency matrix.

7.4.3 Cable Sizing Approach

Another tool that was created to evaluate the architectures was the cable sizing model. Two models were developed (a room temperature cable model and a superconducting model) which are easy to implement and rapidly provide weight estimates for the cables. The models created are able to size either type of cable using cable length, voltage, and material properties. The results of the models demonstrated the effect

of voltage on cable size. They also can help determine the thermal management requirements for either cable.

7.4.4 Power System Reliability Calculation Method

Another important tool that was developed was the approach to calculating system reliability. An essential step in the tool development was defining survival functions for each component in the system. For the superconducting system, this was difficult due to the long lifetime of superconductors and lack of published data. However, research revealed that the component most likely to fail in the system is the cryocooler; therefore, component reliabilities were linked to the estimated reliability of the cryocooler.

Next, stochastic flow network analysis, a concept from the communication and computer engineering fields, was adapted for the power distribution design problem. This allows for a multi-state reliability analysis of the multiple source and multiple sink system. The method that was presented would work for a variety aircraft power distribution problems.

7.4.5 Architecture Optimization Strategy

Since there were too many architecture and technology combinations to evaluate, an architecture down-selection method was created which relies on global optimization to locate candidate architectures. A variety of global optimization methods were tested for the problem to determine if a certain methodology was best suited for this type of design problem. One of the methods used was ant colony optimization which is typically used for single source and single sink problems, so a modified version of the algorithm was created for the multiple source and multiple sink problem.

After testing all the algorithms, it was found that genetic algorithm was the best method for the power distribution problem. The primary reason this occurred was that the design space contained many discontinuities and the genetic algorithm had

the best coverage of the design space.

7.4.6 Architecture Insights

The final contribution of the thesis is the insights that it provided into the design of the turboelectric power distribution system. The analysis showed that the system was best suited for a three-bus architecture with 16 motors. Adding a fourth bus to the architecture adds additional weight with little reliability benefit. On the other hand, since the motors were found to be the most critical point in the system, motor redundancy led to a higher overall system reliability. In other words, the lightest architectures have a greater number of small motors rather than fewer larger motors.

The performance and stability showed that architectures that minimized the number of buses with multiple sources had the best dynamic response. If a three-bus architecture is used, at least one bus will have multiple sources; therefore, controller design will be important to ensure that the connections remain stable.

7.5 Future Studies

While the methodology presented has made a number of contributions to power system architecting, some improvements could be made in the future. Each change will increase the complexity of the analysis, but will provide further insight into the performance of the system being designed.

7.5.1 Superconducting Component Reliability

The failure rates of superconducting components is fairly uncertain due to lack of data. In the future, as more superconducting components have been tested, a more accurate reliability estimate will be available. Also, the reliability of crycoolers will most likely improve when cryocoolers are developed for this application. Most cryocoolers are for ground-based applications where reliability is not a huge concern. When developed for aerospace applications, more emphasis will be placed on reliability during design;

thus, the failure rates will most likely decrease.

7.5.2 Shock Modeling

In the reliability analysis that was performed, simple exponential distributions with estimated failure rates were used to define component survival functions. While this serves as an acceptable estimate for a first-cut analysis, to truly capture reliability some changes must be made.

Perhaps the most important change to the reliability analysis is to include shock modeling. Shock modeling is used to model the degradation of the components over time. Under certain conditions a component will undergo a 'shock' which is a condition that stresses the component. An example would be fault that causes current to rapidly rise on the bus. The rapid rise in current will cause degradation to the cable, thus decreasing its expected lifetime. Shock modeling is able to capture the effect of the degradation and appropriately update the survival function of the component, thus providing a better estimate of the reliability of the system over time.

7.5.3 Protection Components

The components that were considered in the analysis presented in this thesis were generators, rectifiers, buses, inverters, and motors. In reality the system will require several other components. One category of components that will be needed is protection components, such as circuit breakers and fault current limiters. The methodology could be expanded to include these components, but the time needed for analysis would greatly increase. Also, if shock modeling is used, the placement of the protection components would be important for the reliability analysis. The protection components would reduce the amount of stress on a component during a 'shock' so that the degradation of the component is minimized.

7.5.4 Multi-state Analysis

The reliability analysis that was presented relied on stochastic flow networks which enables multi-state analysis. To decrease run time for the optimization, the analysis used for the thesis used a binary (on or off) approach to the flow capacity of each component to decrease run time for the optimization. The analysis could be expanded to multiple flow states for each component. In order to apply this change, a distribution for the probability of the flow state for each component would need to be specified. Also, the optimization run time would be increased.

7.5.5 Large Signal Stability

The stability analysis that was presented only addressed small signal stability analysis. Eventually, the architecture selected should undergo large signal stability analysis. Large signal stability analysis is used to define a stable operating range for the system. Two primary methods exist for large signal stability analysis: Lyapunov methods and bifurcations analysis [115] [69] [149]. Lyapunov methods can be used in conjunction with an optimization method, such as a GA, to define a region of asymptotic stability (RAS) [86] [127]. If the system encounters a disturbance that remains within the bounds of the RAS, the system will return to equilibrium. Bifurcation analysis is used to identify operating points in the system where a small change to the parameters of the system causes a sudden "qualitative" change in the system behavior [69].

7.5.6 Uncertainty

Since the system was designed is in the conceptual design phase, there is uncertainty in the component efficiencies, power-to-weight ratios, and failure rates. Uncertainty analysis could be incorporated into the methodology to address this problem. Using uncertainty analysis would allow the user to determine which architectures are robust to the variability in the variables that were listed. If a robust architecture is chosen, it is less likely that costly design changes would have to be made during later stages

of the system design.

7.6 Final Thoughts

The methodology that was formulated in this thesis has provided a method for rapidly evaluating and locating architecting designs that meet power system capacity and reliability requirements. The capabilities that were developed will be useful as the electrical load demands on aircraft increase and power distribution designs change. The analysis has shown that redundancy allocation is an important factor that must be addressed during the system architecting phase. If the system does not contain the correct amount of redundancy, the reliability gap may not be closed by component changes. By addressing redundancy allocation in this phase of design, a balance between system reliability and weight can be found.

APPENDIX A

AC STABILITY RESULTS

The results of the AC stability analysis for each architecture are shown in this appendix. As discussed in the stability section of the thesis, the AC stability results for each connection will have four plots (dd, dq, qd, and qq regimes). For each architecture, generator to rectifier connections and inverter to motor connections were studied. In general, the results show that the designs are stable. However, the results do show that connections where multiple sources are feeding a single load the stability margin is much smaller than cases that have a single source and single load.

The figures also show that stability margins are smaller for generator to rectifier connections versus inverter to motor connections. However, there was much more variation in load admittance values for the inverter to motor connections. The large variation in load admittance values could lead to instability problems at frequencies between the measured values. Therefore, once a final design is selected, large signal stability analysis should be performed to define the operational limits of the system.

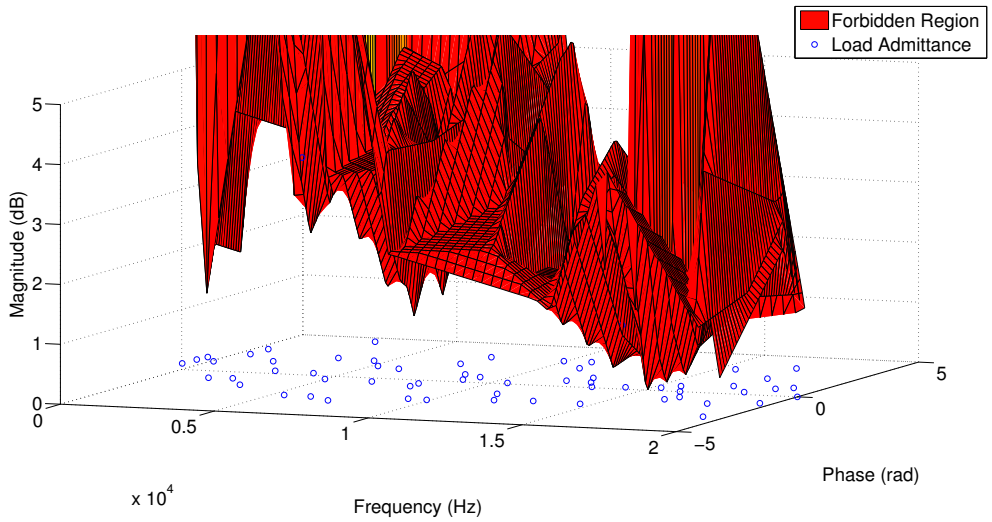

Figure 190: Architecture 1 generator 1 to rectifier 1 connection stability (dd)

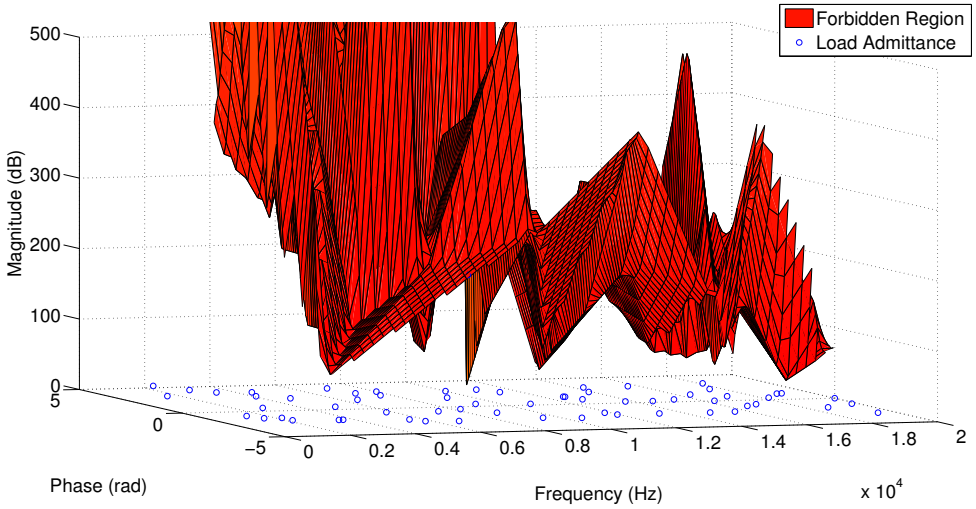

Figure 191: Architecture 1 generator 1 to rectifier 1 connection stability (dq)

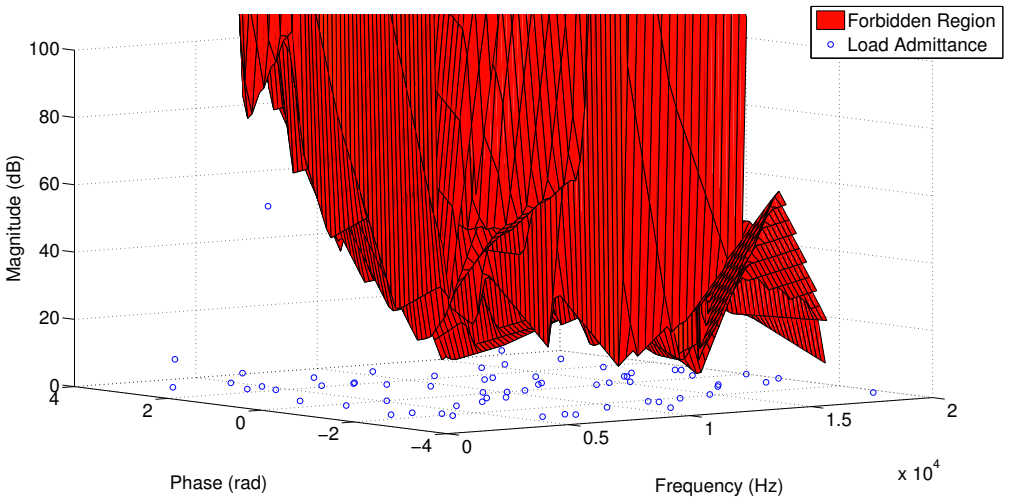

Figure 192: Architecture 1 generator 1 to rectifier 1 connection stability (qd)

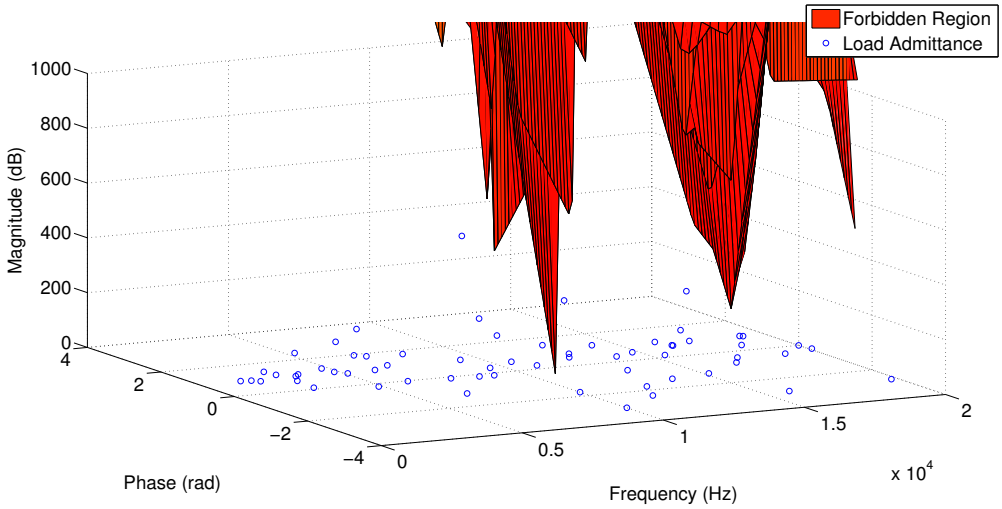

Figure 193: Architecture 1 generator 1 to rectifier 1 connection stability (qq)

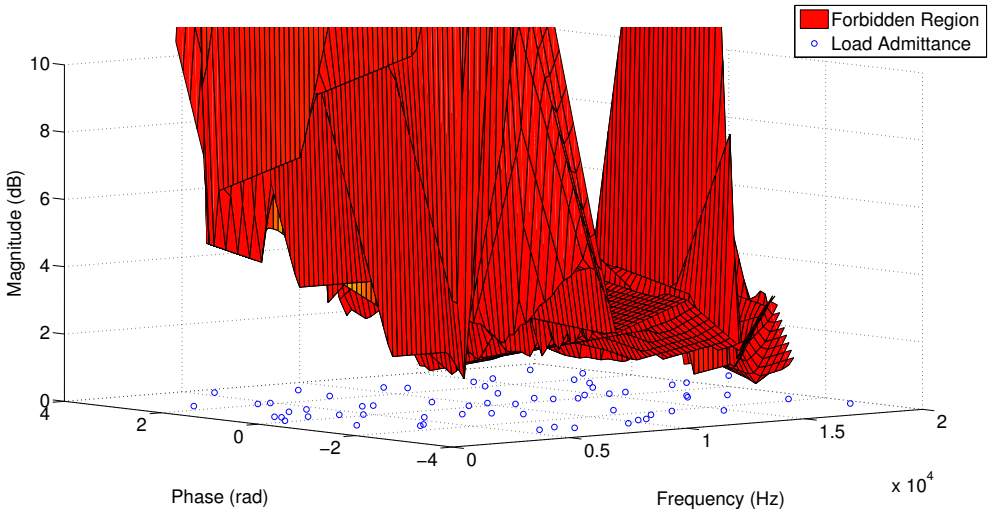

Figure 194: Architecture 1 generator 2 to rectifier 2 connection stability (dd)

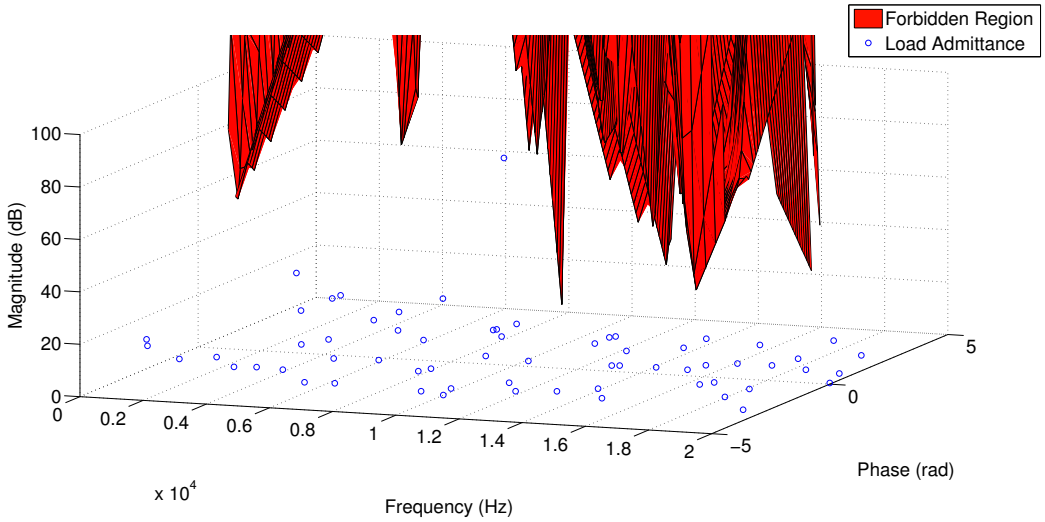

Figure 195: Architecture 1 generator 2 to rectifier 2 connection stability (dq)

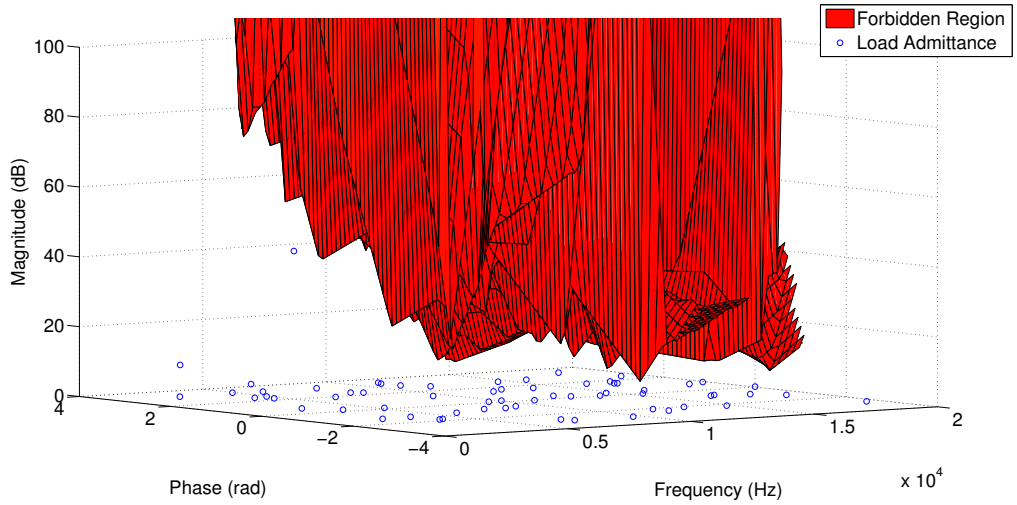

Figure 196: Architecture 1 generator 2 to rectifier 2 connection stability (qd)

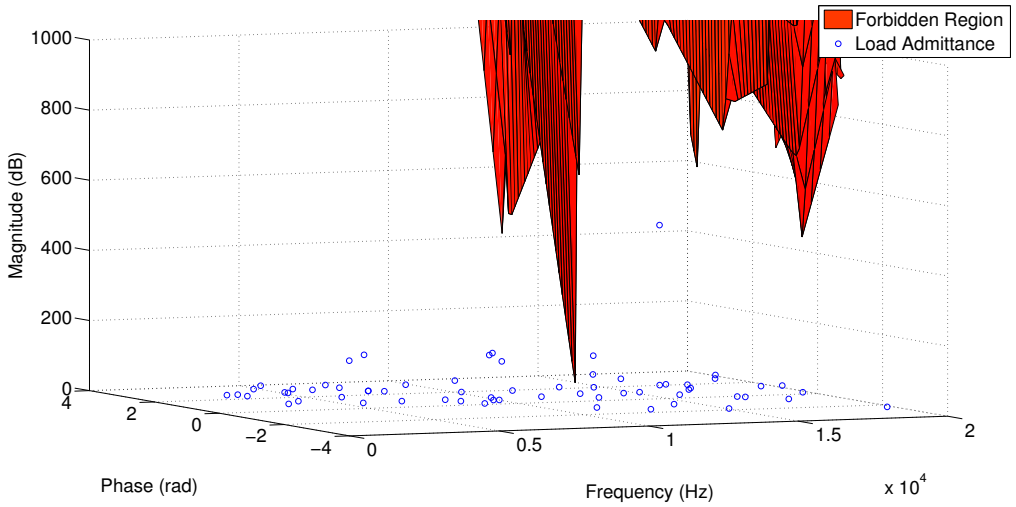

Figure 197: Architecture 1 generator 2 to rectifier 2 connection stability (qq)

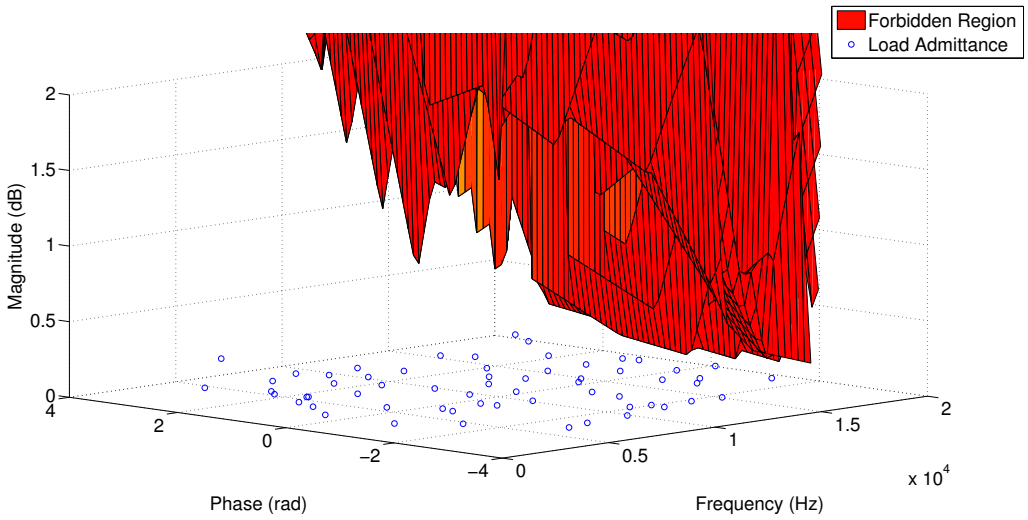

Figure 198: Architecture 1 generator 4 to rectifier 4 connection stability (dd)

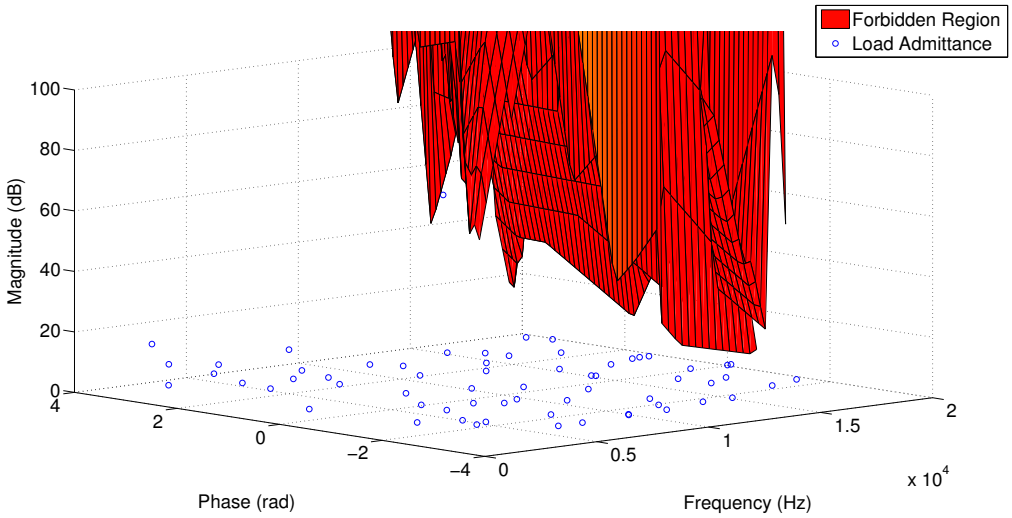

Figure 199: Architecture 1 generator 4 to rectifier 4 connection stability (dq)

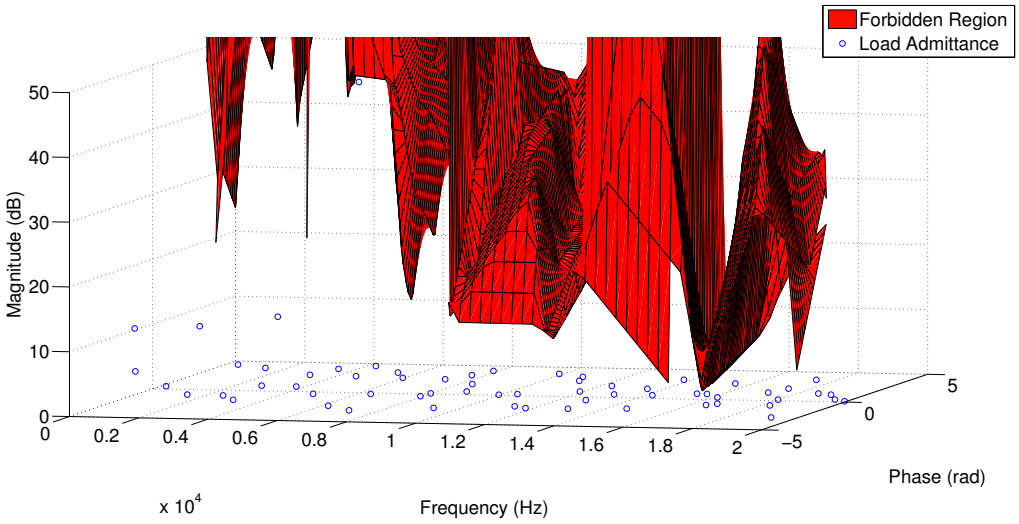

Figure 200: Architecture 1 generator 4 to rectifier 4 connection stability (qd)

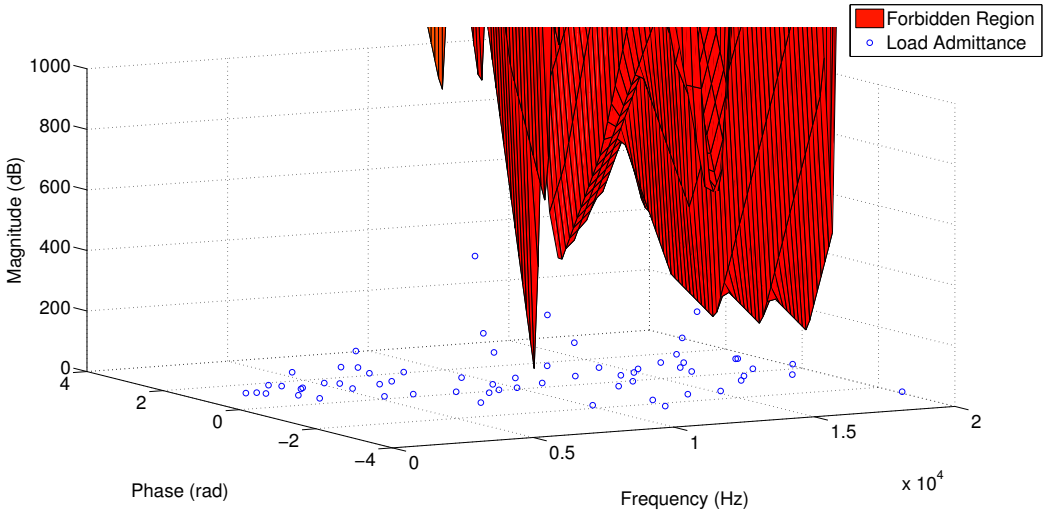

Figure 201: Architecture 1 generator 4 to rectifier 4 connection stability (qq)

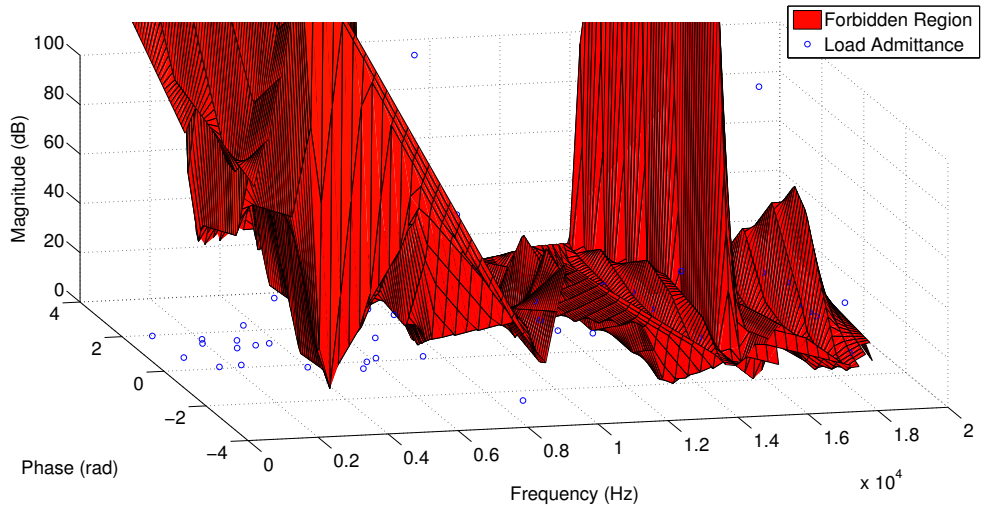

Figure 202: Architecture 1 inverter to motor connection stability (motor group 1) (dd)

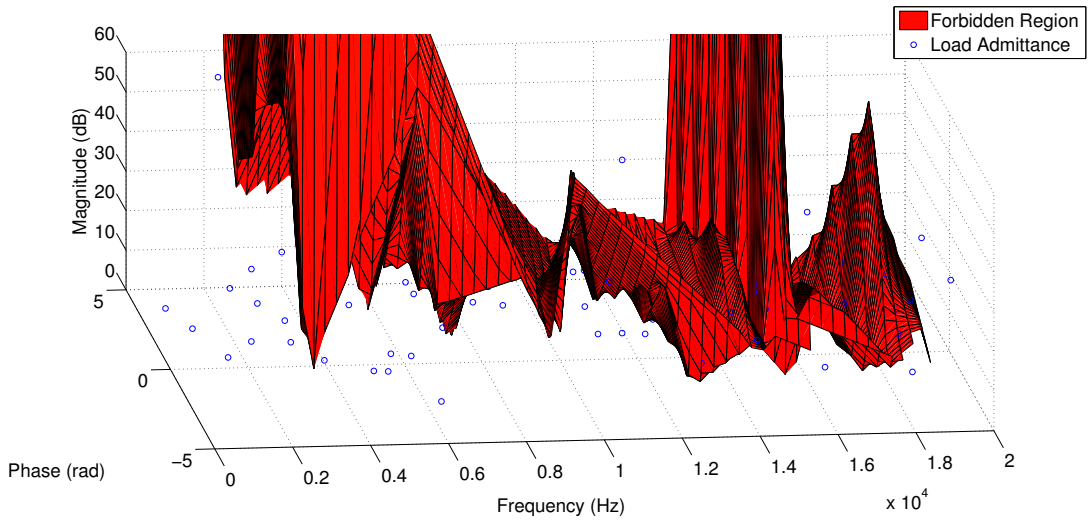

Figure 203: Architecture 1 inverter to motor connection stability (motor group 1) (dq)

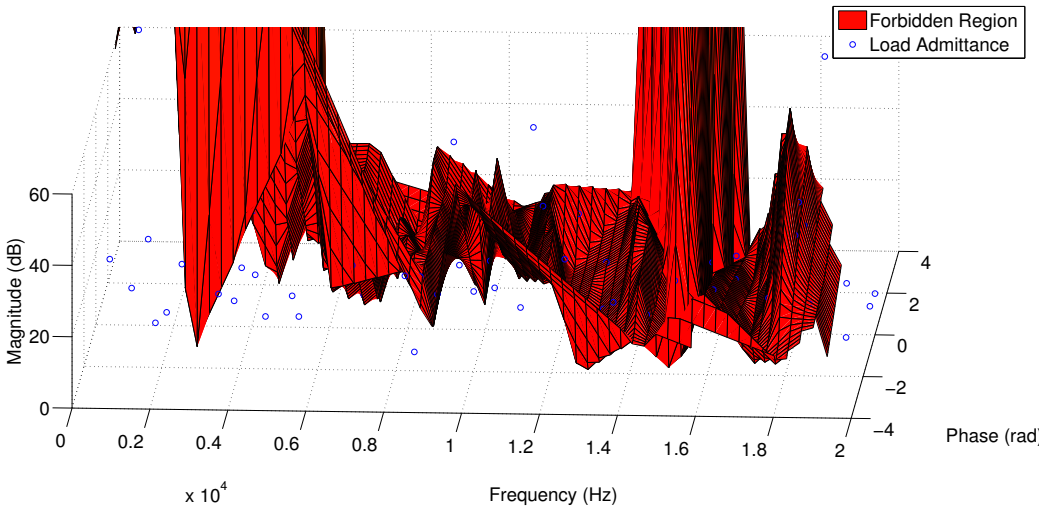

Figure 204: Architecture 1 inverter to motor connection stability (motor group 1) (qd)

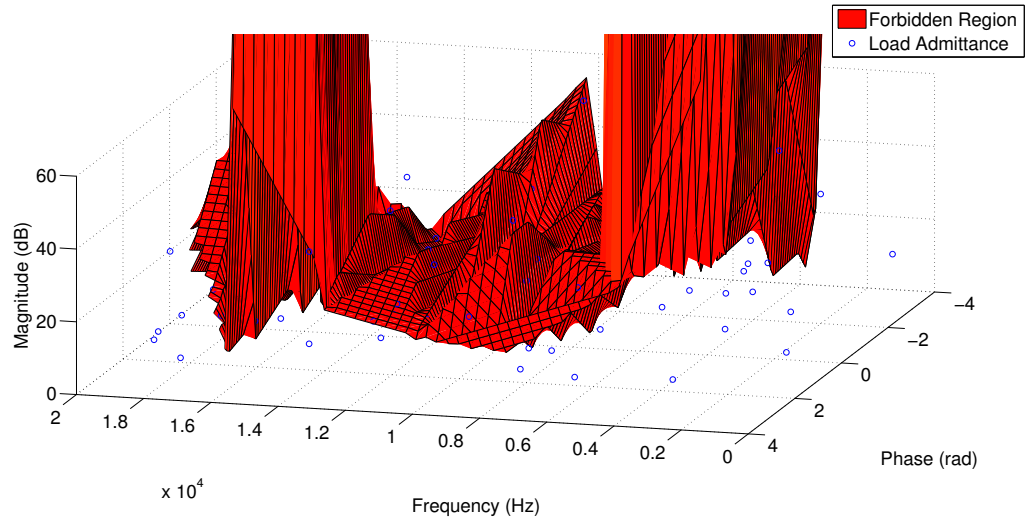

Figure 205: Architecture 1 inverter to motor connection stability (motor group 1) (qq)

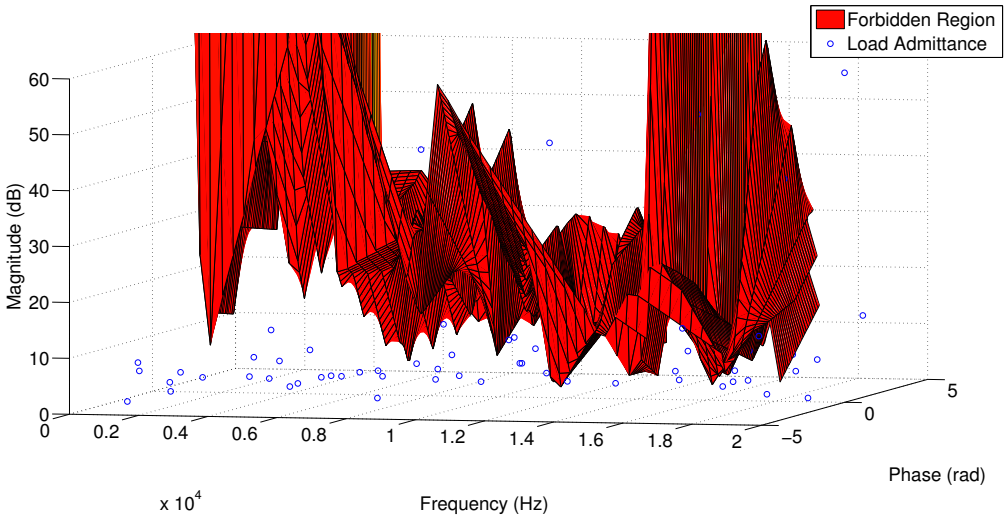

Figure 206: Architecture 1 inverter to motor connection stability (motor group 2) (dd)

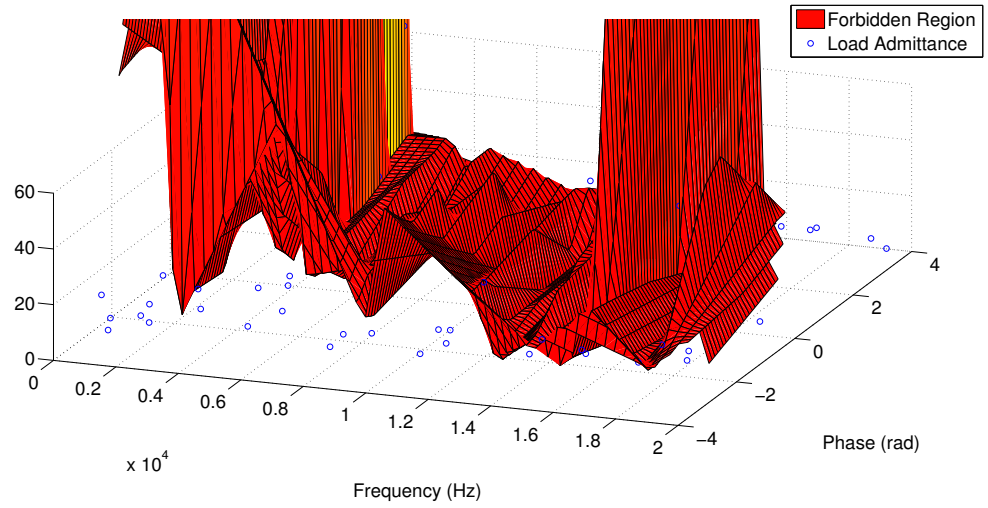

Figure 207: Architecture 1 inverter to motor connection stability (motor group 2) (dq)

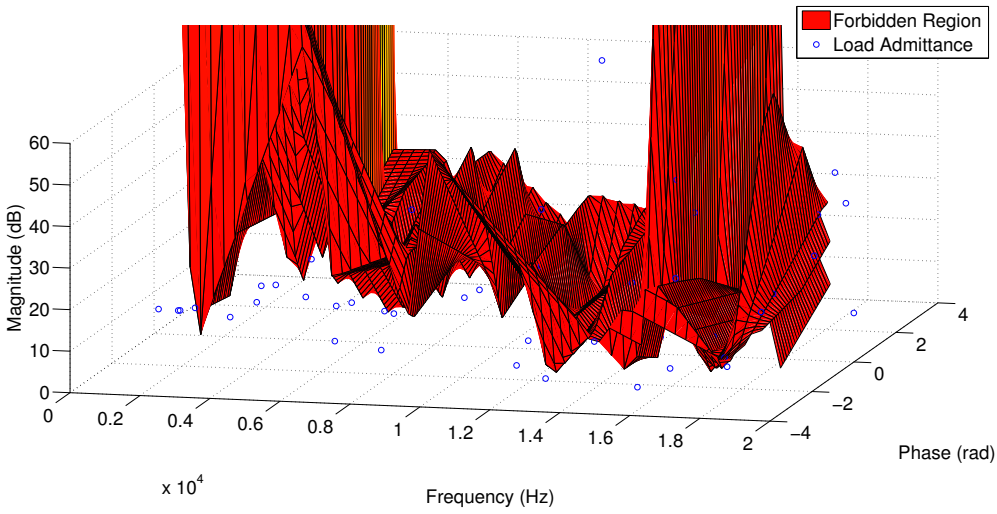

Figure 208: Architecture 1 inverter to motor connection stability (motor group 2) (qd)

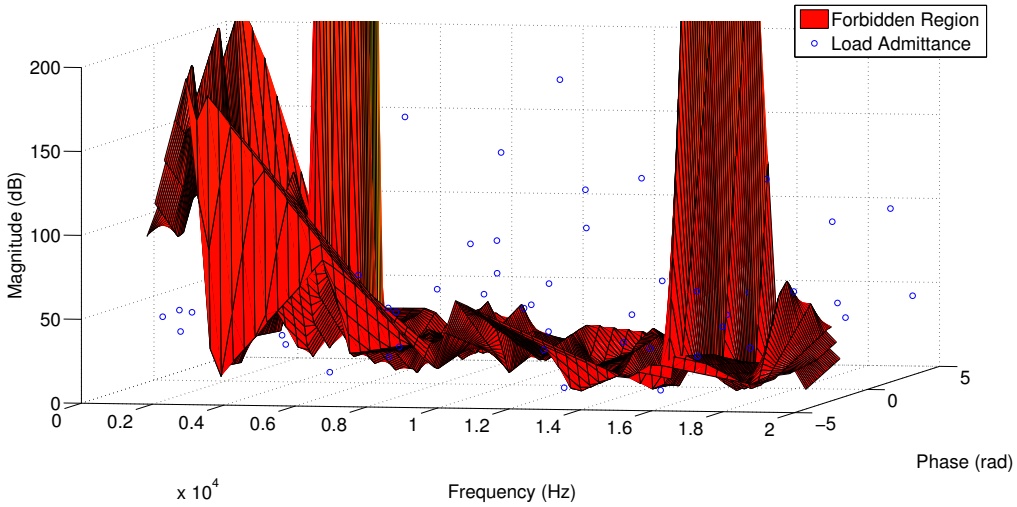

Figure 209: Architecture 1 inverter to motor connection stability (motor group 2) (qq)

A.1 Architecture 2

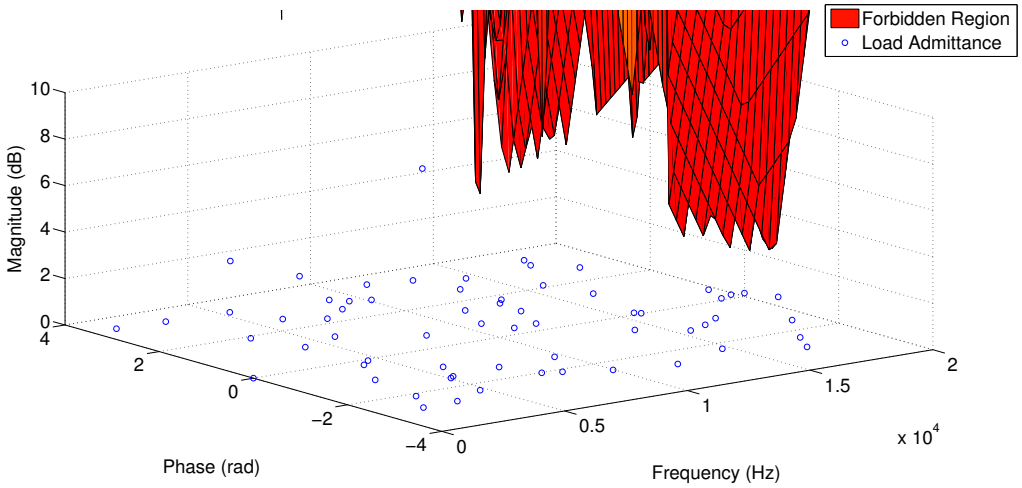

Figure 210: Architecture 2 generator 3 to rectifier 3 connection stability (dd)

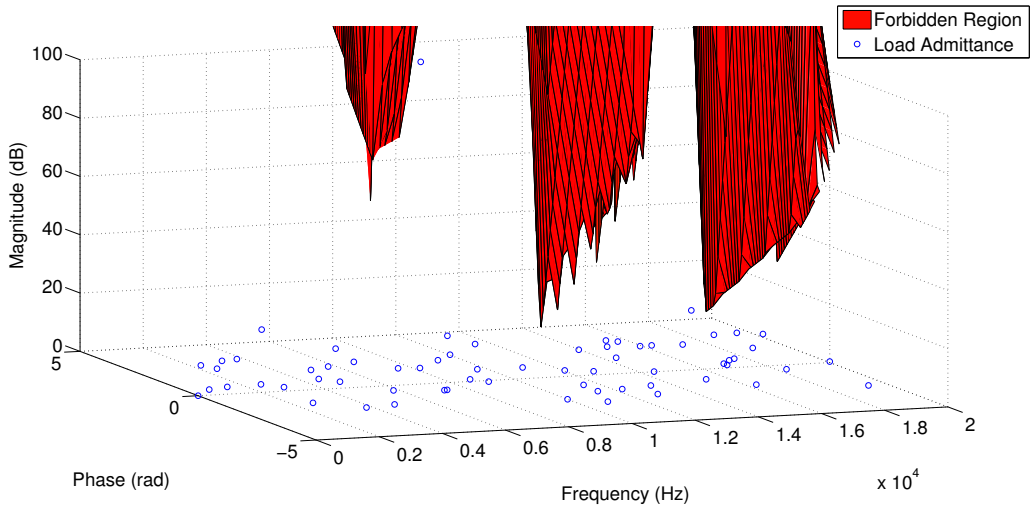

Figure 211: Architecture 2 generator 3 to rectifier 3 connection stability (dq)

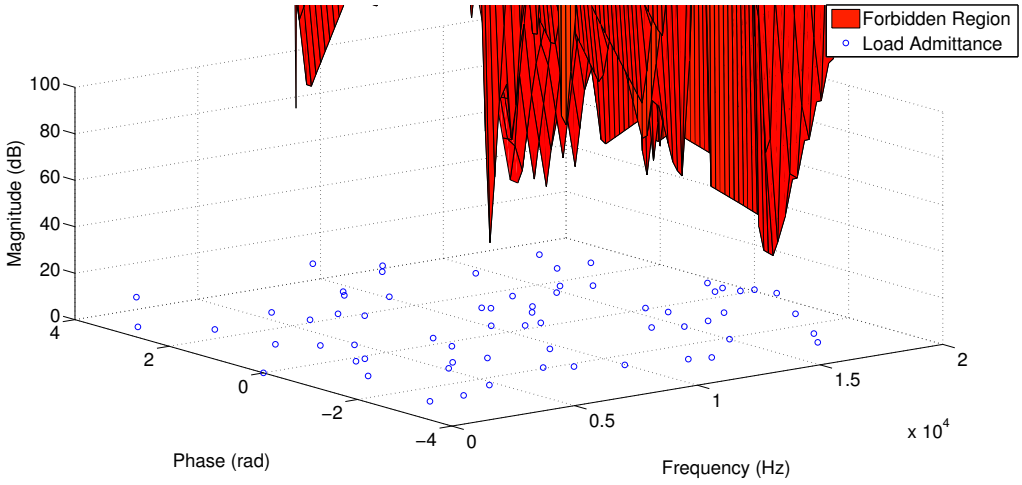

Figure 212: Architecture 2 generator 3 to rectifier 3 connection stability (qd)

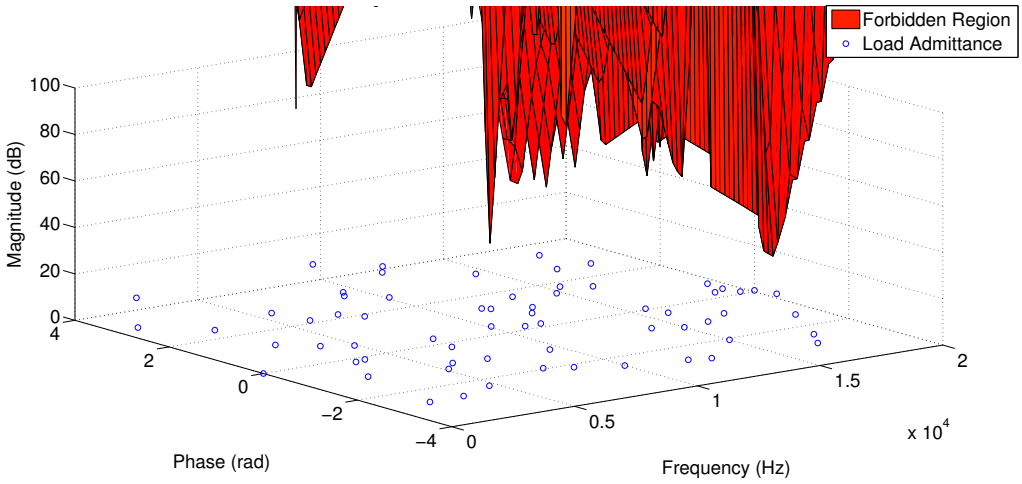

Figure 213: Architecture 2 generator 3 to rectifier 3 connection stability (qd)

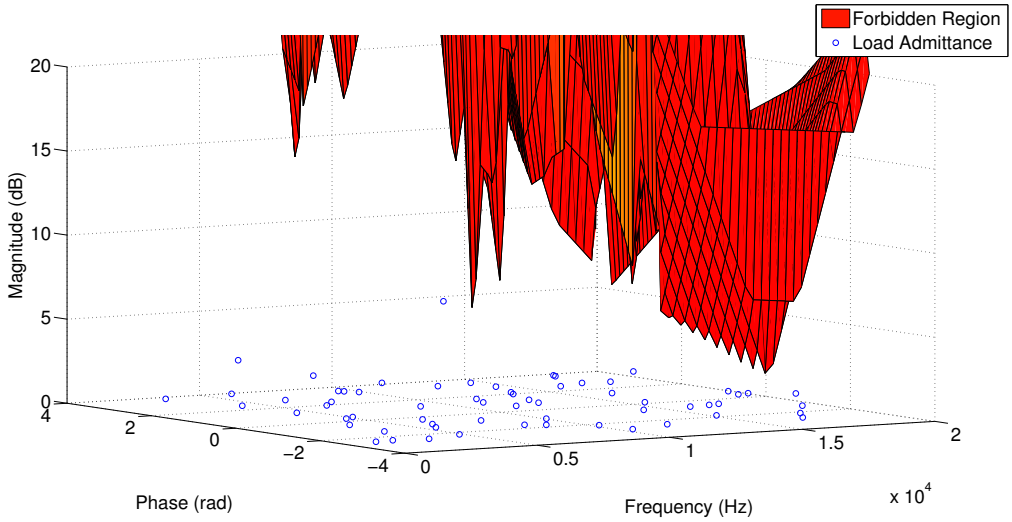

Figure 214: Architecture 2 generator 4 to rectifier 4 connection stability (dd)

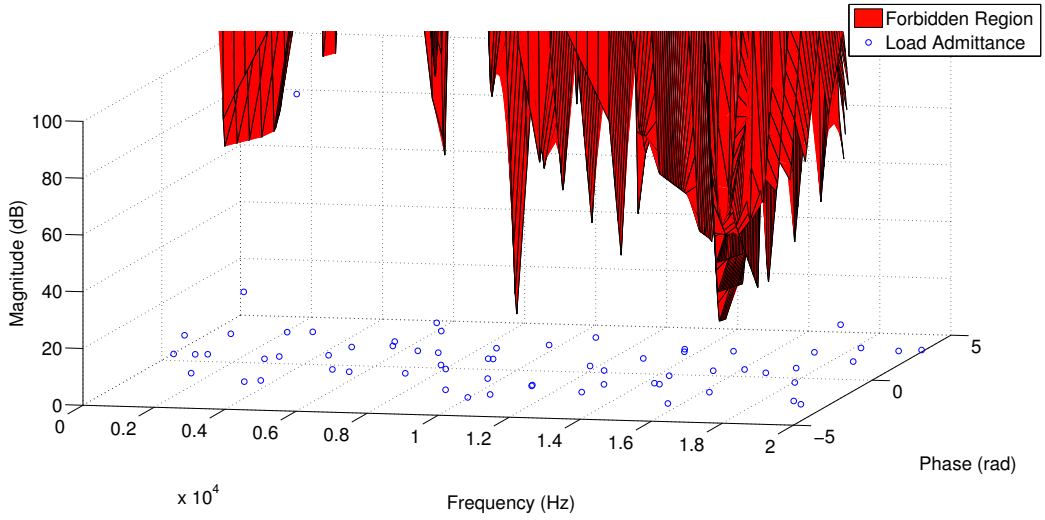

Figure 215: Architecture 2 generator 4 to rectifier 4 connection stability (dq)

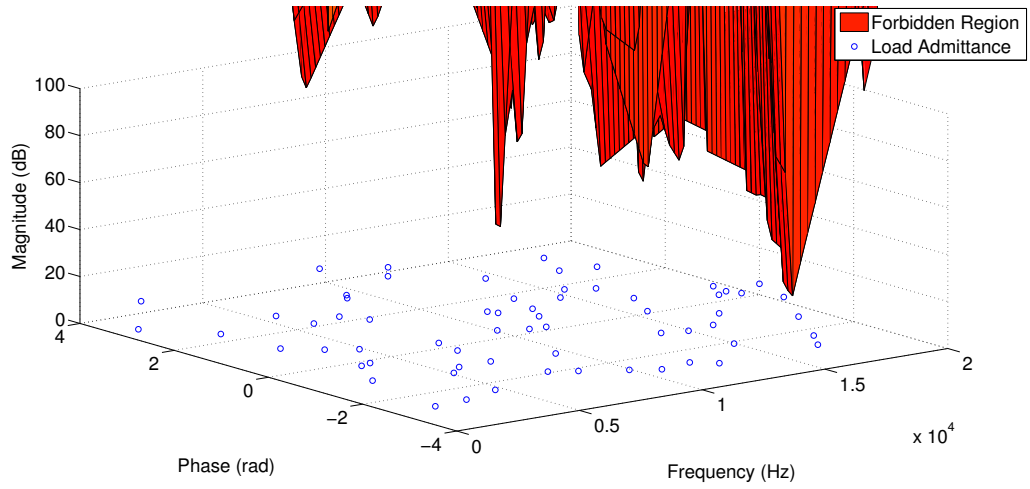

Figure 216: Architecture 2 generator 4 to rectifier 4 connection stability (qd)

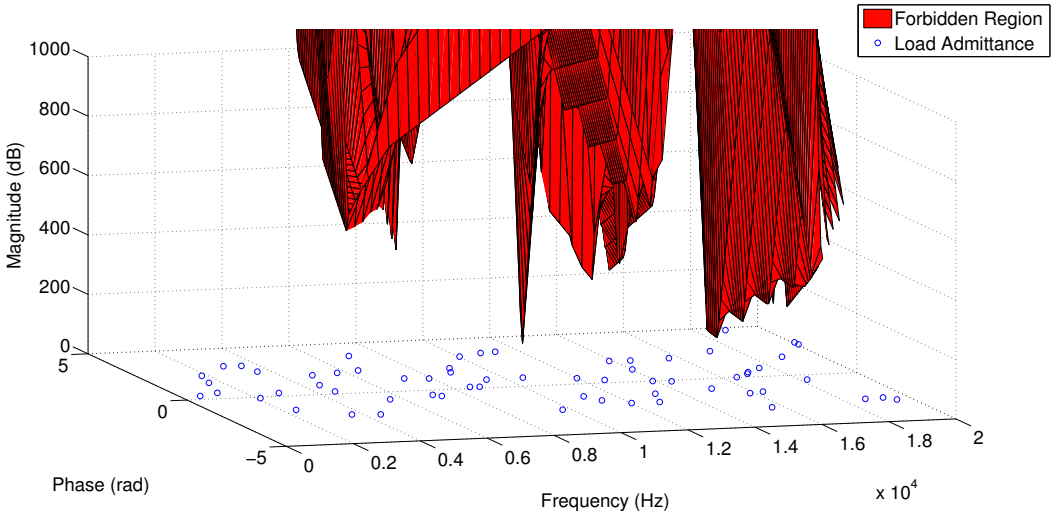

Figure 217: Architecture 2 generator 4 to rectifier 4 connection stability (qq)

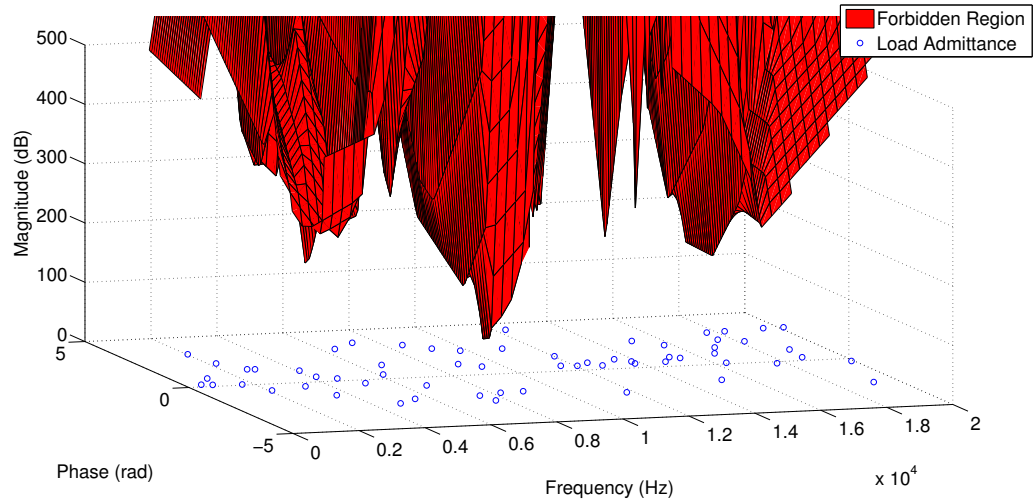

Figure 218: Architecture 2 inverter to motor connection stability (motor group 1) (dd)

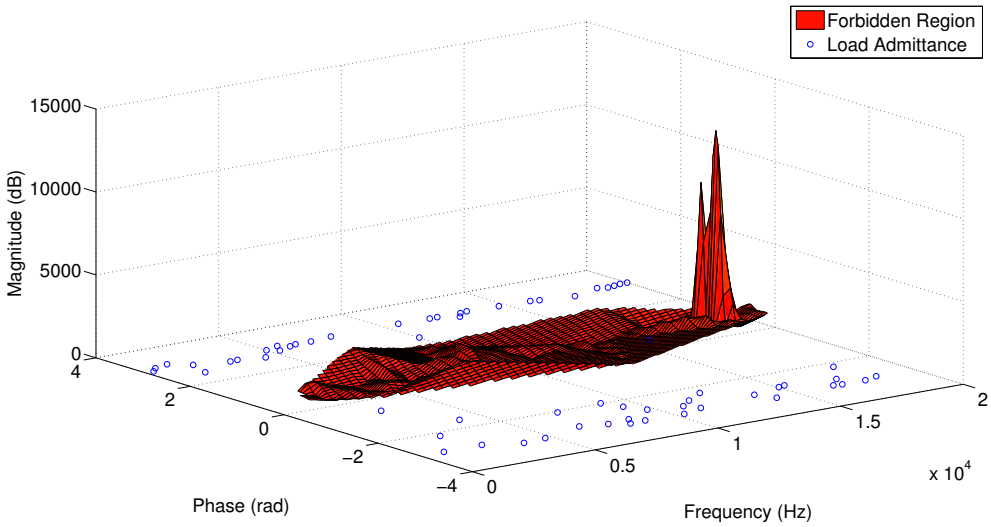

Figure 219: Architecture 2 inverter to motor connection stability (motor group 1) (dq)

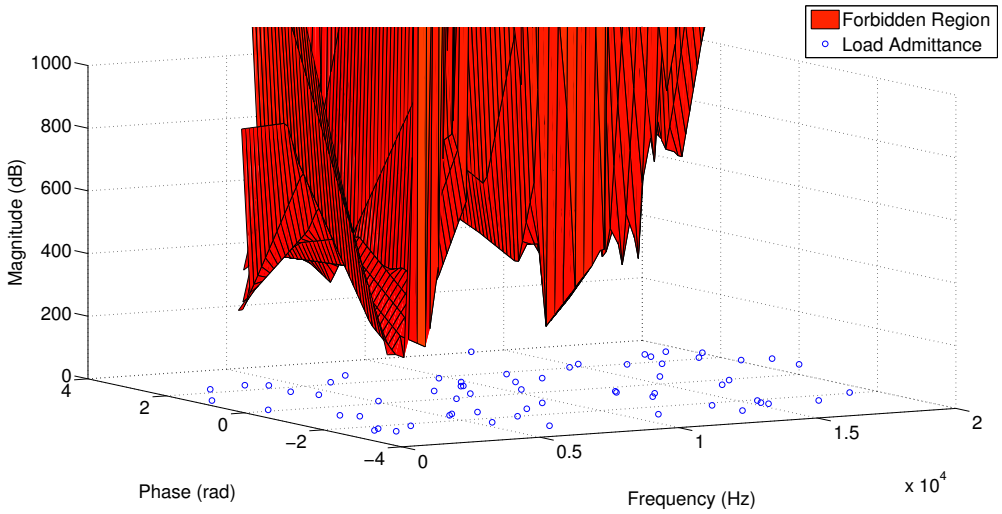

Figure 220: Architecture 2 inverter to motor connection stability (motor group 1) (qd)

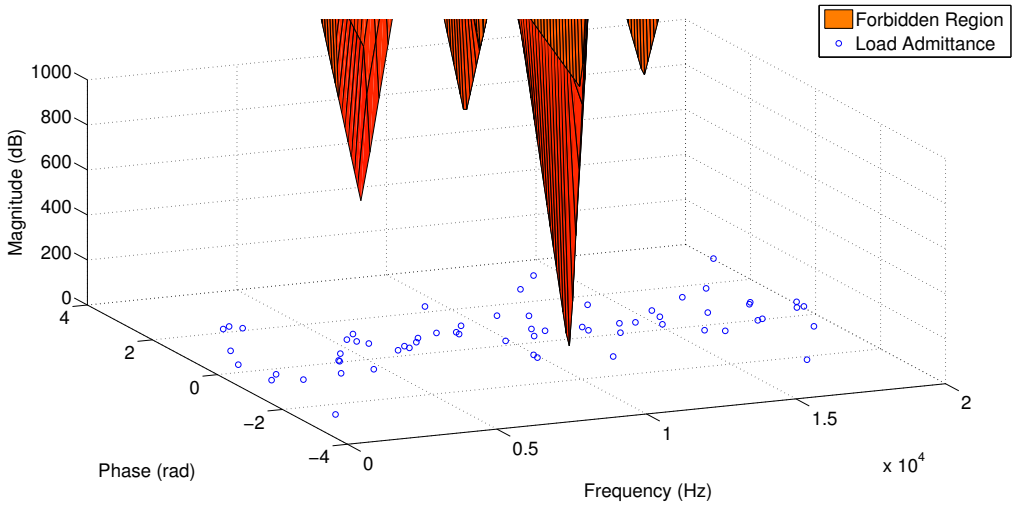

Figure 221: Architecture 2 inverter to motor connection stability (motor group 1) (qq)

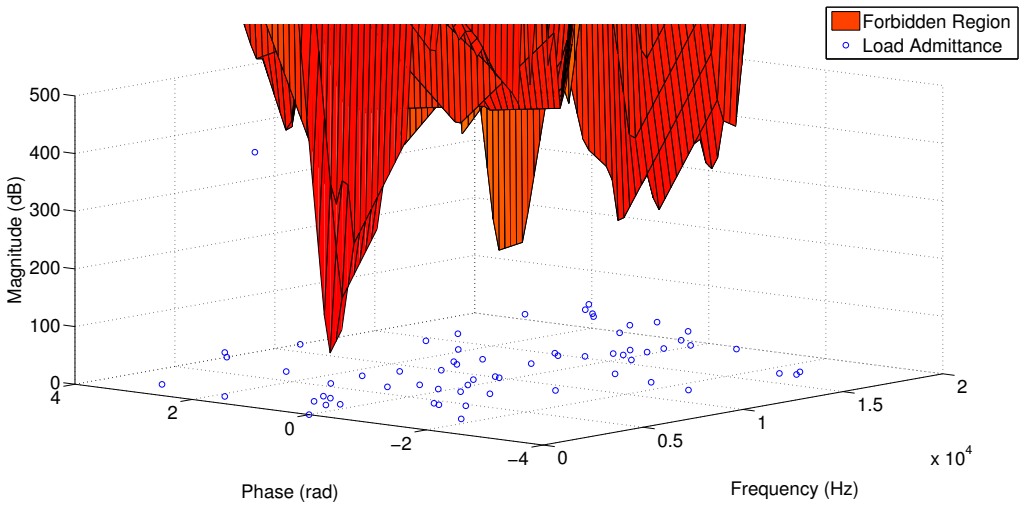

Figure 222: Architecture 2 inverter to motor connection stability (motor group 2) (dd)

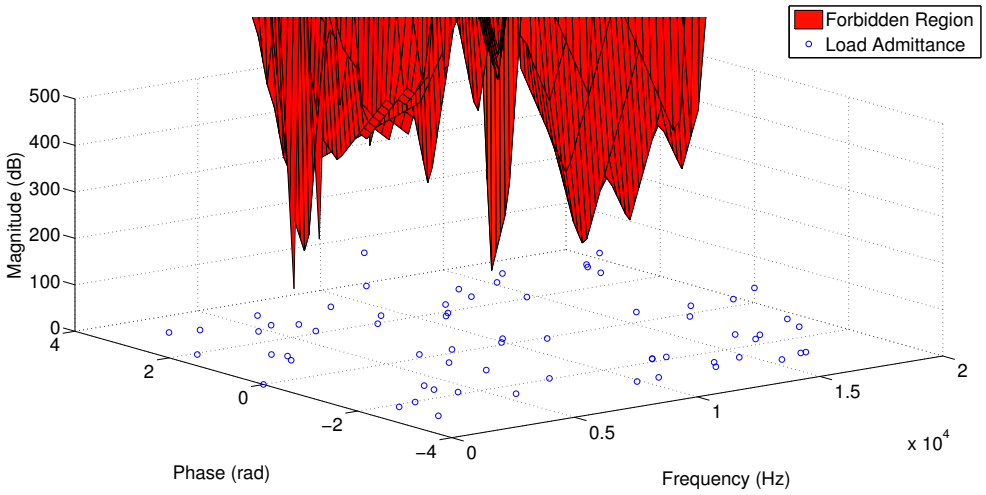

Figure 223: Architecture 2 inverter to motor connection stability (motor group 2) (dq)

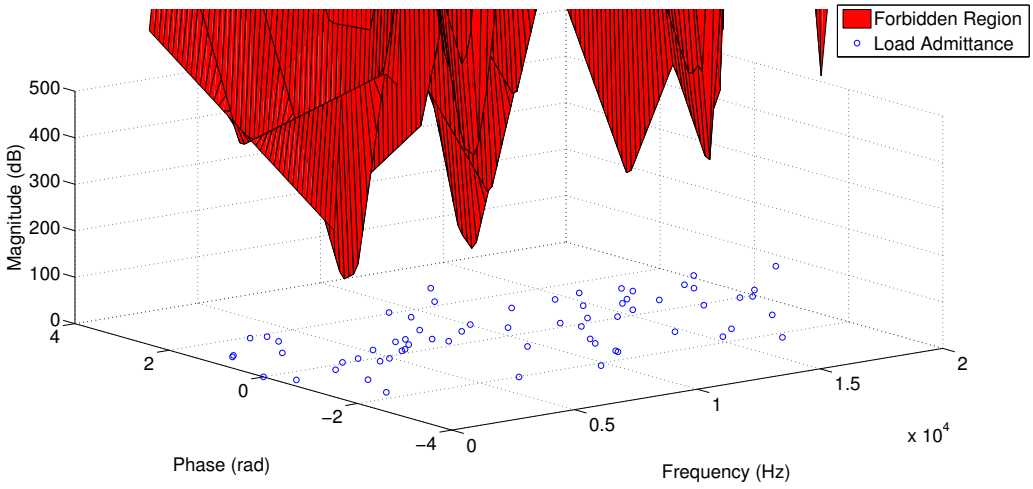

Figure 224: Architecture 2 inverter to motor connection stability (motor group 2) (qd)

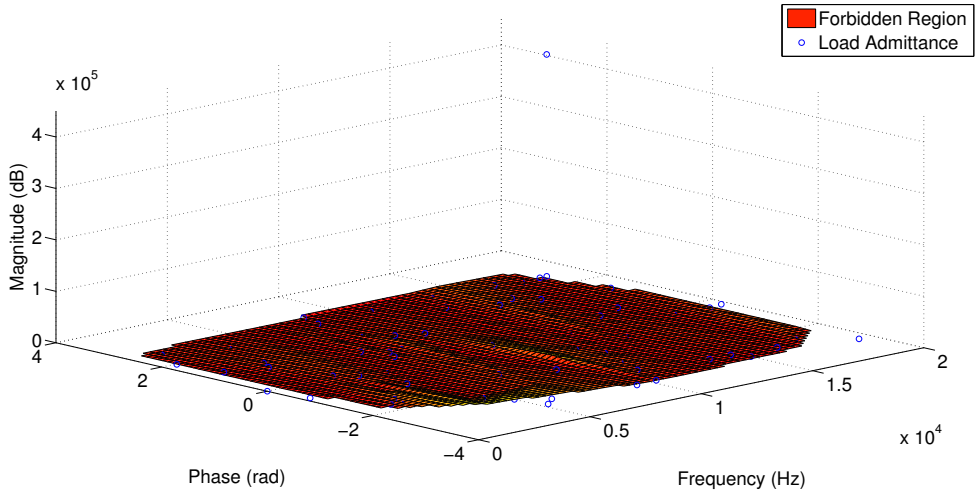

Figure 225: Architecture 2 inverter to motor connection stability (motor group 2) (qq)

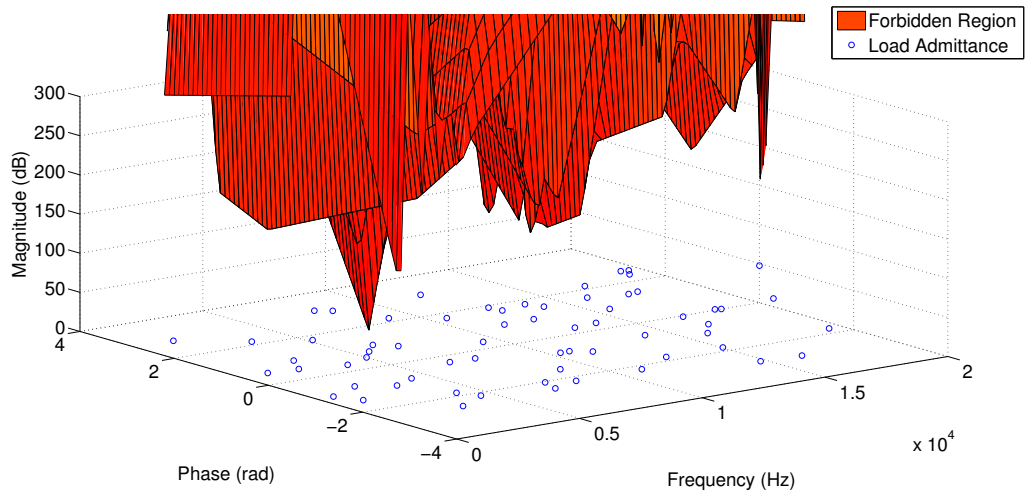

Figure 226: Architecture 2 inverter to motor connection stability (motor group 3) (dd)

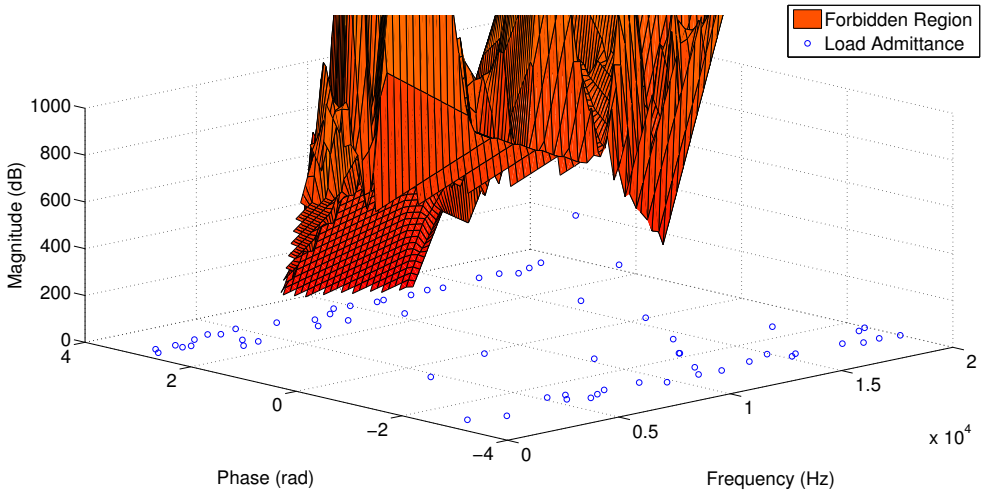

Figure 227: Architecture 2 inverter to motor connection stability (motor group 3) (dq)

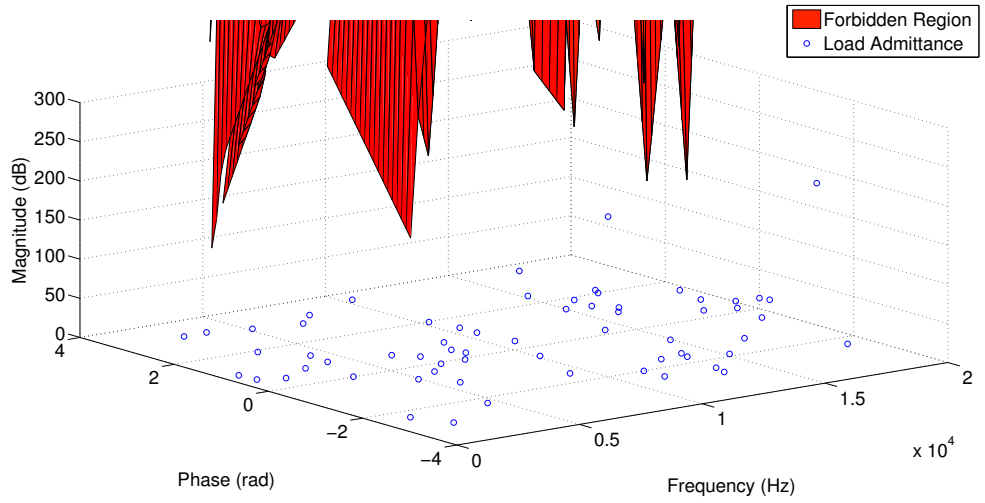

Figure 228: Architecture 2 inverter to motor connection stability (motor group 3) (qd)

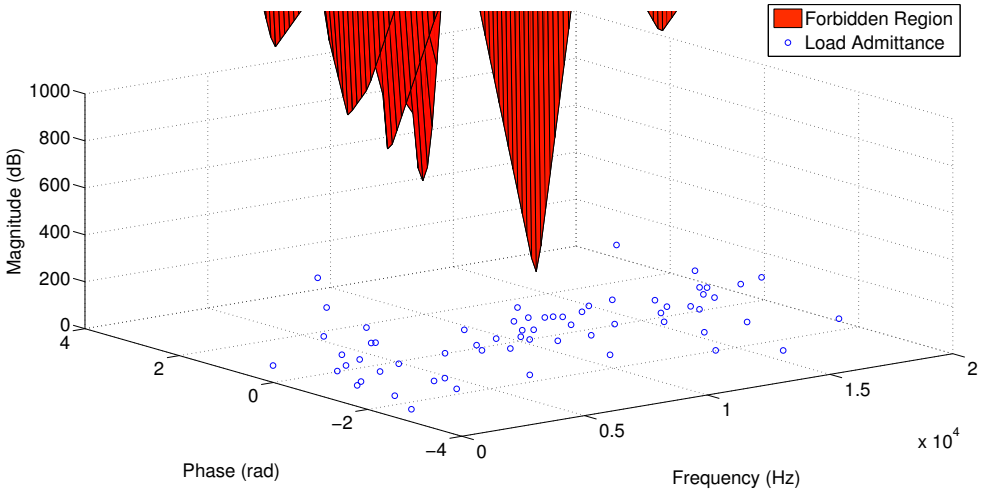

Figure 229: Architecture 2 inverter to motor connection stability (motor group 3) (qq)

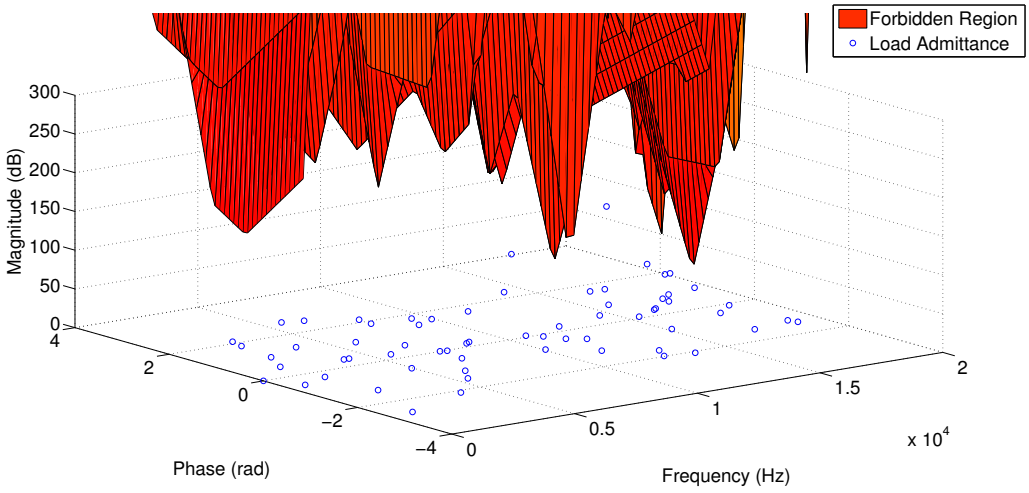

Figure 230: Architecture 2 inverter to motor connection stability (motor group 4) (dd)

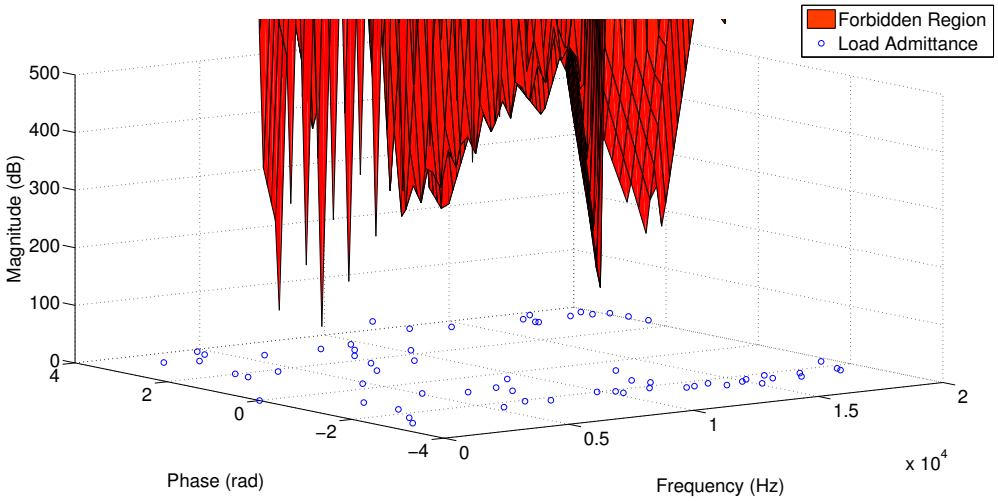

Figure 231: Architecture 2 inverter to motor connection stability (motor group 4) (dq)

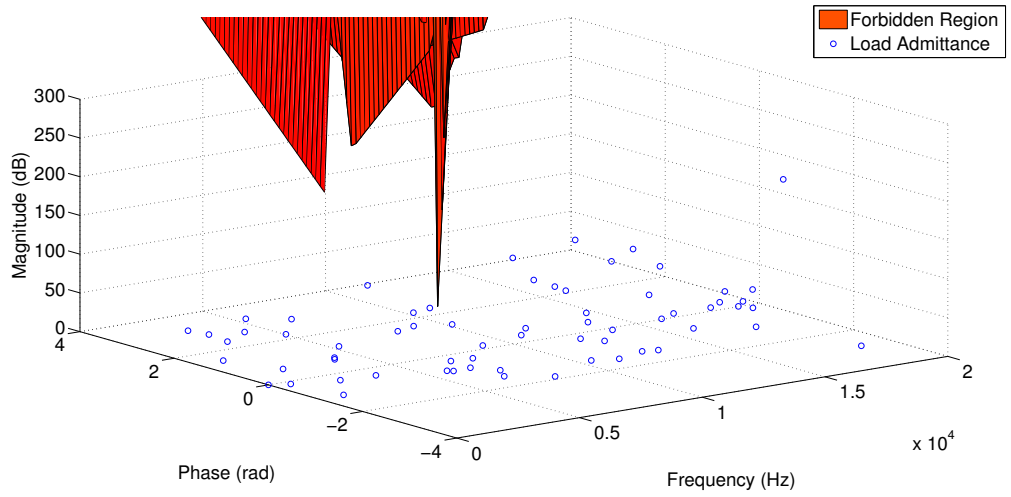

Figure 232: Architecture 2 inverter to motor connection stability (motor group 4) (qd)

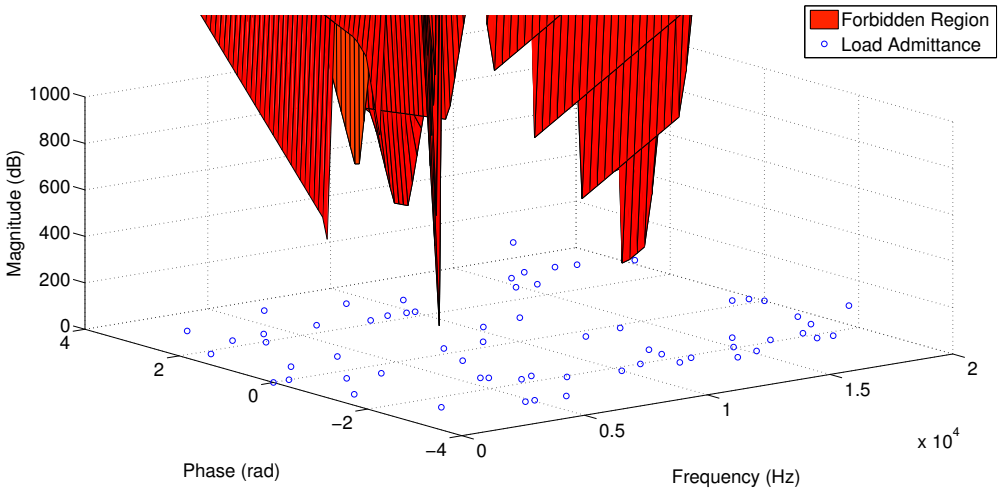

Figure 233: Architecture 2 inverter to motor connection stability (motor group 4) (qq)

A.2 Architecture 3

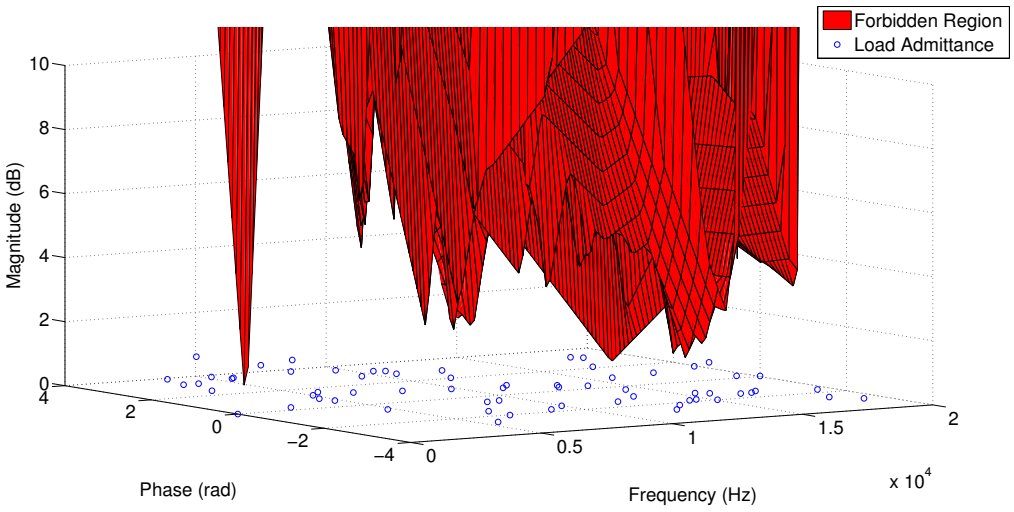

Figure 234: Architecture 3 generator 1 to rectifier 1 connection stability (dd)

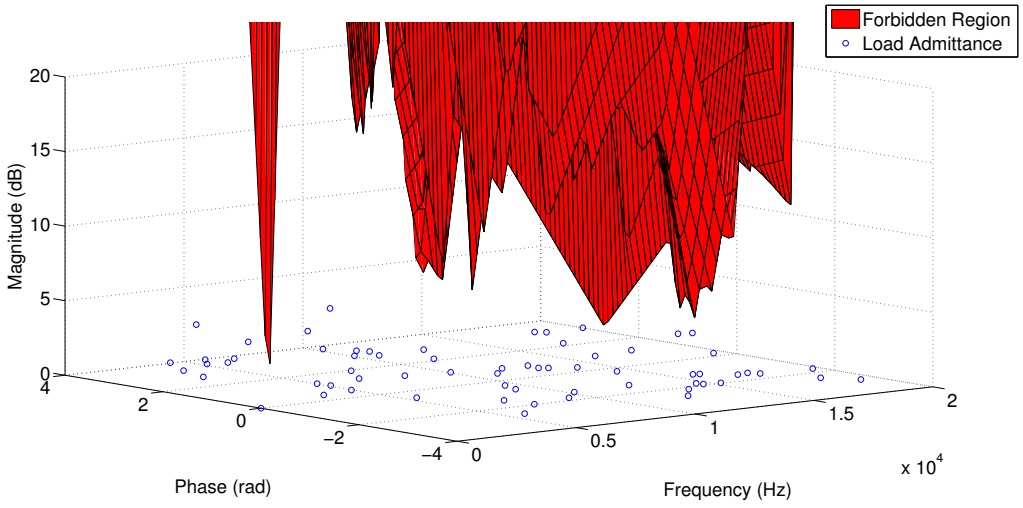

Figure 235: Architecture 3 generator 1 to rectifier 1 connection stability (dq)

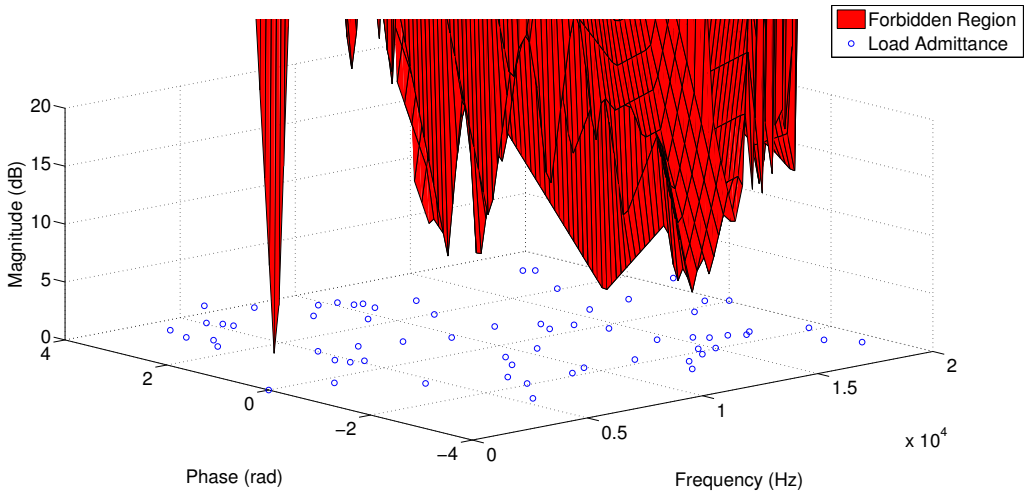

Figure 236: Architecture 3 generator 1 to rectifier 1 connection stability (qd)

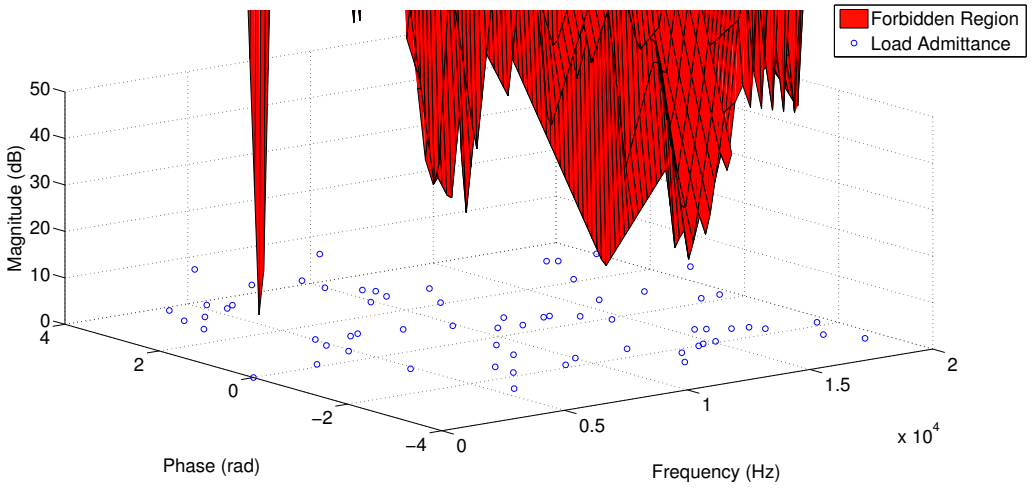

Figure 237: Architecture 3 generator 1 to rectifier 1 connection stability (qq)

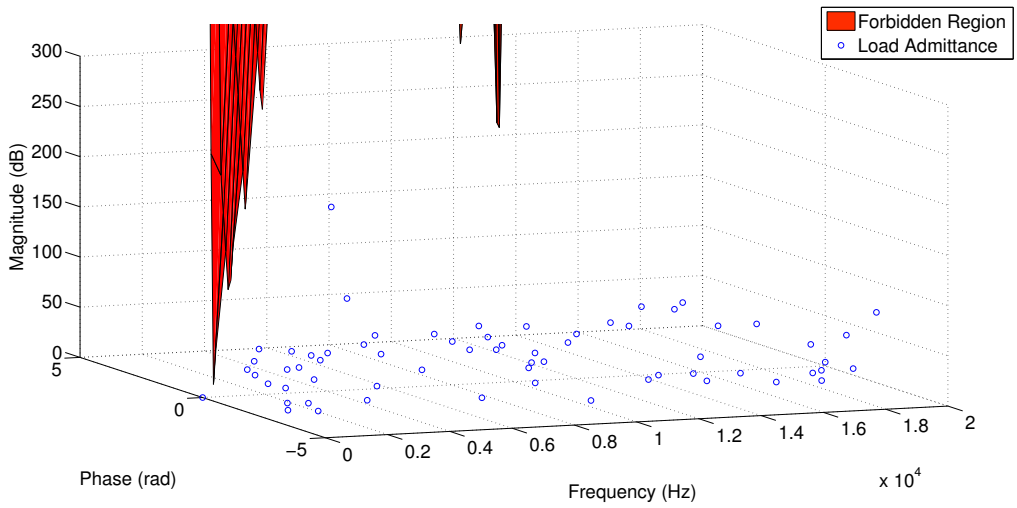

Figure 238: Architecture 3 inverter to motor connection stability (motor group 1) (dd)

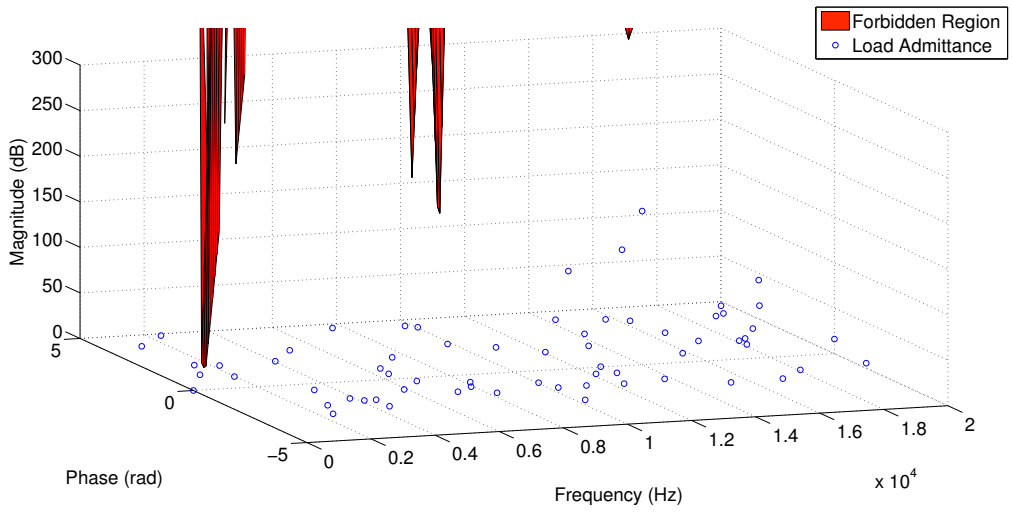

Figure 239: Architecture 3 inverter to motor connection stability (motor group 1) (dq)

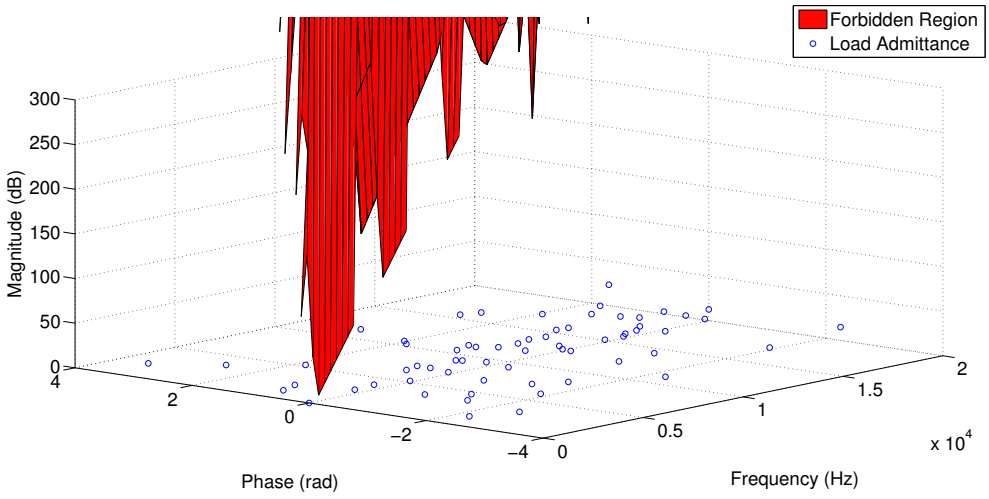

Figure 240: Architecture 3 inverter to motor connection stability (motor group 1) (qd)

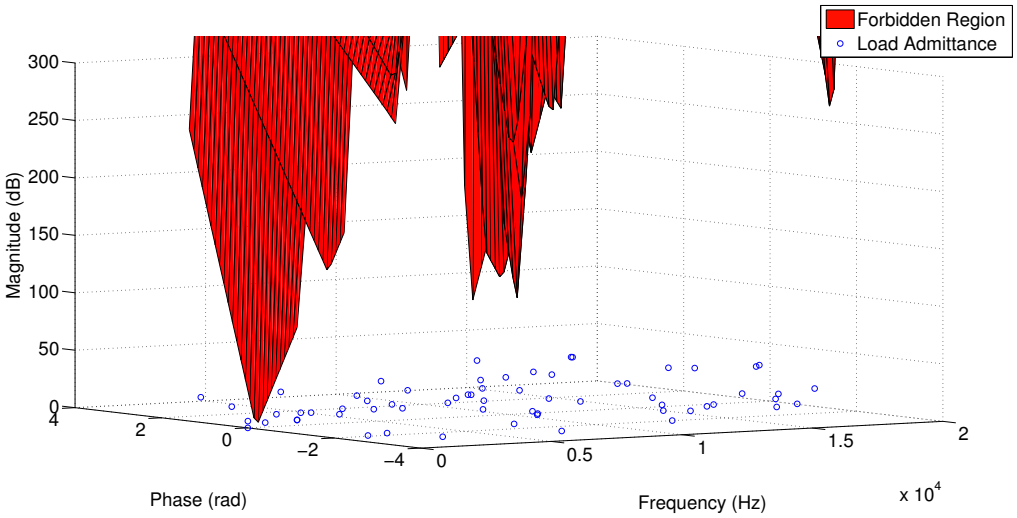

Figure 241: Architecture 3 inverter to motor connection stability (motor group 1) (qq)

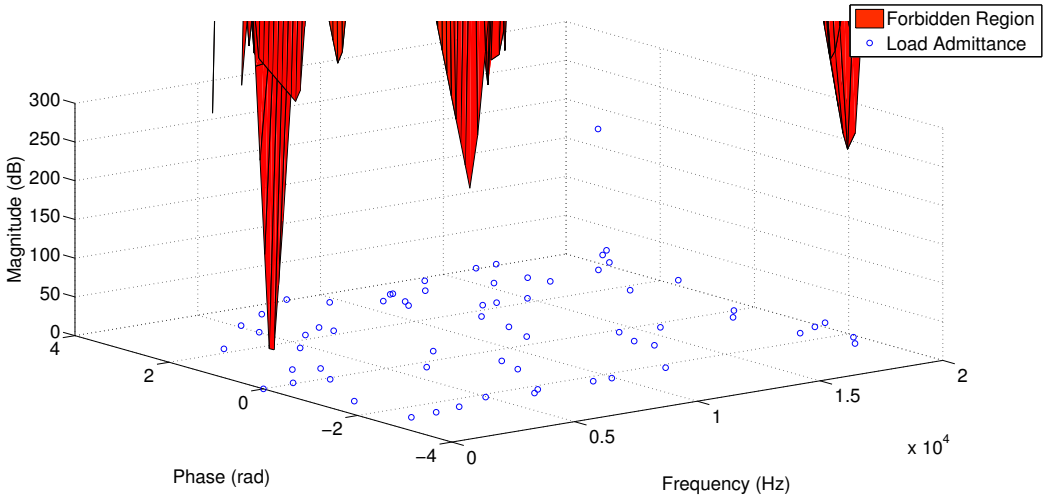

Figure 242: Architecture 3 inverter to motor connection stability (motor group 2) (dd)

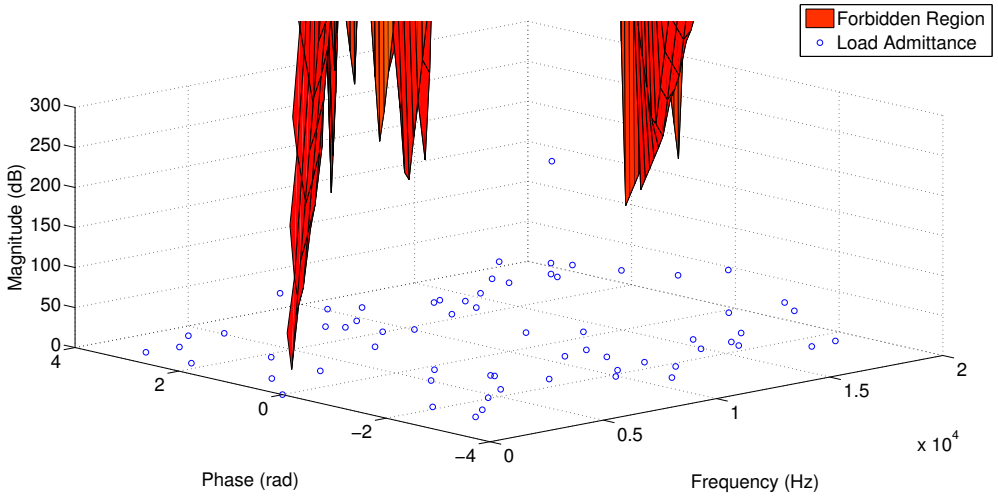

Figure 243: Architecture 3 inverter to motor connection stability (motor group 2) (dq)

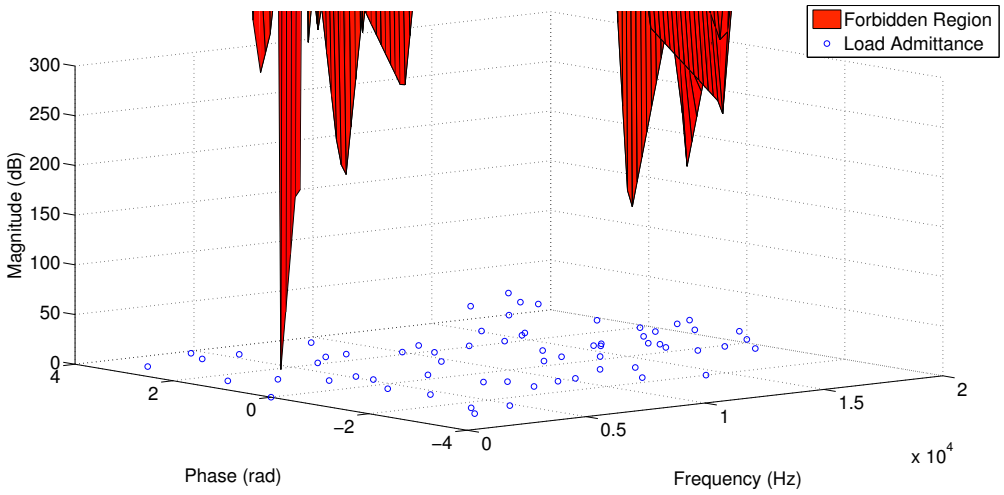

Figure 244: Architecture 3 inverter to motor connection stability (motor group 2) (qd)

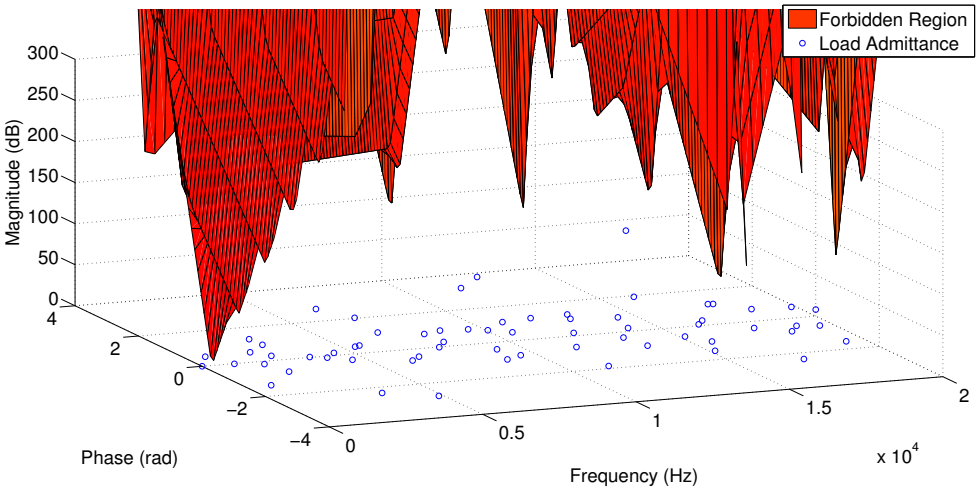

Figure 245: Architecture 3 inverter to motor connection stability (motor group 2) (qq)

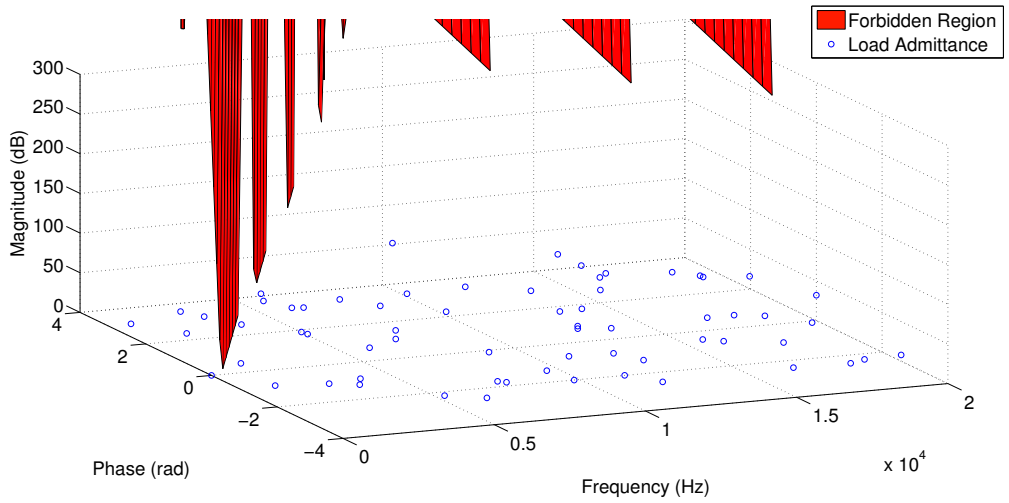

Figure 246: Architecture 3 inverter to motor connection stability (motor group 3) (dd)

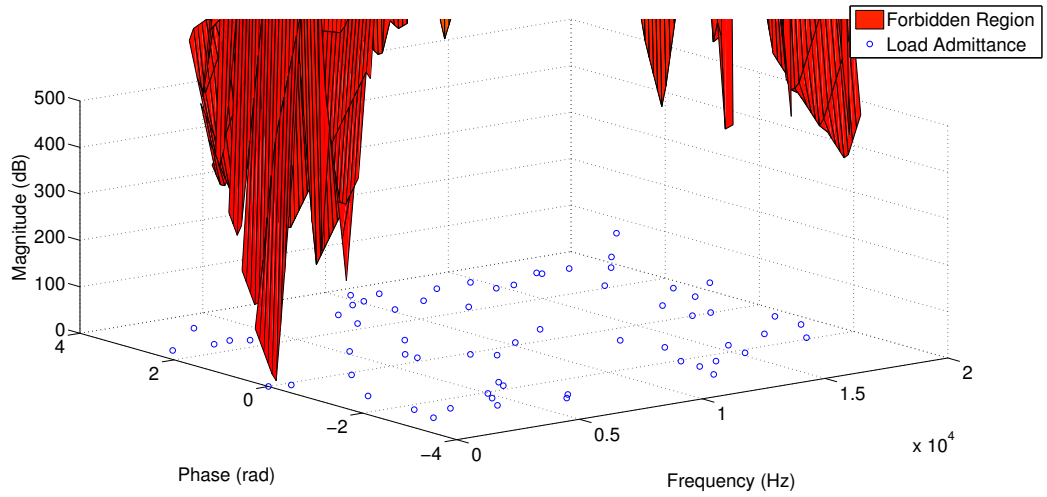

Figure 247: Architecture 3 inverter to motor connection stability (motor group 3) (dq)

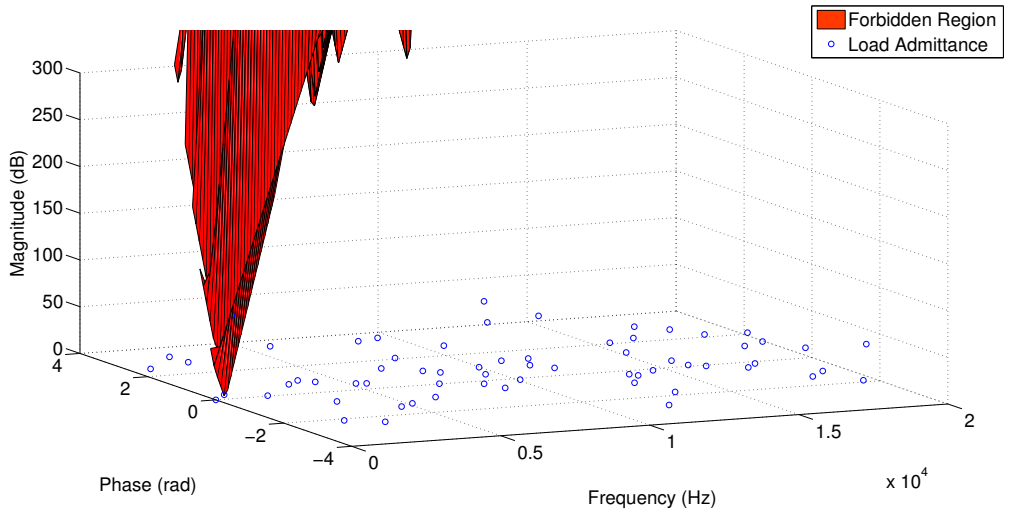

Figure 248: Architecture 3 inverter to motor connection stability (motor group 3) (qd)

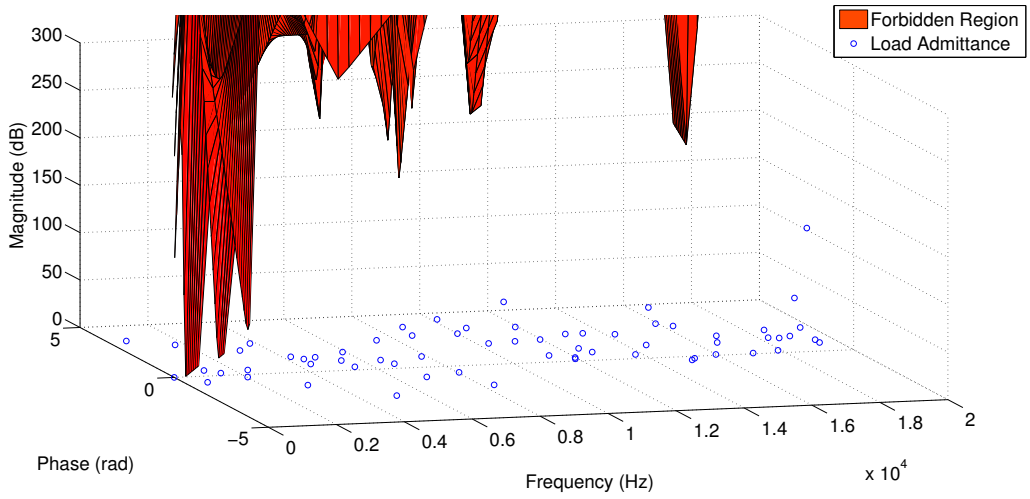

Figure 249: Architecture 3 inverter to motor connection stability (motor group 3) (qq)

REFERENCES

[1] "Janaf thermochemical tables," 1971.

[2] "Determining reliability for complex systems part 1 - analytical techniques," April 2001.

[3] "Determining reliability for complex systems part 2 - simulation," May 2001.

[4] Airbus, "A319/a320/a321 flight deck and systems briefing for pilots," tech. rep., 1998.

[5] AlRashidi, M. R. and El-Hawary, M. E., "A survey of particle swarm optimization applications in electric power systems," *IEEE Transactions on Evolutionary Computation*, vol. 13, pp. 913–918, August 2009.

[6] Andrade, L. and C., T., "Design of the boeing 777 electric system," *IEEE AES Magazine*, July 1992.

[7] Anixter, "Iec medium voltage cable standards," June 2012. `http://www.anixter.com/AXECOM/AXEDocLib.nsf/(UnID)/AE64734E04E4F4E980256F24007506FC/%24file/I-4_24.pdf`.

[8] Armstrong, M., "A process for function based architecture definition and modeling," Master's thesis, Georgia Institute of Technology, April 2008.

[9] Armstrong, M. J., Ross, C. A. H., and Blackwelder, M. J., "Propulsion system component considerations for nasa n3-x turboelectric distributed propulsion system," *SAE International Journal of Aerospace*, vol. 5, December 2012.

[10] Armstrong, M. J., Ross, C. A. H., Blackwelder, M. J., and Rajashekara, K., "Trade studies for nasa n3-x turboelectric distributed propulsion system electrical power system architecture," *SAE International Journal of Aerospace*, vol. 5, December 2012.

[11] Asuri, S., "Modelling and control of sparse converter fed induction motor drives," Master's thesis, Tennessee Tech University, 2005.

[12] Aven, "Reliability evaluation of multistate systems with multistate components," *IEEE Transactions on Reliability*, vol. 34, no. 5, pp. 473–479, 1985.

[13] Avery, C., Burrow, S., and Mellor, P., "Electrical generation and distribution for the more electric aircraft," in *Universities Power Engineering Conference*, pp. 1007–1012, IEEE, September 2007.

[14] Bazovsky, I., *Reliability Theory And Practice*. Courier Dover Publications, 2004.

[15] Bernstein, B. S., *Electrical Power Cable Engineering*. Marcel Dekker, Inc., 2nd ed., 2003.

[16] Birtles, P., *Boeing 777*. Zenith Imprint, 1998.

[17] Boeing, "Boeing and aviation safety," 2014. `http://www.boeing.com/boeing/commercial/safety/faq.page`.

[18] Boroyevich, D., Cvetkovi, I., Dong, D., Burgos, R., Wang, F., and Lee, F., "Future electronic power distribution systems a contemplative view," in *12th International Conference on Optimization of Electrical and Electronic Equipment*, pp. 1369–1380, 2010.

[19] Boyle, R., "Lightweight cable made of braided nanotubes could replace copper wires," September 1999.

http://www.popsci.com/technology/article/2011-09/lightweight-cable-made-braided-nanotubes-could-replace-copper-wires.

[20] Broeck, H. W. V. D., Skudelny, H.-C., and Stanke, G. V., "Analysis and realization of a pulsewidth modulator based on voltage space vectors," *IEEE Transactions on Industry Applications*, vol. 24, pp. 142–1510, January/February 1988.

[21] Brown, G., "Weights and efficiencies of electric components of a turboelectric aircraft propulsion system," in *AIAA Aerospace Sciences Meeting*, 2011.

[22] Brown, G., Kim, H. D., and Felder, J. L., "Materials aspects of turboelectric aircraft propulsion," tech. rep., NASA, 2009.

[23] Brugg, "High voltage xlpe cable systems technical user guide." http://nepa-ru.com/brugg_files/02_hv_cable_xlpe/03_web_xlpe_guide_en.pdf.

[24] Casanellas, "Losses in pwm inverters using igbts," *IEEE Proceedings Electric Power Applications*, vol. 141, pp. 235–239, September 1994.

[25] Center, N. G. R., "Making future commercial aircraft quieter," November 2004. http://www.nasa.gov/centers/glenn/about/fs03grc.html.

[26] Center, R. I. A., "Handbook of 217plus reliability prediction models," tech. rep., 2006.

[27] Chaijarurnudomrung, K., Areerak, K.-L., and Areerak, K.-N., "Modeling and stability analysis of ac-dc power system with controlled rectifier and constant power loads," *WSEAS Transactions on Power Systems*, vol. 6, pp. 31–41, April 2011.

[28] Chaijarurnudomrung, K., Areerak, K.-N., and Areerak, K.-L., "Modeling of three-phase controlled rectifier using a dq method," in *2010 International Conference on Advances in Energy Engineering*, pp. 56–59, 2010.

[29] Chandrasekaran, S., Ragon, S., Lindner, D., Gurdal, Z., and Boroyevich, D., "Optimization of an aircraft power distribution system." August 2002.

[30] Chen, Y. and Jin, X., "Modeling and control of three-phase voltage source pwm rectifier," in *Power Electronics and Motion Control Conference*, vol. 3, pp. 1–4, IEEE, August 2006.

[31] Chevtchenko, O., "Modeling of high temperature superconducting tapes, arrays and ac cables using comsol," in *COMSOL Conference*, 2010.

[32] Chowdhuri, P., "Electrical characteristics of a dc superconducting cable," *Cryogenics*, pp. 171–180, 1982.

[33] Chowdhuri, P., "Feasibility of electric power transmission by dc superconducting cables," *IEEE Transactions on Applied Superconductivity*, vol. 15, pp. 3917–3926, December 2005.

[34] Christou, I., Nelms, A., Cotton, I., and Husband, M., "Choice of optimal voltage for more electric aircraft wiring systems," *IET Electrical Systems in Transportation*, vol. 1, no. 1, pp. 24–30, 2010.

[35] Committee on Aeronautics Research and Technology for Environmental Compatibility, National Research Council, *For Greener Skies: Reducing Environmental Impacts of Aviation.* The National Academics Press, 2002.

[36] Corporation, R. A., "Reliability modeling: k out of n configurations." Online, September 2011. http://www.reliabilityanalytics.com/blog/2011/09/02/reliability-modeling-k-out-of-n-configutation/.

[37] de Tenorio, C., *Methods for collaborative conceptual design of aircraft power architectures*. PhD thesis, Georgia Institute of Technology, 2010.

[38] Dixon, J. W., *Power Electronics Handbook*. Butterworth-Heinemann, 3rd ed., 2011.

[39] Dorigo, M., Birattari, M., and Stutzle, T., "Ant colony optimization: Artificial ants as a computational intelligence technique," *IEEE Computational Intelligence Magazine*, November 2006.

[40] Douglas, J., Zalewski, M., and Romeu, J.-L., "Power transmission using high voltage dc to decrease infrastructure burden," in *SAE International Power Systems Conference*, October 2012.

[41] Emadi, A., Khaligh, A., Rivetta, C., and Williamson, G., "Constant power loads and negative impedance instability in automotive systems: definition, modeling, stability, and control of power electronic converters and motor drives," *IEEE Transactions on Vehicular Technology*, vol. 55, pp. 1112–1125, July 2006.

[42] Erickson, R. and Maksimovic, D., *Fundamentals of Power Electronics*. Kluwer Academic Publishers, 2nd ed., 1999.

[43] Feenstra, R., Gapud, A. A., List, F. A., Specht, E. D., Christen, D. K., Holesinger, T. G., and Feldmann, D. M., "Critical currents ic(77 k) 350 acm width achieved in ex situ ybco coated conductors using a faster conversion process," *IEEE Transactions on Applied Superconductivity*, vol. 15, pp. 2803–2807, June 2005.

[44] Felder, J. L. and Kim, H. D., "Control volume analysis of boundary layer ingesting propulsion systems with or without shock wave ahead of the inlet," in *AIAA Aerospace Sciences Meeting*, 2011.

[45] Felder, J. L., Kim, H. D., and Brown, G., "Turboelectric distributed propulsion engine cycle analysis for hybrid-wing-body aircraft," in *47th AIAA Aerospace Sciences Meeting*, AIAA, 2009.

[46] Felder, J. L., Kim, H. D., Brown, G., and Chu, J., "An examination of the effect of boundary layer ingestion on turboelectric distributed propulsion systems," in *AIAA Aerospace Sciences Meeting*, 2011.

[47] Finemech, "Liquid nitrogen." Online, 2012. `http://www.finmech.com/tech_resources/liquid_nitrogen.html`.

[48] Firestine, T. and Guarino, J., "A decade of change in fuel prices and u.s. domestic passenger aviation operations," tech. rep., U.S. Department of Transportation Research and Innovative Technology Administration, March 2012.

[49] for Transport (Air Accidents Investigation Branch), D., "Aircraft accident report 2/2009," April 2009.

[50] Forsyth, A., Yang, S., Mawby, P., and Igic, P., "Measurement and modelling of power electronic devices at cryogenic temperatures," *IEE Proceedings Circuits Devices Systems*, vol. 153, pp. 407–415, October 2006.

[51] Gagnon, "The element of copper." Online. `http://education.jlab.org/itselemental/ele029.html`.

[52] Gallagher, S., "Boeings dreamliner batteries inherently unsafe and yours may be too," January 2013. `http://arstechnica.com/business/2013/01/boeings-dreamliner-batteries-inherently-unsafe-and-yours-may-be-too/`.

[53] Ganev, E., Warr, W., and Salam, A., "Lead-unity-lag electric power generation system," *SAE International Journal of Aerospace*, vol. 5, December 2012.

[54] Gano, S. E., Kim, H., and Brown II, D., "Comparison of three surrogate modeling techniques: Datascape, kriging, and second order regression," in *11th AIAA/ISSMO Multidisciplinary Analysis and Optimization Conference*, AIAA, September 2006.

[55] Gap, T., "Brushless motors & generators with high power & torque density," 2014. `http://www.thingap.com/`.

[56] Gibson, A., Hall, D., Schiltgen, B., Foster, T., Keith, J., and Masson, P., "The potential and challenge of turboelectric propulsion for subsonic transport aircraft," in *AIAA Aerospace Sciences Meeting*, 2010.

[57] Gibson, A., Hall, D., Waters, M., Schiltgen, B., Foster, T., and Papathakis, K., "Superconducting electric distributed propulsion structural integration and design in a split-wing regional airliner," in *AIAA Aerospace Sciences Meeting*, AIAA, January 2011.

[58] Gorissen, D., Couckuyt, I., Demeester, P., and Dhaene, T., "A surrogate modeling and adaptive sampling toolbox for computer based design," *Journal of Machine Learning Research*, vol. 11, pp. 2051–2055, 2010.

[59] Guida, B. and Cavallo, A., "Average models for aeronautical electrical networks: An application for intelligent load power management," in *SAE International Power Systems Conference*, October 2012.

[60] Guynn, Berton, Tong, and Haller, "Advanced single-aisle transport propulsion design options revisited," in *2013 Aviation Technology, Integration, and Operations Conference*, August 2013.

[61] Hampton, Harlein, Lennartsson, Orton, and Ramachandran, "Long-life xlpe insulated power cable." Online, 2007. http://www.neetrac.gatech.edu/publications/jicable07_C_5_1_5.pdf.

[62] Hartani, K. and Miloud, Y., "Control strategy for three phase voltage source pwm rectifier based on the space vector modulation," *Advances in Electrical and Computer Engineering*, vol. 10, no. 3, pp. 61–65, 2010.

[63] Hartmann, Miniboeck, K., "A three-phase delta switch rectifier for more electric aircraft applications employing a novel pwm current control concept," in *Applied Power Electronics Conference and Exposition*, IEEE, 2009.

[64] Hasson, R., Cohanim, B., and Weck, O., "A comparison of particle swarm optimization and the genetric algorithm." Electronic, 2004.

[65] Haugan, T., Long, J. D., Hampton, L. A., and Barnes, P. N., "Design of compact, lightweight power transmission devices for specialized high power applications," in *SAE International Power Systems Conference*, 2008.

[66] Hirose, M., Masuda, T., Sato, K., and Hata, R., "High-temperature superconducting (hts) dc cable," *SEI Technical Review*, vol. 61, pp. 29–35, 2006.

[67] Hiscocks, P. D., "A laplace transform cookbook." Electronic, March 2008.

[68] Hsieh and Lin, "Reliability-oriented multi-resource allocation in a stochastic-flow network," *Reliablity Engineering & System Safety*, vol. 81, pp. 155–161, 2003.

[69] Huang, M., Wong, S.-C., Tse, C., and Ruan, X., "Catastrophic bifurcation in three-phase voltage-source converters," in *Fourth International Workshop on Chaos-Fractals Theories and Applications*, pp. 147–151, 2011.

[70] Hui, W., Jihua, C., Shoudao, H., and Yaonan, W., "The investigation of pwm rectifier control method," in *Power Electronics and Motion Control Conference*, vol. 2, pp. 673–675, IEEE, August 2004.

[71] Husain, *Air Breathing Engines*. I. K. International Pvt Ltd, 2010.

[72] indexmundi, "Jet fuel - daily price." Web, March 2013. `http://www.indexmundi.com/commodities/?commodity=jet-fuel`.

[73] Jarosz, P. R., Shaukat, A., Schauerman, C. M., Cress, C. D., Kladitis, P. E., Ridgley, R. D., and Landi, B. J., "High-performance, lightweight coaxial cable from carbon nanotube conductors," *Applied Materials and Interfaces*, vol. 4, pp. 1103–1109, 2012.

[74] Jones, R. I., "The more electric aircraft - asssing the benefits," *Journal of Aerospace Engineering*, vol. 216, pp. 259–269, May 2002.

[75] Jordanian, R., *A318/A319/A320/A321 Flight Crew Operating Manual*, August 2012.

[76] Karimi, K. J., "Future aircraft power systems- integration challenges," tech. rep., Boeing, 2007.

[77] Kaymaz, I., "Application of kriging method to structural reliability problems," *Structural Safety*, vol. 27, pp. 133–151, 2005.

[78] Kim, H. D. and Felder, J. L., "Control volume analysis of boundary layer ingesting propulsion systems with or without shock wave ahead of the inlet," in *AIAA Aerospace Sciences Meeting*, 2011.

[79] Kim, H. D., Brown, G. V., and Felder, J. L., "Distributed turboelectric propulsion for hybrid wing body aircraft," in *International Powered Lift Conference*, July 2008.

[80] Laboratory, B. N., "Properties of liquid nitrogen." Online, 2013. http://www.bnl.gov/magnets/staff/gupta/cryogenic-data-handbook/Section6.pdf.

[81] Lee, B. K. and Ehasani, M., "A simplified functional model for 3-phase voltage source inverter using switching function concept," in *Industrial Electronics Society*, vol. 1, pp. 462–467, 1999.

[82] Lee, J. J., "Historical and future trends in aircraft performance, cost, and emissions," Master's thesis, Massachusetts Institute of Technology, 2000.

[83] Leemis, *Reliability: Probabilistic Models and Statistical Methods*. 2009.

[84] Lim, D., Ong, Y.-S., and Jin, Y., "A study on metamodeling techniques, ensembles, and multi-surrogates in surrogate-assisted memetic algorithms," in *Genetic and Evolutionary Computation Conference*, pp. 1288–1295, July 2007.

[85] Lisnianski, A., Levitin, G., Ben-Haim, H., and Elmakis, D., "Power system structure optimization subject to reliability constraints," *Electric Power Systems Research*, vol. 39, pp. 145–152, 1996.

[86] Loop, B. P., Sudhoff, S. D., and andEdwin L. Zivi, S. H. Z., "Estimating regions of asymptotic stability of power electronics systems using genetic algorithms," *IEEE Transactions on Control Systems Technology*, vol. 18, pp. 1011–1022, September 2010.

[87] Losic, N. A., "Reduced order tracking 3-ph phase-locked loops in aerospace applications," in *SAE International Power Systems Conference*, 2012.

[88] Louganski, K. P., "Modeling and analysis of a dc power distribution system in 21st century airlifters," Master's thesis, Virginia Polytechnic Institute and State University, September 1999.

[89] Luongo, C., Masson, P. J., Nam, T., Mavris, D., Kim, H. D., Brown, G. V., Waters, M., and Hall, D., "Next generation more-electric aircraft: A potential application for hts superconductors," *IEEE Transactions on Applied Superconductivity*, vol. 19, no. 2, pp. 1055–1068, 2009.

[90] Maglev, "Frequently asked questions and answers about maglev," 2001. `http://www.maglev2000.com/works/how-08.html`.

[91] Mahdavi, J., Emaadi, A., Bellar, M. D., and Ehasani, M., "Analysis of power electronic converters using the generalized state-space averaging approach," *IEEE Transactions on Circuits and Systems*, vol. 44, pp. 767–770, August 1997.

[92] Malik, Z. and Rashid, K., "Comparison of optimization by response surface methodology with neurofuzzy methods," *IEEE Transactions on Magnetics*, vol. 36, pp. 241–257, January 2000.

[93] Malinowski, M., *Sensorless Control Strategies for Three - Phase PWM Rectifiers*. PhD thesis, Warsaw University of Technology, 2001.

[94] Masson, Nam, Choi, Tixador, Waters, hall, Luongo, and Mavris, "Superconducting ducted fan design for reduced emissions aeropropulsion," *IEEE Transactions on Applied Superconductivity*, vol. 3, pp. 1662–1668, 2009.

[95] Masson, P., Brown, G., Soban, D. S., and Luongo, C. A., "Hts machines as enabling technolgy for all-electric airborne vehicles," *Superconductor Science and Technology*, vol. 20, pp. 748–756, 2007.

[96] Masson, P. and Luongo, D., "Hts machines for applications in all-electric aircraft," in *Power Engineering Society General Meeting*, pp. 1–6, IEEE, June 2007.

[97] Masuda, T., Yumura, Watanabe, Takigawa, Ashibe, adn Kato, S., Odura, Yamada, Hirose, Yatsuka, Sato, and Isojima, "High temperature superconducting cable technology," *SEI Technical Review*, vol. 59, pp. 8–13, 2005.

[98] Mavris, D. N., Baker, A. P., and Schrage, D. P., "Ippd through robust design simlation for an affordable short haul civil tiltrotor," in *American Helicopter Society 53rd Annual Forum*, 1997.

[99] Meziane, R., Massim, Y., Zeblah, A., Ghoraf, A., and Rahli, R., "Reliability optimization using ant colony algorithm under performance and cost constraints," *Electric Power Systems Research*, vol. 76, pp. 1–8, 2005.

[100] Middlebrook, R. D. and Cuk, S., "A general unified approach to modelling switching-converter power stages," in *IEEE Power Electronics Specialists Conference*, pp. 73–86, 1976.

[101] Minervini, J., "Superconductors for power transmission and distribution." PPPL Colloquium, May 2009.

[102] Minitab, "Distribution models for reliabilty data." `http://www.minitab.com/support/documentation/Answers/Reliability_Distribution.pdf`.

[103] Mohanta, D. K., Sadhu, P. K., and Chakrabarti, R., "Deterministic and stochastic approach for safety and reliability optimization of captive power plant maintenance scheduling using ga/sa-based hybrid techniques: A comparison of results," *Reliability Engineering and System Safety*, vol. 92, pp. 187–199, 2007.

[104] Moir, I. and Seabridge, A., *Aircraft Systems: Mechanical, Electrical and Avionics Subsystems Integration*. John Wiley & Sons, 3rd ed., 2008.

[105] Mukoyama, S., Yagi, M., Hirano, H., Yamada, Y., Izumi, T., and Shiohara, Y., "Development of hts power cable using ybco coated conductor," *Physica C*, vol. 445-448, pp. 1050–1053, 2006.

[106] Mukoyama, S., Yagi, M., Hirata, H., Suzuki, M., Nagaya, S., Kashima, N., and Shiohara, Y., "Development of ybco high-tc superconducting power cables," *Furukawa Review*, vol. 35, pp. 18–22, 2009.

[107] Myers, R. H. and Montgomery, D. C., *Response Surface Methodology: Process and Product Optimization Using Designed Experiments*. Wiley-Interscience, 2nd ed., 2002.

[108] Nakayama, T., Yagai, T., Tsuda, M., and Hamajima, T., "Micro power grid system with smes and superconducting cable modules cooled by liquid hydrogen," *IEEE Transactions on Applied Superconductivity*, vol. 19, pp. 2062–2065, June 2009.

[109] Nelson, T., "787 systems and performance," 2005. `http://dibley.eu.com/documents/B787SystemsandPerf-GeorgeBeyle-31mar09.pdf`.

[110] Norman, P., Alt, J. T., and Burt, G., "Parametric average-value converter modeling for aerospace applications," *SAE International Journal of Aerospace*, vol. 5, December 2012.

[111] Norris and Wagner, *Douglas Jetliners*. MBI Publishing, 1999.

[112] O'Connel, T. C., McCarthy, K., Yeu, R., Pigg, P., Bowman, T., and Lamm, P., "Software tools for efficient model-based design of energy optimized aircraft," *SAE International Journal of Aerospace*, vol. 5, December 2012.

[113] of Defense, D., "Military handbook 217f reliability prediction of electronic equipment," tech. rep., 1991.

[114] of Inspector General, O., "Aviation industry performance: A review of the aviation industry, 20082011," tech. rep., United States of America Department of Transportation, 2012.

[115] Pai, M. A. and Sauer, P. W., "Stability analysis of power systems by lyapunov's direct method," *IEEE Control Systems Magazine*, January 1989.

[116] Pallett, E., *Aircraft Electrical Systems*. Piman Publishing, 2nd ed., 1980.

[117] Paranthaman, M. P. and Izumi, T., "High-performance ybco-coated superconductor wires," tech. rep., Materials Research Society, August 2004.

[118] Penner, J. E., Lister, D. H., Griggs, D. J., Dokken, D., and McFarland, M., "Aviation and the global atmosphere," tech. rep., Intergovernmenal Panel on Climate Change, 1999.

[119] Phipps, W., *Mechanics of Flight*. John Wiley & Sons, 2004.

[120] Phipps, W., *New Generation Three-Phase Rectifier*. PhD thesis, University of Canterbury, July 2008.

[121] Politano, D., Sjstrm, M., Schnyder, G., and Rhyner, J., "Technical and economical assessment of hts cables," in *Applied Superconductivity Conference*, IEEE, September 2000.

[122] Poole, C., Farach, H., Creswick, R., and Prozorov, R., *Superconductivity*. Elsevier Ltd., 2nd ed., 2007.

[123] Raczkowski, B. C., Loop, B., Amerhein, M., Walters, E., and Wasynczuk, O., "Large displacement stability by design for robust aircraft electric power systems," in *SAE International Power Systems Conference*, October 2012.

[124] Radebaugh, R., "Cryocoolers." Electronic, February 2009.

[125] Rashid, M. H., *Power Electronics Handbook*. Academic Press, 2001.

[126] Rogers, "Electric drive status and challenges." PDF, July 2012. url-http://www1.eere.energy.gov/vehiclesandfuels/pdfs/eveverywhere/4rogersed.pdf.

[127] Rosado, S. P., *Voltage Stability and Control in Autonomous Electric Power Systems with Variable Frequency*. PhD thesis, Virginia Polytechnic Institute and State University, September 2007.

[128] Rosero, J., Ortega, J. A., Albadas, E., and Romeral, L., "Moving towards a more electric aircraft," *IEEE A&E Systems Magazine*, pp. 3–9, March 2007.

[129] Ross, "Active versus standby redundancy for improved cryocooler reliability in space," in *13th International Cryocooler Conference*, 2004.

[130] Rostila, L., Soderlund, L., Mikkonen, R., and Lehtonen, J., "Modelling method for critical current of ybco tapes in cable use," *Physica C*, vol. 467, pp. 91–95, 2007.

[131] Rudenko and Schubnikow, "The viscosity of liquid nitrogen, carbon monoxide, argon and oxygen as a function of temperature." Online, August 1968. `https://ia600705.us.archive.org/13/items/nasa_techdoc_19680021813.pdf`.

[132] Salam, Z., "Power electronics and drives," tech. rep., 2002.

[133] Sanjuan, S. L., "Voltage oriented control of three-phase boost pwm converters," Master's thesis, Chalmers University of Technology, 2010.

[134] Sato, S., Mody, P., Hall, D., Blanco, E., and Hileman, J., "Assessment of propulsion system configuration and fuel composition on hybrid wing body fuel efficiency," in *AIAA Aerospace Sciences Meeting*, 2011.

[135] Schmidt and Allais, "Superconducting cables for power transmission applications: A review," in *Workshop on Accelerator Magnet Superconductors*, 2005.

[136] Shaw, J. C., Galloway, S., Norman, P., and Burt, G., "Aircraft power and propulsion systems-research challenges and opportunities for electrical systems," in *SAE International Power Systems Conference*, 2012.

[137] Shirai, Y., Tatsumoto, H., Hata, K., Shiotsu, M., Kobayashi, H., Naruo, Y., and Inatani, Y., "Preliminary study on heat transfer characteristics of liquid hydrogen for coolant of htc superconductors," in *Advances in Cryogenic Engineering: Transactions of the Cryogenic Engineering Conference* (II, J. W., ed.), vol. 55, American Institute of Physics, 2010.

[138] Siemens, "Innovative motor technology for electric and hybrid vehicles." PDF, May 2013. `http://www.industry.siemens.com/topics/global/en/electric-vehicle/Documents/innovative-motor-technology.pdf`.

[139] Simpson, T. W., Mauery, T. M., and Korte, J. J., "Comparison of response surface and kriging models for multidisciplinary design optimization," in *AIAA/USAF/NASA/ISSMO Symposium on Multidisciplinary Analysis and Optimization*, 1998.

[140] Singh, C. and Mitra, J., "Monte carlo simulation for reliability analysis of emergency and standby power systems," in *IEEE Industry Applications Conference*, 1995.

[141] Steel, A., "304/304l stainless steel product data sheet." Online, 2013. http://www.adsteel.com/pdf/markets_products/stainless/austenitic/304_304L_Data_Sheet.pdf.

[142] Sudhoff, S. D., Glover, S., Lamm, P., Schmucker, D., and Delisle, D., "Admittance space stability analysis of power electronic systems," *IEEE Transactions on Aerospace and Electronic Systems*, vol. 36, pp. 965 – 973, July 2000.

[143] Sudhoff, S., Glover, S., ?ak, S., Pekarek, S., Zivi, E., Delisle, D., and Clayton, D., "Stability analysis methodologies for dc power distribution systems," in *Thirteenth International Ship Control Systems Symposium*, April 2003.

[144] Synergy, "Main-synergy cables usa ltd.," June 2012. http://www.anixter.com/AXECOM/AXEDocLib.nsf/(UnID)/AE64734E04E4F4E980256F24007506FC/%24file/I-4_24.pdf.

[145] Technolgies, L., "Electric vehicle propulsion," 2014. http://www.launchpnt.com/portfolio/transportation/electric-vehicle-propulsion/.

[146] Thompson, G., "Training syllabus for the b777 electrical load management system," August 2009. http://www.geaviation.com/systems/support/pdf/training/SL-B777-ELMS-L3-03.pdf.

[147] Tinsely, C. T., "Modeling of multi-pulse transformer rectifier units in power distribution systems," Master's thesis, Virginia Polytechnic Institute and State University, 2003.

[148] Tooley, M. and Wyatt, D., *Aircraft Electrical and Electronic Systems: Principles, Maintenance, and Operation*. Elsevier Ltd., 2009.

[149] Umbria, F., Aracil, J., and Gordillo, F., "Singular perturbation stability analysis of three phase two-level power converters," in *18th Mediterranean Conference on Control & Automation*, pp. 123–128, June 2010.

[150] The United States Navy, *Aviation Electricity and Electronics Power Generation and Distribution*, February 2002.

[151] Vanderplaats, G., *Multidiscipline Design Optimization*. Vanderplaats Research and Development, Inc., 2007.

[152] Wan, C., Huang, M., Tse, C., Wong, S.-C., and Ruan, X., "Irreversible instability in three-phase voltage-source converter connected to non-ideal power grid with interacting load," in *Energy Conversion Congress and Exposition*, pp. 1406–1411, September 2012.

[153] Weichmann, E. P., Ziogas, P. D., and Stefanovic, V. R., "Generalized functional model for three-phase pwm inverter/rectifier converters," *IEEE Transactions on Industry Applications*, vol. 23, pp. 236–246, March/April 1987.

[154] Xi, H., Gong, W., Zhang, Y., Bi, Y., Ding, H., Wen, H., Hou, B., and Xin, Y., "Chinas 33.5 m, 35 kv/2 ka hts ac power cables operation in power grid," *Physica C*, vol. 445-448, pp. 1054–1057, 2006.

[155] Xu, W., Kaizheng, H., Shijie, Y., and Bin, X., "Simulation of three-phase voltage source pwm rectifier based on direct current control," in *Congress on Image and Signal Processing*, pp. 194–198, IEEE, 2008.

[156] Ye, H., Efstathiadis, H., and Haldar, P., "Numerical thermal simulation of cryogenic power modules under liquid nitrogen cooling," *Journal of Electronic Packaging*, vol. 128, pp. 267–272, September 2006.

[157] Yufang, S., "Calculation of network system reliability based on improved disjointed minimal path set," in *2010 International Conference on E-Product E-Service and E-Entertainment (ICEEE)*, 2010.

[158] Zangeneh, N., Azizian, A., Lye, L., and Popescu, R., "Application of response surface methodology in numerical geotechnical analysis," in *55th Canadian Society for Geotechnical Conference*, 2002.